Urban Wind Resource Assessment: Predicting the Turbulence Intensity, Excess Energy Available and Performance of Roof-Mounted Wind Turbines in a Built Environments

Francis Chimeziri Emejeamara

Submitted in accordance with the requirements for the degree of
Doctor of Philosophy

The University of Leeds
Energy Research Institute
School of Chemical and Process Engineering

May, 2017

The candidate confirms that the work submitted is his own, except where work which has formed part of jointly authored publications has been included. The contribution of the candidate and the other authors to this work has been explicitly indicated below. The candidate confirms that appropriate credit has been given within the thesis where reference has been made to the work of others.

Chapter 4 includes the published work stated below:

Emejeamara FC, Tomlin AS, Millward-Hopkins JT. Urban wind: Characterisation of useful gust and energy capture. *Renewable Energy*, 2015, 81, pp.162-172.

Chapter 5 includes the published work stated below:

Emejeamara FC, Tomlin AS. A method for mapping the turbulence intensity and excess energy available to building mounted wind turbines over a UK City. *Wind Energy*, 2015.

The original work contained within these papers is all the candidate's own work with guidance from A.S. Tomlin.

Acknowledgements

Completing this research project has been a mammoth challenge, with phases of stress, frustration and lassitude contrasting with moments of exhilaration, fulfilment and relief. This no doubt has required great personal effort, self-motivation and determination. I would like to thank my primary supervisor Professor Alison S. Tomlin for providing the guidance, direct and timely feedback and always demanding the highest of standards in all facets of my research study. I would like to thank the Niger Delta Development Commission (NDDC) for providing the financial assistance during the research.

Thanks must also go to Leena Jarvi, Curtis Wood and Annika Nordbo (The University of Helsinki) and Keith Sunderland (Dublin Institute of Technology) for the high-resolution datasets I dearly needed for the urban wind analysis, James Gooding, Joel Millward-Hopkins and all the parties involved in providing valuable data used in this study. On a personal note, I wish to thank all my friends and colleagues in the Energy Research Institute, of whom there are too numerous to mention, for all the help, support, motivation and the necessary distractions. Hence, I would like to first like to thank God Almighty for the grace and strength in trying times. Finally, I would like to thank my parents, Mr and Mrs G.A. Emejeamara and my siblings (Uzo, Kelechi, Uche, Oluchi and Chidi) for the moral and financial assistance they provided through the ups and downs I experienced while carrying out this research. This story would never have begun and this feat would never have been realized without you.

Abstract

De-centralised renewable energy power generation is proposed to be a significant part of the future of electricity generation technology, with wind energy playing a significant role. With half of the global population residing in urban and suburban areas, the opportunity for individuals or small organisations to generate power locally facilitates the decrease in losses associated with long distance electricity generation and transmission. Small-scale wind turbine applications within suburban/urban areas are exposed to high level of gust and turbulence compared to flow over less rough surfaces (e.g. coastal/offshore areas, open grasslands, rural areas, etc.). There is, therefore, a need for such systems not only to cope with, but to thrive under such rapidly fluctuating, complex urban wind conditions. Assessing the potential of a proposed urban wind turbine project is hindered by insufficient assessment of both the urban wind resource and power capabilities of certain turbine designs within a potential suburban/urban site. This, however, requires estimation of important factors such as local atmospheric turbulence, total energy available to the turbine system and the potential power output to be generated should a certain turbine system design be installed within a potential site.

The research presented in this thesis proposes a methodology for scoping the potential of small wind turbines within a built environment through effective assessment of the urban wind resource and power capabilities of small turbine systems. The aim is to address the lack of accurate and affordable methods for site viability assessment of small wind turbines within a built environment. This methodology encompasses three sub-models which estimate the local atmospheric turbulence (represented by the turbulence intensity, $T.I.$), additional energy within the gusty urban wind (represented by the excess energy content, EEC) and the turbine power capability at different heights within a potential site.

Firstly, to quantify the influence of location on the total energy available to a small wind turbine at a potential site, an in-depth evaluation of the urban wind resource is completed. This includes the development of methods to predict the local atmospheric turbulence at a given turbine mast height, and the additional energy available to the turbine which is usually under-represented when using assessments based only on mean wind speeds. This is achieved using high temporal resolution wind measurement datasets from eight potential turbine sites within the urban and suburban environments and LiDAR building height datasets from three major UK cities namely, Leeds, Manchester and London. Subsequently, new analytical models are developed that allow the mapping of atmospheric turbulence and excess energy at different heights over Leeds, Edinburgh, Manchester and London by combining the $T.I.$ and

EEC estimation models with currently available methods of predicting mean wind speeds over urban areas. The results from these two models highlight the importance of including building height variation and changes in wind direction within the assessment, and also the value of employing detailed building geometric data as model inputs.

A simple low-cost 2-D multiple streamtube vertical axis wind turbine (VAWT) model capable of simulating turbine performance in a fluctuating wind isdeveloped. Combining this VAWT model with dynamic stall features and variable speed control strategy, enables a system based design of wind turbines operating within suburban/urban environment. A method of estimating the performance of a turbine operation within an urban wind resource is developed by assessing the power capabilities of the VAWT model using high-resolution wind measurement datasets as model inputs. This is combined with the $T.I.$ and EEC estimation models in developing a new model known as the turbine power estimation (TPE) model used in mapping turbine performance at different heights over Leeds, Edinburgh, Manchester and London. Comparison between the TPE model and a generic power curve is made, hence suggesting the possibility of using a simple model to estimate the power capabilities of a certain turbine design while accounting for local turbulence within an urban wind resource.

Finally, the investigation of the cumulative potential of small wind turbine power generation in Leeds, Edinburgh, Manchester and London indicates a largely untapped wind resource available (represented by high EEC values estimated within small distances in each city) which could be harnessed if gust tracking solutions were to be commercially available. It also highlights the importance of site viability assessment and its financial implications illustrated by capacity factor maps over the four cities, which has practical value for turbine manufacturers and urban planners alike. Thus, for urban wind applications to achieve their optimum deployment potential, this research study proposes a simple, effective and affordable tool for preliminary scoping the potential of certain small wind turbine designs within a suburban/urban environment, and hence encouraging effective carbon savings. In order to maximize the impact of this research study, it would be valuable that these maps be extended to other towns/cities and made available and easily accessible to individuals and interested parties, and hence this is a major objective of future work.

Table of Contents

List of Tables

List of Figures

CHAPTER 1

1 Introduction

1.1 Background

Half of earth's population today resides in suburban/urban environments. In view of the growth of the world population and rural-urban migration statistics, this fraction is expected to increase in the future [1]. This significant growth in the population within these areas has simultaneously stimulated the increase in the demand for energy as a result of increasing human activities within the suburban/urban environment, thus leading to increases in intensive energy consumption within these densely populated areas.

The rising uncertainties over the future of the oil market (i.e. volatile oil prices, remaining reserves, etc.) as a result of the recurring effect of the two global energy crisis (1973 and 1979), the current drop in oil prices, decrease in reserves and a fear of a third energy crisis looming, coupled with the upsurge in the awareness of anthropogenic global warming and the rising atmospheric concentration of greenhouse gases (GHG) awareness have, fuelled huge interest in the search for alternative, sustainable and cleaner energy resources. It has become one of the most important tasks assigned to modern science and technology in recent times. This quest has thereby created a strong awareness among the public, instigating the generation of their own energy at a reduced carbon footprint and at the same time reducing their energy bills. This has induced a new energy market with an extensive opportunity for other alternative green energy sources to compliment popular energy sources like the fossil fuel sources (oil and gas, coal, etc.). These alternative sources are known as Renewable Energy Sources (RES) and they include solar thermal and photovoltaic, tidal, biomass, wind, geothermal, wave, etc. The environmental impacts of the dispersion of pollutants within a suburban/urban region, as well as the provision of power through RES, with wind energy as one focus, have prompted the necessity to understudy the climate around these suburban/urban areas, knowing that this will strongly affect the quality of life.

Prior to modern industrialisation, wind energy technologies were used to harness energy from wind for either pumping water or grinding grains. Due to high energy demands at the beginning of modern industrialisation, the fluctuating wind energy supply was replaced by more consistent energy supplies from coal, oil and gas resources [2]. However, global shocks from the energy crisis led to the re-emergence of wind energy technologies, with much focus on the generation of electricity. Perceptions about wind turbines have changed over the decades, from the concentration on single turbine developments to maximizing collective

power generation through an array of turbines (known as wind farms) by the end of the eighties. Manufacturers and energy companies are now heavily involved in the development of wind farms for commercial power generation which was their target business objective and not just wind turbine business. With its emergence in recent years as one of the most cost effective forms of renewable energy, wind energy is currently enjoying the status of a proven technology to great commercial effect. This has led to significant increase in the global annual installed capacity, with the rate of increases in sale of small-scale wind turbines growing to a record of 40% per year since the energy crisis of the 1970s [3]. Due to its cost-effectiveness, most developing countries have embraced the idea of utilizing wind and solar energy resources and the hybrid technology for their rural electricity needs [4].

The expansion of the wind energy industry into rural and urban areas has occasionally been met with public disapproval. From a financial perspective, factors strongly hampering wind energy success within these environments have been cost, revenue and desired return on investment. Other factors include government policies, such as incentives (like tax credit, etc.) or disincentives (like tax, etc.). However, from a technological perspective, insufficient urban wind resource assessment, noise-level of turbine operations, inefficient turbine power capability analysis as a result of the complex gusty urban wind resource and the availability of commercial gust tracking algorithms among other factors, all provide major setbacks to urban wind applications. Thus, smaller and quieter wind energy systems that have been developed for use within a built environment may be less subject to these concerns. These small-scale wind turbines can easily blend into a built environment through the incorporation of building-mounted wind turbines in high rise city centres, or ground mounted wind turbines in suburban regions. This would compensate for the losses experienced within the electricity supply system [5], as well as create greater public awareness for renewable energy options.

1.2 Research Objectives

Due to the complex nature of the urban wind resource as a result of inherent complex local building structures, atmospheric instabilities, etc., effective urban wind resource analysis and turbine performance assessment tends to play a significant role in the success and future of urban wind applications/projects. In order to achieve this, efficient and effective wind resource assessment in potential turbine sites as well as relevant affordable tools for estimating the power capabilities of certain turbine designs if they were to be installed within suburban/urban sites, should be made available. For this reason, this study presents a novel cost effective methodology for estimating the level of atmospheric turbulence at different hub heights over a complex suburban/urban environment based on parameterisations of the surface

aerodynamics. It also suggests that such a method can be used in quantifying the total (kinetic) energy resource available as well as estimating the power capabilities of a potential turbine system at different hub heights within a built environment, if the wind speed and turbulence intensity are provided. In developing this methodology, some of the most significant issues that arose when assessing the urban wind resource as well as the turbine power assessments within a built environment will be rectified using novel modelling techniques.

1.3 Overview of Thesis Structure

This research is divided into different stages, each with distinct intermediate goals:

a) First, a literature review covering the fundamentals of wind energy with an introduction to the concept of turbulence are presented in Chapter 2. This includes an overview of the various parameters used in evaluating turbulence within the wind energy industry and an introduction to boundary layer and urban meteorology. Various approaches employed by different studies in the study of turbulence are also presented thus laying the foundation for the purpose of this study. A review of wind turbine systems and their applications is also presented within this section. This includes turbine system characteristics, aerodynamics fundamentals (with focus on the actuator disk and the blade element momentum theory) and turbine control systems. This chapter also presents a view on the socio-economic importance of wind turbine systems hence highlighting the environmental and financial viability of wind energy projects.

b) The methodologies adopted within this study is presented in Chapter 3. This covers site description and instrumentation employed, data processing and analysis. A brief description of the wind prediction model, which was first proposed by Joel Milward-Hopkins and employed in this study, was also presented in this Chapter. Chapter 3 also presents a review of various turbine modelling approaches employed by different authors. It also goes on to present the basic framework for a simple low-cost small vertical axis wind turbine model which was employed in turbine power performance analysis and the power output estimation model proposed in Chapter 6. This turbine model was tested under various operating conditions and results presented. Finally, two control strategies namely fixed-speed and variable speed controls were also compared and hence the VSC selected for use in the turbine power assessment carried out in Chapter 6.

c) With the techno-economic performance of wind turbine systems being sensitive to the site's wind resource, Chapter 4 focuses on the characterisation of a typical urban wind

resource based on high resolution data collected from sonic anemometers located at roof-top locations within a built environment. The concept of 'excess energy' is presented in this chapter, with the effect of averaging time on the excess energy available within this rapidly fluctuating, turbulent wind resource also demonstrated. Hence, assessing the relationship between the level of turbulence and the excess energy available within a built environment, an analytical model for predicting the excess energy and/or the total kinetic energy available at a potential turbine site is proposed.

d) In Chapter 5, a methodology to estimate the level of atmospheric turbulence at a given hub height above a complex urban surface is tested. This methodology, based on parameterisation of the surface aerodynamics, is combined with the excess energy prediction model proposed in Chapter 4 in estimating the additional energy and hence total energy that would be available to a turbine system at different hub heights were effective control systems to be employed. This methodology was tested at the city-scale over four major UK cities namely, Leeds, Edinburgh, London and Manchester. Results at different hub heights within each city are shown, allowing for preliminary evaluation of city-scale potentials for generating wind energy in suburban/urban areas.

e) The potential of a small wind turbine system within a built environment at different response times was assessed in Chapter 6 using the turbine model presented in Chapter 3. Assessing the turbine system's performance at eight different sites, a new methodology for estimating the power output for a given turbine system within a suburban/urban environment was proposed. This methodology known within this study as the turbine power estimation (TPE) model takes into account the effect of turbulence and the excess energy available these features are neglected in most turbine power assessments using the widely popular power coefficients supplied by manufacturers. This methodology was tested at different hub heights over Leeds, Edinburgh, London and Manchester with results highlighting the need for effective wind resource and turbine performance assessment for potential wind turbine projects within suburban/urban areas. A comparison between power estimation using a generic turbine power curve and the TPE model proposed within this study is presented. Maps of the capacity factor of a turbine system estimated at a given hub height over the four cities (i.e. Leeds, Edinburgh, Manchester and London) was presented and discussed. Finally, a method of assessing the performance of a gust tracking control within an urban wind resource is proposed.

f) Finally, in Chapter 7, conclusions of the research study are summarised and their implications and impacts discussed.

1.3 Bibliography of published work

Due to the research performed in this PhD programme, the following paper publications and conference presentations have been produced so far:

Chapter 4:

Emejeamara FC, Tomlin AS, Millward-Hopkins JT. Urban wind: Characterisation of useful gust and energy capture. *Renewable Energy*, 2015, **81**, pp.162-172.

Chapter 5:

Emejeamara FC, Tomlin AS. A method for mapping the turbulence intensity and excess energy available to building mounted wind turbines over a UK City. *Wind Energy*, 2015.

Conferences attended:

- Oral Presentation at the American Meteorological Society (AMS): 21st Symposium on Boundary Layers and Turbulence in Leeds, United Kingdom; 9-13 June 2014.
  Paper Title: A Method of Mapping the Turbulence Intensity and Excess Energy over a major UK city (Leeds).
- Poster Presentation at the American Wind Energy Association (AWEA) WINDPOWER Conference and Exhibition 2015 in Orlando Florida, USA; 18-21 May, 2015.
  Paper Title: Mapping the Turbulence Intensity and Excess Energy over three major UK cities.
- Oral Presentation at the 17th International Conference on Renewable Energy Resources and Applications in Paris, France; 20-21 July, 2015.
  Paper Title: Mapping the Turbulence Intensity and Excess Energy over four major UK cities.

CHAPTER 2

2 Literature Review

2.1 Wind Energy Fundamentals

Wind can be simply characterised by its speed and direction, which are affected by various factors like surface topography, climate characteristics, geographic location, etc. Wind turbines tend to generate energy as a result of their interaction with the wind, thus converting the kinetic energy harnessed by the system into useful energy. This chapter is devoted to the fundamentals of wind energy as well as introducing the concepts of "*turbulence*" and wind flow over a built environment thus setting a foundation for the research goals which will be presented later on.

2.1.1 Extracting Energy from the Wind

2.1.1.1 The Wind Resource

Wind can simply be defined as air movement across the surface of the earth, from a region of high pressure to a region of low pressure. This can be as a result of differential heating and cooling of the land and sea (also known as the land and sea breeze [6, 7]), the formation of westerly winds from air streams that collide as a result of Coriolis effect, the forming of easterlies from warm air streams that flow around the equator [2], etc. The Coriolis force (or effect, as described by some studies) can be defined as:

$$f = 2\Omega \sin(|\Upsilon|) \qquad \text{Equation 2. 1}$$

where Υ is the latitude and Ω is the angular velocity of the rotation of the earth. It is popularly used for temperate regions (latitude) as it is zero around the equator. Coriolis forces induce a circular motion of air as it tries to move from high- to low-pressure regions thus resulting in a large-scale global circulation pattern [2].

Apart from other characteristics of wind resource, the most striking is its variability (temporal and geographical). This variability continues both in time and space, over a wide range of scales [2]. This is of importance due to the amplification by the cubic relationship with wind

power [8, 9]. Large-scale variability is as a result of different climatic regions in the world, whereas factors such as vegetation, physical geography – the size and shape of land mass, effect of topography (mountains and plains), height above the ground and the fraction of land and sea within a climatic region, influence the small scale variability of a specific wind resource [7, 10]. Temporal variability on a large-scale (represented by the 'Macro' section in Figure 2.1) means wind resources may vary from one year to the next, with even more variations occurring over a decade or longer. As shown in Figure 2.1, analysis carried out by Van der Hoven [11] on a 200-day wind data suggested the peak at a period of 0.01 cycles per hour (~ 4days) to result from seasonal large-scale wind fluctuations due to passage of large, synoptic-scale pressure systems. Thus, all wind turbines can respond to these changes which occur on the time-scale of days or hours [12].

Longer time-scales, on the other hand, are fairly predictable considering seasonal variations within a year or diurnal variations (i.e. variations with the time of the day). However, shorter time-scales within minutes and seconds (represented by the 'Micro' section in Figure 2.1) tend to house higher kinetic energy (represented by an energy peak at a period of 60 cycles per hour (i.e. ~ 1 min)) as well as an important factor known as turbulence. This high-energy turbulent wind within the micrometoeorological range makes wind resource fairly unpredictable, thereby affecting the design of wind energy conversion systems, the quality of power delivered to the grid (as in the case of wind turbines), and the resultant effect on its consumers. The unpredictability of the day-to-day wind resource can be attributed also to the non-linear and highly complex manner in which these variations interact. All these variations, if not well understood, will create difficulties in predicting the economic viability of specific wind energy projects such as wind farms, etc., and proper design and planning of wind energy generating plants, especially the amount of power supply to the grid [13, 14]. In general, if Figure 2.1 is considered a basic representative of the energy spectrum of a horizontal wind velocity, two energy peaks were suggested by Van der Hover to occur at periods of 4 days and 1 min. A spectral gap centered at a period of 1 hour (or 30 mins as suggested by Ref [11, 15]) also observed suggests lack of physical processes present that could support wind velocity fluctuations within this period. Consequently, this suggests that very little energy in the regions between approximately 2 hrs and 10 min. This so-called spectral gap suggests that the synoptic and diurnal variations can be treated as quite distinct from the short-period fluctuations of turbulence (represented by the micrometeorological region) which have significant effect on wind turbine operations [2]. Hence, considering small-scale wind energy within the built environment, urban wind applications need to be able, not only respond accurately to, but also thrive in short-period fluctuations dominant within the period housing the second energy peak (i.e. at 1 min). Detailed analysis of the total energy located within the

micrometeorological time-scale within a built environment will be discussed further in Chapters 4 and 5.

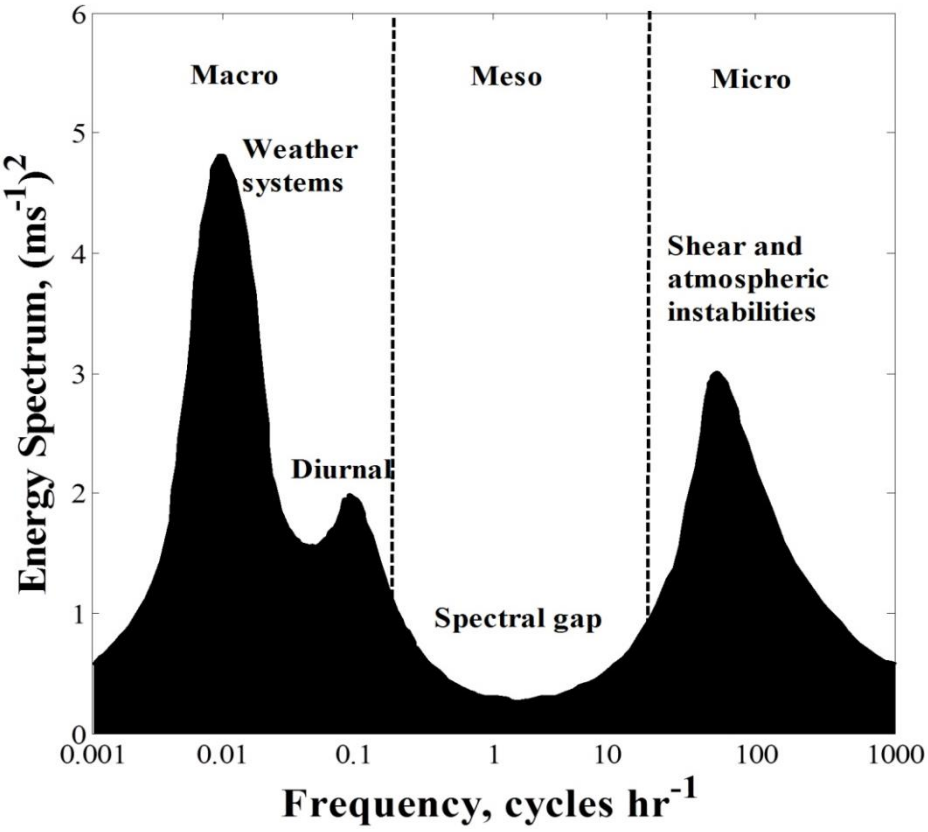

Figure 2. 1: Frequency distribution of fluctuating wind energy within the internal sub-layer, adapted from Van Der Hover [11]

It is rightfully true that underlying tendencies, which are responsible for climate differences within regions, exist. These differences are moderated by meso-scale (local thermal and topographical) effects. Thermal effects are responsible for local variations while topography (like mountains, hills, etc.) initiate regions of high wind speed, as wind speed generally increase with height above the ground [2]. These thermal effects can be as a result of differential heating of the land and sea [7], or due to differences in altitude as cold air on high altitude flows downwards to plains below, creating a highly stratified, strong downslope wind. Topographical effects are developed due to flow over elevated grounds or funnelling effects as wind flows through valleys which are aligned to the wind flow.

2.1.1.2 Nature of the Wind

Wind has proved to be a valuable resource through history with various systems designed to harness its energy for various purposes and these include wind mills, sailing of ships, etc. In recent times, increased exploitation of wind energy for both industrial and domestic purposes has prompted various studies for the purpose of a better understanding of the complex nature of the wind resource. Factors that are of great importance to the nature of the wind resource in a chosen site include:

a) The temporal variability of wind velocity over different time scales
b) The spatial variability factor within a mean wind velocity and
c) The cubic relationship between wind velocity and wind power

Previous studies have showed that the most striking characteristic of the complex nature of wind resources can be attributed to these three factors [2]. In a bid to analyse the distinctive nature of the wind resource and how its inherent characteristics affect power generation via wind turbine systems, various authors have obtained long-term measurements from different sites for study. Wind resource in thunderstorms and foehn winds (a type of dry wind that occurs at the lee side of elevated topographic features usually mountains or hills), tornadoes, hilly-land with complex topographical characteristics, and offshore terrains have shown to be more complex when compared with flat surfaces [10]. While in built environments, the complex nature of the wind resource has shown to be greatly enhanced by the inherent complex urban boundary characteristics. Thus, investigating power generation in a built environment via small-scale wind turbines requires an in-depth study of the wind resource within such environments. In order to achieve this, frequency distributions of the wind resource over a given time interval are developed from statistical averages. This will aid in examining turbulence properties inherent in the suburban/urban climate as well as analysing its effect on the performance of a wind turbine system.

Several methods of wind resource data collection like the Sound Detection And Ranging, or acoustic radar (SODAR), Light Detection And Ranging, or laser radar (LiDAR), etc., have been employed over the years [16], with the most popular method being through an anemometer employed at the target site. Large-scale wind projects like onshore or offshore wind farms require collecting wind data over a larger time scale (for example, 1-3 years) in order to develop adequate statistics to define the required wind velocity averages [17], while small wind turbine systems require shorter time scale statistics considering its shorter response time to the varying wind speed characteristics. Considering the significant amount of energy at shorter time-scale fluctuations representative of an urban wind resource (as shown in Figure 2. 1), this study attempts to characterise the urban wind resource in Chapter 4 as well

as propose a method of estimating the additional energy available within this fluctuating, turbulent wind resource in Chapter 5.

2.1.1.3 Wind Energy Physics

The power in the wind can be derived from the kinetic energy of the flow acting on the turbine blades and forcing rotation of the rotor. This rotor rotation is transmitted through the rotor shaft and a gearbox thereby producing a rotating magnetic flux at the generator which in turns produces electrical energy. The kinetic energy in a particular moving mass (m) of air can, therefore, be given as:

$$K.E_w = \frac{1}{2}\dot{m}V_\infty^2 \qquad \text{Equation 2. 2}$$

where $\dot{m}$ is the mass flow rate of air, and V_∞ is the upwind instantaneous flow velocity.

The mass flow rate for an element of air through an area A in steady streamline conditions can be defined as:

$$\dot{m} = \rho A V_\infty \qquad \text{Equation 2. 3}$$

where ρ is the air density.

Hence, power in the wind can be defined as the kinetic energy of the wind over a given time period (e.g. 1 second) and is given as:

$$P_w = \frac{1}{2}\rho A V_\infty^3 \qquad \text{Equation 2. 4}$$

Hence, when estimating the wind resource at a potential site, slight inaccuracies in predicting wind velocities can result in significant errors in estimating the energy yields of the system.

From the equations above, it is justified that power is proportional to the cubic value of the wind velocity. This means that if the wind velocity is doubled, we will get eight times the power. Hence, it is very important to have an understanding of the basics and characteristics of wind resource with respect to wind energy exploitation.

Power also increases with increasing air density (for example cold conditions present at sea level) and reduces with lower air density (for example hot climates at altitude). Therefore, it is important to consider atmospheric effects in wind turbine power computations.

2.1.2 Urban Wind and Turbulence

Climatologies present in suburban/urban environments are different from those in rural and coastal environments. Various applications like building design, air pollution modelling and wind engineering have prompted the detailed study of these inherent climatologies within built environments. The urban boundary layer provides within its area, various characteristic features that tend to influence or serve as obstacles at the wake of oncoming wind. These obstacles, for example, arrays of buildings, completely impede on the wind flow thus creating a "*wind shade*". This wind shades allows higher energy losses due to the slowdown effect, leading to a characterized high level of resultant turbulent wind at the wake downwind of these obstacles. Terrain roughness height, however, is one major factor responsible for the difference in energy distribution with length scales between the suburban/urban wind environment and large rural wind farms. In order to ensure that the wind turbine system operates at an optimum aerodynamic efficiency, one however, needs to evaluate this turbulent wind resource within these built environments. This, therefore, leads us to the need for understanding the important phenomenon known as "*turbulence*".

2.1.2.1 Turbulence

Wind velocity and turbulence are the most important factors that influence the amount of energy available to a wind converter system within a built-up area and the ability of the wind converter system to extract useful work. Wind velocity is not a strictly stationary function, hence it changes with time (as shown in Figure 2.2 below). The instatenous value of the wind velocity (V_t) can, however, be represented as the sum of the mean wind velocity ($\bar{V}$) and its fluctuating component (i.e $V' = V_t - \bar{V}$). In a turbulent wind flow, the mean values of the wind velocity tends to be smooth and slowly varying whereas the fluctuations (V') are characterised by extreme spartial and temporal variations. Hence, turbulence, in relation to wind turbines, can be referred to wind velocity fluctuations in a relatively fast time-scale, usually less than 10-15 minutes (as represented by the micrometeorological range in Figure 2.1) [18, 19].

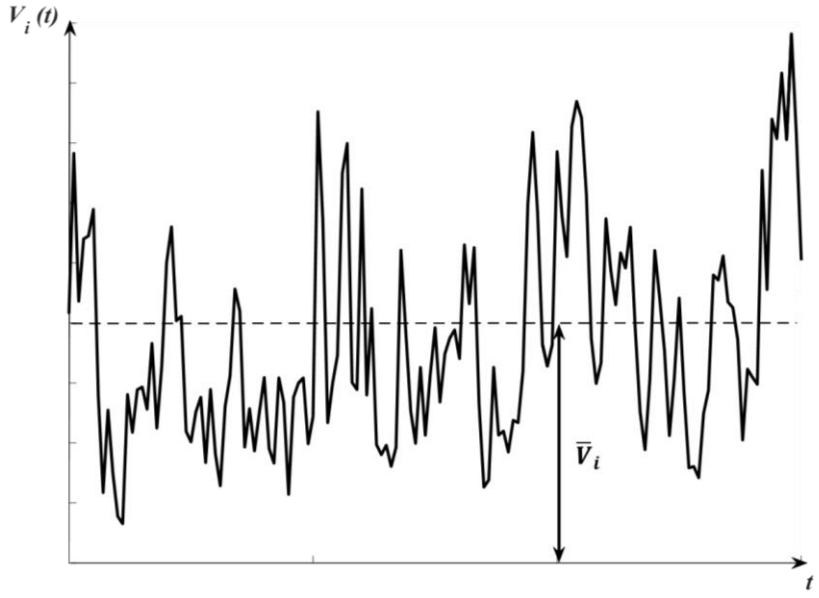

Figure 2. 2: Typical record of a turbulent wind flow within a built-up area.

Mean wind velocity is well defined and easily calculated, whereas turbulence, in its broadest sense, represents a greater challenge. Turbulence, observed closer to the earth surface, is believed to be caused by two factors; topographical and thermal factors [2]. It is understood that complex (heterogeneous) terrains have a significant impact on the local wind climate. Thus, the wind velocity and the wind direction, as well as the inherent ambient turbulence, are all highly influenced by the local terrain heterogeneity. Thermal effects, which are also important factors, could be as a result of either differential surface heating or differences in altitude (buoyancy driven). Wind energy development over complex terrain areas like built environments has revealed the critical issues that underlie complex terrain flows. Hence, this clearly calls for flow modelling of increased accuracy. In extreme cases, an inversion of the wind shear and a downstream flow separation is possible, which is followed by an increase in turbulence, that renders not all locations within a built environment appropriate for wind turbine siting [20, 21]. Also the wake of turbines in wind farms and buildings or obstacles within built environments, tend to inherit turbulence created by the obstacle effect upstream of the wind. The gradient between the wake of turbines or buildings/obstacles and free-stream wind outside the wake also tend to create an added shear-generated turbulence.

Turbulence, due to its complexity, cannot easily be represented by deterministic equations [2, 22], rather it can be described in terms of statistical properties through the use of time-averaged physical laws such as conservation of mass, momentum and energy while taking into account factors such as pressure, temperature, humidity, density and the

three-dimensional motion of air. These statistical properties range from turbulence intensity, gust factor, friction velocity, to detailed description of how as a function of frequency, the three components of turbulence (i.e. longitudinal, lateral and vertical components) vary in space and time. A starting point is invariably Newton's second law, which when applied to a lump of wind flow takes the form of the Navier-Stokes equation given in Equation 2.5 [23-25]. This is popularly used when explaining a great variety of incompressible flows in fluid mechanics studies.

$$\frac{dV}{dt} = -V \cdot \nabla V - \frac{1}{\rho}\nabla P + \nu \nabla^2 V + F_o \qquad \text{Equation 2. 5}$$

where V represents the mean wind velocity, ν is the kinematic viscosity, P is pressure and ρ represents the density of air. Assuming constant air density and neglecting other external forces acting on the flow (F_o), various studies have modelled the changes in the directional velocity of the wind flow (i.e. complex nature of turbulence) using three components. These are represented by the three terms on the right-hand side of Equation 2.5. The first term represents the inertial force, the second term represents the pressure force while the third term simply represents the viscous force. An inverse proportional measure of the viscous forces acting on the flow is known as the Reynolds number (Re). This is a dimensionless parameter popularly used in characterising different types of flow [2] and is defined as the ratio of the inertial forces and the viscous forces acting on the flow (as shown in Equation 2.6). It consequently quantifies the relative importance of these two types of forces for a given flow condition.

$$Re(L_e) = \frac{Inertial\ force}{Viscous\ force} = \frac{VL_e}{\nu} \qquad \text{Equation 2. 6}$$

where V is the characteristic mean wind velocity of the flow, L_e is the appropriate length-scale and ν is the kinematic viscosity. At high Reynolds numbers, the motion of the characteristic wind flow results in the formation of eddies, thus giving rise to turbulence. This, however, suggests the viscous forces to be very small when compared to the inertial forces, hence the third term in Navier-Stokes equation can be neglected. Thus, Equation 2.5 can, therefore, be rewritten as:

$$\frac{dV}{dt} = -V \cdot \nabla V - \frac{1}{\rho}\nabla P \qquad \text{Equation 2. 7}$$

For low Reynolds number, the inertial term is smaller than the viscous term (as deduced from Equation 2.6), hence the first term in Equation 2.5 can be neglected. Thus, Equation 2.5 can be rewritten as:

$$\frac{dV}{dt} = -\frac{1}{\rho}\nabla P + \nu\nabla^2 V \qquad \text{Equation 2. 8}$$

A flow can also be characterised as laminar, transitional or turbulent depending on its local Reynolds number [2]. A flow is classified as laminar when its Reynolds number is less than 2300, transitional when the Reynolds number is greater than 2300 and less than 4000, and turbulent when the Reynolds number is greater than 4000.

Considering a turbulent flow where $Re(L_e)$ is large (coinciding with the micrometeorological range in the Van der Hoven spectrum shown in Figure 2.1), V is represented by the typical value of its fluctuating component (i.e. $|V'|$) and L_e is the typical length-scale of the large-scale turbulent eddies. The largest eddies, which are basically created by instabilities in the mean wind flow, rapidly break up or evolve into smaller eddies due to inertial instabilities. These smaller eddies are themselves unstable and in turn, pass their energy onto even smaller structures and so on. Since the Reynolds number is large, the whole process is essentially driven by inertial forces while the viscous stresses are considered negligible. Thus, at each instant, there is continual transfer (or cascade) of energy from large-scale down to small eddies. This is known as the *cascade process* [26]. However, when the eddy size becomes so small and the Reynolds number, based on the size of the smallest eddies, is in the order of unity, the cascade comes to a halt. At this point, the flow becomes laminar and the viscous forces become significant [22]. The Navier-Stokes equations were formulated between 1921-45 by Claude-Louis Navier and George Gabriel Stokes [27, 28]. Averaging these equations gives what is known as the Reynolds-Averaging Navier-Stokes equations, which govern the mean wind flow. These equations, however, serve as the bedrock for most computer-simulated turbulent flow models such as the Reynolds-Averaged Navier-Stokes (RANS), Large Eddy Simulation (LES), etc., which will be discussed further in Section 2.3.

Despite the random nature of wind flow within a turbulent environment, statistical properties of the velocity field, such as $\bar{V}$ and $\overline{(V')^2}$, seem to be quite reproducible [22]. Thus, in a bid to develop dynamic equations for these statistical quantities, studies have shown that solving the Navier-Stokes equations lead to the apprearance of more statistical unknowns than the equations relating them, hence non-linearity on the right of Equation 2.5 [22, 29, 30] . This is known as the *turbulence closure problem.* Thus, various studies have introduced various concepts in a bid to resolve the closure problem, thus leading to the development of different turbulence models. These include the eddy viscosity model, the k-epsilon (k-ε) model, the k-omega (*k*–ω) turbulence model, shear stress transport (SST) model, etc. The k-epsilon (k-ε) model is the most common model used to simulate mean wind flow characterisitics for turbulent wind conditions [22]. This is a one-point closure model (i.e. evaluates statistical

quantites at one point in space) which seeks to predict the Reynolds stresses, thus allowing the mean flow to be calculated. Reynold stress (also referred to as wind shear stress) indicates that velocity fluctuations lead to a transport of momentum from one lump of flow to another [26], and only occurs when the atmosphere is turbulent. This can be estimated using Equation 2.9 [31].

$$\tau = -\rho\overline{u'w'} \qquad \text{Equation 2. 9}$$

where ρ represents the air density, the overbar represents temporal averaging over a burst period and the prime indicates that fluctuations of the wind speed components (i.e. u' for longitudinal and w' for vertical) are also considered. Various models have been developed based on the k-epsilon (k-ε) model approach and are widely used by engineers and researchers in estimating the influence of turbulence on mean wind flow. These models use time/spatially averaged approaches such as RANS where turbulence is expressed in terms of simple quantities such as turbulence kinetic energy (TKE) or turbulence dissipation, and have also employed various statistical parameters, a few of these are presented below.

2.1.2.2 Turbulence Evaluation Parameters

Turbulence is an inevitable phenomenon in both offshore and onshore wind. Turbulent wind speed variations can be said to be roughly Gaussian (i.e. normally distributed) although the tail of this distribution is, maybe to a large extent, non-Gaussian, thereby making it unreliable for estimations [2]. As earlier stated, the turbulence level at different sites can be evaluated using different statistical properties. This has been demonstrated in the past by various studies (such as building design, pollution dispersion, wind energy, etc.) through the use of different parameters. In the wind energy industry, there are a number of statistical descriptors of turbulence that have been employed for this cause. A few are listed below. These turbulence evaluation parameters were partly based on theoretical considerations, and partly on empirical fits to a wide range of data (observations) from various researchers taken in various atmospheric conditions and in various sites.

Turbulence Intensity

Turbulence intensity is one of the popular parameters in characterising the turbulence level in any given site. It is simply an overall measure of turbulent variation of the wind velocity component over a given period of time across an area [32], and is dependent on the height of

the flow from the ground surface, the topography of the flow terrain and the thermal behaviour of the atmosphere. It is mathematically calculated using Equation 2.10:

$$T.I._u = \frac{\sigma_u}{\overline{V_u}} \qquad \text{Equation 2. 10}$$

where $T.I._u$ is known as the longitudinal turbulence intensity, σ_u represents the standard deviation of the longitudinal wind velocity component which is given as:

$$\sigma_u = \sqrt{\frac{1}{T}\sum_{i=1}^{T}(V_{ui} - \bar{V}_u)^2} \qquad \text{Equation 2. 11}$$

where $\overline{V_u}$ represents the mean longitudinal wind velocity over a burst period and *T* defines the sample burst period (usually 10 minutes according to wind energy industry standards [12]).

V_{ui} represents the longitudinal free-stream wind velocity upstream and is given as:

$$V_{ui} = u_u \cos\theta_u + v_u \sin\theta_u \qquad \text{Equation 2. 12}$$

where θ_u is the longitudinal free-stream wind direction which is derived from the horizontal wind components, u_u (*x*-direction) and v_u (*y*-direction) as follows:

$$\theta_u = \tan^{-1}(v_u/u_u) \qquad \text{Equation 2. 13}$$

The lateral ($T.I._v$) and the vertical ($T.I._w$) turbulence intensities are also similar to that of the longitudinal, and are given as:

$$T.I._v = \frac{\sigma_v}{\overline{V_v}} \qquad \text{Equation 2. 14}$$

$$T.I._w = \frac{\sigma_w}{\overline{V_w}} \qquad \text{Equation 2. 15}$$

where u, v and w represent the longitudinal, lateral and vertical components of the wind. σ_u, σ_v and σ_w are the standard deviations about the mean wind velocity for the different wind components.

It is important to note that methods of estimating turbulence intensities vary across the wind energy industry. An example is the Danish standard turbulence intensity parameter which is estimated using Equation 2.16 [2, 33].

$$T.I._{danish(u)} = \frac{1}{\ln \frac{z}{z_0}} \qquad \text{Equation 2. 16}$$

where z represents the height above the ground and z_0 represents the local roughness length of the specific site, with the lateral and vertical components of the turbulence intensities defined as:

$$T.I._{danish(v)} = 0.8\, T.I._{danish(u)} \qquad \text{Equation 2. 17}$$

$$T.I._{danish(w)} = 0.5\, T.I._{danish(u)} \qquad \text{Equation 2. 18}$$

Equations 2.16 – 2.18 represent empirical estimations based on surface roughness for neutral conditions which may be employed in modelling turbulence over a given area where high resolution wind measurements were not available. This will be discussed further in Chapter 5.

Friction Velocity

Friction velocity is a reference wind velocity which describes profiles in a surface layer where fluxes are assumed to be independent of height (for example in Monin-Obukhov similarity theory) [31]. Friction velocity is another important parameter used in the measure of atmospheric turbulence while taking into account atmospheric stability. This can be estimated using various methods. Taking reference from the typical roughness length of a specific terrain, frictional velocity can be estimated using Equation 2.19 [2].

$$u_* = \frac{k_a \bar{V}}{\ln\left(\frac{z}{z_0}\right) + \Psi} \qquad \text{Equation 2. 19}$$

where z_0 is the roughness length of the terrain, z is the selected height above the ground, k_a is Von Karman's constant (in the value of 0.41), $\bar{V}$ is the mean wind velocity across a given burst period and Ψ is the coefficient of atmospheric stability (this is negative in unstable conditions and positive in stable conditions whereas for neutral conditions (often assumed in most wind energy studies), it is typically small and can be ignored [2, 34]).

Friction velocity can also be represented as a function of Reynold stress as shown in Equation 2.20 [33, 35, 36].

$$u_* = \sqrt{\frac{\tau}{\rho}} \qquad \text{Equation 2. 20}$$

where τ represents the Reynolds stress and ρ represents the density of air.

Friction velocity is commonly used in defining the level of surface homogeneity. After carrying out analysis on high resolution measurement data collected at different sites in a bid to characterise the local turbulence at different heights within an urban boundary layer, Roth [37] proposed an empirical relationship for estimating friction velocity which is represented by Equation 2.21.

$$u_* = \bar{V}\,(0.094 + 0.353\exp(-0.946(z/h_m))) \qquad \text{Equation 2. 21}$$

where h_m is the local mean building height and z is the height of measurement above the ground.

This takes into account the variation in building heights and can be applied over built environments where high resolution measurements of turbulent properties are not available. Other methods suggested by different studies in estimating friction velocity under different atmospheric conditions can be found in Refs [31, 38-41].

Gust Factor

Gust factor can be defined as the ratio of the gust wind speed or the peak gust (which is equivalent to the maximum wind speed (V_{max}) within a given burst period) to the mean wind speed across the burst period. This is mathematically represented as [33, 42]:

$$G.F(T) = \frac{V_{max}}{\bar{V}(T)} \qquad \text{Equation 2. 22}$$

However, gust factor can be represented as a function of turbulence intensity as well as time dependent as shown in Equation 2.23 [2, 33].

$$G.F_{(T)} = 1 + 0.42T.I_u \ln\frac{3600s}{T} \qquad \text{Equation 2. 23}$$

where T is in seconds and represents the burst period.

From detailed analysis of onsite measurements, a modification of Equation 2.23 was proposed by Wieringa [33] which calculates the gust factor while accounting for the roughness length, hub height and time dependence. This is given by Equation 2.24:

$$G.F_{(T)} = 1 + \frac{1.42 + 0.3013\ln\left[\left(\frac{990m}{\bar{V}T}\right)\right]}{\ln(z/z_o)} \qquad \text{Equation 2. 24}$$

where $\bar{V}$ is the mean wind speed over the burst period (T).

Gustiness present in a wind resource initiates dynamic loading effects on a turbine system, which can be examined in terms of the gust loading factor, which relies on the gust factor. This has led to the factoring of the expected mean wind speed of a given probability distribution into the design codes of wind turbines so as to accommodate the effect of gustiness into the system's design. In the past, gust factor was a major factor used in structural engineering for examining gust loading on structures in order to proffer better designs. Both time and space averaging play an important role in the development of gust factor [43]. Thus, in structural engineering, 3 s gust factors are used in examining cladding, roofing and glazing, 5 s gust factors are used for structures with horizontal and vertical dimensions less than 50 m, 15 s gust factors are used for structures with horizontal and vertical dimensions greater than 50 m [44], while in the wind engineering industry, the standard gust factor interval is 10 minutes, which is the industry standard time interval in examining wind turbine response to wind gustiness [45]. While the turbulence intensity is used in characterizing the overall gustiness across a wind data, gust factor is used to define the peak gusts in the same interval.

In smaller systems like small-scale and micro wind turbines, short duration gusts (ranges like 30 s, 1 min gusts and 10 min gusts) are very relevant in examining the system's response to the effect of gustiness. This property has also been extended to larger wind turbine systems whereby the maximum gust loading on each individual component is examined and the occurrence over the entire system is put together in order to find out the maximum most probable overall loading. Having presented various statistical descriptors of turbulence proposed by different studies, one should be aware which definition is required or used for a

specific purpose. Further comparison and discussion of methods of estimating the level of turbulence at different heights within a built environment in relation to urban wind characterisation is presented in Chapter 5.

2.1.2.3 Boundary Layer and Urban Meteorology

As the height above the ground increases, the turbulent wind variations which are caused by the interaction in the ground surface become weaker. However, a height is attained where the wind velocity variations are considered to be governed by rotation of the earth and large-scale synoptic pressure differences and free from surface influences [46]. At this height, the air moves so that a balance is achieved between the Coriolis force and the pressure gradient. This is known as the geostrophic balance. In their study, Seinfeld and Pandis [26] suggested that the component of the Coriolis force at this height is exactly balanced by the pressure gradient, thus resulting in what is known as the geostrophic wind. As stated earlier, low Reynolds flow ($Re \ll 1$) suggests frictional effects dominate and for large Reynolds number flows ($Re \gg 1$) we may neglect friction. Thus, geostrophic wind can be described as large Reynolds number flow. Below this height, the effect of the earth surface can be felt and should be considered in flow characterization. This area is known as the boundary layer area. Wind turbines are energy systems specifically built to harness the wind within the boundary layer. Boundary layer conditions are influenced by regional conditions as well as the energy transfer between undisturbed high-energy geostrophic wind and the layer below [2]. Wind velocity changes with height within a built environment [47] and this leads to wind shear across the rotor of the turbine system causing varying loads across the rotor. Thus, the understanding of this boundary layer's inherent properties is very important in characterizing local turbulence [2, 37] and its effect on wind turbine systems [12].

These are defined by boundary layer meteorology and a brief overview of the various boundary layer processes is given in the following section.

Atmospheric Boundary Layer

The roughness of the earth surface and the height above this surface, the topography and thermal effects significantly influence the local turbulence within a given area. The boundary layer within the troposphere (i.e. the lowest layer of the Earth's atmosphere), known as the planetary boundary layer (PBL) or atmospheric boundary layer (ABL), houses a lot of important processes. However, in order to understand the turbulence experienced by wind

converter systems, it is important to understand the properties of this boundary layer and the principal effect governing these properties.

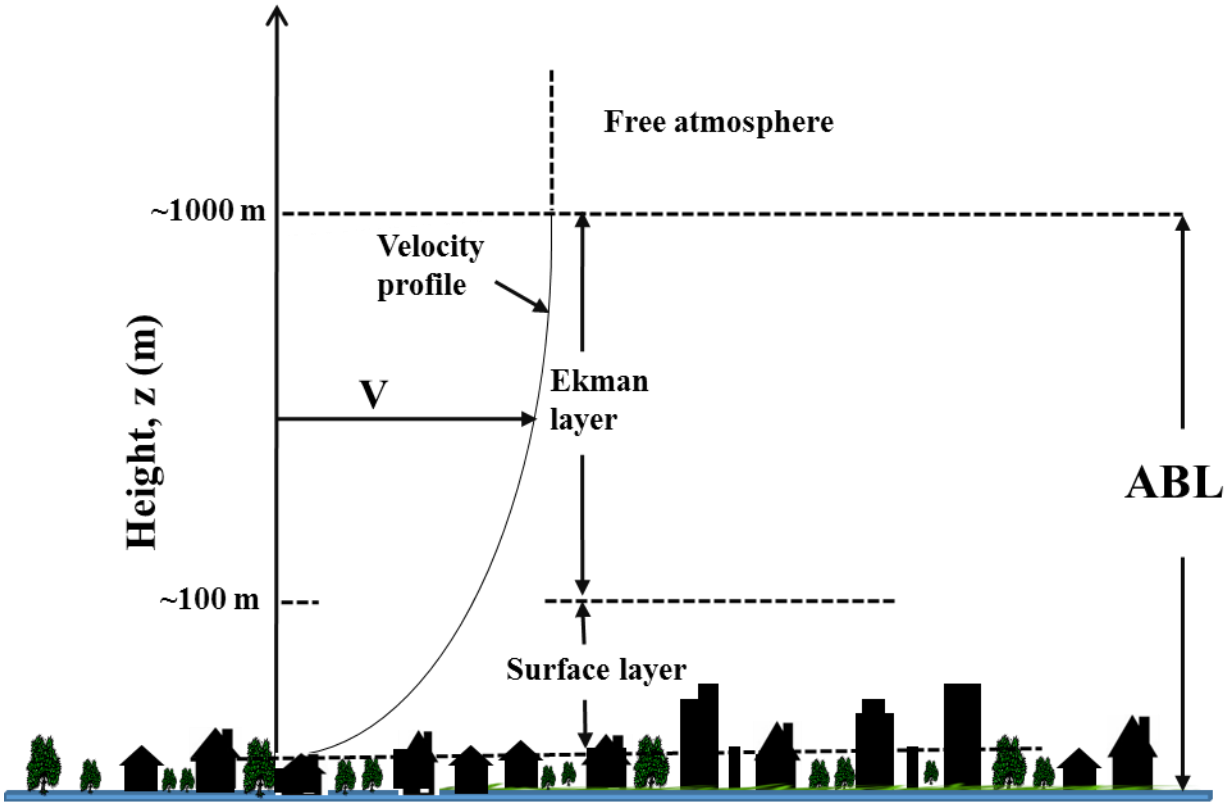

Figure 2. 3: Subdivision of the Atmospheric Boundary layer (ABL) into further sub-layers [46]

As illustrated in Figure 2.3, this layer can be divided into two regions; the surface layer height typically 50 – 100 m above the earth surfaces and the region above that layer (usually referred to as the Ekman layer) extending to a height of 500 – 1000 m [46]. The depth of this layer varies according to the time of the day (with the upper limits, known as the daytime and nighttime boundary layers, forming what is called the *inversion layer capping*). The geostrophic wind driven by synoptic-scale weather events tends to be in control of the wind velocity within the upper layer of the atmospheric boundary layer (ABL) [48]. The geostrophic balance tends to control the wind direction at heights above the ABL [26]. Factors like the shear forces due to roughness elements and buoyancy forces initiated by solar heating up of the earth, considerably affect the motion of the air within the upper layer of the ABL. Its results are turbulent eddies which are controlled by free or forced convection [49]. As one descends in the ABL boundary, the effect of the inherent roughness elements which individually exact a drag force on the wind flow increases and the wind velocity within this layer tends to vary

greatly in magnitude and direction compared to that of the geostrophic wind. The drag force exerted by the roughness elements on the wind produces turbulent stresses which expand upwards thus creating shear in the vertical wind profile. The magnitude of these shear forces depend on the roughness element characteristics (i.e. density, height, etc.). Thus, as suggested by Newton's law of viscosity, studies have shown typical wind profiles over uniform and extensive surfaces within the ABL (as demonstrated in Figure 2.3) to have a large vertical wind shear $\left({}^{dV}/_{dz}\right)$ near the ground, and decreasing gradually as the height above the ground increases [2, 46, 50, 51]. Hence, wind shear produced by mechanical process $\left({}^{dV}/_{dz}\right)$ can be expressed as [46, 51]:

$$\frac{dV}{dz} = \frac{u_*}{k_a z} \qquad \text{Equation 2. 25}$$

where k_a is the Von Karman constant, u_* is the friction velocity, which has a relationship with Reynolds stress through the expression represented in Equation 2.20. In wall bounded flows, it is assumed that the average length-scale of the turbulent eddies is restricted by the presence of the wall. Hence, '$k_a z$' in Equation 2.25 can be defined as the mixing length [52].

Integrating this expression give a common logarithmic vertical wind profile [50]:

$$V_z = \frac{u_*}{k_a} \ln z + \mathrm{C} \qquad \text{Equation 2. 26}$$

where C is a constant of integration, V_z represents the mean wind speed at a given height z. This can be re-written with a constant (known as the roughness length z_0) inside the logarithmic term, such that $V_z = 0$ at $z = z_0$:

$$V_z = \frac{u_*}{k_a} \ln\left(\frac{z}{z_0}\right) \qquad \text{Equation 2. 27}$$

In general, four factors govern the properties of a boundary layer and they are inherent thermal effects, surface roughness, the strength of the geostrophic wind and the Coriolis effect due to the rotation of the earth [2].

Thermal effects in a boundary layer can be classified into three stratifications namely [2]:

1. The unstable stratification: In this stratification, increased heating of the earth surface causes air close to the surface to rise. This rising air expands due to reduced pressure at increasing height thereby causing the air to cool adiabatically. Insufficient cooling

of this air tends to cause it to rise further until it gains thermal equilibrium with surrounding air. This, therefore, develops large convection cells which result in a thick boundary layer with large eddies.

2. The stable stratification: The rising air, in this stratification, becomes colder than its surrounding air due to the adiabatic cooling effect with height, resulting in the suppression of the vertical movement of the rising air. This usually occurs at night time, of which a property like wind shear is large and turbulence is determined by friction with the ground.
3. The neutral stratification: The rising air is in thermal equilibrium with the surrounding air due to its adiabatic cooling effect. This is usually observed in strong winds where the roughness of the terrain causes sufficient mixing in the boundary layer. Neutral stratification is the most important category when it comes to wind energy applications.

Most wind energy studies have developed models based on neutral stability atmospheric conditions (or neutral stratification) since unstable conditions give rise to sudden gusts and turbulent winds thus resulting in significant wind loads which are critical in wind turbine designs. In neutral stratification, the properties of this layer are dependent on the Coriolis effect and the surface roughness.

The surface roughness is described by the roughness length, z_o, and this varies in different terrains (as presented in Table 2.1). The roughness length (z_o) generally represents the vertical height within a terrain at which the wind speed is theoretically equivalent to zero. Wind shear profile gradually changes downwind of the transition with changing surface roughness.

Table 2.1: A summary of the standard roughness lengths for different terrains (where [A] is adapted from Ref [2] and [B] is adapted from [12]).

Types of Terrain	Roughness length z_o (m)
Cities, Forests	> 0.7[A,B]
Suburbs, wooded countryside	0.3[A], 0.2[B]
Villages, countryside with trees and hedges	0.1[A]
Open farmland, few trees and buildings	0.03[A], 0.05[B]
Flat grassy plain	0.01[A]
Flat desert, rough sea	0.001[A], 0.005[B]

The height of a boundary layer in the neutral atmosphere can be estimated as a function of the friction velocity (as represented in Equation 2.28 [2])

$$h = u_*/\,6f \qquad \text{Equation 2. 28}$$

where f is the Coriolis effect and u_* is the friction velocity.

Based on theoretical considerations, Burton [2] suggested that the wind velocity at the top of the boundary layer can be estimated by combining Equations 2.19 and 2.28 at h = z ,

$$\bar{V}(\mathrm{h}) = \frac{u_* \left[\ln(u_*/f\, z_0) - \ln 6 + \Psi\right]}{k_a} \qquad \text{Equation 2. 29}$$

where z_0 represents the roughness length of the terrain (as provided in Table 2.1) and Ψ represents the coefficient of stability and is assumed to be 5.75 for neutral conditions [2].

This is similar to the equation describing the geostrophic wind, of which is referred to as geostrophic drag law. This is given as:

$$G = \frac{u_*}{k_a}\sqrt{\left[\ln\left(\frac{u_*}{f z_o}\right) - A\right]^2 + B^2} \qquad \text{Equation 2. 30}$$

with $A = ln6$ and $B = 4.5$ for neutral conditions.

Although these simple laws may be applied above the boundary layer where pressure gradients and Coriolis forces significantly influence the wind flow, these simple definitions will be modified when considering wind velocities at heights closer to the ground. Hence, this study aims to demonstrate how urban surfaces (as a result of increased surface friction) disrupt these simple laws.

The Built Environment Canopy

The built environment has a significant concentration of structures, of varying shapes and sizes and basically one climatic element that can be changed in this canopy is its inherent wind. The built environment canopy can be grouped into urban, suburban and semi-rural areas, with the variation between the urban and rural environment meteorology created by the density of the roughness elements and thermal effects. In this study, we restrict our discussion to the areas within the urban and suburban environment which is herein referred to as built environment. The increased roughness in this built environment causes larger mechanical turbulence with the thermally induced turbulence caused by the urban heat island (UHI) [49] thereby creating the need for better turbulence modelling through sound meteorological input data. Previous analysis on turbulence within the built environment through creating models and generating scenarios in an artificial environment have fallen short of expected results since these models based on simple arrays entertained inaccuracies due to the inability to recreate specific urban meteorological characteristics. Clearly, the complexity of interpretation and design of the built environment's elements has led to the avoidance of meticulous description of the individual structures and its influence on urban wind.

Structures (such as building, trees, etc.) within the built environment tend to influence the wind flow characteristics in the ABL such that surface shear associated with these structures basically influences the wind speed and the degree of turbulence [53, 54]. Thus, for flows over the built environment canopy, a modification to Equation 2.27 is made in order to account for the blocking effect of the obstacles. This is achieved through a correction to the height above ground level using the parameter known as the zero plane displacement height d. Thus, the horizontal wind velocity is expressed using Equation 2.31 [55].

$$V_z = \frac{u_*}{k_a} \ln\left(\frac{z-d}{z_0}\right) \qquad \text{Equation 2. 31}$$

where V_z represents the mean wind speed at a given height z, k_a is the Von Karman constant, z_0 is the roughness length, u_* is the friction velocity. The use of the expression in Equation 2.31 in predicting the wind speed in the ISL depends on the knowledge of the parameters z_0 and d. Both parameters (the displacement height and the roughness length) play an important role in defining the influence of surface roughness elements on form drag. The start point from which the velocity profile is measured, typically depends on the displacement height, while the roughness length adjusts the wind speed by a given constant [56]. Garrat [57] pointed out that the values 0.1 and 0.7 multiplied by the average height of the buildings is commonly used in representing the z_0 and d in a lot of natural surfaces. This is not the case for built environments, as these parameters are functions of the size, shape and the area covered by the roughness elements within the given environment [58]. In order to understand these effects better, it would be ideal to further classify the ABL into sub-layers and discuss in detail.

The Urban Boundary Layer

The internal boundary layer above a built environment known to have modified itself based on the surface characteristics of the given environment is known as the urban boundary layer (UBL). This strong modification can be attributed to the thermal turbulence produced by anthropogenic heat emissions and the storage of heat in urban structures, as well as the high surface roughness within this boundary layer. The UBL develops downwind from a built environment's edge (See Figure 2.4) with its height depending on the surface roughness and atmospheric stability [59]. Thus, the flow characteristics within this layer are strongly influenced by its inherent structure geometry.

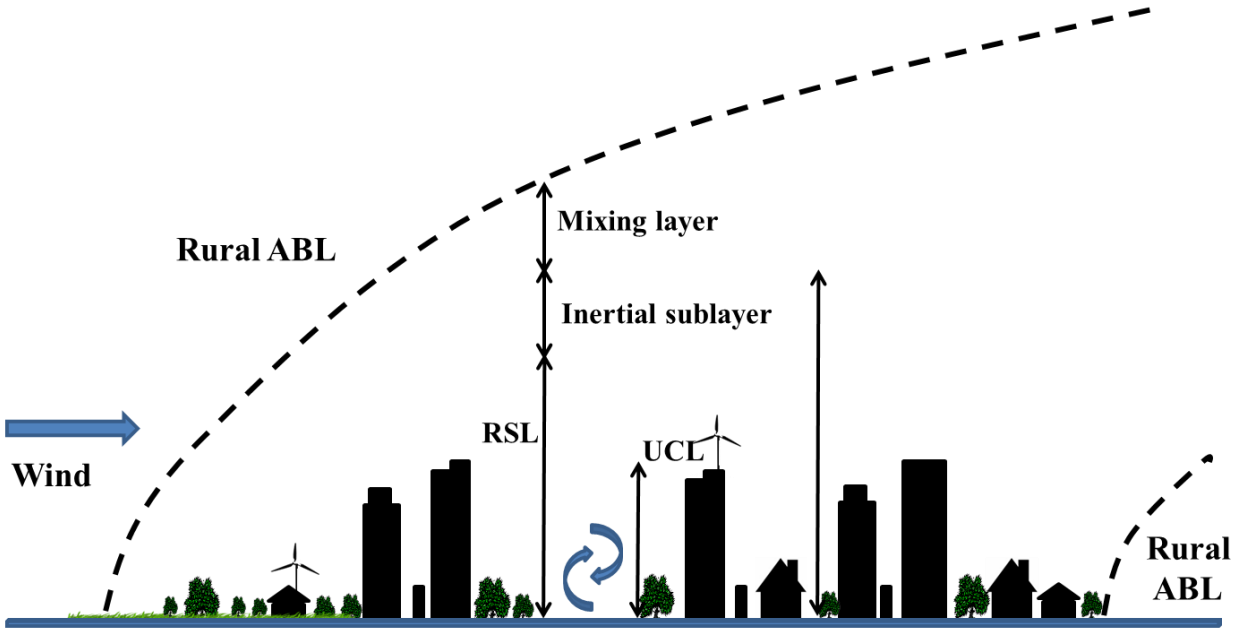

Figure 2. 4: Schematic diagram representing UBL and ABL, with indications of the RSL and UCL at the atmospheric boundary layer. (Adapted from [49])

Inertial Sub-layer

The state of the atmospheric boundary layer is governed by the lowest level of turbulent exchange, which is known as the surface layer. The upper part of the surface layer where the change of the turbulent flux with height is less than 10% is known as the inertial sub-layer (ISL). In this layer, the wind speed is considered to be horizontally homogenous while the Reynolds stress is assumed constant [52]. Various studies have suggested different approaches in estimating the minimum height of this layer (usually represented as the blending height). Refs [60, 61] proposed a method of estimating blending height within a built environment by solving iteratively a combination of two equations which individually accounted for growth of the boundary layer as a result of incoming wind direction and the total local surface forces over the terrain respectively. The methodology developed by the UK Met Office [62] suggested this height to be twice the maximum canopy height within a 1 km square grid whereas Millward-Hopkins *et al* [63] suggested this height to be twice the local mean building height within a 250 m square grid. This will be discussed in further detail in Chapter 3.

Roughness Sub-layer

For small scale wind energy studies, the roughness sub-layer is of great importance. Considering the fact that the small-scale wind applications are generally located within this boundary sub-layer, a clear investigation of the wind characteristics and principal elements governing the climate within this sub-layer is necessary. A roughness sub-layer (RSL) can be separated from the surface layer where individual effect of the roughness elements on the flow is eminent [46] in the presence of roughness elements on the ground. Some studies suggest that turbulence measurements should be carried out above the RSL since spectral theories and conventional flux-profile relationships are normally applied to the inertial sub-layer [37]. The turbulent flow above the RSL can be defined by a single dominant length scale, provided the ABL is adiabatic and is in equilibrium with the underlying roughness elements. The upper part of the atmospheric boundary layer (ABL), as shown in Figure 2.4, where the turbulent fluxes decrease upwards is called the mixing layer.

However, other studies have indicated the possibilities of extending the logarithmic profile from the ISL down through the RSL in a bid to describe the spatially averaged wind speed [37, 63] although the constant τ, which describes the effect of the wind stress on the ground, is not valid in this layer [64]. The choice of z_0 and d is of great importance [47, 64, 65], as results achieved through the extraction of the parameters from a fitted log law to the ISL can be of high significance in predicting the wind within the RSL. Application of this log law would only provide one with the predicted mean wind speed at a given height (i.e. height for the proposed turbine installation). This however, would be useful in predicting the turbulent properties at that height [37, 66, 67] and possibly its effect on the turbine's performance, which will be discussed later on. Due to the little knowledge about the flow in the RSL and the roughness canopy, the expression (i.e. Equation 2.31) is often applied outside its validity range which involves extrapolating it to levels as low as $z = d + z_0$ (the theoretical zero-velocity level) [68]. Although extrapolating down to the theoretical zero plane using Equation 2.31 is acceptable for studies on the flow above the urban structures where the details of the near-surface flow are less important, recent studies have however, suggested valid methods of using an exponential profile which accounted for the boundary layer growth as a result of the influence of incoming wind direction in predicting mean wind speed of flow within the roughness sub-layer [63, 69]. This will be discussed in further details in Chapter 3.

The Urban Canopy Layer

Due to channelling and recirculation effects in the urban canopy layer (UCL), the ability to define the average wind profile in this layer has, in the past, proved more problematic than that within the RSL. The depth of this layer may also depend on the wind speed, shrinking as stronger flow allows influences from above to penetrate [70]. Understanding the vertical wind profile in the UCL is less relevant to urban wind resource estimation given the fact that the wind speed within the UCL might be quite low for a viable turbine installation and the best location for roof mounted turbines would be the boundary between the UCL and the RSL. However, this study aims at proposing cost effective methods of estimating the energy available to roof mounted wind turbines within a built environment using high resolution wind measurements. It also demonstrates city-scale variation of wind speed, turbulence and the total wind energy at different mast heights over a few major cities in the UK, hence presenting a tool for viable wind resource assessment for micro wind projects within suburban/urban areas.

2.2 Wind Turbines

2.2.1 Introduction

A wind turbine can be defined as a machine which extracts the kinetic energy from the wind and converts it to useful power [8]. For over three thousand years, wind power has been harnessed for various purposes. This includes windmills for grinding of flour, pumping water, and also directional sailing in ships [71]. These historic designs (i.e. wind mills), constructed from cloth, wood and stone, were typically large, heavy and inefficient [72]. Presently, wind turbines are a source of generating electricity, heating and cooling using vapour compression heat pumps, pumping water, desalinating water by reverse osmosis, heating water by fluid turbulence, mixing and aerating water bodies. With global energy issues and questions caused by the different oil crises in the seventies, the dwindling popularity of nuclear plants in some countries, the increasing concern of climate scientists on the effect of greenhouse gases like carbon dioxide from coal plants and the changing economic and regulatory environment as well as technological innovations, the resurgence of wind energy was inevitable. Fifty years ago, no one would have predicted the recent extraordinary popularity of machines powered by wind energy.

With the first wind turbines for electricity generation arriving on scene at the beginning of the twentieth century, wind energy technology has developed step by step, and is now seen as one

of the most important sustainable energy resources. Wind technology has witnessed rapid development since the 300 kilo watts (kW) wind turbine emerged at the end of the eighties. Ten years later, a 1.5 megawatts (MW) wind turbine was unveiled [2]. 2 – 3 MW wind turbines were made commercially available prior to 2004 [73], and 5 – 6 MW wind turbines are currently present in the market. The 8 MW wind turbine model has been completed by Vestas, with the first turbine prototype estimated to power approximately 7,500 homes per year installed at the Danish National test centre for Large Wind Turbines in Østerild where it will be closely monitored for the purpose of validating its reliability and energy output [74], whereas Siemens plans to unveil a 10 MW wind turbine by the end of the decade.

Although wind energy has been utilized for over three thousand years now, it still remains a very complex technology required detailed understanding of technical subjects like aerodynamics, electrical engineering, mechanical engineering and structure dynamics.

2.2.1.1 Wind Turbine Classification

Several wind turbine designs have been devised throughout the times. Most of them comprise a rotor driven by lift and drag forces, which result from its interaction with the incoming wind. Based on rotor design, wind turbines are grouped into two (2) different categories:

1. Horizontal Axis Wind Turbines (HAWT)
2. Vertical Axis Wind Turbines (VAWT)

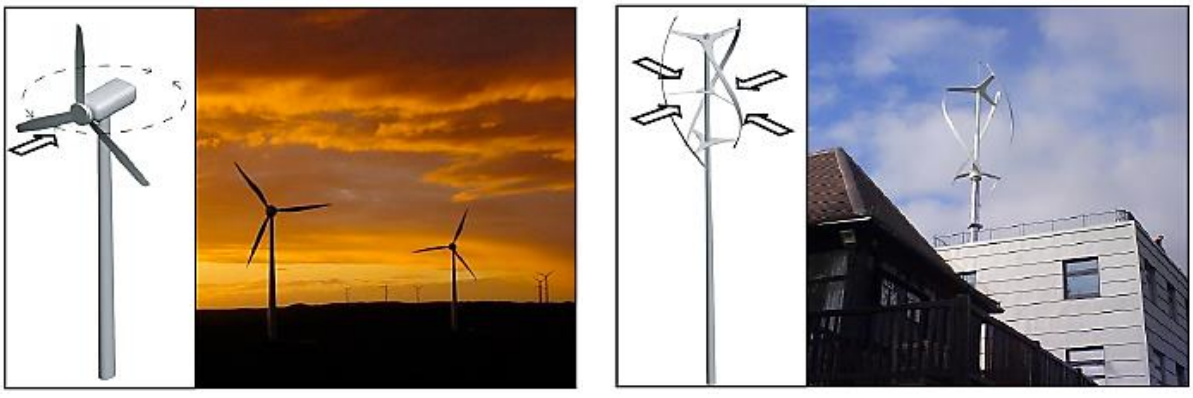

(a) Horizontal axis wind turbine (HAWT) **(b) Vertical axis wind turbine (VAWT)**

Figure 2. 5: Representation of a horizontal axis wind turbine and a vertical axis wind turbine design [75]

Horizontal Axis Wind Turbine (HAWT)

These are turbine designs which have their rotor rotation axis parallel to the wind flow and the ground. The main components visible are the blades, tower and nacelle (See Figure 2.5). The generator and the high-speed shaft are found in the nacelle compartment. The majority of grid-connected commercial wind turbines are built on this design concept. Most HAWTs built today, are usually two- or three-bladed, although we have turbines with less or more blades. A few of many interesting horizontal axis wind turbine concepts are provided in Figure 2.4.

Based on their rotor orientation, horizontal axis wind turbines can be classified into two types namely [76]:

1. Upwind HAWT
2. Downwind HAWT.

Upwind HAWTs have their rotor facing the wind and a complex steering system that steers the rotor to face the direction of the wind, thereby causing it to run smoothly. The basic advantage of this design is to avoid wind shade behind the turbine structure, decreases in power output and reduce the noise level [77]. The downwind HAWTs have their rotor located on the lee side of the turbine, with the rotor and nacelle having a suitable mechanism that allows the nacelle to follow the direction of the wind flow passively thereby generally resulting in fatigue, higher noise levels and reduced power output. This design is less popular than the former, with the latter not requiring the installation of any kind of steering mechanism to ensure the rotor faces the wind during operation (also known as the yaw mechanism) [76]. The future of economic development of horizontal wind turbines faces stiff walls, partly due to high stress loading on the blades and noise levels.

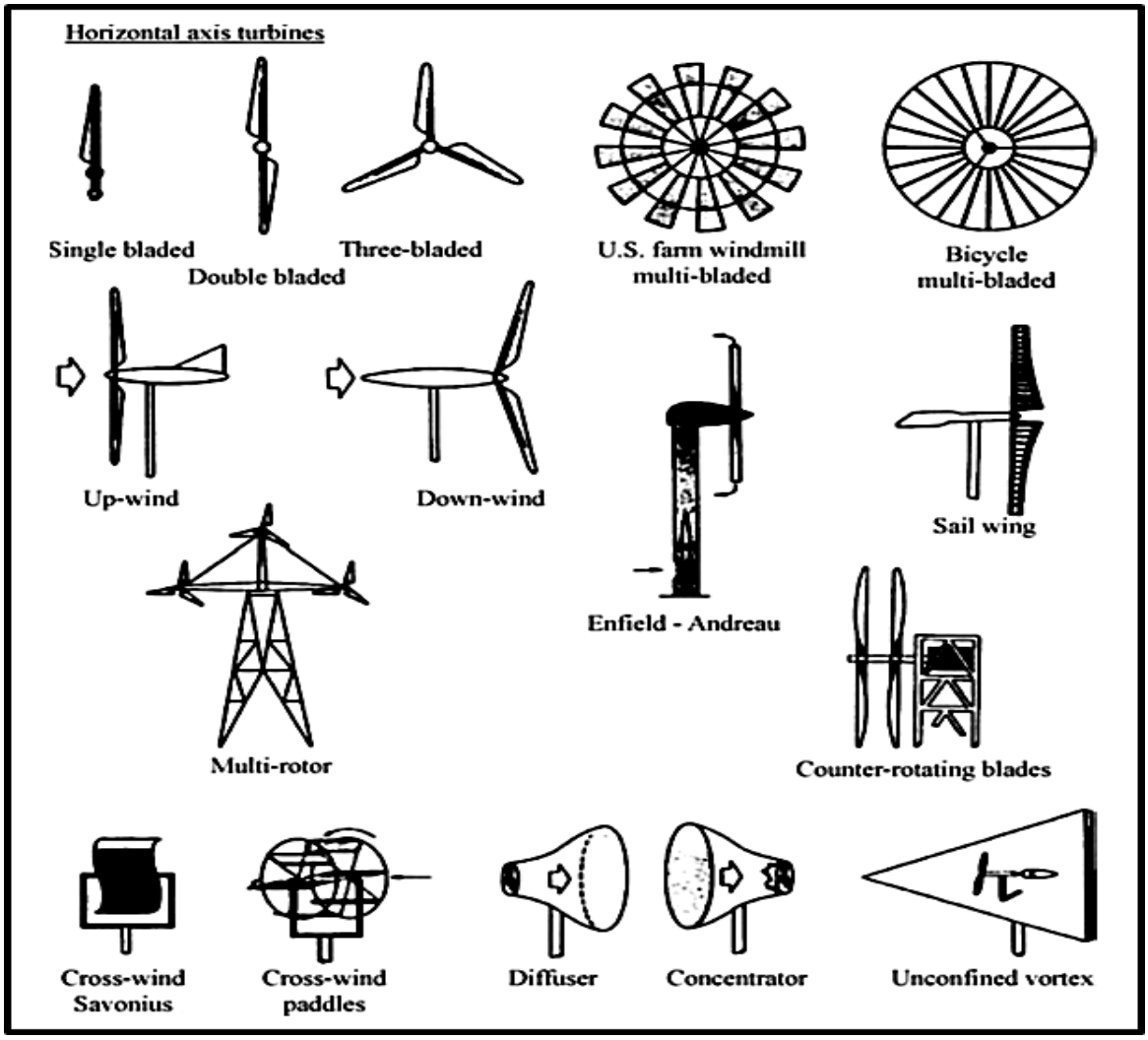

Figure 2. 6: Various concepts of horizontal axis wind turbines [78].

Vertical Axis Wind Turbine (VAWT)

These are turbine system designs which have their rotor rotation axis perpendicular to the wind flow and the ground (See Figure 2.5). The most important advantage of VAWTs is their simplicity in design, having a single moving part (rotor) where no yaw mechanisms are required (i.e. the ability to capture the wind from any direction) and with almost all components requiring maintenance located at the ground level thereby allowing easy and accessible maintenance services [79, 80]. There are three main types of VAWTs namely:

1. Darrieus vertical axis wind turbine design
2. Savonius vertical axis wind turbine design
3. H-Rotor vertical axis wind turbine design.

In the 1980's, there were two distinctive types of the vertical axis wind turbine namely: The Darrieus and the Savonius wind turbine designs, with the H-Rotor design developed later on. The first low-cost Darrieus rotor was developed by Sandia National Laboratories in 1974 [81] and in later years, new types of smaller-sized vertical axis wind turbines were being introduced particularly for applications within built environments where they would be considered more relevant due to the low wind speed and changing wind direction that characterises the urban wind. The Darrieus and H-Rotor VAWT designs operate in a similar principle like the common HAWT design, making use of the aerodynamic principles based on the lift force principle. The Savonius rotor operates using the principle of drag, such that it rotates at a slower speed or at a speed close to that of approaching wind speed thus producing a tip speed ratio that is less or equal to one and has a maximum power coefficient not more than 25% [82]. These forces (lift and drag) will be explained later in this section. Unlike the Darrieus and the H-Rotor VAWT designs, the Savonius VAWT design is robust and has a very low power factor, with the most successful VAWT design being the Darrieus-type [83].

These vertical axis wind turbines, as stated earlier, generally are relatively quieter, need no yaw mechanism, are simpler in design, cost competitive and do not suffer much from constant varying gravitational loads. They also have reduced risks associated with their slower rates of rotation and are commonly designed for medium- and small-scale power generation [84]. For this reason, they seem a potentially good choice of configuration for the urban environment and have become dominant in the commercial wind power market as well as widely favoured in recent building integration concepts, as compared to HAWTs. However, they suffer from issues such as narrower operating ranges (e.g. higher cut-in wind speeds than HAWTs), lower peak efficiencies and low starting torques. Many of these issues can be addressed through turbine controls [85, 86]. A few of many interesting vertical axis wind turbine concepts are provided in Figure 2.7. An example of VAWT and HAWT applications within a built environment can be seen in Figure 2.8.

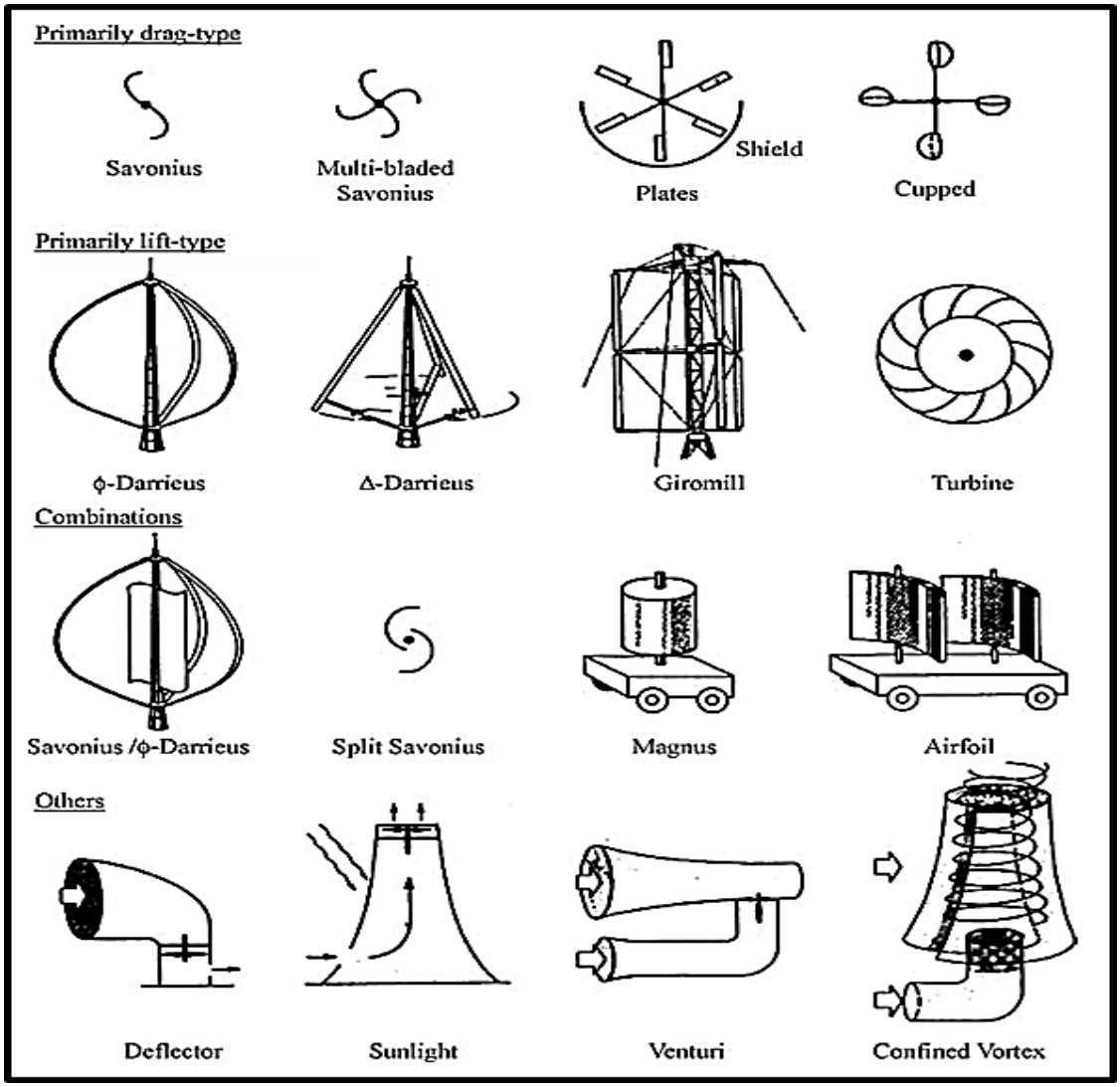

Figure 2. 7: Various concepts of vertical axis wind turbines [78]

Figure 2. 8: An example of VAWT and HAWT applications within a built environment in UK.

Wind turbines can also be classified based on their capacity. There are two types of wind turbines under this classification.

Large-scale Wind Turbines

Large scale wind turbines are mostly found in HAWT designs. They stand approximately over 50 m high and are usually of the design capacity of 100 kW and above. Most large-scale turbines are grid-connected and used in wind farms (both onshore and offshore) considering that they are economically viable in large wind energy projects for grid connection [84]. At present, we have wind farms housing wind turbine capacities of 2 MW, 3 MW, 5 MW and of recent 6 – 7 MW capacities.

Small-scale Wind Turbines

These were designed to encourage the public to buy into the wind micro-generation market by making wind turbines affordable as well as to provide for the increasing energy needs in suburban/urban areas. They stand approximately 10 – 50 m high, specially designed for micro-generation in built environments and remote areas. They can be connected to the grid or for domestic use (i.e. off-grid for purposes such as charging batteries, powering home appliances, etc.) and are found either as a HAWT or a VAWT design. It is fast becoming an increasingly promising way to provide electricity in developing countries. This category can be split further into three (3) categories [87], namely:

a. Micro Wind Turbines: They have the capacity range of 0 – 1.5 kW rated. They are designed to generate electricity at heights between 10 – 18 m above the ground.
b. Small-scale Wind Turbines: They have rated capacities of 1.5 – 15 kW. They are designed to generate electricity at heights between 12 – 25 m above the ground.
c. Small-Medium-scale Wind Turbines: They have rated capacities of 15 – 100 kW. They are designed to generate electricity at heights between 15 – 50 m above the ground.

Distinctively, small wind turbines may serve as roof-mounted turbines and can be used for various applications ranging from short period power supply for domestic tasks like battery charging through producing maximum power over long periods grid export. The smallest turbine in this category (i.e. micro wind turbines) can generate several hundreds of kilowatt hour (kWh) in one year which is approximately between 5 and 20% of the energy demand of

a standard UK home annually [87]. The small-medium-scale turbine at maximum height can generate enough power for a factory, farmstead, or 60 standard UK homes [88]. Analysis carried out later on within this study is focused on micro vertical axis wind turbine designs.

2.2.1.2 Wind Turbine Characteristics

Modern wind turbines use very little materials to capture energy in the wind resource of a chosen site [4]. Theoretically, the wind encounters the blades of the wind turbine, causing the turbine rotor to spin. The low-speed shaft connected to the rotor transfers the energy to the gearbox which steps up the speed and spins the high-speed shaft. The high-speed shaft causes the generator to spin, producing electricity [89]. This principle applies to HAWT and VAWT designs, with the former possessing a yaw system which is used to navigate the nacelle so that the rotor faces the wind. As the wind flows across the turbine rotor, the ring-shaped rotor frame rotates freely on guide wheels under the force induced by the impact of the wind on the airfoil blades. As the wind turbine extracts kinetic energy from the wind flow across the rotor disc, it slows down the wind flow thereby forming a stream tube-like boundary layer with circular cross sections separating it with the unaffected airflow that does not pass through the rotor disc. The approaching wind causes the building up of pressure which tends to absorb the decreasing kinetic energy from the static wind within the boundary. Because of the slowing down of the wind flowing through this boundary, the boundary layer must be expanded to accommodate this slowing down wind since the slow wind cannot be compressed [2].

As the wind flows through the streamtube boundary as illustrated in Figure 2.9, it witnesses a drop in the static pressure such that the pressure of the exiting wind (i.e. P_{R2}) is lower than the atmospheric pressure level. This resultant flow downstream of the wind turbine possesses a lower static pressure and velocity thereby creating a region called *wake* [2]. As the windflow moves further away downstream of the turbine, equilibrium is reached as its pressure returns to the atmospheric pressure (P_a) at the expense of kinetic energy. So evidently, there are no static pressure changes at the far upwind and far downwind regions, but a drop in kinetic energy at the downwind region.

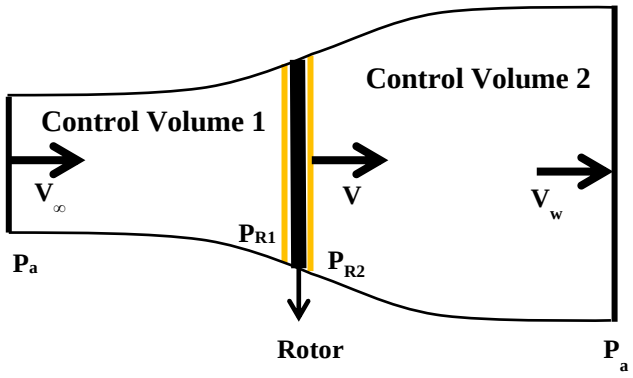

Figure 2. 9: Principle of Energy extraction from airflow in a wind turbine.

Wind Turbine Stages of Operation

The turbine operation fundamentally, as illustrated in Figure 2.10, is divided into three (3) operating regions:

1. Region 1: In this region the wind speed is not enough for the turbine start-up. Once the wind speed approaches the cut-in speed (cut-in speed varies with turbine design), the wind turbine starts up. Below the cut-in speed, the available energy in the wind is too low to compensate for operation costs and losses [83].
2. Region 2: In this region, the available power is lower than the turbine's rated power. This region usually follows a cubic parabola [83] and can be divided into two sub-regions. The first sub-region covers the period the turbine begins power generation while operating within a range of wind speeds and generating torques which are below 'rated'. The second sub-region encompasses turbine operation as wind speeds approach those that provide rated power. This is a very sensitive and important region of the operation and control as good turbine designs ensure that rated torque is reached before the rated generator speed.
3. Region 3: In this region, the available power exceeds the rated power and the wind speed has reached the rated speed. Thus, the turbine power is kept constant and as it exceeds the rated, it stalls. Stalling is a simple way to control power and preserve the turbine system. A turbine is in a state of stall when the blades are no longer moving, which could be due to an increase in the angle at which the relative wind strikes the blade. The basic reason for the stalling action in both large and small-scale wind turbines is to avoid exceeding the safe mechanical and electrical loading limits. Improvements in turbine blade and control designs have led to changes in the turbine's

operational behaviour in Region 3. High wind cut-out ideally occurs at wind speeds above 20 – 30 ms^{-1} for large wind turbines and 12 – 15 ms^{-1} for small wind turbines. Above this cut-out wind speed, the wind turbine system is shut down to avoid structural, mechanical and electrical overloads.

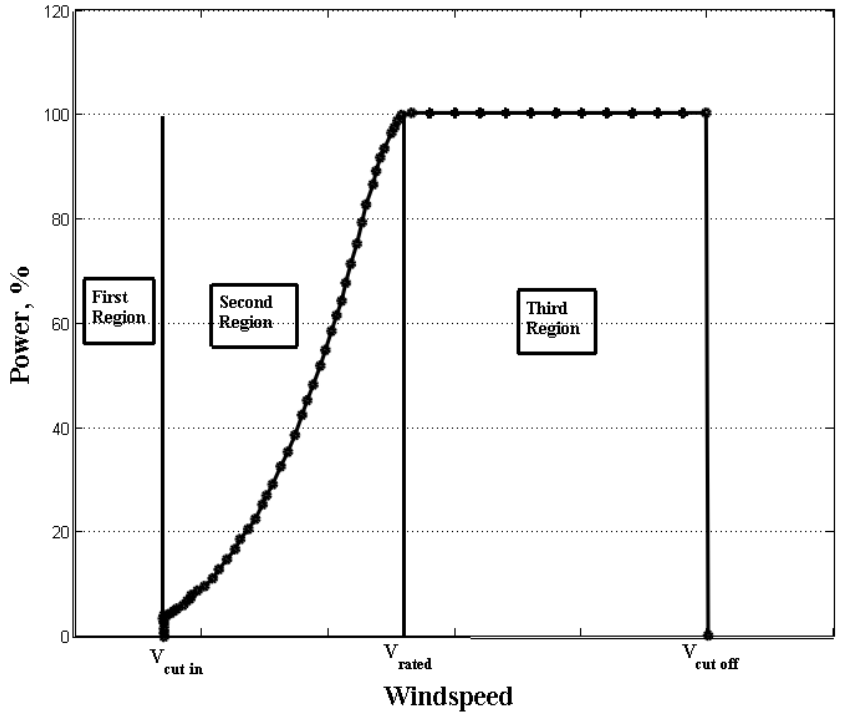

Figure 2. 10: An ideal power curve for a typical wind turbine.

There are no perfect wind turbines as they cannot fully capture the power available in the wind. Reasons for this can be said to be the energy losses at different components of the turbine during the conversion process, and also the wind still possesses some kinetic energy after passing the turbine for the flow to be continuous. Hence, the performance of a turbine design can be judged using a coefficient known as the turbine power coefficient (C_p). This is basically defined as the percentage of wind power the turbine can convert to mechanical power and is mathematically represented by:

$$C_p = \frac{P_T}{P_w} \qquad \text{Equation 2. 32}$$

where P_T is the power captured by the turbine, P_w is the power available in the wind for the size of turbine. C_p also varies with the tip-speed ratio (λ) (which is defined as the ratio of the rotor tip speed to free wind speed). This will be further discussed in Chapter 3.

2.2.2 Wind Turbine Aerodynamics

2.2.2.1 Fundamental Rotor Disc Theory

The energy extracted by a wind turbine model depends on the interaction between the rotor/blades and the wind. The manner of energy extraction and how much of this energy is actually extracted in a built environment depends upon the particular turbine design. The major reasons for the choice of VAWT over HAWT in this study, is to mitigate the effect of changes in wind direction and increased turbulence on the turbine operation. Most small-scale VAWTs, depending on the purpose of application, employ a rotor with a number of blades, of which there is no consensus as to the standard number of blades. As stated earilier, the nature of the force acting on the blades, vary with different VAWT models. Thus, a wind turbine system can be classified depending on the force which does the work on the blades of the turbine system (i.e. lift- or drag-type wind energy converter) [90]. This leads us to the question, what do we mean by the 'lift' and 'drag' forces and what is the physics behind these forces as it relates to the VAWT performance? Before discussing the lift and drag forces, a brief summary on airfoils and their terminologies, is necessary.

Airfoils and Their Basic Terminologies

Early wind turbine designs employed the use of airfoils developed by the National Advisory Committee for Aeronautics (which was also known to be NACA airfoils designs) in their blade designs. These NACA airfoil sections were developed using specific geometric shapes that generate mechanical forces under the relative motion of the airfoil and a surrounding fluid, and were previously designed with equations describing the aerodynamic properties of airfoil blade profile for aircraft wings. The length and width of a chosen blade are tantamount to the desired aerodynamic performance, the assumed airfoil properties and strength considerations and finally the maximum desired rotor power [91].

A simple diagram of an airfoil section is given in Figure 2.11 showing the leading and trailing edges of an airfoil section. A few important airfoil terminologies are briefly defined as follows:

a. Chord length: The straight line connecting both edges of an airfoil section is called the chord line. The airfoil chord length 'c' is defined as the measured distance from the leading to the trailing edge, along the chord.
b. Camber: This is the measured perpendicular distance from the mean camber line to the chord line.

c. Angle of attack: This represents as the angle between the relative wind velocity and the chord line.

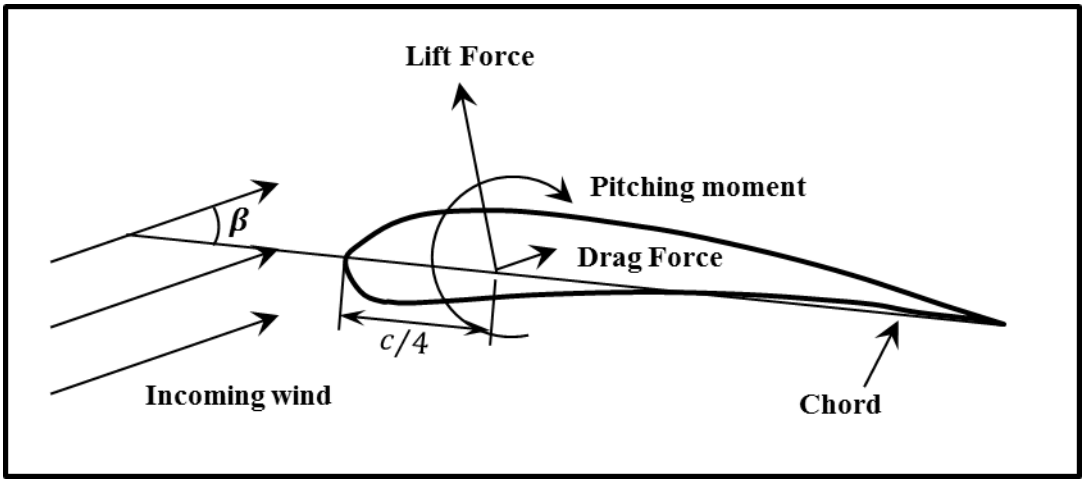

Figure 2. 11: Forces acting on a blade, also demonstrating chord and the angle of attack relative to the blade and the direction of the positive forces described by the direction of the arrows, c represents the blade chord length and β represents the pitch angle (Adapted from [91]).

The basic geometric parameters that affect a desired aerodynamic performance of an airfoil (blade) include the trailing edge angle, maximum blade thickness and the thickness distribution of the blade profile, mean camber line and the leading edge radius [91]. Many types of airfoils used in wind turbine blade designs have been developed [92, 93] with improvements of airfoil design for small-scale wind turbines mainly aimed at achieving airfoil sections with lesser weight, better strength and aerodynamic characteristics [94].

The Principle of Lift Force

Most modern wind turbines (HAWTs and VAWTs) operate on the principle of lift, with the majority of HAWTs designed on the same principle of lift employed in aircraft wings and propellers in the Aerospace and Aeronautic industry [91]. Basically, as the wind flows across the blade's rounded leading edge (See Figure 2.11), there is a pressure drop which results in a negative pressure gradient. Surface pressure increases when the wind flow decelerates as it approaches the blade's trailing edge, thereby resulting in a positive pressure gradient.

Considering the airfoil design and the angle of attack, if the wind velocity in the upper surface of the blade is higher than that at the lower surface, then there is a net force [91]. The blade's angle of attack is determined by the prevailing wind velocity and the velocity of the blade's motion [2]. So basically, lift force results from unequal pressures on the upper and lower surfaces of the blade and it is defined to be perpendicular to the direction of the prevailing wind flow (See Figure 2.11). This principle is employed by the Darrieus type, H-Rotor type VAWT and also in most modern wind turbines for generating electricity [90].

The Principle of Drag Force

Drag forces result from both the friction developed as the wind flows across the blade surface and the pressure difference across the blade section. The resultant drag component due to friction is as a function of the viscosity of the fluid (in this case, air) which transmits energy into the flow field, whereas the resultant drag component due to pressure is a function of the pressure distribution in the direction of the prevailing wind flow [2, 91]. Therefore, in summary, drag forces result from a combination of the viscous friction forces at the blade surfaces and the unequal pressure across the blade surfaces facing towards and away from the prevailing wind flow. It is defined to be parallel to the direction of the prevailing wind flow (See Figure 2.11). This principle is employed by the Savonius type VAWT which is used in applications like water pumping.

Over the centuries, many types of wind turbine designs have emerged, and some of the more distinguishable designs with their power coefficients as well as propulsion principle (i.e. lift or drag) are provided in Table 2.2.

Table 2.2: Historical and modern Wind Turbine designs (Adapted from [95]).

No.	Design	Orientation	Use	Principle of propulsion	C_{pmax}
1	Savonius Rotor	VAWT	Historic Persian windmill to modern day ventilation	Drag	16%
2	Cup	VAWT	Modern day cup anemometer	Drag	8%
3	American farm Windmill	HAWT	18th century to present day, farm use for grinding wheat, corn, etc., pumping water and generating electricity	Lift	31%
4	Dutch Windmill	HAWT	16th century, used for grinding wheat, corn, etc.	Lift	27%
5	Darrieus Rotor (egg beater)	VAWT	20th century, used for generating electricity	Lift	40%
6	Modern Wind Turbine	HAWT	20th century, used for generating electricity	Lift	43% (1-bladed) 47% (2-bladed) 50% (3-bladed)

2.2.2.2 Turbine Aerodynamics

The turbine system aerodynamics describes the forces developed on a wind turbine while operating within a given wind resource. Based on a linear momentum theory, the simple turbine aerodynamic model employed within this study was developed using two major approaches [83] namely:

a. The Actuator disc theory which describes the energy extraction process and also provides the theoretical upper bound to the turbine system's conversion efficiency.
b. The Blade Element Momentum (BEM) theory provides details of the forces acting on the blade element as a result of incoming flow.

A. Actuator Disc Model

This approach regards the turbine system as an actuator disc (i.e. a generic device that extracts kinetic energy from the wind) immersed in an airflow, which is assumed to be incompressible as shown in Figure 2.12. This simply analyses the actuator disc theory as a controlled volume in which the boundaries are the surface walls of the streamtube (outlined in Figure 2.12) and the two cross sections (represented at the free-stream and wake regions). For this analysis, three points (i.e. the free-stream region, the blade region and the wake region) will be considered.

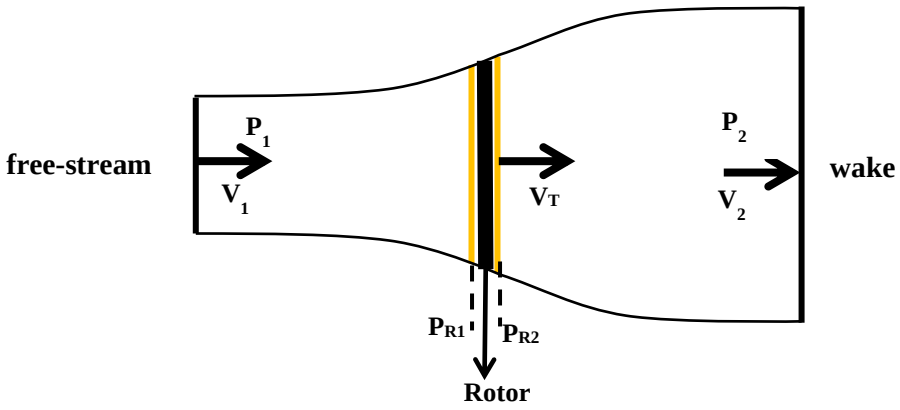

Figure 2. 12: 1D Actuator Disc.

Hence, the mass flow rate remains the same throughout the stream tube. Thus, the continuity equation along the stream tube can be given as:

$$\rho A V_1 = \rho A V_T = \rho A V_2 \qquad \text{Equation 2. 33}$$

For steady state flow the mass flow rate across the rotor can be calculated using Equation 2.34.

$$\dot{m} = \rho A V_T \qquad \text{Equation 2. 34}$$

Given that the mass flow rate must be the same across the stream tube, the upstream cross-sectional area of the streamtube enclosing the disc becomes smaller than the downstream cross-sectional area. Hence, the turbine experiences a thrust equal to the change in the wind's linear momentum. This is expressed by applying conservation of linear momentum on both sides of the actuator disc rotor (as expressed in Equation 2.35).

$$F_T = \dot{m}(V_1 - V_2) \qquad \text{Equation 2. 35}$$

where V_1 and V_2 are the wind velocities upstream and downstream and $\dot{m}$ is the mass flow rate of air across the turbine rotor.

Since the flow is assumed to be frictionless and there is no work or energy transfer done, Bernoulli equation can be applied on both sides of the rotor. Thus, applying energy conservation using Bernoulli equation on both sides of the rotor will result in Equations 2.36 and 2.37.

$$P_{R2} + \tfrac{1}{2}\rho A V_T^2 = P_2 + \tfrac{1}{2}\rho A V_2^2 \qquad \text{Equation 2. 36}$$

$$P_1 + \tfrac{1}{2}\rho A V_1^2 = P_{R1} + \tfrac{1}{2}\rho A V_T^2 \qquad \text{Equation 2. 37}$$

where P_{R1} and P_{R2} are the pressures at both sides of the actuator disc as shown in Figure 2.12.

Combining Equations 2.36 and 2.37 gives the pressure decrease as:

$$\Delta P = \tfrac{1}{2}\rho(V_1^2 - V_2^2) \qquad \text{Equation 2. 38}$$

The thrust acting on the actuator disc rotor can be calculated as the sum of the forces on each side of the rotor.

$$F_T = A\Delta P \qquad \text{Equation 2. 39}$$

where

$$\Delta P = P_{R1} - P_{R2} \qquad \text{Equation 2. 40}$$

Thus, substituting Equation 2.38 into Equation 2.39, we have

$$F_T = ½\rho A(V_1^2 - V_2^2) \qquad \text{Equation 2. 41}$$

The rate at which the force (F_T) does work is expressed as $F_T V_T$, where V_T is the wind velocity across the wind turbine (which is represented as an actuator disc) and can be expressed by combining Equations 2.34, 2.35 and 2.41. Thus, the wind velocity across the rotor is given as:

$$V_T = \frac{V_1 + V_2}{2} \qquad \text{Equation 2. 42}$$

We could however, express the wind velocity downstream relative to the wind velocity upstream, giving the fractional decrease in wind speed across the wind turbine in terms of a reference factor known as the induction factor 'a'. This is expressed as:

$$a = \frac{V_1 - V_T}{V_1} = \frac{V_1 - V_2}{2V_1} \qquad \text{Equation 2. 43}$$

Hence from Equation 2.43, the wind velocity at the actuator disc V_T and the wind velocity downstream V_2 can be expressed as:

$$V_T = (1 - a)V_1 \qquad \text{Equation 2. 44}$$

$$V_2 = (1 - 2a)V_1 \qquad \text{Equation 2. 45}$$

The momentum theory applies up to $a = 0.5$, with V_2 becoming negative at higher values of a, which is obviously impossible [2, 83]. Therefore, the force of the actuator disc on flow as a result of the pressure drop introduced by the actuator disc (i.e. thrust force) can be expressed as [83]:

$$F_T = (V_1 - V_2)\rho A V_1(1 - a) \qquad \text{Equation 2. 46}$$

where A is the turbine rotor swept area and ρ is the air density.

Combining Equations 2.44, 2.45 and 2.46, the thrust force can be re-written as:

$$F_T = 2\rho A V_1^2 a(1 - a) \qquad \text{Equation 2. 47}$$

Thus, the thrust coefficient can also be obtained using:

$$C_T = \frac{2\rho A V_1^2 a(1-a)}{½\rho A V_1^2} = 4a(1-a) \qquad \text{Equation 2. 48}$$

The power extracted by the wind turbine is now given as:

$$P_T = F_T V_T = 2\rho A V_1^3 a(1-a)^2 \qquad \text{Equation 2. 49}$$

Since in this context, $V_\infty = V_1$, power available in the wind (P_w) could be re-written to be:

$$P_w = ½\rho A V_1^3 \qquad \text{Equation 2. 50}$$

Substituting Equations 2.49 and 2.50 into Equation 2.32**,** the power coefficient can then be expressed as:

$$C_p = \frac{2\rho A V_1^3 a(1-a)^2}{½\rho A V_1^3} = 4a(1-a)^2 \qquad \text{Equation 2. 51}$$

Betz Limit

In 1962, a German physicist called Albert Betz established a standard limit for the maximum theoretical power coefficient for an ideal wind turbine [9]. This he achieved by applying the axial momentum theory in his analysis while considering an expanding stream tube as shown Figure 2.10. Betz, however, pointed out that the maximum value of the expression in Equation 2.51 occurs when $a = 1/3$. Substituting the maximum value of 'a' into Equation 2.51, C_p = 16/27 = 0.593. He, therefore, proposed that the theoretical maximum aerodynamic efficiency for a wind turbine is in the value of 59.3% approximately, which is called the Betz limit. In practice, considering factors like electrical power losses due to transmission (η_e), mechanical losses (η_m), etc., the power coefficient of a commercial wind turbine is much lower than the Betz limit. This is as a result of taking into account, different losses while calculating the actual power generated, as expressed in Equation 2.52.

$$P_T = \eta_m \eta_e C_p P_w \qquad \text{Equation 2. 52}$$

Tip-Speed Ratio (λ)

As briefly explained earlier, tip-speed ratio is mathematically represented as:

$$\lambda = \frac{\omega \mathrm{R}}{V_{\infty}}$$ Equation 2. 53

where ω is the rotor rotational speed and R is the rotor radius.

A slow rotating rotor will result in unperturbed flow through the gaps of the wind turbine blade and consequently low power extraction, while a rapidly rotating rotor cases the turbine blades to act as a solid wall to the wind flow which also leads to low power extraction. Considering all these, it is therefore important in the design of the wind turbine to match the angular velocity of the rotor to the wind speed in order to obtain optimal rotor efficiency or tip-speed ratio in order to extract as much power as possible from the wind stream [96]. Due to the aerodynamic properties of the wind turbine, the power coefficient (C_p) varies with both wind speed and the rotational speed of the turbine blades. This is represented by the C_p- λ relationship which is a strong factor in determining the performance of a wind turbine (See Figure 2.13).

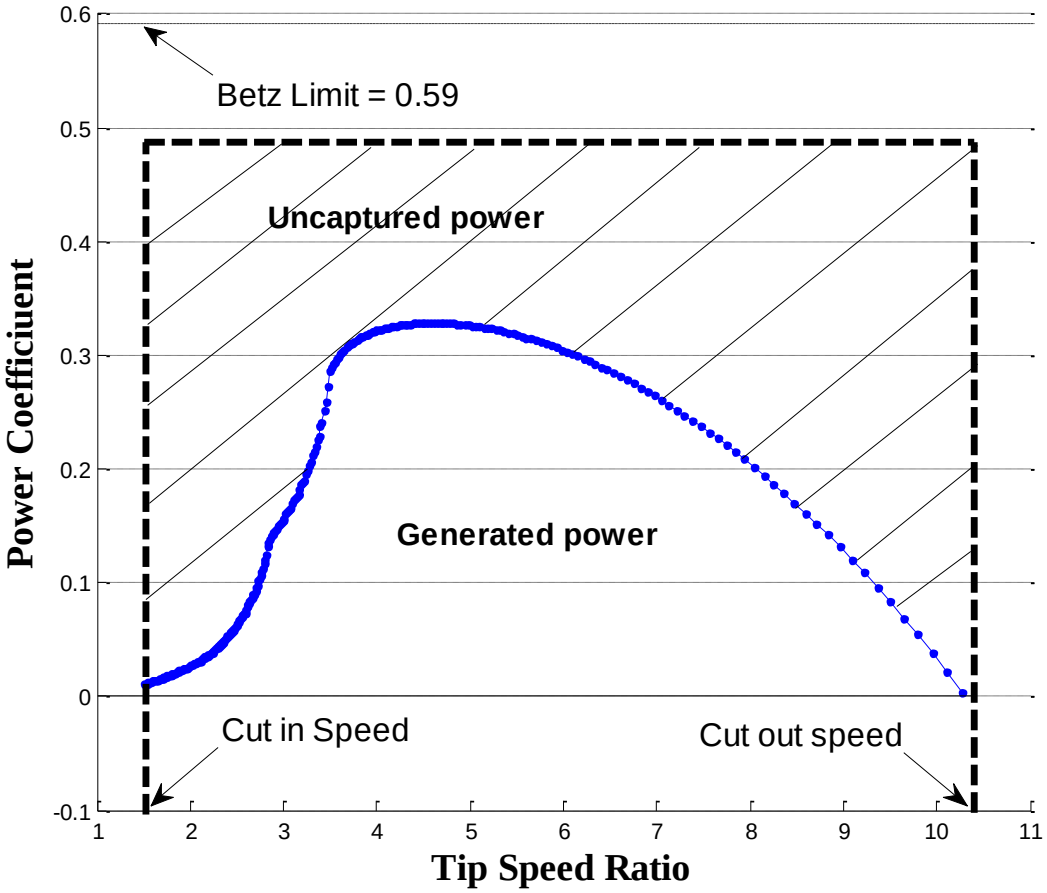

Figure 2. 13: A simple plot of C_p- λ relationship for a small wind system (Adapted from [96]).

B. Blade Element Momentum (BEM) Theory

The blade element momentum (BEM) theory is popularly used in turbine blade design and assessment. The BEM theory is useful to derive the expressions for the torque, power and thrust force experienced by the turbine blade element while under operation. In order to achieve this, detailed analysis of aerodynamic forces acting on the blade element is carried out.

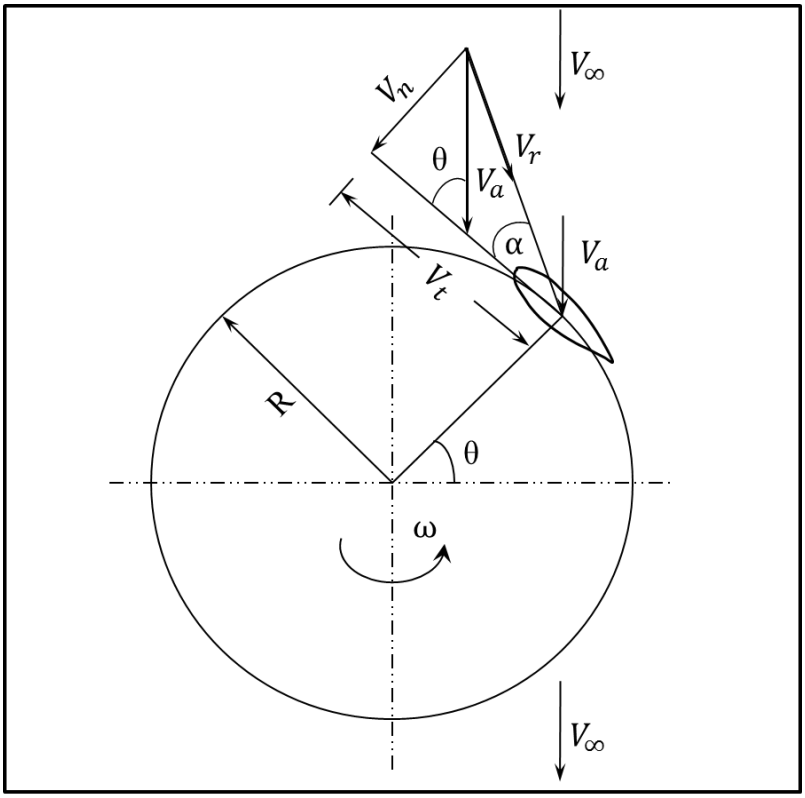

Figure 2. 14: Schematic diagram illustrating the flow velocities of a straight-bladed Darrieus-type VAWT (Adapted from [90]).

From Figure 2.14, the tangential velocity (V_t) and the normal velocity (V_n) components are obtained from the expressions below [90]:

$$V_t = R\omega + V_a \cos\theta \qquad \text{Equation 2. 54}$$

$$V_n = V_a \sin\theta \qquad \text{Equation 2. 55}$$

where V_a represents the induced flow velocity and can be obtained by substituting V_T as V_a in Equation 2.43, ω is the rotational speed, R is the radius of the turbine and θ is the azimuth angle. The angle of attack (α) is then derived from the expression:

$$\alpha = \tan^{-1}\left(\frac{V_n}{V_t}\right) \qquad \text{Equation 2. 56}$$

From Equations 2.54 – 2.56, the angle of attack can be expressed in terms of the axial induction factor of the system which is given as:

$$\alpha = tan^{-1}\left(\frac{(1-a)sin\theta}{(1-a)cos\theta + \lambda}\right)$$ Equation 2. 57

where λ is the tip speed ratio as defined in Equation 2.53.

The turbine blade is assumed to move in the airflow at a relative velocity (V_r), which is a composition of the upstream wind speed (V_∞) and the blade velocity ($U_b = \omega r$) and can be expressed as:

$$V_r = \sqrt{{V_t}^2 + {V_n}^2}$$ Equation 2. 58

Thus, substituting Equation 2.54 and 2.55 into Equation 2.58, the relative velocity can be expressed as:

$$V_r = \sqrt{(V_a sin\theta)^2 + (V_a cos\theta + U_b)^2}$$ Equation 2. 59

Substituting V_T as V_a in Equation 2.59 and normalizing using upstream velocity, Equation 2.59 can be re-written as:

$$\frac{V_r}{V_\infty} = \sqrt{((1-a)sin\theta)^2 + ((1-a)cos\theta + \lambda)^2}$$ Equation 2. 60

The normal force coefficient (C_n) can be derived by the difference between the normal component of lift and drag forces while the tangential force coefficient (C_t) is the difference between the tangential components of the lift and drag. The expressions can be written as:

$$C_n = C_l cos\alpha + C_d sin\alpha$$ Equation 2. 61

$$C_t = C_l sin\alpha - C_d cos\alpha$$ Equation 2. 62

where C_l and C_d are the blade lift and drag coefficients. The net normal and tangential forces (as illustrated in Figure 2.15) are obtained from the expressions:

$$F_n = \frac{1}{2}\,\rho C_n c\, H\, {V_r}^2$$ Equation 2. 63

$$F_t = \frac{1}{2}\,\rho C_t c\, H\, {V_r}^2$$ Equation 2. 64

where c is the chord length and H is the height of the turbine blade.

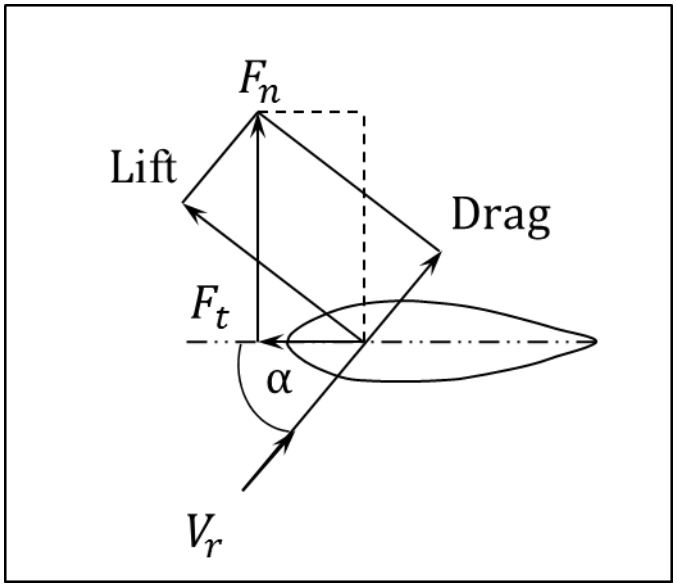

Figure 2. 15: Force diagram acting on the blade (Adapted from [79]).

The tangential force as a function of the azimuth angle (θ) is given as:

$$F_{ta} = \frac{1}{2\pi}\int_0^{2\pi} F_t\,(\theta)d\theta = \frac{0.5\rho cH}{2\pi}\int_0^{2\pi} C_t\,V_r^2 d\theta \qquad \text{Equation 2. 65}$$

The instantaneous torque T_b generated by the blade is given as:

$$T_b = RF_{ta} \qquad \text{Equation 2. 66}$$

The total power P_b is obtained from the expression:

$$P_b = \omega T_b \qquad \text{Equation 2. 67}$$

The stream wise instantaneous drag force (F_d), as a result of change in momentum is given as:

$$F_d = \rho A\,V_a\,(V_\infty\ -\ V_w) \qquad \text{Equation 2. 68}$$

and the rotor drag coefficient (C_{dd}) given as:

$$C_{dd} = \frac{\mathrm{F}_d}{\frac{1}{2}\rho A {V_a}^2} \qquad \text{Equation 2. 69}$$

Substituting Equation 2.68 into Equation 2.69, we have:

$$C_{dd} = 4\left(\frac{\mathrm{V}_\infty - V_a}{V_a}\right) \qquad \text{Equation 2. 70}$$

The interference factor (a_i) can be expressed in terms of the rotor drag coefficient and is given as:

$$a_i = \frac{V_a}{\mathrm{V}_\infty} = \left(\frac{1}{1 + C_{dd}/4}\right) \qquad \text{Equation 2. 71}$$

One method of calculating the overall torque and power of the VAWT with a given number of blades (*N*) from Equations 2.66 and 2.67 is by introducing the velocity ratio expression (or interference factor) obtained in Equation 2.71 into the equations of torque and power above. In summary, an overview of the basic theories/approaches in developing turbine aerodynamic models has been presented. The relevance of these theories will be highlighted in the development of the VAWT stream tube model employed within the study later on (See Chapter 3).

2.2.3 Wind Turbine Control Systems

2.2.3.1 Introduction

Control has risen to be an important part of turbine design due to the increase in turbine capacity and size as well as the emergence of studies on the complex nature of the wind resource in recent years. Also, complexity in design generated by the coupling of different structural modes has required sophisticated control methods to deal with its effects. Fundamentally, the objectives of the wind turbine control system are to improve power production, ensure that the turbine operates within the desired operating conditions (i.e. close to the C_{pmax}), and at the same time reduce load on the system thereby ensuring safe operations with a minimal number of system failures [91]. The choice of control components and configuration of small-scale HAWTs or VAWTs depends greatly on the specific design and configuration of the turbine [97]. For example, the choice of upwind or downwind configuration/design in small scale HAWTs affects the choice of yaw controller as well as the turbine dynamics and structural design.

In designing turbine control, it is usually assumed that wind speed flow is uniform across the rotor. This leads to complexities in the design process due to the wind speed deviations caused by the behaviour of instantaneous wind fields which vary in space and time across the rotor. Turbulent wind causes the wind input to vary across the blade section and also different wind speeds to be observed across each blade. This has led to the continuous improvements in wind

turbine controls, be they applied to the blade pitch, generator, etc. For example, considering HAWT misalignments resulting from turbulence, studies suggest a 10% decrease in power with a 20° yaw misalignment [98], which makes it difficult for the turbine to operate within its optimal operating condition (i.e. maximum C_p) as was discussed in Section 2.2.1. However, the increased efficiency and lower loads of wind turbines creates enough benefits to make power electronics cost effective [99].

As stated by Bellarmine and Urquhart [100], although VAWT and HAWT designs are efficient, both are presently being rigorously tested and improved. Considering the aerodynamic characteristics (as discussed in Section 2.2.2) and the designed operating conditions for any given wind turbine model, the aim of the control system is to improve or maintain aerodynamic performance of the wind turbine within the desired operating conditions while reducing load (fatigue) in the system. Although the control system for different types of turbines (large- and small-scale) vary, we can agree that they all have one purpose: the conversion of wind energy to electrical energy [91]. Since small-scale wind turbines have higher rotational speeds and are more apt to be influenced by local turbulence, as compared to large-scale wind turbines, choice of control strategy of the small-scale wind turbines is a very important element in the system's design [101]. Fundamentally, the wind turbine control system might attempt to maximize the aerodynamic torque/power at wind speeds below rated, and also attempt to limit its aerodynamic torque at wind speeds above rated [91]. A simplified wind turbine system model (as shown in Figure 2.14) is useful for understanding the basic concept of control systems in modern wind turbines.

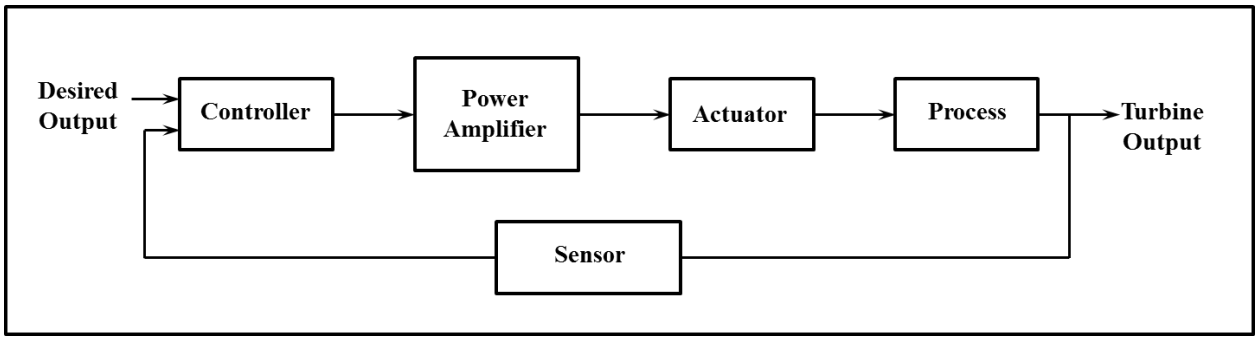

Figure 2. 16: A schematic diagram showing basic control system components (Adapted from [91]).

A basic example provided in Refs [91, 102], classified the control systems of a wind turbine into three levels namely:

a) Supervisory control which monitors the well-being of the turbine, and determines the start and stop of the turbine by measuring the wind speed flowing across the rotor. Wind turbines have anemometers installed on them for this purpose.
b) Operational control determines how the turbine achieves its design objectives at Region 2 and 3. This control loop houses the incoming wind sensors and actuators while treating the subsystem controls as black boxes.
c) The Subsystem/dynamic controller causes the generator, pitch drive, yaw drive (as in the case of HAWTs), power electronics and other actuators to perform as designed.

In the past, control modelling techniques have neglected the incorporation of the dynamic and stochastic aspects of the wind and the turbine in their consideration. This has led to various researchers investigating different advanced control methods in order to proffer solutions to the effect of damage loads on the roots of the turbine structure and blades. These different approaches are distinguished by plant uncertainties, like the variation observed in a turbulent profile as the rotor turns to position the blades, which spatially varies, even at constant wind conditions, with the rotor disk [91, 102].

2.2.3.2 Basic Control Design Strategies

There are two popular control strategies within the wind engineering industry [2, 91, 103]. These are:

a) Fixed-Speed Wind turbine
b) Variable-Speed Wind Turbine

Fixed-Speed Wind Turbine

This type of design is sometimes called the 'Danish Concept'. This is because it was developed by the Danish and is widely used in Danish wind turbines. Fixed-speed wind turbines operate sub-optimally except under wind speeds corresponding to their optimal tip speed ratio [2]. This means that the peak efficiency of the turbine rotors is developed at one rotational speed. This fixed-speed wind turbine is usually found in large-scale wind turbines, is combined with stall control and has an asynchronous squirrel caged induction generator (SCIG) connected to a transformer which is directly connected to the grid. Fixed-speed wind turbines due to their nature, always draw reactive power from the grid they are connected to [73, 104, 105], and at

most times, the amount of the reactive power drawn from the grid varies with corresponding grid voltage fluctuations. This is why a capacitor is incorporated into their design so as to compensate for reactive power (See Figure 2.17). A smoother grid connection can, however, be achieved with the fixed speed wind turbine concept by incorporating a soft-starter [73].

One important characteristic of a fixed-speed wind turbine system is its inability to modify the torque characteristics thus leading to an overall poor performance with the conversion efficiency far from optimal. In addition to low conversion efficiency, fixed speed turbines suffer from other shortcomings such as poor regulation properties (due to lack of flexibility of the operation mode) and poor control action to inject damping to the drive-train subsystem thus resulting in mechanical stresses that reduce the lifetime of the turbine system [83]. However, since no extra hardware or control designs/features are added to implement this control strategy, fixed speed wind turbines are very simple and low-cost.

Variable-Speed Wind Turbine

This type of turbine control concept can be found in both large- and small-scale turbine designs. It has become very popular in commercial wind turbines, particularly for operations in environments with low wind speeds. One very important feature of the variable-speed wind turbine is its capability to accelerate or decelerate the rotational speed of the wind turbine according to changes in the wind speed. This is achieved using suitable power electronic equipment, thus ensuring that the turbine system operates in its highest level of aerodynamic efficiency under fluctuating wind flow [106]. Hence, the power quality impact of the variable-speed configuration can be enhanced compared to the fixed-speed turbine.

Variable-speed turbines are becoming more and more common in commercial wind turbines and can also be found in three (3) different types (as shown in Figure 2.17). These include:

1. Variable-Speed Wind Turbine system with Variable Rotor Resistance: This configuration is known as Optslip design and denotes a limited variable-speed controlled wind turbine design with variable generator rotor resistance and pitch control. It has been made popular by the Danish wind turbine manufacturer Vestas Wind Systems since the mid-1990s. It uses a wound rotor induction generator (WRIG) and is directly connected to the grid. The slip and the power output in this type of turbine design are controlled by varying the rotor resistance, as the optical coupling removes the need for slip-rings [73]. The size of the variable rotor resistance typically within 0 – 10% above synchronous speed, determines the dynamic speed control

range. Reactive power compensation and a soft-starter are needed for this design, as compared to fixed-speed wind turbine designs.

2. Variable-Speed Wind Turbine system with Full-scale Frequency Converter: This is a fully variable speed, pitch controlled wind turbine design with a full-scale frequency converter connecting the system to the grid. The full-scale power converter performs smooth grid connection over the entire speed range as well as performing reactive power compensation [73]. The generator can be excited either by a permanent magnet excited type or electrically. This design has a full 0 – 100% control of the synchronous speed range and supports reactive power compensation and smooth grid connection [103]. Due to the passage of the generated power through a power converter, it has a higher power loss. It is also very expensive in cost.

3. Variable-Speed Wind Turbine system with Partial-scale Frequency Converter: This design uses a double-fed induction generator (DFIG) and is actually similar to a variable-speed controlled wind turbine design with a WRIG, a pitch control and a partial frequency converter on the rotor circuit [103]. Compared to the previous turbine design, this design supports a wider range of dynamic speed control (within the range ± 30% of the nominal speed [105]), depending on the size of the frequency of the rotor and also its speed. This design proves economical as the partial-scale power converter is basically 25 – 30% of the full-scale converter [105], although requires the use of slip-rings which is a constraint. However, compared to variable speed design with full-scale power converter, it has lower power loss in the power electronics [73].

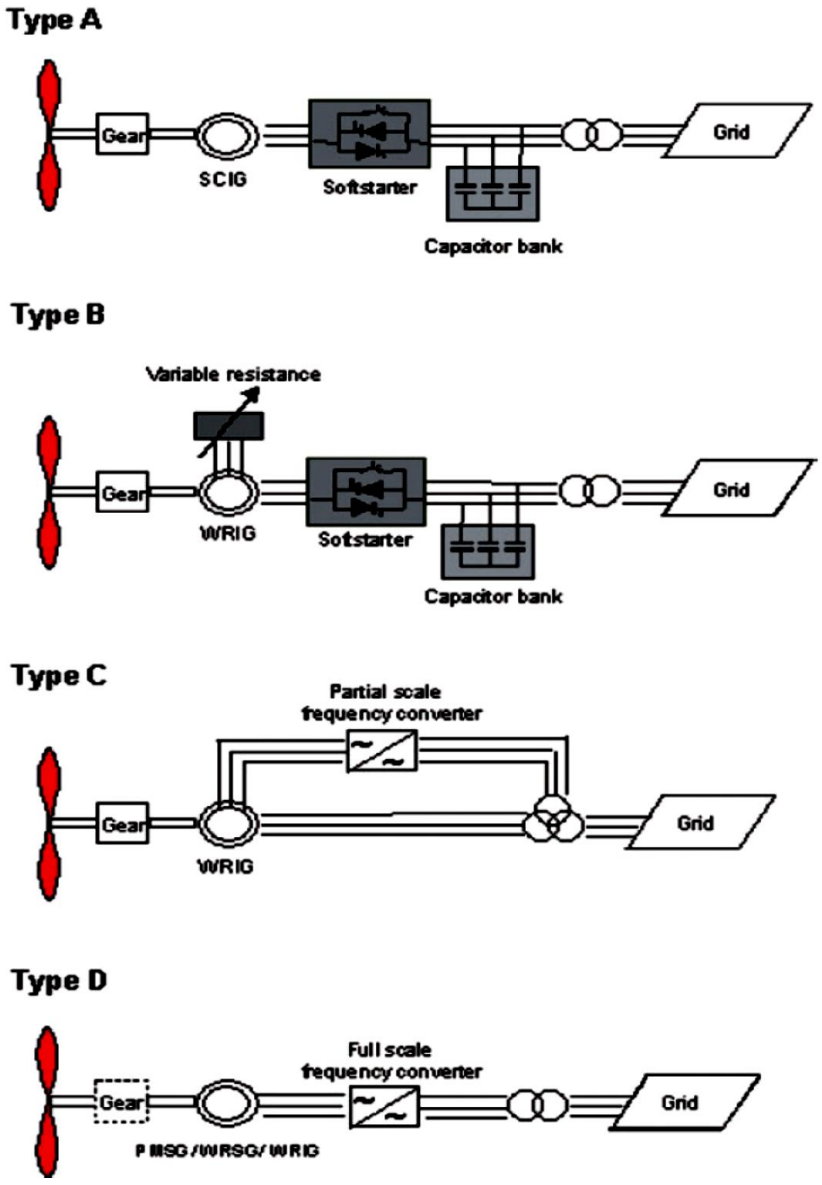

Figure 2. 17: Different wind turbine system designs based on control system configuration; Type A: Fixed Speed Wind Turbine; Type B: Variable Speed Wind Turbine with Variable Rotor Resistance; Type C: Variable Speed Wind Turbine design with Partial-scale Frequency converter; Type D: Variable Speed Wind Turbine design with Full-scale Frequency converter [103].

Wind turbines may be either fixed- or variable-pitch, which means that the turbine blades may or may not rotate along their longitudinal axes [91]. Fixed-pitch configurations are simple and low cost and are also commercially available for domestic and other applications [85]. Although less expensive, inability to control loads and aerodynamic torque in fixed-pitch turbines have made them less popular and thus, they are becoming obsolete. Under the

variable-pitched design, there are turbines that can rotate all parts of the blade along the pitch axis while we have other designs that can rotate just part of their blades along the pitch axis. Variable-pitch turbines tend to limit power by pitching to full feather or stall as the turbine operation enters the aerodynamic stall regime above the rated wind speed [102]. In the past, VAWT manufacturers employed the fixed-pitch concept in their traditional VAWT designs. Modern VAWTs are incorporating the variable-pitch concept into its system's design so as to optimize power production at minimal system failures. Previous studies have shown that fixed-pitch configurations provide inadequate starting torque [85], whereas variable-pitch configuration has the potential to overcome starting torque problem but it is overly complex, thus rendering it less practical for small-scale applications [79].

2.2.3.3 Past and Present Control Strategies

Past Control Strategies

Basically, classic control methods for common wind turbines (HAWTs or VAWTs) have two single-input single-output loops (SISO) for the pitch and generator controls (one control being used in a situation where the pitch and torque commands are identical as represented in Figure 2.18) [107].

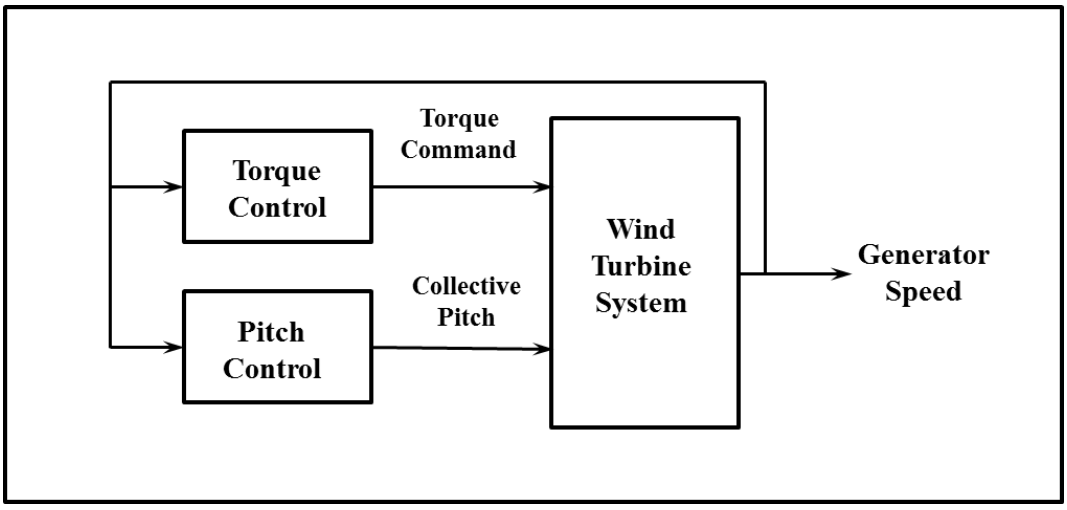

Figure 2. 18: Schematic diagram of a traditional turbine control based on generator speed feedback alone, with pitch and torque controllers treated as separate SISO loops [107].

As the turbine progresses across the various operating regions as discussed in Section 2.2.1, this classic type of control model captures changes at different operating points [107]. These changes are described as follows:

Region 1: The control objectives here are to

1. Pitch at the normal Region 1 angle that will generate minimum aerodynamic torque
2. When the speed is large enough, pitch at the normal Region 2 angle in order to produce torque and accelerate the rotor.

Region 2: The control objectives for this region are

1. To command torque so that the rotor rotational speed tracks the wind speed that gives the optimal tip-speed ratio λ*, thereby tracking the C_{pmax} (as described earlier).
2. To command torque such that rated torque is reached before rated generator speed. In this transition region, the torque command is commonly computed as a function of the generator speed.

Region 3: At this region, the control objective is to keep the generator torque constant and to regulate the turbine speed at the rated value which simultaneously limits the aerodynamic power. In the past, VAWT models had blades that could easily fold in high wind speeds thereby avoiding speeding of the turbine in this operating region [84].

Present Control Designs

In present control designs employed by HAWTs and VAWTs, actions like the control of speed are being achieved by adjusting individual blade pitch angles [107]. Hence, therefore, this suggests that a single multiple-input multiple-output (MIMO) controller (as shown in Figure 2.19) might be adequate when the turbine is operating at rated power.

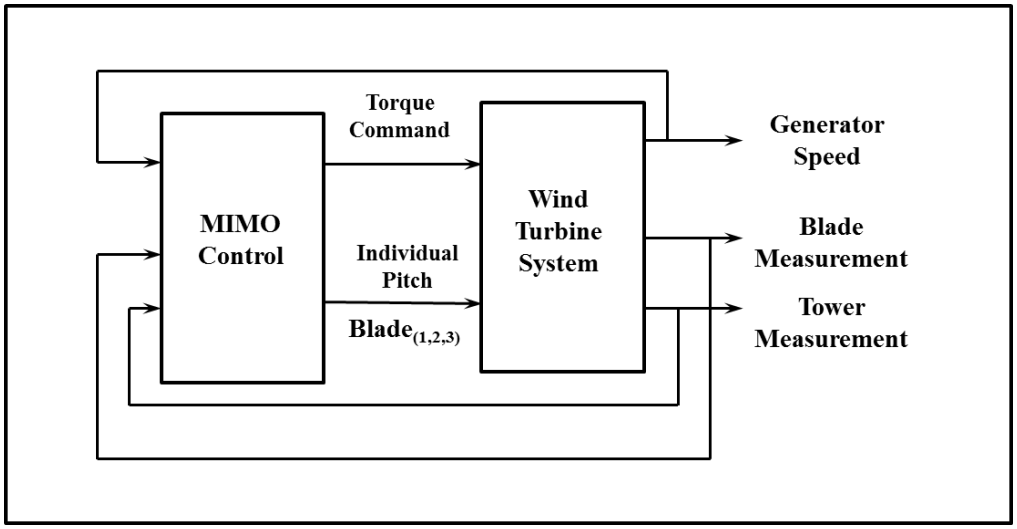

Figure 2. 19: Schematic of the MIMO controller. This controller has access to individual blade measurement and generator speed [107].

The principal control objectives are as follows:

Region 2: As wind speed changes, the control commands the balance of the rotor speed to the correct value by adjusting the generator torque so as to achieve optimal tip speed ratio λ^* [108].

Region 3: In this region, the use of blade-pitch controllers, designed using a classic proportional integral derivative (PID) control technique, is employed to regulate turbine speed and damp out drive train resonance in varying wind conditions through its notch filtering/compensating quality [109].

Advanced Control

Most research in this area has been split into investigations incorporating optimal capture in variable wind conditions in Region 2 and load mitigation in Region 3. Considering progress made with the Region 2 control, much effort has been put into research in the generator electro-mechanical section, with the use of maximum power point tracking (MPPT) in developing the majority of the models that increases the wind power output at around 11 - 50% while it tracks wind speed changes as fast as 0.2 Hz thus suffering low stress on the shaft and gears. This is said to be an improvement to that of the constant speed systems [110, 111] or the use of extremum control strategy (ECS) model approaches [112]. The MPPT and the ECS techniques are considered non-linear although they begin their designs in a linearized form.

Other studies [113, 114] did relate the nonlinear relationship between the wind speed, aerodynamic torque and pitch in their control modelling techniques as well as demonstrate an adaptive approach towards optimization of turbine power output. Basically, as electrical controls are used for maximum power point tracking (MPPT), aerodynamic controls are used to limit the turbine rotational speed and power at high wind speeds.

Advanced Region 3 Control: Frost *et al* [115] demonstrated novel adaptive applications which used a direct model reference adaptive control (DMRAC) approach in designing a collective pitch controller. The sole objective was to regulate generator speed in Region 3 and also to reject step disturbance without regulating the rotor speed although this may lead to reduced energy capture and undesirable torque-controller interaction [108]. This tends to improve on the proportional integrator pitch controller model, while Kumar and Stol [116] demonstrated a model of schedule modelled predictive controller (SMPC) and linear modelled predictive controller which showed considerable reduction in tower and drive train loads in Region 3, when compared with single-input single-output controllers. Nevertheless, multiple-input multiple-output (MIMO) time invariant methods tend to dominate advanced control research in Region 3; most of these improved MIMO control models in question are state-space based rather than transfer function based.

Proposed Improvements

A lag in response time emanating from the measurements taken from the wind turbine which is used for control feedback for the control algorithms introduced a need for preview controllers in order to mitigate resulting load before the disturbance arrives [107]. LiDAR technologies that measure the upwind speed at a sample rate of 10's of Hz can prove to be advantageous as a feedback to preview controllers. This preview controller can be designed together with the feedback controller in a bid to improve performance without large actuation increase [107]. Although large improvements and promise in control technologies are emerging from the preview control concept, a few other issues need to be investigated and developed. These include a noise-free measurement technology that will work in unison with the preview controller, proper characterization of the wind inflow to the turbine at sites with complex terrain features, reduced distortion of such technologies and optimizing the preview control model for operation by good modelling of the stochastic nature of upcoming wind profile. This proposed controller concept can suffice for large performance gains considering rate limitations in large-scale wind turbines via pitch actuation and might be useful for small wind turbines in built environments. In a bid to optimize control of the turbine system, this study aims to provide methodologies of evaluating the additional energy available at sites with

complex terrain features (such as suburban/urban areas) as well as assessing the performance of a given control system within such environment. This information can be used for improvements in preview control algorithms.

Also, various small-scale vertical axis wind turbines (VAWT) control methods such as the constant speed soft-stalling concept have been proposed to regulate the rotor speed or the output dc-side voltage of the generator rectifier [117-119] which stalls the turbine and reduces the power extracted by the VAWT. This method also houses a problem, as the power output is greater than the rated power, of which the generator and power electronics must be rated accordingly. Another proposed control improvement is the blade optimal pitch control model. This computes the optimal variation of the blades' pitch angle of the VAWT in order to maximize the torque generated at any given operational condition either by controlling the blades individually [120] or all the VAWT blades at once [121].

With the proposed use of autoregressive statistical models for short-term wind predictions for power tracking seeming to be expensive for small-scale VAWTs, an approach to resolving the difficulty of identifying target operating points of a small-scale VAWT by reversing the normal power-tracking control algorithm was proposed by Ahmed *et al* [119]. This control scheme is designed to regulate the speed according to the measured current thereby driving the turbine into a stall mode as soon as the wind speed exceeds the maximum power tracking range. The aim of these proposed improvements described above, is to improve the efficiency at reduced load in the wind turbine system. This is to ensure its cost effectiveness (i.e. cost to energy generated value). Since incorporating power electronics and other control technologies into a small-scale wind turbine's system design increases its initial cost, this study proposes cost effective methods of estimating how much total energy is available within a given turbine site as well as assessing the performance of the control system employed in a bid to improve efficiency within a small VAWT operation. The control methods relevant to this study will be discussed further in Chapter 3.

2.2.3.4 Turbine Control System Components and Devices

Control has proved to be an inevitable difficulty when designing VAWTs unlike HAWTs, with the overall design of the HAWT providing the opportunity to easily adjust the blades at the central hub in order to overcome problems during the periods of start-up, stall and braking. These control concerns in the VAWTs are severely increased by the increasing rate of turbulence within built environments, where they are commonly deployed.

In the presence of this complex turbulent wind, blade design, brake and circulation control of these VAWTs are prospective areas for improved future solutions.

Control of Blade Angles

One control technique popularly employed in the wind industry is the control of the blade angles. Three independent angles define the geometry of straight-bladed VAWTs (See Figures **2.20 and 2.21**). These are the:

- **Tilt angle** – the angle between the longitudinal axis of the blade and the rotor axis
- **Incidence angle (or angle of attack)** – the angle between the tangent of the swept circle and the blade chord
- **Swept angle** – describing the angle between the blade axis and the plane tangent to the swept cylinder.

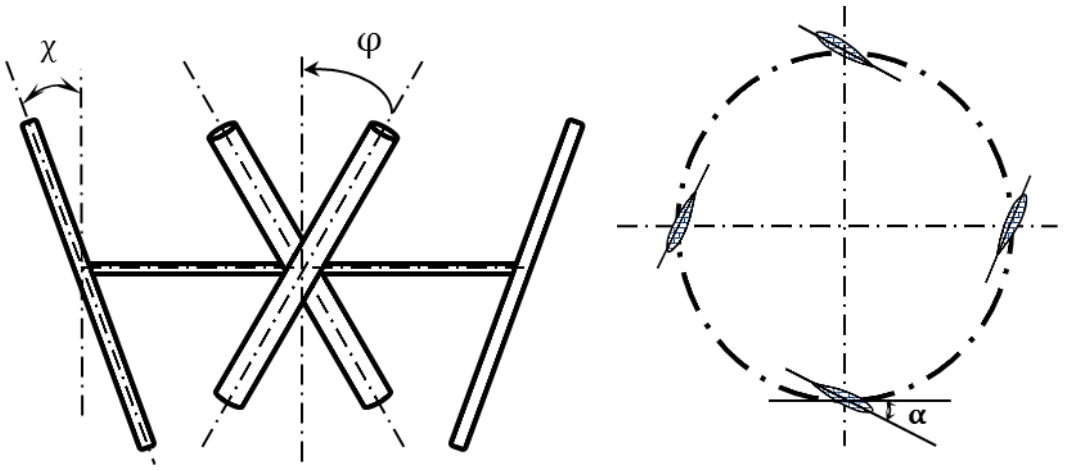

Figure 2. 20: A diagram describing the three independent angles; tilt(χ), incidence (α) and sweep (φ) angles (Adapted from [122]).

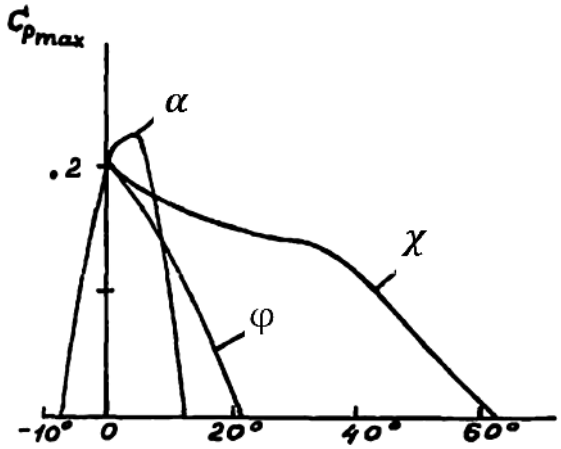

Figure 2. 21: The influence of the sweep (φ), incidence (α) and the tilt (χ) angles on C_{pmax} of a VAWT model (Adapted from [122]).

In trying to maintain optimal power coefficients, adjusting the angle of attack (α) is actually the most common and more realizable method of aerodynamic control, whereas the swept angle variation is preferred over changes in tilt angle if a more significant C_{pmax} change is required (swept and tilted blades are subject to high inertia and centrifugal loads, increased material consumption and strength issues and require complex mechanical designs thereby making them less attractive).

The variation of these angles strongly influences the maximum value of the turbine's power factor, with the variation in the angle of attack (α) showing more influence on C_{pmax} than the tilt and swept angle variations. As stated earlier, utilising the angle of attack is a common control method but is considered more difficult in VAWT designs as compared to HAWTs. This means that the control element needed in altering the blade angle of attack must be controlled through the spars linking the blades to the hub [122].

Control using Air Brake Flaps

One method of ensuring the VAWT operates within its designed wind speed limits is by the use of air-brake flaps. Air-brake flaps are another control method that can be used to effect VAWT brake, and this can be set up on the blade tips or struts. Neglecting flap induced velocities and lift at oblique flow and assuming flap and blade aerodynamic freedom, the braking moment (M_f) from the brake flap can be given as:

$$M_f = {}^1/_2\, j\rho C_{xf}((\omega R_f)^2 + {}^1/_2\, V_\infty^2)A_f R_f \qquad \text{Equation 2. 72}$$

where j is the flap number, C_{xf} is the flap drag factor, A_f is the area of the flap, R_f is the radius of the aerodynamic centre, ω is the angular velocity, ρ is the air density while V_∞ is the upstream wind velocity.

The braking moment ratio is given as:

$$C_{mb} = \frac{M_f}{({}^1/_2\, \rho R_f V_\infty^2)} \qquad \text{Equation 2. 73}$$

Samsonov and Baklushin in [122] estimated the braking moment developed by flaps from the difference between the moment of the model with and without flaps.

Control using Jet Brake Flaps

Another control method is the use of Jet brake flaps. This is described as a change in the flow around the pattern of the blade with the help of an interceptor (spoiler) extending from the leading edge area of the blade, which will extremely influence the torque of the VAWT. This is a circulation control where the decrease of the blade pulling force is achieved by making control flow stall from the blade. This is the most difficult type of control considering the fact that the blade is the weakest and most vulnerable element of the VAWT, making it unattractive to fit a control device inside or on the blade [122].

This method eliminates the chances of using complex mechanical control systems, having low reliability and operating in a field of centrifugal loads. There is also a possible way of increasing the VAWT performance by reversing the blown-out jet to the trailing edge [123].

Other devices employed in turbine control designs for power measurement as well as tracking the energy generation in the wind turbine include:

- Torque transducers
- Accelerometers
- Position encoders on the blade pitch and drive shaft actuation system and
- Strain gauges on the blade and tower.

Large wind turbines basically have a minimum of two (for VAWTs) or three (for HAWT) actuators [99, 124]. The first is the yaw control actuator, nearly included in large turbines (mostly for horizontal axis wind turbines), consists of a yaw motor which turns the turbine to align it with the direction of the wind. In small turbines, the yaw control is designed either in the form of a fan-like tail or as the rotor downwind of the turbine. Due to dangerous gyroscopic forces in large turbines, it is not safe to yaw the turbine at a high rate, mostly at rates less than 1 degree per second [124]. However, it is of less concern with small wind turbines thus making it yaw with every change in wind direction. The second actuator is the generator as generator torque can be an effective control actuator. Depending on the power processing equipment and type of generator, this actuator sends out commands at specific conditions in order to achieve desired loads or torque as it controls the acceleration and deceleration of the rotor. The last actuator is that of the blade pitch motor. This motor is designed based on type and design of the turbine blades. The blade pitch motor controls the pitch angle through feedbacks from the differential loading at different parts of the blades. Pitch actuators can be used to control the aerodynamic torque from the inflowing wind. For example, a 5 MW turbine has a pitch rate range of 8 degrees per second, while a 600 kW turbine has a typical maximum pitch rate range of 18 degrees per second [102].

In conclusion, due to increased investigation and research on the nature of wind flow within different sites (coastal, rural, urban, etc.), turbine controls tend to have made significant improvements from classic control designs through advanced control mechanisms. Over a decade, improved control methods have been investigated considering the fact that the behaviour of wind turbines is time varying and intrinsically nonlinear. This nonlinearity has resulted in cause for concern in the aerodynamic performance in wind turbines. Nevertheless, good results have emerged as new control models have been developed by either analysing a two degree of freedom linearized turbine model at an operating point to determine aerodynamic effects like blade flap (for both VAWTs and HAWTs), tower fore-aft motion from nonlinear simulation design codes like FAST [125] or secondary effects like rotating central tower, struts and spoilers from simulation design codes based on the 'Double-Multiple Stream tube' model like CARDAAV [126]. This study however, aims to demonstrate a new method of assessing the performance of control models within a site with complex terrain features based on stream tube models as well as estimating control model performance at different heights in a city-wide scale (see Chapter 6).

2.3 Review of Previous Studies

A summary of the various approaches employed by various authors in investigating turbulence in different terrains is presented within this section, which served as stepping stones to improved turbulence analysis in relation to wind turbine performance in different terrains and the wind energy industry at large.

2.3.1 Turbulence Analysis via Field Data

Most previous urban studies tend to have concentrated on near-idealised, two-dimensional building arrays. The first documented observation of urban turbulence properties was probably performed in 1946 in Tokyo from the Central Meteorological Observatory tower [127] with works in the early 1950s until the 1970s mainly focused on the mean properties of flow and temperature [37]. The modern approach to the study of turbulence and boundary-layer flows could be said to have started theoretically in 1974-5, with the first useful field experiment and data obtained five years later [128]. Many field studies, especially the early experiments, were made for the purpose of heat energy conservation investigation [129, 130] or pollution dispersion studies [131-133] within an urban canyon. The connection between field studies and their relative theoretical advances illustrated by the way mathematical models were introduced together with the field data inspiring them were presented in Ref [128]. The DAPPLE project which was tested in the London area [134], suggested changes in flow direction at street level based on the northerly or southerly component to the forcing rooftop winds. Field studies of detailed turbulence statistics are rare and most are focused on height variation in one profile [132, 135] or for the purpose of pollution dispersion applications [134, 136-138]. Studies focused on full-scale, reduced scale and real world field observations of wind flow and turbulence over built environments are provided in Refs [139-144]. However, very few field studies on turbulence were carried out for the purpose of wind energy analysis. The cost of field data studies (data collection and analysis) stemming from enormous logistical efforts required in mounting field experiments led to the development of other methods of turbulence study (and mathematical models) as illustrated below. Thus, this study will be proposing efficient and cost effective methods for predicting turbulence and characterizing the wind resource available over a built environment.

2.3.2 Turbulence Analysis via Wind Tunnel Experiments

The cost of field experiments led to the development of the outdoor wind tunnel in Askervein [145] and Blasheval [146] in Cooper's Ridge [147] in south-east Australia, which required enormous logistical effort to mount. The first wind tunnel simulation was dated 1978 with fifteen wind tunnel simulations and ten documented experiments listed in a review by Finnigan [148] between 1978 and 1985.

Many wind tunnel experiments have been performed since then. Wind tunnel experiments have long been a major source of obtaining turbulence data for urban wind analysis, although the make-up of most urban canyons (i.e. artefacts of the suburban/urban environment) in these experiments, have been homogenous in nature. It was, however, shown by means of wind tunnel modelling, that the nature of the flow over a built environment essentially depends on the geometry of the elements (for example depth-to-width and length-to-depth ratios, building roof shapes, etc.) within this particular boundary layer [149-152]. Very few wind tunnel experiments where turbulent components of three-dimensional flow in the canyon were measured with spatial resolution sufficient enough for a quantitative description of the canyon's flow pattern, have been performed so far [153].

Early works on turbulence faced with practical problems of modelling some terrains, for example real hills, for comparison with field data, ignored the roughness restrictions in their model design and constructed ones that were not fully rough so that the inner layer could be analysed in the tunnel [145]. This brought to light, the limitations to modelling (for example complex terrains) under wind tunnels as well as prompted questions on the nature of flow near the surface of these smooth models (surface turbulence), flow separation features and how this can be matched with the real world. With improvements in modelling techniques, some of the earlier discrepancies for these simple models were removed or explained. Wind tunnel studies conducted later on, investigated the measurement of flow around bluff generic shape model buildings (rectangular, prismatic and cubical) within a two-dimensional urban street canyon in simulated atmospheric shear layer [131, 154], while others [64, 150, 155] analysed flow across a built environment while comparing homogenous and heterogeneous arrays of symmetrical building structures. However, there still exists limitations of these models to fully replicate the real-time turbulent properties in wakes within these built environments given the level of the unsymmetrical features of the building (rooftop) shapes, spacing and height, in a real suburban/urban setting, which still calls for more standardized wind tunnels for more accurate turbulence prediction results.

2.3.3 Turbulence Analysis via Computational Fluid Dynamics (CFD) Simulations

Flow within and around buildings and other structures plays an important role in determining the urban climate within a built-up area. Steady-state and transient wind loadings are very important inputs in wind turbine design, considering the flow/structure interaction aspect which might lead to structural failure especially structures that maybe exposed to severe weather conditions. At a basic level, these wind-induced phenomena obey the same fundamental laws of physics. However, large-scale wind engineering considers the atmospheric boundary layer, as influenced by surface roughness, Coriolis, thermal stratification and other effects more statistical in character than deterministic. This is specifically because of the uneconomical and unavailability of the necessary meteorological data to assemble a well-defined boundary condition [156]. Various simulation techniques have been applied as a means of studying the turbulent flow and other range of flows in this suburban/urban terrain.

Before the advent of the digital computers, different modelling techniques that produced an integral sense or a macro-scale of the flow properties were used in estimating the effect of high frequency velocity perturbations within a flow field. But since the inception of supercomputers in the 1960s, flow analysis has been carried out numerically using a range of techniques which is now known as Computational Fluid Dynamics (CFD). This has made simulation techniques well established with simulation results best presented in combination with experimental data for that particular flow. In a bid for a more accurate and economical modelling technique for analysing the urban climate phenomena led to Computational Fluid Dynamics (CFD). For this reason and also strong interests in large-scale unsteady effects, wind-related studies are often performed on wind tunnel models, which are used for acquiring data for design purposes or for CFD calibration and verification [157]. However, wind tunnels provide controllable and well-defined conditions but fail to recreate the range of conditions in the ABL, which limits their use for real applications. These, therefore, presents further challenges for both CFD and wind tunnel studies.

A major characteristic of problems in wind engineering and that of the built environment is that they basically involve a wide range of scales such as simultaneous analysis of region of the ABL, characterisation of the flow around an array of buildings embedded within this layer and the localised details around a particular point or a building within this array (for example flow separation, impinging, vortex shedding, etc.). It should be noted that analysis of the built environment most times requires a total system approach which would involve more than one tool especially in cases of complex flow. The complex nature of turbulence can be attributed to a simple set of equations known as Navier-Stokes equation with no available analytical solutions to even the simplest turbulent flow [158].

A large family of models for turbulence have been developed in the past, ranging from simple algebraic expressions for eddies to more elaborate descriptions introducing separate transport equation for each component of the Reynold stress. The most common models available are the standard $k-\varepsilon$ model [159], lower Reynolds number $k-\varepsilon$ model [160], Re-Normalisation Group (RNG) $k-\varepsilon$ model [161], standard $k-\omega$ model [162] and Steady-State Turbulence (SST) $k-\omega$ model [163]. Turbulent flow behaviour can be predicted via six (6) common approaches namely: correlations, integral methods, single-point Reynolds-Averaged closures, two point closure, large eddy simulations (LES) and direct numerical simulations (DNS). In the context of computational fluid dynamics (CFD), turbulent flows are computed using three approaches:

1. The Reynolds-Averaged Navier-Stokes (RANS) equations
2. The Large Eddy Simulation (LES)
3. The Direct Numerical Simulation (DNS).

The Reynolds-Averaged Navier-Stokes (RANS) Approach

For the purpose of modelling turbulent flows, the fundamental building block of industrial CFD is the Navier-Stokes equation set which is expressed in terms of suitably-averaged velocities and pressures to make them acquiescent to numerical solution without excessive computing overheads [164]. This equation has been known for more than a century to govern the physics of (Newtonian) fluid flow. This is a widely used conventional approach in which the dependent variables take their time-averaged values known as Reynolds averaging (or time averaging) with the equations referred to as the Reynolds-Averaged Navier-Stokes (RANS) set. Additional pseudo-stresses arising from turbulent flow of all scales are obtained from averaging results of the unknown terms in the RANS equation in an additional set. These additional pseudo-stresses are termed Reynolds stresses while the additional equations that are derived through a substantial degree of approximation due to complexities of the turbulence to determine these stresses are known as the turbulence models. This has led to the development of a lot of models for different turbulent scenarios or conditions, each model working for the specific condition which was designed for, but not for the others.

The task of a modelling approach is to relate the Reynolds stresses to known quantities such as geometric parameters, flow scales and strains, thereby providing closure relations for them. It is, therefore, important to note that the RANS equations can only provide limited

information about the unsteady aspects of the turbulent flow which makes its application limited except for some specific cases. In the past, the RANS framework faced numerical accuracy concerns with available RANS models (i.e. RANS) ranging from full differential Reynolds stress transport models to large number and buoyancy effect in both near wall and bulk flow regions, although there have been recent advances in these areas. Certain applications such as flow around structures proved to be difficult to be accurately captured using previous RANS models especially at points where wake structures, pressure distributions and turbulence characteristics on or near its surfaces [165, 166]. Although, not accounting for different scales of turbulence, recent studies have demonstrated that at least in the spatial/temporal average sense that RANS approach can be successfully applied within a built environment [167].

The Large Eddy Simulation (LES) Approach

Large Eddy Simulation (LES) has proved to be a promising alternative approach over the past decade, overcoming the limitations and deficiencies of Reynolds averaging of larger scaled motions faced by the RANS approach. The averaging deficiencies in the RANS approach are now being handled in LES by performing a spatial averaging on the scale of the computational grid spacing (spatial filtering), making the LES better suited in predicting unsteady effects than the RANS approach with the result that modelling is only required of the pseudo-stress term that represents turbulent motions below this scale (example are the sub-grid scale (SGS) models representing small-scale motions) [164]. This means that the turbulent large scales are explicitly calculated while sub-grid closure rules are used in modelling the smaller ones [168]. In view of the overall acceptable predictions, the level of fidelity of the sub-grid model depends in several factors including the type of problem being solved, fineness of the resolved mesh, and what aspect of the flow are critical [169].

LES deals with coarser grids and higher Reynolds number but requires sub-grid models. Although many SGS models have been proposed in the past, it is still unclear the feasibility of LES in simulation of turbulence [170] with the nature of the Reynolds stress still unknown. With respect to a reference state, the flow solutions exhibited by LES are very sensitive to small perturbations (which might cause new instabilities) and changes in initial conditions. Other sources of error with LES include discrete representation of variables, numerical discretization, aliasing and SGS modelling [171] as well as difficulty in handling boundary conditions. The implicit contribution of the numerical methods to turbulence modelling should be well understood in order to avoid double-counting the effect of turbulence through the properties of the numerical method as well as the explicit turbulence model.

The Direct Numerical Simulation (DNS) Approach

The Direct Numerical Simulation (DNS) approach was first initiated by Orszag and Patterson in 1972 at the National Centre for Atmospheric Research [172]. They achieved this by using spectral methods to solve a 32^3 computation of an isotropic turbulence based on Taylor micro-scale and at a Reynolds number of 35. This method was improved on by Rogallo [173] in 1981 for the purpose of computing homogenous turbulence subjected to mean strain by combining transformed Navier-Stokes equations with an extension of the Orszag-Patterson algorithm. The results were compared with theory and experimental data and used to evaluate several turbulence models. This set a framework for DNS of homogenous turbulence which has undergone various improvements and modifications based on computational resources [174] and turbulence computational methods [175-178]. Basically, DNS solves the full Navier-Stokes equations thereby capturing the effect of all turbulent scales without any model for the turbulent motions. With this approach, the flow variables are known as a function of space and time and can be obtained by solving the Navier-Stokes equations. DNS has a more accurate prediction as it is usually used in computing fully nonlinear solutions of the Navier-Stokes equations which capture important phenomena in turbulence as well as the process of transition, with its application limited to simple geometric flows and somewhat low Reynolds number. It solves turbulent velocity field without the need for turbulent models. This approach is used in creating simplified situations that cannot be recreated in an experimental facility. The greatest advantage of DNS is actually its stringent control over the flow being studied.

DNS is mathematical and its codes are time consuming and usually higher spatially resolved thereby requiring extensive storage capacity. One major problem of the DNS approach is that turbulence contains a wide spectrum of vortices, increasing the size ratio of the largest to the smallest vortices as the Reynolds number increases, thereby making it difficult for DNS to effectively function at higher Reynolds numbers. Considering computing power constraints, it is believed that DNS does not deliver fully resolved results [171], needing careful grid convergence studies for verification purposes. For higher Reynolds numbers, RANS and LES (which computes only scales with large energy contents thus a good choice for investigating flows of large-scale) are more prevalent than DNS [158]. Boundary conditions are always critical in the use of DNS with specifying boundary conditions at open boundaries a very difficult issue. It is a general belief that the use of non-conventional methods like multi-grid, will lead to affordable DNS solutions, and development of nonlinear methodologies of analysis will prove very productive. In general, DNS can be said to be the best desirable solution to a much more computationally intensive turbulent flow problem, with the LES a

second choice considering its less complex nature and finally RANS which is the least complex. Basically for turbulent flow modelling using the three CFD approaches, all turbulent scales are modelled through the RANS approach, all scales are resolved through the DNS approach while for the LES, larger scales are explicitly computed leaving the effect of the smaller ones to be modelled [168]. However, basic limitations in these CFD studies includes studying mostly flow across symmetrical building/obstacle shapes and spacing, and the high cost of computing involved while employing CFD in the study of turbulent models.

In summary, some studies from wind tunnel experiments and CFD models have shown limitations in fully modelling the wakes in a built environment and incorporating the real-time turbulent properties produced by the unsymmetrical building/obstacle layout (height, spacing and shapes) within such urban setting. Most of these studies have not really analysed turbulence from the point of view of wind energy applications (i.e. most focused on dispersion applications). However, wind tunnel studies have delivered some very useful results based on idealised arrays aiming to mimic urban surfaces. Examples include the demonstration that a log law may be extended into the RSL if appropriate z_0 and d are defined [47, 64]. Also, they have illustrated the importance of representing heterogeneous building heights when defining surface aerodynamics [64, 150, 155, 179]. However, wind tunnel models of specific cities are extremely rare and hence we have to rely on modelling approaches for city-wide wind assessments. Whilst LES has been performed for some cities currently, it is too expensive to be rolled out for a large number of cities quickly whereas DNS modelling approach tends to be too expensive and impractical. This leads us to the use of time/spatially averaged approaches such as RANS where turbulence is expressed in terms of simple quantities such as turbulence kinetic energy (TKE) or turbulence dissipation. From the point of view of wind energy assessment, therefore, it would be useful to be able to relate such quantities to the estimated excess energy available to roof mounted turbines. Ideally, for wind resource analysis, high-resolution measurements (for example, using sonic anemometers) would be used over extensive time periods. This is impractical on a city-wide scale, and hence generally, field observations are used to validate modelling approaches (as shown later within this study).

2.3.4 Wind Turbine Economics

2.3.4.1 Introduction

One major factor limiting the popularity of most renewable energy technologies is the high generation cost. With recent improvements in technology and institutional support, wind energy has become economically competitive with other conventional sources like coal and

natural gas, with the cost of wind energy dropping by approximately 80% within the last two decades and the trend expected to continue in future years [9]. Having been rated the fastest growing renewable energy technology in the nineties, wind is not evenly distributed around the world. Economic merits of a wind system heavily depend on the local conditions. Computing the cost to energy generated value for wind turbine systems is quite simple and straight-forward whereas assessing the benefits is rather a complex process. In the past, studies were undertaken to determine optimum size of turbines by balancing the complete cost of building the turbine, installation and also the operations of various sizes of turbines against the revenue generated. Results showed minimum costs of energy to be obtained with wind turbine diameters in the range of 35 – 60 m, and even cheaper with offshore wind turbines, depending on which assumptions were made. Considering small-scale wind systems, Mathew [9] argued that the cost of wind turbines can be reduced considerably by scaling up the size of the wind system, although the cost of many components (such as safety features, electronic circuits, etc.) for these small wind turbines does not scale up at the same rate as the turbine size.

2.3.4.2 Environmental and Financial Viability

The environmental and financial payback periods are strong factors that determine the viability of a potential wind turbine project and thus influence the motivation to invest in small wind turbine systems. These periods could be influenced by various factors like available financial subsidies, turbine model type, carbon intensity of the electricity offset by that produced by the turbine system, and above all, the wind resource available at the potential site [180, 181]. A wind turbine project can be said to be environmentally viable if the carbon savings during its lifetime are sufficient to replace the carbon released in its manufacture, transport, operation and disposal. In order to achieve this, two inputs are required; (a) a cradle-to-grave audit of the carbon emissions and (b) the predicted energy yield over the lifetime of the turbine system [182]. This can be achieved by employing a parameter known as the capacity factor which is given as:

$$CF = \frac{Average\ power\ delivered}{Maximum\ rated\ power} \qquad \text{Equation 2. 74}$$

Capacity factors are generally calculated annually from the actual energy generated by the turbine and also provide a measure for the performance of the turbine system in a given site. Assessment of a 600 W turbine performance and operation at various rural and urban areas carried out by Allen *et al* [180], based on a capacity factor of 23%, suggested a standard

carbon payback of less than 12 years for the urban area and less than 3 years for the rural areas.

Financial viability assessment tends to be more challenging compared to environmental viability. This is as a result of various factors like the instability of the wind energy market, electricity market and changing UK Government policies. One major support provided by the Government for small wind installations is the Feed-in Tariff (FiT). Following recent reviews in FiT, the current value of the tariff valid between 8th of February and 31st March, 2016 for small-scale wind turbines in the UK is a flat rate of 8.53 p/kWh for installations up to 50 kW with an additional 4.85 p per kWh exported to the grid [183]. Thus, the level of financial support by the Government will influence the viability of any wind energy project within a potential site. Considering FiT revenues and costs of a pole mounted 6 kW turbine, study published by Sissons *et al* [184] suggested a payback period of 7 years with a capacity factor of 25%, which corresponds to the period for a MW onshore turbine.

2.3.4.3 Current Trends

The 2012 review of the Feed-in Tariff (FiT) Scheme (i.e. the Phase 2B review) led to a fall in the annual deployment rates of small wind turbines and massive cuts in staff numbers in many small wind turbine companies across the UK in 2013 [185, 186]. However, current industry reports show positive changes in the market with 2,237 small-scale and small-medium-scale wind turbines representing a total generating capacity of 248 MW installed in the UK alone in 2014, while 2,614 units were exported to markets like Asia, USA and Europe [185]. This was over double the capacity delivered in 2012 within the UK alone, with a 48% growth in the UK export revenue recorded for 2014. Yet many UK companies still raise concerns about the stability of the UK markets and the commitment of the government towards its continued success.

The growth in the UK wind industry (small- and large-scale) over the last three years has been majorly attributed to the support from the government via schemes like the Feed-in Tarrif (FiT), the Green Deal energy efficiency scheme, and various green energy initiatives which aim to provide support for community energy projects. These initiatives include the Community Energy Strategy set up in 2014 by the Department of Energy and Climate Change (DECC) to broaden the support for community energy projects, English Community Benefit Register to record community benefits from wind projects above 5 MW in size, Shared Ownership Framework that will be offered by all wind developments with a project cost of over £2.5 million (excluding aviation and grid costs), etc. [185].

2.3.4.4 Future Potentials

Studies suggest approximately 37% of direct energy use is consumed within urban areas globally and this could triple by 2050 [187], leading to propositions for the adoption of micro-generation to ease the fall in the carbon savings within the suburban/urban areas. This led to micro-generation becoming subject to a number of legislative drivers in the UK, such as micro-generation strategy, Renewable Obligation Order, Feed-in Tariffs Order, etc. [188], as the UK government aimed for net zero carbon new build housing by 2016 [189]. This has prompted a boost in the sale of small-scale wind turbines within the last decade as well as stimulating the growth of micro-wind turbine technologies. A list of small-scale wind turbines currently certified under the UK Microgeneration Certification Scheme (MCS) can be seen on their website [190], including product and installer details, feed-in tariff and installation guidelines.

If the power generated by the wind system is consumed domestically, the financial advantage stalling the turbine is decided by the local electricity tariff of which surplus electricity could be sold to the local utility company [9]. The cost of wind turbines is evaluated based on cost per generated energy, cost/kWh [84]. VAWTs generally could be cost competitive considering the simplicity of their design, low cost of manufacturing as well as installation, operation and maintenance [191]. For a wind system to produce a reasonable economic power in a given location, accurate wind energy and wind potential assessment must be conducted beforehand considering the fact that approximately 90% of all the life cycle costs of a small wind turbine system are upfront. Prevalent wind resource at any given location is site specific. In the case of a built environment, this will depend on many factors such as topography of the choice location, building density, building height, etc.

Recent studies such as Adam *et al* [192], Millward-Hopkins et al [69], Sunderland et al [193] and Drew et al [194, 195] have shown the potential of wind turbines (i.e. both ground level and building mounted) within the built environment. Field analysis and modelling have shown suburban/urban environments to be highly turbulent as explained in Chapter 2. Therefore, it is likely that advanced control options which can respond to rapid fluctuations in wind will improve the efficiencies of urban wind applications. Control methods however have cost implications. Methods are needed which are able to assist in estimating the excess energy available to turbines should the control methods be implemented. These need to be applicable on a city-wide scale and therefore rapid to calculate. The methods outlined in this study contribute to the development of such city-wide appraisal methods.

Poor judgement of the wind resource potentials and characteristics in a site and of the energy output could lead to either under or oversizing of such wind energy system in determining its economic viability, as the consumer's prime goal is achieving a shorter payback period as well as efficient power production. The lack of such analytical tools, tend to prevent small-scale wind turbines from becoming techno-economically successful in operation and hence more likely from being installed at all. This, however, is one major goal for this study, as it tends to investigate short term wind variations, like gust and turbulence. It will also propose an analytical tool that will not just estimate the total wind energy available, but also predict the performance of a given turbine system at a potential turbine site thus encouraging effective energy planning.

CHAPTER 3

3 Methodology

3.1 High Resolution Measurements and Data Processing

Whilst there are a number of sources of UK climatology data with varying degrees of temporal and spatial resolution such as the Met office NCIC (National Climate Information Centre) [62, 196] and Numerical Objective Analysis of Boundary Layer (NOABL) database [197], high frequency wind datasets for urban environments are much scarcer, since datasets acquired for weather forecasting purposes tend to be sited in regions of uninterrupted flow. For a more effective urban wind assessment, given the complex nature of the wind resource within an urban environment, specific high resolution wind data measured above roof heights typical of roof-top wind turbines are required. The temporal resolution should be high enough to capture the time-scales of the turbulent motion and hence needs to be in the order of 1 Hz [12, 198]. Such measurements tend therefore to be collected for research purposes rather than for routine forecasting applications.

3.1.1 Site description and Instrumentation

In this Chapter, eight high resolution wind datasets obtained from eight potential turbine sites within five (5) different cities namely Leeds, Manchester, London, Dublin and Helsinki were selected for this study. Aerial views of all eight sites are shown in Figure 3.1 with brief descriptions of these sites provided below.

Leeds Site

The first two wind datasets were collected at a location within the University of Leeds Campus, Leeds, UK. Three-dimensional wind speed data was captured using sonic anemometers (Research-Grade Gill Scientific Instruments model R3-50) at a sampling frequency of 10 Hz located at two different mast heights of 6 m and 10 m, on the top of the Houldsworth building (roof height approximately 24 m; Lat.: 53.809963°, Long.: -1.5574005°). Within this study, Unileeds (H1) represents data collected at mast height of 10 m, whilst Unileeds (H2) represents data collected at a mast height of 6 m above the roof-top. This site is surrounded by a range of building types, from two-storey urban properties to high rise block of flats. It also has at its north-west direction, a popular park called Hyde

park (See Figure 3.1), and lie within a local area that can be broadly categorised as residential area or university campus.

Manchester Site

The third wind data set was obtained at a sampling frequency of 20 Hz from a sonic anemometer (Gill Windmaster Pro Sonic Anemometer) mounted on a 5 m mast located on the roof-top of the George Kenyon building within the University of Manchester South campus (also known as the Whitworth Meteorological Observatory site with a building height of 49m; Lat.: 53.467371°, Long.: -2.232006°). This site lie within within local areas that can be widely categorised as university campus, residential or city centre. The observatory, established in 2010, is located within the city of Manchester and is surrounded by a range of building types, from medium-rise city centre buildings to high-rise block of flats or office complexes. An aerial view of the site is shown in Figure 3.1, with the Kilburn building located north-east, the Manchester museum at the south-west, Williamson building at the south, and the George Kenyon hall and the Physics Schuster building located at the east of the observation site.

London Site

The London city wind data was collected as part of the Dispersion of Air Pollution and its Penetration into the Local Environment (DAPPLE) project [136, 198, 199] using a Gill R3-100 sonic anemometer at a sampling frequency of 20 Hz and mounted on a Clark mast (mast height approximately 3.5 m) located at the roof-top of the Westminster city council building (roof height approximately 15 m; Lat.: 51.521588°, Long.: -0.160074°). The London site, conversely, can be characterized by rough and impervious land use in all directions and is located at the intersection of the busy seven-lane dual carriage Marylebone Road and a three-lane Gloucester Place road. With reference to Figure 3.1, the London site is surrounded by buildings less than 40 m in height within a 250 m radius around the study area [199].

Dublin Site

Wind datasets for the Dublin sites were collected at two locations; St. Pius X National (Girls) School located in Terenure, Dublin 6W (Lat.: 53.337767° , Long.: -60.305283°) and Dublin City Council Building in Marrowbone Lane, located in Dublin 8 (Lat.: 53.337767° ,

Long.: -6.286186°), Ireland. The first observation site is located on the roof-top of a one-storey school building. This site can be characterised as an extensive residential area consisting of two-storey buildings with pitched roof-tops, significant green space and mature trees [193]. The second site is located within the city centre area and is surrounded by a range of building types, generally 2 – 3 storey residential/commercial buildings (See Figure 3.1). At both sites, wind speed measurements were taken with a Campbell Scientific CSAT3 three-dimensional sonic anemometer at a sampling frequency of 10 Hz and a total height of 12 m for Dublin (St Pius) and 17 m for Dublin (Marrowbone) above ground level (a.g.l.).

Helsinki Site

The wind dataset for Helsinki was collected at two different locations within the city. The first wind dataset, which is referred to as Helsinki (Urban) within this study, was taken from the rooftop of Hotel Torni (Lat.: 60.167803° , Long.: 24.938689°) at a height of 45 m above ground level (a.g.l.) (mast height approximately 2.3 m; total building height approximately 42.7 m). The second site, SMEAR III (Station for Measuring Ecosystem-Atmosphere Relationships), is located 4 km north-east of the city centre (Lat.: 60.202817°, Long.: 24.961128°). Measurements were taken from a mast at the height of 31 m with the anemometer located on a horizontal boom, 1.3 m south-west from the measurement mast which in this study is referred to as Helsinki (Suburban). At both sites, the wind speed measurements were taken with a Metek USA-1 three-dimensional ultrasonic anemometer at a sampling frequency of 10 Hz. The Helsinki (Urban) site is located within a mixed commercial/residential/industrial area characterized by high roughness and impervious urban land use in all directions, while the Helsinki (Suburban) site is located within an extensive residential area with a high vegetation fraction [200, 201].

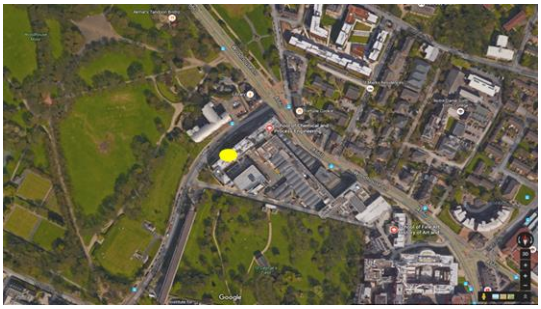

Leeds

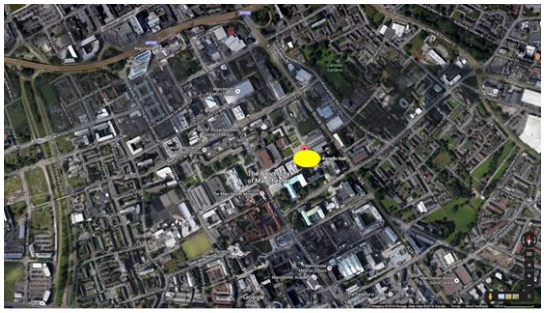

Manchester

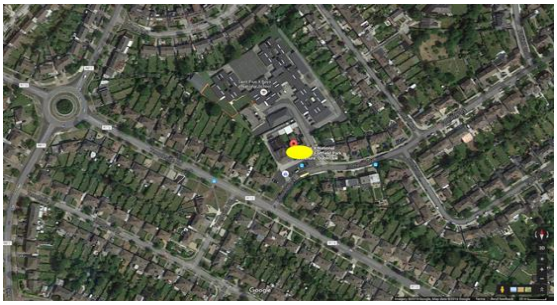

Dublin (St Pius)

Dublin (Marrowbone)

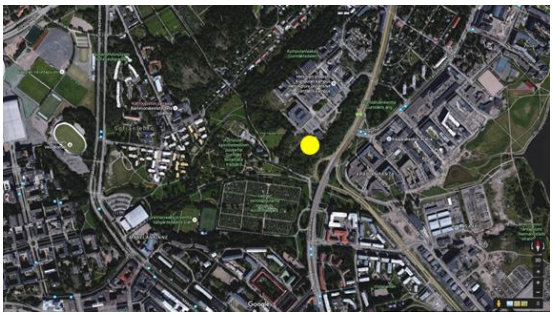

Helsinki (Suburban)

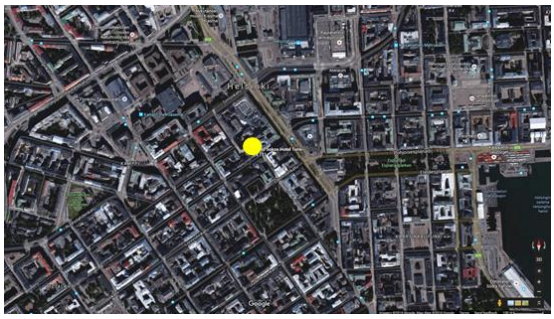

Helsinki (Urban)

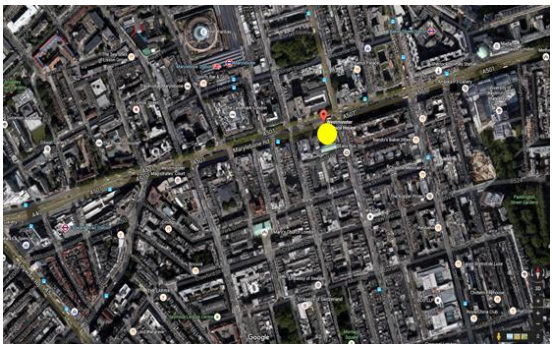

London

Figure 3. 1: Aeriel view of the eight (8) sites; the yellow spot represents the specific location at which measurements were collected (Google © Earth Maps).

3.1.2 Scope of data collected and analysis

The high resolution wind data described in the previous section were collected at the eight sites between the years 2008 and 2011, with a year-long dataset for each site selected for analysis within this study. The sites are considered as potential turbine sites for the purposes of the current analysis based on evaluation of their mean wind speeds. The high resolution wind data collected from the eight potential turbine sites were subject to a quality assurance procedure. For Leeds, Manchester and London sites, physical limits were first imposed on the raw data with values outside this limit excluded and hence replaced with an error flag. Thus, probability density function plots of daily raw files were produced to check for problematic datasets and to allow visual identification of outlying values. 15-min statistics were employed in performing further quality assurance on the raw daily files with data outside a window of mean values ±3 times the standard deviation were flagged as outliers [199]. Also, hourly intervals were rejected if outliers were greater than 600 records out of 36,000. Thus, less than 1% of the data were rejected overall. For the Helsinki datasets, a 2-dimensional coordinate rotation was applied on the raw data, and quality assurance was performed using turbulent fluxes calculated as averages of the covariance of vertical wind speed and considered scaler [200]. Stationary tests were performed and clear peaks were removed by visual inspection. 30-min statistics were employed in performing further quality assurance with physical limits imposed on the raw data to remove outliers and missing data points. For datasets from Dublin sites, 15-min statistics were employed in performing a quality assurance on the raw data, with probability distributions (Weibull and Rayleigh) employed to allow for visual identification of outlying values. These were used in interrogating the raw data every 15 mins and the data processed to yield half-hourly observations. Hence, after carrying out the necessary quality assurance on the one year raw data and elimination of erroneous or missing data, there were 8603 and 7515 hours from Dublin St Pius and Dublin Marrowbone sites respectively.

Due to the unavailability of data across the whole period (2008-2011), the datasets selected are not entirely overlapping but this does not compromise the analysis carried out. As presented in Chapter 2, the longitudinal free-stream wind speed (V_u) and wind direction upstream of the rotor (θ_u) are derived from the horizontal wind components, u_u (x-direction) and v_u (y-direction**).** Hence**,** θ_u, V_u and the longitudinal standard deviation (from henceforth represented by σ) were derived using Equations 2.10 – 2.13.

The high resolution wind data, collected from all sites selected in this study, was averaged at a sample frequency of 1 Hz to ensure data consistency between different sites, and to remove very fast transients. It was then parsed into contiguous 10-min bursts (i.e. T = 10 min), in accordance with the wind energy industry certification standards [45]. In characterising the

degree of turbulence within a burst in terms of statistical properties, the standard parameter of turbulence intensity presented in Section 2.2.2 is employed [2]. This can be rewritten as follows:

$$T.I.(\%) = \frac{\sigma}{\bar{V}} \times 100\% \qquad \text{Equation 3. 1}$$

The standard deviation of the fluctuating component of the wind speed provides a measure of the degree to which the magnitude of the wind is changing during a given burst period. The turbulence intensity for all observation sites presented within this study were obtained using Equation 3.1**.** As a result of $T.I.$ sensitivity to averaging time, turbulence intensities obtained within this study were compared for equivalent burst durations. The average power available in the wind is calculated using Equation 2.50. However, there exists extra energy within shorter frequencies in these urban wind conditions which is usually under-reported due to the use of mean wind speed in calculating the wind power over a given period. This can be defined by two parameters; the Gust Energy Coefficient (GEC) and the Excess Energy Content (EEC). The GEC is defined as the ratio of the total integral kinetic energy in the wind over a given period of time to the assumed energy by only considering the mean of the wind speed within the same period [12]:

$$GEC = \frac{\int_0^T {V_i}^3 \, \mathrm{dt}}{\bar{V}^3 \, .T} \qquad \text{Equation 3. 2}$$

where *T* represents the burst period and V_i represents the instantenous longitudinal free-stream wind velocity upstream.

The extra energy contained within transient fluctuation about the mean over a given burst period is represented in this paper as EEC (which is closely related to the GEC) and is expressed as a percentage of the total integral energy:

$$EEC(\%) = (GEC - 1) \times 100\% \qquad \text{Equation 3. 3}$$

The values of *EEC* will be sensitive to the length of the burst periods chosen which in this study is 10 mins (i.e. *T* = 10 min). From herein, for simplicity we drop the overbar when discussing mean wind speeds.

3.2 Wind Prediction methodology

As discussed in Chapter 2, various studies have proposed several methodologies of estimating the wind resource over a built environment. However, considering the availability of wind

speed measurements, the wind prediction model developed by Millward-Hopkins *et al* [63] for mapping mean wind speeds over cities (referred in this study as the MH model) was adopted in this study. Firstly, this model divides the city map into a grid of neighbourhood regions, with aerodynamic parameters for each region subsequently estimated using geometric parameters derived from digital elevation models (DEM) based upon LiDAR data [69] as inputs into a morphological model [47]. The data employed within the LiDAR-based DEM, which are available from Landmap, are measured by survey aircraft using remote sensing equipment which accurately detects the elevation of any obstructions above the ground. This is further processed to remove erroneous height measurements in order to provide the city's geometry in greater detail [69] in a bid to improve the accuracy of the aerodynamic parameter estimation and consequently the predictive accuracy of the MH model proposed in Ref [63]. Maps of the aerodynamic parameters over the city are calculated on two grids: a coarse uniform grid (of 1 km resolution) is used to represent regional scale (fetch) aerodynamic parameters, while a fine uniform grid (of 250 m resolution) is used to represent the local aerodynamic parameters, with both maps accounting for the aerodynamics of the upwind urban surface as a result of the influence of the incoming wind direction. These aerodynamic parameters were used as inputs in calculating mean wind speeds at different heights over the city.

For the purpose of complete parameterisation of the city's aerodynamics, neighbourhoods with plan area densities (λ_p; defined as the ratio of total roof area to the ground area in a neighbourhood region) within the range of 0.03 – 0.75 use aerodynamic parameters as calculated by the Millward-Hopkins model [179], while the aerodynamic parameters for neighbourhood regions outside this range are selected as follows:

a. when $0.75 < \lambda_p < 1$, the neighbourhood region is assumed to consist of mostly woodland and therefore we assume: z_0 = 1 m and $d/h_m = 0.67$ as recommended by Refs [62, 202] where h_m is the mean building height within the neighbourhood,
b. when $0.01 < \lambda_p < 0.03$, the neighbourhood is assumed to be a 'low density urban' area, and hence $z_0/h_m = 0.06$ m and $d/h_m = 0.35$ as provided by Ref [203],
c. when $\lambda_p < 0.01$, the neighbourhood is assumed to be open terrain, with the number of buildings assumed to negligible. Hence, $z_0 = 0.14$ m and $d = 0$ [62].

The MH model predicts wind speed at a hub height within the city in three different steps:

Step 1: The model takes the long-term average wind speed (V_N) from a regional wind climate database available at 10 m as input and scales this up to the urban boundary layer height (z_{UBL}) using a standard logarithmic wind profile:

$$V_{UBL} = V_N \frac{\ln(z_{UBL}/z_{0-ref})}{\ln(10/z_{0-ref})}$$ Equation 3. 4

where z_{0-ref} is the open country roughness length of 0.14 m.

The regional wind climate is obtained from a relevant climatology dataset such as the Met Office NCIC database [196], or the NOABL database [197], which provide wind speeds at a given resolution (e.g. 1 km for Met Office NCIC) over the whole of UK and are valid at a height of 10 m above a smooth surface. These data sets represent long-term averages of 30 years and 10 years for the NCIC and NOABL databases respectively.

Step 2: The second step involves down-scaling U_{UBL} through the urban boundary layer to the blending height (z_{bl}) using the logarithmic wind profile while considering the flow at z_{bl} to be homogenous [203]. Hence, the mean wind speed at z_{bl} is given as:

$$V_{bl} = V_{UBL} \frac{\ln\left(z_{bl} - \frac{d_{fetch}}{z_{0-fetch}}\right)}{\ln\left(z_{UBL} - \frac{d_{fetch}}{z_{0-fetch}}\right)}$$ Equation 3. 5

z_{bl} is set to be twice the mean building height while the aerodynamic fetch parameters $z_{0-fetch}$ and d_{fetch} reflect the influence of the incoming wind direction. Taking into account boundary layer growth as a result of the influence of incoming wind direction, the height of z_{UBL} is estimated as a function of the distance from the upwind edge of the city 'X' using Elliot's formula [204] as shown in Equation 3.6:

$$z_{UBL} = \min\left\{z_{0-fetch}[0.65 - 0.03\ln(z_{0-fetch}/z_{0-ref})] \times \left[\frac{X}{z_{0-fetch}}\right]^{0.8}, 500\right\}$$ Equation 3. 6

Here, z_{UBL} is set to a maximum height of 500 m [63] and the constant "0.65" in Equation 3.6 was slightly modified from its original value of 0.75 as recommended by the Met Office [62].

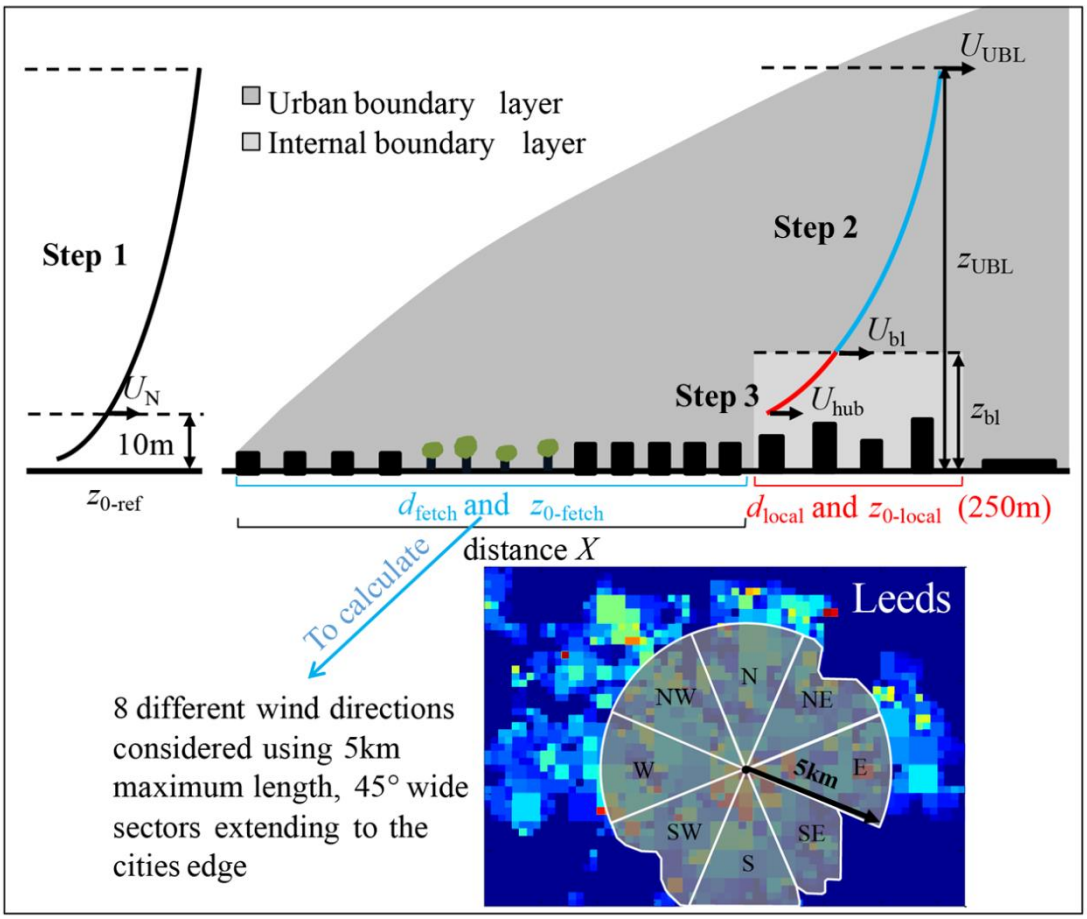

Figure 3. 2: Schematic representation of the wind prediction methodology referred to as MH model (Adapted from Ref [63]).

Step 3: Given the complex nature of the flow at the lowest region of the urban boundary layer, predicting the wind speed at heights below the blending height is divided into two stages:

a. For a hub height (z_{hub}) above the mean building height, the wind speed is calculated using local scale aerodynamic parameters d_{local} and $z_{0-local}$ and a logarithmic profile as shown in Equation 3.7:

$$V_{hub} = V_{bl}\frac{\ln\left(z_{hub} - \frac{d_{local}}{z_{0-local}}\right)}{\ln\left(z_{bl} - \frac{d_{local}}{z_{0-local}}\right)} \qquad \text{Equation 3. 7}$$

b. For hub heights (z_{hub}) below the mean building height, the wind speed is calculated using an exponential profile while accounting for the influence of height variation upon the wind profile [205]:

$$V_{hub} = V_{hmeff} \exp\left[9.6\lambda_f(1 - \sigma_h/h_{hm-local}) \times (z_{hub}/h_{hmeff} - 1)\right] \quad \text{Equation 3. 8}$$

where $h_{hm-local}$ is the normal mean building height within each neighbourhood region, σ_h is the standard deviation of the building heights in each local neighbourhood, h_{hmeff} is a modification of $h_{hm-local}$ that takes into account the disproportionate effect of tall buildings upon the wind flow in areas with heterogeneous building heights [179] and V_{hmeff} is the wind speed at h_{hmeff} obtained using Equation 3.7.

In order to obtain the final average wind speed predictions, a weighted average of the directionally dependent predictions for the eight compass wind directions (N,NE,E,SE,S,SW,W and NW) based upon the temporal frequency of the wind as recorded at a nearby reference station is calculated.

In a bid to validate the MH model, Milward-Hopkins *et al* [47, 52, 63] tested for the effect of building height variability and surface area density upon aerodynamic parameters on surfaces while estimating the profile of spatially averaged, horizontal mean wind velocity within a built environment using the experimental data. First, they compared z_0, d and other aerodynamic parameters predicted by the MH model with experimental data. Considering heterogenous arrays (i.e. buildings with varying heights), MH model predictions for z_0 and d as well as the linear increase of z_0 with increasing building height variation showed good agreement with experimental data. Secondly, as shown in Figure 3.3, the logarithmic wind profiles predicted by the MH model were also compared with measured wind profiles from experimental data as well as wind profiles predicted using the Macdonald's model [206] (popular wind speed prediction methodology employed in most studies such as Drew *et al* [194], Kastner-Klein and Rotach [207], Macdonald [68], Di Sabastino *et al* [208], etc.). The experimental data were obtained from studies published by Cheng *et al* [65], Jiang *et al* [205], Hagishima *et al* [155] and Zaki *et al* [150, 209] and referred to in Figure 3.3 as CC, Jia, Hag and Zaki respectively. Hence, tests carried out at different heights down to the h_{hmeff} and under increasing building height variability showed the logarithmic wind profiles predicted by MH model to have excellent agreement with measured wind profiles from Hagishima et al [155], Zaki et al [150] and Cheng et al [65]. Although, as σ_h increases, a slight divergence was observed when MH model results were compared to experimental data published by Jiang *et al* [205], a good agreement was still observed for $\sigma_h/h_{hm-local}$ = 0.5, which is the greatest magnitude of height variability found in many major cities [47, 210]. Also, results published by Ref [47] showed that Macdonald's model significantly overestimates wind profiles above these heterogenous building arrays, thus highlighting the significant inaccuracies that could occur when a model

that does not account for building height variation is used to estimate wind profiles above a built environment. In general, Ref [47] suggested that the MH model offers good estimates of z_0 and d, and hence wind velocity profile above heterogenous surfaces (for example, suburban and urban areas), particularly when compared to previous models that do not consider the influence of building height variability such as the Macdonald *et al* [206], Raupach [211, 212] and Bottema [211, 213, 214].

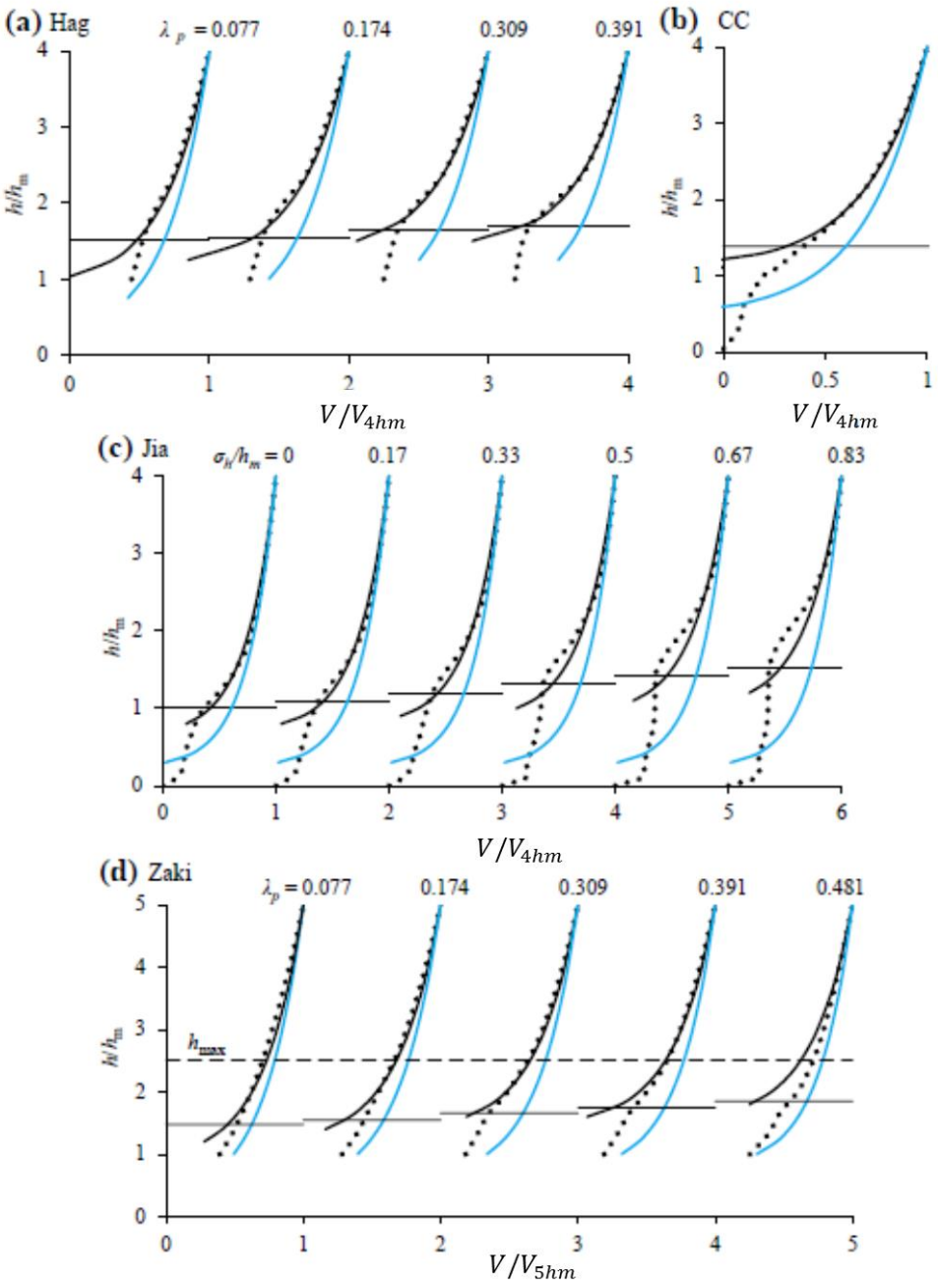

Figure 3. 3: Logarithmic wind speed (V) profile predicted by MH model (solid lines) over arrays set up and compared with wind profiles (dotted lines) from experimental data presented by (a) Hagishima *et al* [155], (b) Cheng *et al* [65], (c) Jiang *et al* [205], (d) Zaki *et al* [150, 209], and also the predictions of the model of Macdonald *et al* [206] (blue lines). The solid horizontal lines indicate h_{hmeff}. In (a-c), the wind profiles are normalised by wind speed at 4hm (i.e. 4 times the $h_{hm-local}$), and in (d) by wind speed at 5hm (i.e. 5 times the $h_{hm-local}$). Note: h_{hm} represents $h_{hm-local}$ (Adapted from Ref [52]).

In their extensive study on wind speed estimation within built environments, Milward-Hopkins *et al* [63] also compared the performance of the MH model with the Carbon Trust wind speed estimation tool while evaluating its accuracy using 23 test sites within five UK cities. The Carbon Trust tool (herein referred to as CT model) is a wind speed estimation tool which applies the UK Met Office methodology [62, 63] in predicting the wind speed over a city. From their analysis, MH model showed an improvement in accuracy, by about 18% when compared with the CT model. Further analysis showed an average percentage error of 11.7% for well-exposed sites, which is an improvement on that of the CT model with an average percentage error of 30.7%. This suggested a reduction in the uncertainties within the building height data which may have contributed to prediction errors. Thus, to maximize the accuracy of wind speed predictions, the MH model essentially suggests that the height based inputs such as the mean building heights, displacement heights, etc., should be estimated with a high degree of accuracy [69]. Extensive details on the MH model can be found in Refs [63, 69].

3.3 Vertical Axis Wind Turbine Modelling

3.3.1 Introduction

With increased resurgence of interests regarding wind turbines in recent times, several research institutions have developed numerous vertical axis wind turbines (VAWT) designs based on several aerodynamic computational models for the purpose of optimal design parameters and predicting the performance of these VAWTs before manufacturing models or prototypes. This study aims at assessing the performance of a small-wind turbine as well as estimating the energy available within a built environment. In order to achieve this, a two-dimensional VAWT model is employed. Although this study is not solely focused on the design and optimization of vertical-axis wind turbines and their operation within a built environment, an outline of the development of a simple low-cost VAWT model is presented herein. Having introduced the different concepts of wind turbine designs and also briefly the fundamentals of wind turbine aerodynamics in Chapter 2, this section goes on to present the basic development framework for modelling a simple VAWT system which will be employed in wind energy assessment within a built environment in Chapter 6. An overview of different types of modelling techniques suggested by various studies is presented in Section 3.3.2. Section 3.3.3 presents the VAWT model, the dynamic stall feature and also highlights other important factors influencing the performance of VAWT operations. Finally, an overview of

two popular control strategies employed in turbine operations is presented with a comparison of their performances demonstrated in Section 3.3.4.

3.3.2 Background

For the purpose of analysing turbine performances in a bid to optimize VAWT designs, several methodologies have been employed in order to allow design parameters to be altered with the effect of these alterations studied. This has led to the development of mathematical models substituting physical prototyping which requires a lot of time and resources. It is, therefore, important that these mathematical models must be developed approximating real life as close as possible for improved turbine design testing. Different mathematical models available for testing of VAWTs are discussed below.

3.3.2.1 Momentum Models

Different momentum models are based on the circulation of flow velocity through the wind turbine by equating the streamwise aerodynamic force on the blades with the rate of change of momentum of air (this is equivalent to the overall change in velocity times the mass flow rate), with the force equal to the average pressure difference across the rotor. Over the years, several model approaches such as single stream tube, multiple or double multiple model approaches have been developed by applying Bernoulli's equation to each stream tube. It is, however, apparent that the momentum equations do not fully describe the effect of the highly turbulent conditions produced thereby making the momentum models inaccurate at high tip speed ratios and high solidities [79]. Various momentum models used by various studies are listed below.

Single Stream tube Method

The single stream tube method was proposed in 1974 by Templin for the calculation of performance characteristics of Darrieus-type VAWTs [79, 215]. In this type of model, the basic assumption is that the entire turbine is enclosed within a single stream tube (as shown in Figure 3.4) with the induced velocity (i.e. rotor axial flow velocity) constant throughout the rotor and calculated by equating the stream-wise drag with the change in axial momentum. It is also assumed that the actuator-disk is considered as a surface of the imaginary body of revolution, with the upstream and downstream side of the swept volume having a constant flow velocity. Thus, the uniform velocity through the rotor V_T is given as:

$$V_T = \frac{V_\infty - V_{wa}}{2} \qquad \text{Equation 3. 9}$$

where V_∞ is the upstream velocity, V_{wa} is the wake velocity and all calculations are performed for a single blade whose chord length equals the sum of the chord lengths of the actual rotor blades.

This theory takes into account the effect of airfoil stalling and the zero-lift-drag coefficient on the performance characteristics, the effect of geometric variables such as rotor height-diameter ratio and blade solidity. It cannot, however, incorporate the effect of wind shear into the model. This model is viable for performance prediction of light-loaded VAWTs. Its limitations include predicting higher power than experimental results, neglecting wind velocity variations across the rotor (as these variations increase with increasing blade tip speed ratio and solidity)[79]. An improvement on the single stream tube model for cyclically pitched straight-bladed VAWTs with the addition of the effect of turbulent wake state, strut drag and dynamic stall, was proposed by Noll and Ham in 1980 [216].

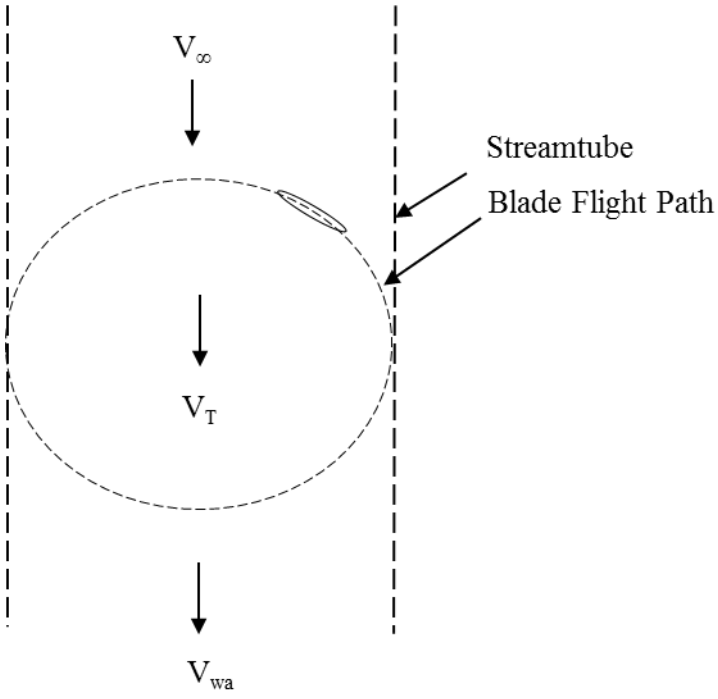

Figure 3. 4: Schematic diagram of a Single Stream tube Model.

Multiple Stream tube Model

The multiple stream tube model was first introduced in 1974 by Wilson and Lissaman [79, 217], and improves upon the single stream tube model in a number of ways. In this type of

model approach, the flow is assumed inviscid and incompressible for the calculation of the induced velocity, while the swept volume of the turbine is divided into a number of adjacent, aerodynamically independent parallel stream tubes (shown in Figure 3.5). The blade element momentum (BEM) theories are applied to each stream tube with the possibility of adding the effect of atmospheric wind shear into the model. Wilson and Lissaman considered the lift force to only appear while calculating the induced velocity (which varies over the frontal disk area both in vertical and horizontal directions) and is given by:

$$F_L = 2\pi \sin\alpha \qquad \text{Equation 3. 10}$$

and the induced velocity ratio also given as:

$$\frac{V_a}{V_\infty} = 1 - \left(\frac{k}{2}.\frac{Nc}{R}.\frac{R\omega}{V_\infty}.sin\theta\right) \qquad \text{Equation 3. 11}$$

where α is the angle of attack, R is the rotor radius, N is the number of blades, c is the blade's chordlength, V_∞ is the upstream (or freestream) wind velocity, θ is the rotor azimuthal angle, ω is the rotor rotational velocity and k is a factor found through iteration [79]. The induced velocity for each stream tube can also be obtained by using Equation 2.43. This model is limited to fast running light-loaded VAWTs which is a major drawback.

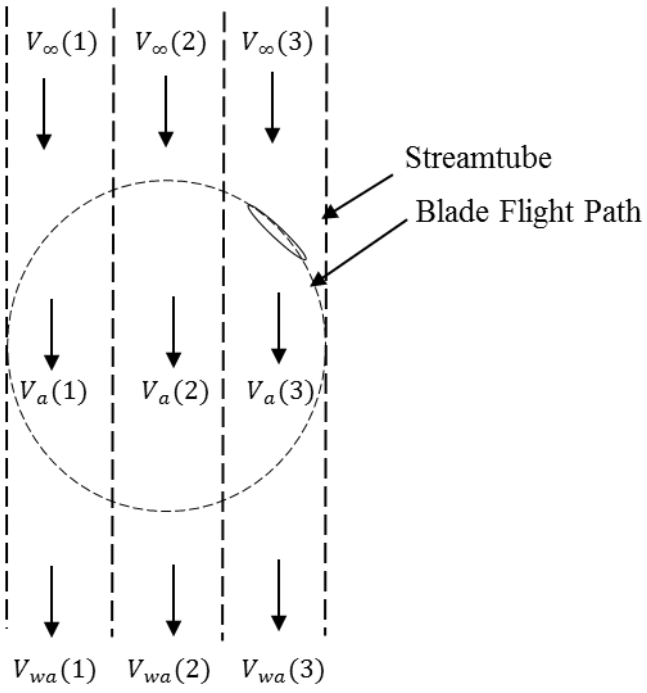

Figure 3. 5: Schematic diagram of a multiple stream tube model of a VAWT.

Strickland [218] produced an improved multiple stream tube model that included wind shear effects and calculated its induced velocity by equating the blade elemental forces and the change in the momentum along each stream tube. Compared to experimental data, the results of this model were quite impressive as it predicted the overall power capabilities reasonably, especially with a lightly-loaded rotor. The difference between Strickland's model and that proposed by Wilson and Lissaman was that Wilson and Lissaman only used theoretical lift force in the induced velocity calculation which gave a fast convergence, while Strickland added the effect of drag force for similar calculations and this resulted in slower convergence due to added complexity [79]. Muraca *et al* [219] also suggested another multiple stream tube model theory by including the effect of support struts, airfoil geometry, blade aspect ratio, turbine solidity and blade interference, with the effect of flow curvature assessed by considering flow over a flat plate. An expression for the distribution of the lift on the plate was developed within the variable angle of attack from the leading to the trailing edge points of the plate, and then the distributed lift force was averaged over the whole plate surface. From their theory, Islam *et al* [79] suggested that the effect of flow curvature for a low chord to radius ratio on the performance characteristics is negligible.

In 1977, Sharpe [220] presented a well-detailed description of a multiple stream tube which was similar to that of Strickland's but added the effect of Reynolds number in calculating the rotor drag coefficient. Hence, for a multiple stream tube model, a single blade passes each stream tube twice (i.e. the upstream and downstream) per revolution.

Double Multiple Stream tube Model

In order to incorporate the upstream and downstream induced velocities, given the existence of velocity deficit as the wind flow across the turbine, the double multiple stream tube model (DMST) was proposed. This model was proposed in 1981 by Paraschivoiu [221] for the purpose of predicting the performance of a Darrieus VAWT. The basic principle of this model is calculating the upstream and downstream half cycles of the turbines separately (as shown in Figure 3.6), with the induced velocities at the downstream and upstream calculated using the principle of two actuators in a cycle [222]. For these half cycle calculations, this model considers the vertical variation of the induced velocity (similar to that of the multiple stream tube model), while the horizontal component of the induced velocity is kept constant (similar to the single stream tube model).

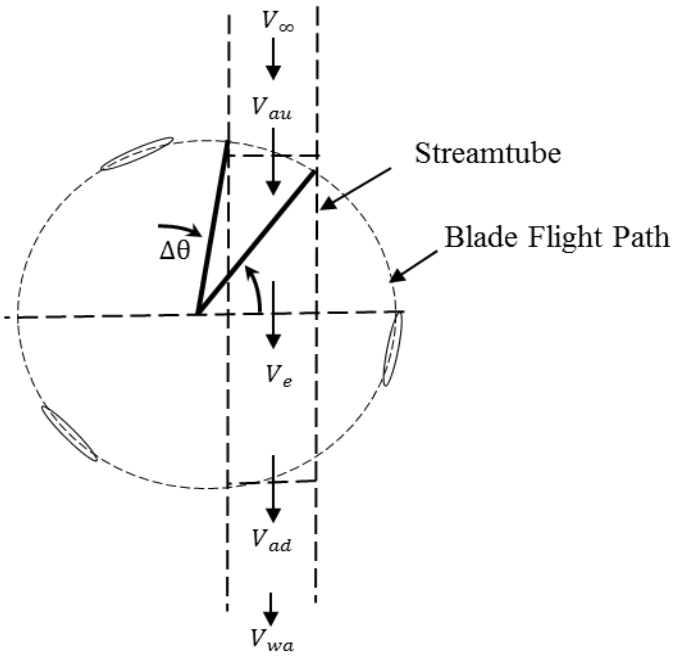

Figure 3. 6: A schematic diagram of a double multiple stream tube model [79].

The wake velocity for the upstream half cycle V_{au} is given by:

$$V_{au} = V_{\infty i}(1 - a_u) \qquad \text{Equation 3. 12}$$

where V_{au} is the upstream induced velocity, $V_{\infty i}$ is the ambient wind velocity (with wind shear effect causing it to vary at different heights of the turbine blade). The induced velocity for the downstream half-cycle V_{ad} is given in the expression

$$V_{ad} = V_e\,(1 - a_d) \qquad \text{Equation 3. 13}$$

where V_e is the downwind input velocity, a_u and a_d are the upstream and downstream induction factors.

Unlike the multiple stream tube model that uses one induced velocity for the upstream blades as well as the downstream blades, the DMST incorporates velocity deficit within its model thereby recreating a more realistic model of flow across the turbine blades. The DMST model over-predicts the power for some turbines (especially high solidity designs) and experiences a convergence problem on the downstream side at higher tip speed ratios. However, it gives a better correlation between experimental and calculated results when compared with multiple

stream tube models, especially for local aerodynamic blade forces with multiple stream tube models [79].

3.3.2.2 Vortex Models

This modelling approach uses the calculation of velocity field around the wind turbine influenced by the vortices in the wake of the blades to develop potential flow models. This idea was first introduced by Larsen [223] whose first model neglected the stall effect (i.e. assuming small angle of attack) and was not fully in two-dimensional form (considering vortex trailing the rotor blade tips). A two-dimensional model was later presented for straight-bladed VAWTs by Fanucci and Walter [224] whereas Wilson's study analysed the performance of a giro mill [225]. This led to further improvements like the two-dimensional vortex model with very a narrow blade and high height-diameter ratio for fast running, lightly-loaded VAWT [226], a three-dimensional model with aerodynamic stall [227]. Other improvements include an improved three-dimensional model with the inclusion of the dynamic effect such as pitching circulation, added mass effects and dynamic stall effects [227] and incorporating flow curvature [228] following the method proposed by Migliore [229] into the original aerodynamic model presented by Strickland [227]. In the Vortex modelling approach, the turbine blade represented in previous model approaches by a blade element is replaced with lifting or bound-line vortices whose strengths are determined using calculated angle of attack and relative flow velocity, and airfoil coefficient datasets. Based on the Helmholtz theorem [230], the strengths of the bound vortex filament (which is sometimes called substitution vortex filament) and each trailing tip vortex are considered to be equal, while the spanwise vortex is shed when its strength is equal to the bound vortex strength (shown by the Kelvin's theorem [230]) thereby leading to relative changes in the shed vortex system.

There are several drawbacks experienced while using the vortex modelling technique. These include very high computational time and reliance on basic significant simplifications like the inclusion of the blade aerodynamic viscosity effects through empirical force coefficients and assumptions of the potential flow in the wake [231].

3.3.2.3 Cascade Models

The Cascade model was first proposed by Hirsch and Mandal [232] for the analysis of VAWTs and is based on the application of the cascade flow theory of turbomachineries. This model assumes the blade airfoils to be positioned in a plane surface (cascade). The blade interspace calculated by dividing the turbine's circumferential distance by the number of blades. The

freestream and wake velocities are established by applying Bernoulli's equation [79]. The induced velocity is related to the wake velocity through a semi-empirical expression as

$$\frac{V_{au}}{V_{\infty}} = \left(\frac{V_e}{V_{\infty}}\right)^{k_i} \quad \text{Equation 3. 14}$$

for the upstream side, and

$$\frac{V_{ad}}{V_e} = \left(\frac{V_w}{V_e}\right)^{k_i} \quad \text{Equation 3. 15}$$

for the downstream side, where V_e and V_w are the wake velocities of the upstream and downstream sides respectively and the value of the coefficient k_i is determined from a fit of experimental results.

This cascade model approach has reasonable computational time compared to the vortex model, incorporates local Reynolds number variation effects at different orbital positions (θ), finite aspect ratio, zero-lift-drag coefficients and flow curvature effects in its calculations. It has a high level of accuracy in predicting overall values for turbines with both high and low solidities, and also improved correlation for instantaneous blade force calculations. Mandal and Burton [233] improved on this model by incorporating effects of flow curvature and dynamic stall with blade pitching, with the resultant wake velocities comparable with those of the complex dynamic vortex model. However, compared to stream tube models, studies show that the cascade model requires higher computational costs.

In summary, an overview of various popular aerodynamic modelling approaches employed for turbine design analysis and better performance prediction of vertical axis wind turbines has been presented in this section. Several studies have suggested the vortex models to be the most accurate models when compared to other approaches. However, considering that vortex and cascade models are computationally very expensive and with the vortex model suffering from convergence problems in some cases, stream tube models have been adopted by many studies focused on VAWT design and power capability analysis [234, 235]. Given its simplicity, low computational cost and suitability for low solidity configurations, the double multiple stream tube (DMST) modelling approach has been adopted in this study for design and power prediction analysis of a micro VAWT operation within a built environment.

3.3.3 Vertical Axis Wind Turbine Modelling

As stated earlier, various studies have assessed the performance of different turbine models while considering several important factors. These include variable blade pitch angles [231], different rotor speed control strategies (such as constant speed control, constant tip speed ratio demand feedback control, etc.) [83], spoke drag effect, turbine response and its effect on grid supply [75], effect of wake structure, blade type and shape [236], wind shear, blade-tip, junction and tower losses [237], strut effect and losses from multiple blade elements [238], etc. However, this study focuses on assessing urban wind energy by employing a straight-bladed fixed pitch low-cost 2-D multiple stream tube vertical axis wind turbine model which was developed using the MATLAB software. A schematic representation of this design is presented in Figure 3.7. This approach is effective in predicting the axial force and the overall performance of a lightly-loaded VAWT whilst minimising computational costs. The choice of simple fixed-pitch configuration makes VAWT designs more feasible for small-scale wind applications despite their self-starting issues (which will be discussed later) [239]. The turbine system modelled is assumed to be a three straight-bladed vertical axis wind turbine which has a rotor radius (R) of 0.75 m, a blade height (H) of 1.5 m (i.e. a rotor height to diameter ratio of approximately 1) and a chord length (c) of 0.08815 m. These parameter choices as represented in Table 3.1, are representative of a typical micro VAWT design employed within an urban wind resource. Considering the flow in each stream tube, the turbine rotor is divided into two halves; first representing the upstream half of the surface swept by the turbine blades ($0 \leq \theta \leq \pi$), and the second representing the downwind half of the rotor ($\pi \leq \theta \leq 2\pi$). The induction velocity is calculated twice, one for the half upstream of the turbine system while the other half downstream of the turbine. This is considered to affect the velocity of the flow across the stream tubes as a result of the forces exerted on the flow by the actuator disk. This causes the velocity to decrease across the stream tubes. The induced velocities for the upwind (V_{au}) and downwind halves (V_{ad}) of the stream tubes were obtained as a function of the induction factor (a) and can be estimated from the expressions:

$$V_{au} = V_{\infty}(1 - a) \qquad \text{upwind half } (0 \leq \theta \leq \pi), \qquad \text{Equation 3. 16}$$

$$V_{ad} = V_{\infty}\,(1 - 2a) \qquad \text{downwind half } (\pi \leq \theta \leq 2\pi). \qquad \text{Equation 3. 17}$$

Values for specific parameters such as number of blades, the height of turbine's blade, the chord length of blades, turbine swept area, inertia, free upstream wind velocity, air viscosity, air density, etc., have been chosen for this VAWT model. These design parameters can, therefore, be changed at will while investigating the turbine performance at different

conditions. This is to aid in observing the performance of the turbine model at different operating conditions.

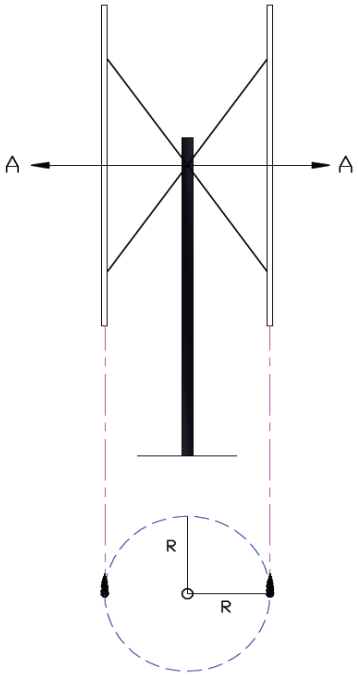

Figure 3. 7: A schematic representation of a simple straight-bladed vertical axis wind turbine where A-A is the plan view and *R* represents the turbine radius.

Table 3. 1: The vertical axis wind turbine model properties.

VAWT Configuration properties	
Turbine Rotor Diameter	1.5 m
Blade Height	1.5 m
Chordlength	0.08815 m
Blade type	Straight - bladed
Airfoil types	NACA0012, NACA0015, NACA0018, NACA0021

The VAWT model developed within this study employs the actuator disk momentum theory as well as the blade element and momentum (BEM) theory as described in Section 2.2.2 to

determine the momentum at the upstream half of the rotor and the deficit downstream of the VAWT model. This is combined with empirical lift and drag coefficients for the blades in calculating the normal and tangential forces on each turbine blade (as described in Chapter 2). The 2-D airfoil lift and drag coefficients were obtained from the stationary attached flow wind tunnel experiment conducted by Sheldahl and Klimas [240], corrected by Lazauskas [86]. The time averaged thrust force on a given number of blades and twice per revolution is given as [235]**:**

$$T_a = \frac{\Delta\theta}{\pi} 2N * \text{Instantaneous Thrust} \qquad \text{Equation 3. 18}$$

where N is the number of blades, and instantaneous thrust on a single blade at a certain azimuth angle (θ) can be expressed as:

$$T_i = \frac{1}{2}\rho H c V_r^2 (C_t cos\theta - C_n sin\theta) \qquad \text{Equation 3. 19}$$

where V_r represents the relative velocity which depends on the rotor azimuthal angle (θ), and is therefore different for each streamtube section (described in section 2.2.2), H is the blade height, c represents the chordlength while the C_n and C_t represent the normal and tangential force coefficients derived from Equations 2.63 and 2.64.

The average non-dimensional thrust coefficient is also given as:

$$C_T = \frac{T_a}{\frac{1}{2}\rho V_r (RH\Delta\theta sin\theta)} \qquad \text{Equation 3. 20}$$

This, however, can be re-written as:

$$C_T = \left(\frac{nc}{2R}\right)\left(\frac{V_r}{V_\infty}\right)^2 \frac{2}{\pi}(C_t cos\theta - C_n sin\theta) \qquad \text{Equation 3. 21}$$

The average torque on the rotor in one full revolution can then be estimated using Equation 6.14.

$$T_{ba} = N \sum_{i=1}^{2m} \frac{\left[\frac{1}{2}\rho H c R V_r^2 C_t\right]}{2m} \qquad \text{Equation 3. 22}$$

where m is the number of stream tubes and $2m$ is the number of $\Delta\theta$.

The torque and power coefficients can then be derived from Equations 3.23 and 3.24**.**

$$C_q = \frac{T_{ba}}{\frac{1}{2}\rho DRHV_\infty{}^2} \quad \text{Equation 3. 23}$$

where ρ is the air density, D is the rotor diameter and H is the blade height.

$$C_p = C_q.\lambda \quad \text{Equation 3. 24}$$

where λ is the tip speed ratio.

Four types of airfoils namely NACA0012, NACA0015, NACA0018 and NACA 0021 were tested within this study. These airfoil blades were initially designed by the National Advisory Committee on Aeronautic (NACA) for aircraft wings [241]. Each NACA airfoil is represented by four numbers which describes the airfoil design (i.e. NACA '****'). The first number represents the percentage of the chordlength that make up the maximum airfoil camber, the second number represents the location of the camber along the airfoil section (i.e. distance from the leading edge) and finally, the last two numbers represent the thickness of the airfoil section as a percentage of the chordlength. For example, NACA0012 simply means the airfoil has no camber (i.e. '00') and the thickness of the airfoil section represented by the number '12' basically means the blade thickness is 12% of the chordlength [241]. Figure 3.8 demonstrates a comparison between the steady-state performance of a 2-D multiple stream tube numerical model of a H-type VAWT proposed by McIntosh *et al* [234] (referred to as the McIntosh model) and the current VAWT model at constant rotational speed and varying wind speeds (i.e. tip speed ratios within the range of 0.1 to (9.7*V_∞/R)). The McIntosh model was developed from a Flowstate methodology which is a graphical solution method that removes complexities arising in a bid to achieve convergence within the momentum model. This methodology examines the flow state (i.e. separated or attached flows) at each stream tube and provides a physical, converged solution by simply selecting an informed choice of solution point. This model has been tested and validated against a number of available experimental datasets for Darrieus VAWTs [234]. The performance of each turbine model presented in Figure 3.8 was evaluated at various flow angles described by the azimuthal angle (θ). From Figure 3.8, results show good agreement between the McIntosh model and the current model. However, Figure 3.8 also shows that employing dynamic stall features demonstrated improvements at higher tip-speed ratios, thus highlighting the importance of dynamic stall in urban wind applications. Although the power curve shown in Figure 3.8 is defined for steady flow conditions, the shape of performance curves in unsteady winds has been shown to be similar [234]. Hence the figure serves to illustrate the region of tip speed ratios at which maximum aerodynamic efficiency (i.e. C_{pmax}) and therefore maximum power can be achieved. As stated earlier, effectively extracting energy from gusty urban wind

containing large fluctuations will require knowledge of the turbine system's maximum aerodynamic efficiency. This will be discussed further when discussing turbine controls design in Section 3.3.4.

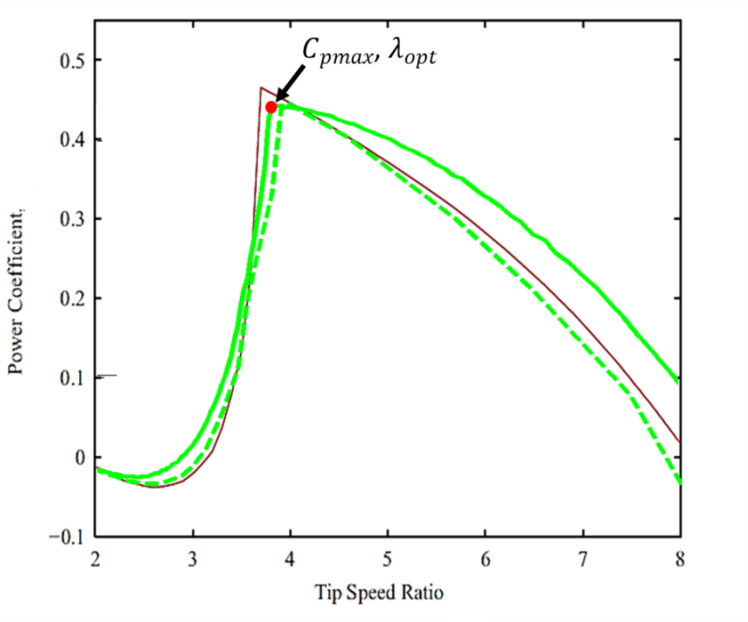

Figure 3. 8: Performance of the numerical model (NACA0012) for different tip speed ratios highlighting the maximum operating point of the VAWT. (a) red plot represents McIntosh numerical model with no dynamic stall [234] (b) green broken lines represents current numerical model with no dynamic stall (c) green solid lines represents current numerical model with dynamic stall.

For the purpose of designing this study, flow across the rotor is assumed to be incompressible, steady and homogenous. This model also assumes uniform thrust over the disk or rotor area and that the static pressure at the far upstream and downstream of the rotor is the same as that of the undisturbed ambient static pressure. There are various factors that influence the performance of a VAWT system. A few of these factors considered within this study are presented below.

3.3.3.1 Thrust Coefficient and Induction Factor

One important parameter in turbine system modelling is the thrust coefficient C_T. The use of Equation 3.21 is widely accepted as a good description for momentum loss across a range of induction factors in wind turbine modelling [2, 75, 235], and thus is adopted within this model. One limitation of the BEM theory is that it becomes invalid when the induction factor is

greater than 0.5 (i.e. as a result of the rotor entering what is known as a turbulent wake state [242, 243]). Thus, after obtaining some experimental data of rotors operating in a turbulent windmill state, Glauert [75, 244] in 1926 proposed an empirical solution to the problem of thrust which is widely experienced in various momentum models. This was in the form of a parabola given by the expression:

$$C_T = 0.889 - \frac{0.0203 - (a - 0.143)^2}{0.6427} \qquad \text{Equation 3. 25}$$

and intersecting the classical momentum theory parabola (defined by Equation 2.48 [2, 235]) at $a = 0.4$.

Thus, various studies have applied the Glauert empirical formula (defined by Equation 3.25) in the region $0.4 < a < 1$ [235]. Recent studies have proposed correction models which are used in correcting both the rotor thrust coefficient and the local coefficient of the individual blade elements when incorporating tip/hub losses thus solving the discontinuity problem arising when plotting the Glauert's curve [243]. Instead of employing the classical C_T - a curve (given by Equation 2.48) widely used in calculating thrust coefficient at different induction factors (a), a modification to the solution defined by Equation 3.26 and illustrated by Refs [2, 231, 245] was employed within this study. This is an empirical fit and is given by Equation 3.26 and is valid for the region $a_T < a < 1$.

$$C_T = C_{T1} - 4(\mathrm{C}_{T1}^{0.5} - 1)(1 - a) \qquad \text{Equation 3. 26}$$

where C_{T1} is 1.816 (representing the best fit to experimental data), and a_T is expressed as:

$$a_T = 1 - 0.5\mathrm{C}_{T1}^{0.5} \qquad \text{Equation 3. 27}$$

Induction factor is sometimes referred to as interference factor [246] but both factors are different. These two factors, as defined in Section 3.3.2, are used to determine the induced velocity at the upstream and downstream region of the VAWT model. However, as suggested by various authors [2, 75, 231, 235, 246], an iterative method is used in VAWT model analysis in deriving the induction factor (as shown in Figure 3.9). Multiple studies applying an iterative actuator-disk method have suggested this to be successful only on lightly loaded wind turbines. In this study, convergence of this iterative method was improved through the use of a relaxation scheme represented by Equation 3.28 as suggested in Refs [75, 247].

$$a_{new} = w a_{new} + (1 - w) a_{old} \qquad \text{Equation 3. 28}$$

where w is an under-relaxation parameter.

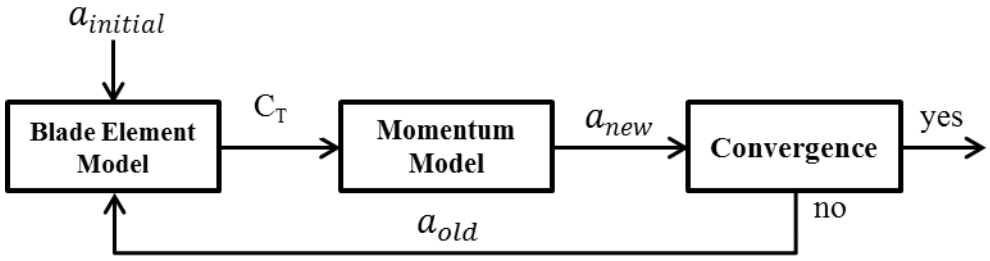

Figure 3. 9: Illustration of the iterative approach employed in double multiple stream-tube models.

3.3.3.2 Dynamic Stall

Wind turbines encounter additional unsteady effects at high or rapidly fluctuating wind speeds and their power outputs are limited by the maximum power ratings of their system components. In order to limit power output or extend the range over which turbines remain operational within these complex wind conditions while avoiding turbine system failure, some studies have suggested stalling methods such as adjusting the turbine blades (i.e. pitching to stall), braking systems, etc. [2, 91]. Others have proposed reducing the turbine's efficiency by reducing the tip speed ratio from the steady state inflow optimum values $\lambda < \lambda_{opt}$ [75]. Previous studies have shown that under stationary attached flow, the lift force acts approximately as a linear function of the angle of attack (when the angle of attack is small) [2]. The VAWT model considered above, however, exhibits flow pattern changes at a limiting value of the angle of attack, with the lift force passing through a maximum. This can be referred to as a static stall model, as described by the experiment carried out by Sheldahl and Klimas [240] which was instrumental in the production of lift and drag coefficient table for the four (4) blade (airfoil) sections (NACA0012, NACA0015, NACA0018, NACA0021) employed herein. The static 2-D airfoil data obtained by Sheldahl and Klimas [240] is frequently used as a steady reference and covered angles of attack ranging from 0 - 180º at Reynolds numbers (Re) from 40,000 to 500,000. This was later corrected by Lazauskas [86] in order to cover for the full 360º range of attack. The use of this static blade (airfoil) data needs to be augmented for low values of reference tip speed ratios (i.e. in high wind speeds or fluctuating inflow) [246]. However, it takes some time for flow under non-stationary conditions to approach the stationary flow pattern due to the inertial and transitory effect of the boundary layer separation and its subsequent re-attachment under high winds or highly

fluctuating wind conditions [75]. This causes a delay in the lift force, with lower lift at increasing angle of attack and higher lift at decreasing angle of attack. Accounting for the delay of lift during fully attached conditions, motion of the separation point, leading edge separation and dynamic interaction between the leading and trailing edge vortices is therefore known as *Dynamic Stall*. Studies have suggested dynamic stall to have significant effect on both the overall power outputs of the turbine system and the generation of cyclic lateral loads when operating at tip speed ratios below λ_{opt} [75].

Dynamic stall tends to occur at the root of the blade where the local tip speed ratio can be considerably less than the reference tip speed ratio. The basic goal of the dynamic stall model is to proffer solutions for the dynamic characteristics of the turbine blades from the available experimental static coefficients (i.e. the lift and drag tables provided by Refs [86, 240]). Gormont [248] proposed the first dynamic stall model used for performance prediction at low tip speed ratios. Gormont's model was first developed for helicopter blades, of which it empirically mimics the hysteresis response of the airfoil. The first step was to define the reference angle of attack at which the two-dimensional static coefficient data is considered [249]. This is achieved by transforming the angle of attack as given in Equation 2.56 to what is now called the reference angle of attack which is given as:

$$\alpha_{ref(L,D)} = \alpha - K_a \Delta\alpha \qquad \text{Equation 3. 29}$$

where $\alpha_{ref(L,D)}$ is the reference angle of attack for the lift and drag respectively,

$$K_a = \begin{cases} 1 & when\ \dot{\alpha}\ \geq 0, \\ -0.5 & when\ \dot{\alpha}\ < 0. \end{cases}$$

$\dot{\alpha}$ is the time derivative of the angle of attack (α), and $\Delta\alpha$ is given as:

$$\Delta\alpha\ = \begin{cases} \gamma_{1(L,D)} S_a & when\ S_a \leq S_b, \\ \gamma_{1(L,D)} S_b + \gamma_2 (S_a - S_b) & when\ S_a\ > S_b, \end{cases} \qquad \text{Equation 3. 30}$$

where

$$S_a = \sqrt{\left|\frac{c\dot{\alpha}}{2W}\right|} \qquad S_c = 0.06 + 1.5\left(0.06 - \frac{t}{c}\right),$$

$$\gamma_{1(L,D)} = \begin{cases} \dfrac{\gamma_{2(L,D)}}{2} & \text{for lift characteristics,} \\ 0 & \text{for drag characterisitcs,} \end{cases}$$

$$\gamma_{2(L,D)} = \gamma_{\max(L,D)} max\left\{0, min\left[1, \frac{M - M_{2(L,D)}}{M_{1(L,D)} - M_{2(L,D)}}\right]\right\},$$

M is the local Mach number and $\frac{t}{c}$ is the relative thickness of the blade (airfoil) section. M_1, M_2 and $\gamma_{\max}$ for the lift and drag are derived from the expressions given in Table 3.2. The dynamic lift and drag coefficients for the Gormont's model are finally derived from the following expressions:

$$C_L^G = \alpha\left[\frac{C_L^S(\alpha_{ref(L)})}{\alpha_{ref(L)} - \alpha_{zero\ lift}}\right] \qquad \text{Equation 3. 31}$$

$$C_D^G = C_D^S(\alpha_{ref(D)}) \qquad \text{Equation 3. 32}$$

$\alpha_{zero\ lift}$ is typically considered as the zero-lift angle of attack, and for the present analysis, considering symmetrical airfoil sections, this quantity is assumed to be zero [246]. The superscript "G" represents the values modified by the Gormont model, while the superscript "S" represents the steady-state, two-dimensional airfoil characteristics which are, for this study, tabulated as functions of Re and α [240]. It will be important to note that the reference angle of attack for the lift is different from that of the drag, as presented in the various expressions of M_1, M_2 and $\gamma_{\max}$ in Table 3.2. Representing the static stall angle as α_{ss} (i.e. the angle below which the lift characterisitics of the airfoil section are strictly linear), it follows that the lift will be modified only when either $\alpha_{ref(L)}$ and α are greater than α_{ss}, then $C_L^G = C_L^S$. It is, however, necessary to employ Equations 3.29 – 3.32 for all angles of attack and not just only angles greater than the static stall angles so as to avoid spurious discontinuities in C_L^G as a function of α.

Table 3. 2: Specific expressions for $\boldsymbol{M_1}$, $\boldsymbol{M_2}$ and $\boldsymbol{\gamma_{max}}$ for the lift and drag.

	Lift Characteristics	**Drag Characteristics**
M_1	0.4 + 5.0 (0.06 – (*t*/*c*))	0.2
M_2	0.9 + 2.5 (0.06 – (*t*/*c*))	0.7 + 2.5(0.06 – (*t*/*c*))
$\gamma_{\max}$	1.4 - 6.0 (0.06 – (*t*/*c*))	1.0 – 2.5 (0.06 – (*t*/*c*))

Strickland, Webster and Nguyen [227] were among the first to propose and employ the adaptation of Gormont's model for VAWTs and suggested a zero value for S_b, since the relative thickness of the airfoils used are greater than 12%. This model was applied only when $\alpha \geq \alpha_{ss}$. It was later suggested by Paraschivoiu, Desy and Masson [250] to apply the adaptation of that proposed by Strickland, Webster and Nguyen [227] only in regions of lower turbulence (with these localised low turbulence regions based on the water tunnel visualization experiment [251]) after prior experiments proved delay in dynamic stall occurring at regions of high turbulence [252].

Studies performed years later speculated that Gormont's model over-predicts the effect of dynamic stall on the performance of VAWTs since Gormont's model was developed for helicopters and the maximum angle of attack reached is lower than that experienced by VAWT blades. Hence Masse [253], in order to evade over-prediction, suggested to compute the dynamic coefficients through a linear interpolation between the static coefficients ($C_{L,D}^{S}$) and the dynamic coefficients predicted by the Gormont's model ($C_{L,D}^{G}$). This he achieved by using the following expressions:

$$C_L^{mod} = \begin{cases} C_L^S + \left[\dfrac{A_M\alpha_{ss} - \alpha}{A_M\alpha_{ss} - \alpha_{ss}}\right]\left(C_L^G - C_L^S\right) & when\ \alpha \leq A_M\alpha_{ss} \\ C_L^S & when\ \alpha \leq A_M\alpha_{ss} \end{cases} \quad \text{Equation 3. 33}$$

and

$$C_D^{mod} = \begin{cases} C_D^S + \left[\dfrac{A_M\alpha_{ss} - \alpha}{A_M\alpha_{ss} - \alpha_{ss}}\right]\left(C_D^G - C_D^S\right) & when\ \alpha \leq A_M\alpha_{ss} \\ C_D^S & when\ \alpha \leq A_M\alpha_{ss} \end{cases} \quad \text{Equation 3. 34}$$

where A_M is an empirical constant proposed by Masse (i.e. A_M = 1.8). Berg [254], after understudying the work of Masse and experiments, suggested the value of A_M (i.e. A_M = 6) to show good agreement between predicted and experimental performances of the Sandia 17 m Darrieus-type VAWT, and α_{ss} as the angle at which the linearity of the changes in lift coefficient as a function of the angle of attack begins to depart, thereby reducing the influence of Masse's model at higher angles of attack and improving its agreement with measured load. Figure 3.10 demonstrates the effect of incorporating dynamic stall on a VAWT operation thus highlighting the reduction in the negative torques observed at lower tip speed ratios and also showing overall improvement at higher tip speed ratios when compared to the system without dynamic stall feature. Although there are other losses encountered within the turbine operations such as blade tip losses, spoke drag effects, strut losses, etc., these were not considered within the present study.

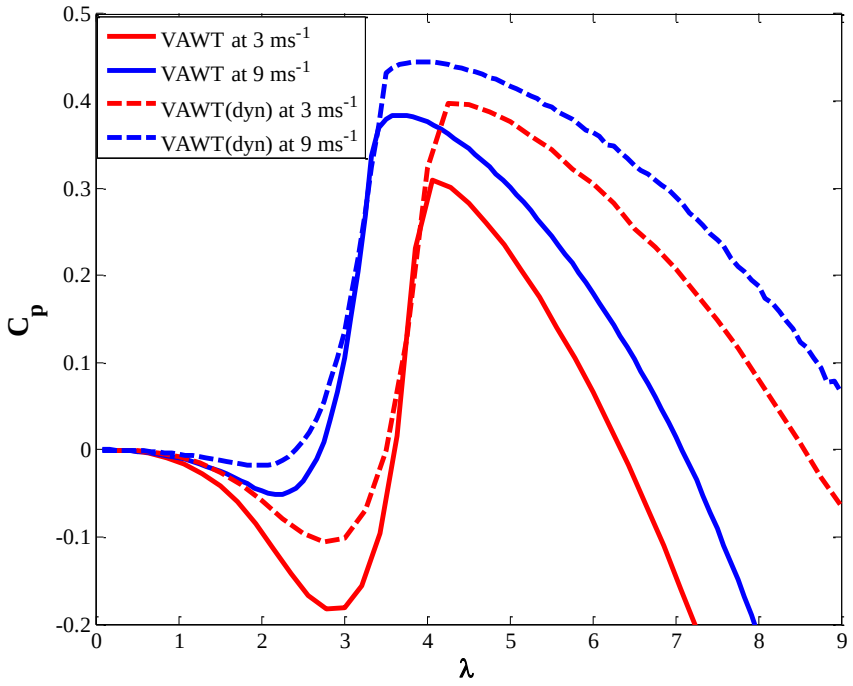

Figure 3. 10: Effect of Dynamic stall on a NACA0018 straight-bladed VAWT at two different wind speeds demonstrated within this study; solid lines represent VAWT model without dynamic stall and broken lines represent the VAWT model with dynamic stall.

3.3.3.3 Turbine Solidity

Based on the $C_p - \lambda$ relationship as discussed earlier, one important parameter responsible for the changes in the turbine performance is known as solidity. This is defined as the total blade area divided by the swept area and could be controlled by the changing of the blade's chordlength or the number of blades. However, the solidity of a VAWT can be given as [75, 79]:

$$Solidity = \frac{Nc}{R} \qquad \text{Equation 3. 35}$$

where N is the number of blades, c is the chordlength and R is the rotor radius.

The effect of solidity on turbine performance, as demonstrated in Figure 3.11, can be described as follows:

a) A low solidity will produce a broader and flatter curve which indicates a little change in the C_p over a wind tip speed ratio range but the C_{pmax} is low because of the high drag losses (note that the drag losses are proportional to the cube of the tip speed ratio).

b) A high solidity will produce a narrow performance curve with a higher C_{pmax} and a sharp peak which makes the turbine very sensitive to the tip speed ratio changes such that very high solidities result in a relatively low maximum C_p which can be attributed to stall losses.

Applications that need turbines of relatively high solidity exist. These include wind-driven water pumps and smaller turbines used in charging batteries. These applications require high starting torque allowing small amounts of power to be developed at very low wind speeds (which is ideal for trickle charging batteries). Although it has been proposed to have a larger number of blades with small individual solidity, it still has its limitations with respect to increased production costs as well as structurally weak and very flexible turbine blades. A clear demonstration of the effect of solidity on turbine performance (for example, NACA0012) is demonstrated in this study (as shown in Figure 3.11). From the VAWT model results, it is seen that the maximum power coefficient increases from 0.4343 to 0.4655 as the solidity rises from 0.1 to 0.2. Additionally, as the solidity is increased further, the maximum power coefficient is reduced. Therefore, given the operating conditions, the maximum power coefficient occurs where the solidity is 0.2. These results are in agreement with vertical axis wind turbine performance observations at different solidities made by McGowan *et al* [255] and Strickland [218] hence aids the validation of this model for urban application.

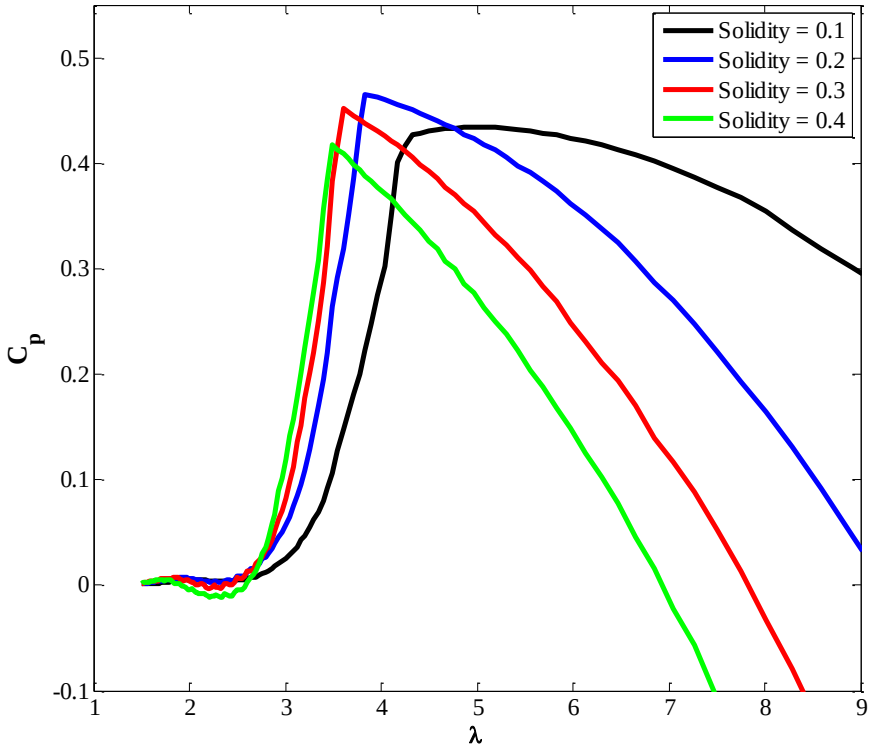

Figure 3. 11: Effect of Solidity on a NACA0012 airfoil-type vertical axis wind turbine performance.

3.3.3.4 Blade (Airfoil) Section

The four symmetrical NACA blade (airfoil) sections, as stated earlier, were employed and tested within this study. Past studies comparing the performance of these four (4) NACA airfoil sections at different operating conditions are rare. However, the major factor observed while employing these blade sections are their minimum or negative torques at lower tip speed ratios as well as their performance at higher tip speed ratios**.** This study considered a fixed-pitch which means that pitch angle changes are neglected in this study (i.e. pitch angle = 0). At a given design solidity and a given upstream wind speed, the model performance plot aids in determining which blade design achieves the highest peak power coefficient (i.e. C_{pmax}). Also given that the turbine operations are sited within a built environment, better performance under higher tip speed ratios will also be advantageous, given that urban wind resource is mostly characterised by low wind speeds. This analysis is aimed at determining which blade design best suits an urban VAWT design. The corresponding power curves for the different blade (airfoil) sections with solidity of approximately 0.35 are presented in Figure 3.12**.**

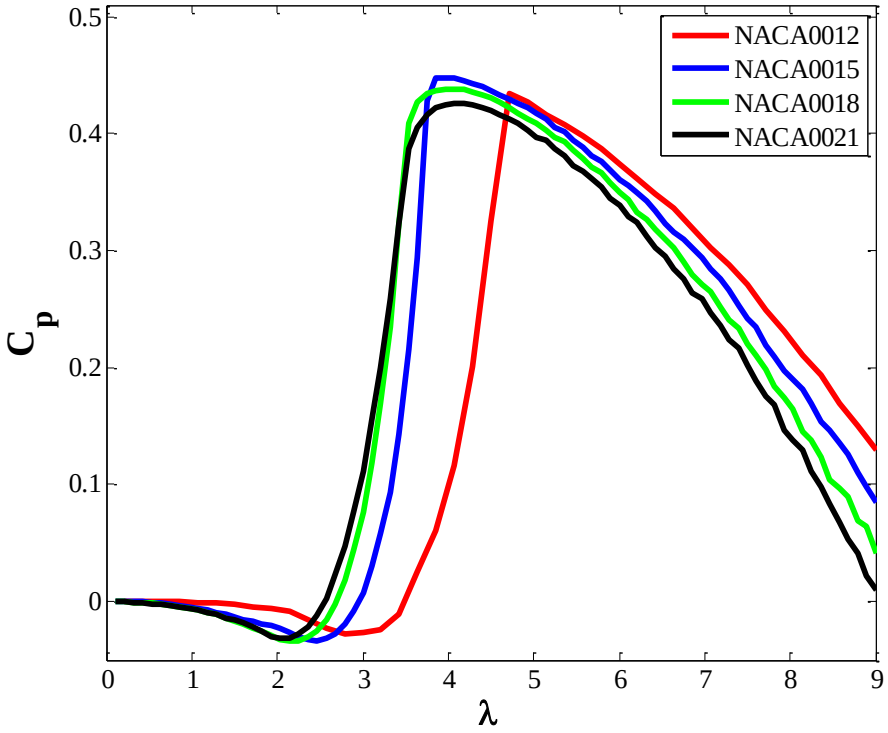

Figure 3. 12: Performance test of the four NACA blades (airfoils) at constant rotational speed and varying wind speeds (i.e. varying tip speed ratios).

Results show NACA0018 and NACA0021 to produce flatter peaks thus suggesting reduced efficiency loss as the tip speed ratio drifts away from the optimal tip speed ratio (i.e. tip speed ratio at C_{pmax}). At lower tip speed ratios, each airfoil section tends to generate negative torques as a result of higher drag forces. Further analysis showed a significant decrease in the negative torques with increasing wind speed. However, Figure 3.12 shows NACA0012 and NACA0015 perform better at higher tip speed ratios compared to NACA0018 and NACA0021. Although NACA0012 produces lower negative torque at lower wind speeds as compared to the other three airfoil sections, NACA0015 was shown to produce higher C_{pmax}. From these results, NACA0015 was considered more suitable for urban wind application and hence is chosen for this study.

3.3.3.5 Reynolds Number

This model resolves the flow across the turbine rotor in two-dimension and the flow field close to the turbine which defines local flow conditions at each rotor blade is characterised by the local Reynolds number (Re). The local Reynolds Number is obtained as a function of the local relative velocity at each flow angle. This is used to predict the turbine performance under free-

flight conditions thereby incorporating (but not fully) the effect of turbulence. The local Reynolds number accounts for the effect of air viscosity, blade chord length and the relative velocity of the blade and is derived from the expression:

$$Re = \frac{V_r c}{\nu} \qquad \text{Equation 3. 36}$$

where c is the chordlength, ν is the kinematic viscosity of air and V_r is the relative velocity of the blade [246, 256]. The airfoil characteristics (i.e. $C_n(\alpha)$ and $C_t(\alpha)$) are incorporated into the BEM model in order to account for changes in effective blade Reynolds number within the model. It was suggested by Blackwell *et al* [257] after conducting a wind tunnel test for a Darrieus-type VAWT wind tunnel test, that the turbine's maximum coefficient of performance (C_{pmax}) increases with increasing Reynolds number (See Figure 3.13) thereby stating the importance of Reynolds number to the given system's operation and a better prediction of the blade's lift and drag forces when it is Reynolds number dependent. Figure 3.14 demonstrates the effect of Reynolds number on the maximum coefficient of performance, thus increase in the Reynolds number results in increased maximum coefficient of performance. Although various experiments have been conducted to predict the global rotor performance by using constant Reynolds number values under different operating conditions [231, 240, 257, 258], in reality, the blade's local Reynolds number changes with varying wind speed and tip speed ratio (as illustrated in Equation 3.36). In determining the lift and drag force coefficients (i.e. C_l and C_d) within this study, values from the lift and drag tables adopted from a wind tunnel test conducted by Sheldahl and Klimas [240], corrected by Lazauskas [86] were two-dimensionally interpolated for each given pair of local Reynolds number and angle of attack. This made it possible to develop and run performance tests for different blade (airfoil) sections (i.e. NACA0012, NACA0015, NACA0018 and NACA0021).

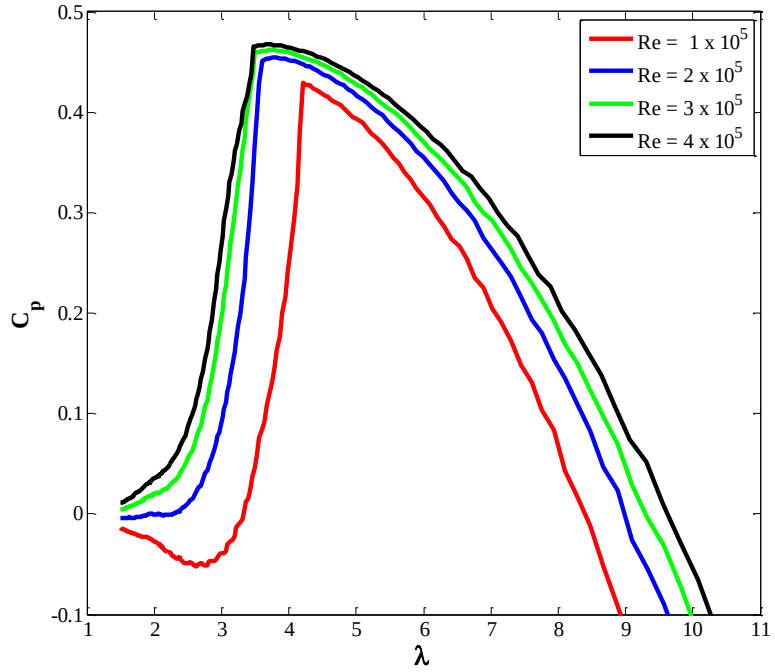

Figure 3. 13: Effect of Reynolds number on Turbine Performance for NACA0015 at constant rotational speed.

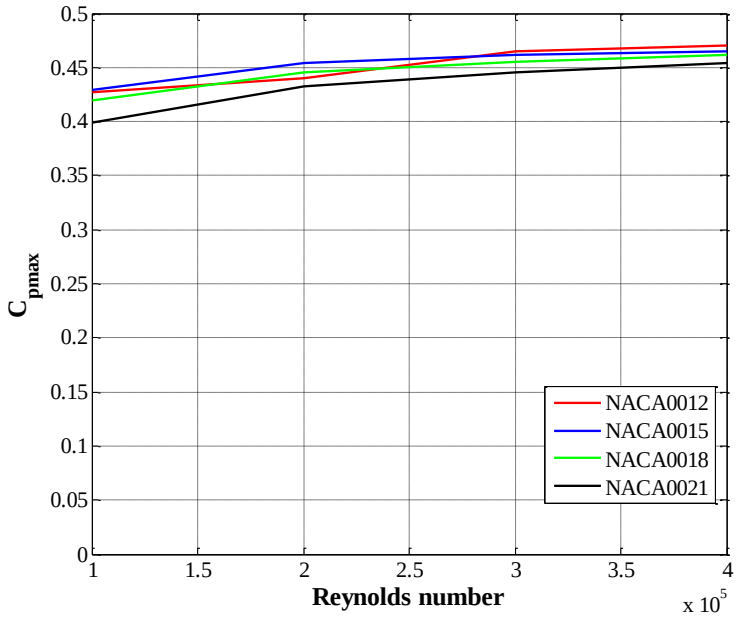

Figure 3. 14: Effect of Reynolds number on maximum power coefficient (C_{pmax}) of a turbine system.

3.3.3.6 Blade Height

In addition, blade height is another factor that influences the performance of a VAWT design. Since the turbine power coefficient is expressed as a ratio of produced power to the maximum

available power and the blade height is a parameter present in both, the power coefficient is not affected by the changes in the turbine blade height. However, the blade height does affect the power and torque produced by the turbine. Thus, Nahas [90] suggested that both values (power and torque) linearly increase with increasing blade height.

3.3.4 Turbine Controls

One important component of a VAWT design in turbine operations within a suburban/urban environment is the control system employed. This plays a major role in the turbine's performance as well as overall energy planning or payback period. As presented in Section 2.2.3, various control schemes have been employed by various studies in assessing the turbine system under different operating conditions. Thus, the response characteristics (i.e. its control architecture and design) determine the ability of the turbine to respond to fluctuations in the wind speed. Neglecting power converter losses as well as other transmission losses and assuming a very rigid rotor, the torque equilibrium equation can be represented as [83, 99, 114, 259, 260]:

$$T_g = T_m - J\dot{\omega} \qquad \text{Equation 3. 37}$$

where T_m represents the torque generated by the turbine rotor, J is the turbine inertia, $\dot{\omega}$ represents the angular acceleration and T_g represents the generator torque (or applied load). Turbine's inertia (J) has been shown to affect the performance of the turbine system within a gusty wind resource [261], with a few studies focused on this area available in literature. Although turbine inertia is incorporated into the VAWT model operation within this study (with inertia J = 9 kgm^2 in the case of variable speed VAWT configuration), Figure 3.15 suggests a decrease in the maximum power coefficient (demonstrated by the C_{pmax}) by 18.5% should the turbine inertia be increased by 20%. Also, a reduction in the inertia (i.e. by 20%) was shown to increase the $C_{pmax}C_{pmax}$ by 21.49%. Further tests to confirm the effect of inertia on the power capabilities of small VAWTs under different operating conditions are suggested for future work, hence not presented herein.

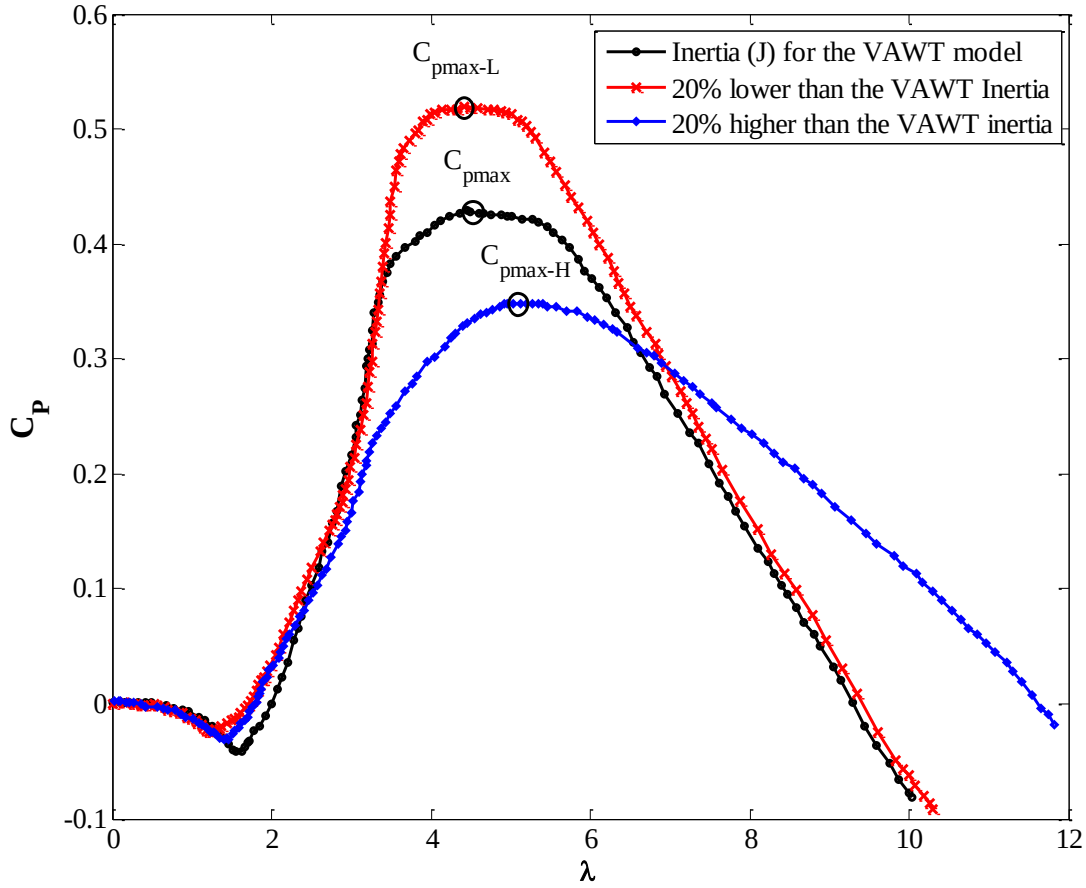

Figure 3. 15: Effect of varying Inertia on Turbine performance; C_{pmax-L} represents the C_{pmax} for turbine operation when the Inertia was reduced by 20%, C_{pmax-H} represents the C_{pmax} for turbine operation when the Inertia was increased by 20%.

Equation 3.37 defines the transient response of the wind turbine to a specific wind resource. However, it is important to note that the numerical model utilizes lift and drag coefficient data valid for steady flow. Thus, transient behaviour in this study is modelled as the infinitesimal variation between two pseudo-steady cases [262].

3.3.4.1 Turbine Self Start

Figure 3.16 demonstrates the performance for the VAWT rotor described earlier, highlighting the change in torque coefficient (described in Equation 3.23) for different tip speed ratios. The average torque coefficients (C_q) for this VAWT design show positive values up to a tip speed ratio of ~ 9, suggesting that turbine self-start would be possible. A closer examination of the VAWT's aerodynamic torque as a function of azimuthal rotor position (for example at λ = 0.2 as shown in Figure 3.17) shows areas with negative torques**.** Accidental self-starts have been

recorded in the past (most notably the unexpected self-start for the case of the Magdalen Islands rotor which eventually resulted in failure [75]). However, regions of negative torque as shown in Figure 3.17, which is in agreement with results from other sitdies focused on optimisation of small VAWT for urban application [75, 263], effectually rule-out a self-starting operational feature for the lift-type VAWT developed within this study.

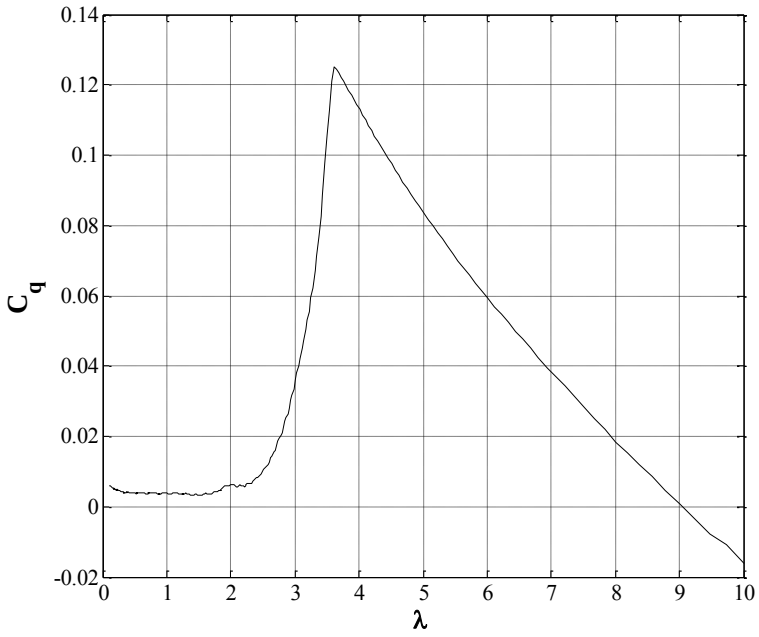

Figure 3. 16: Plot of rotationally averaged aerodynamic torque at different tip speed ratios.

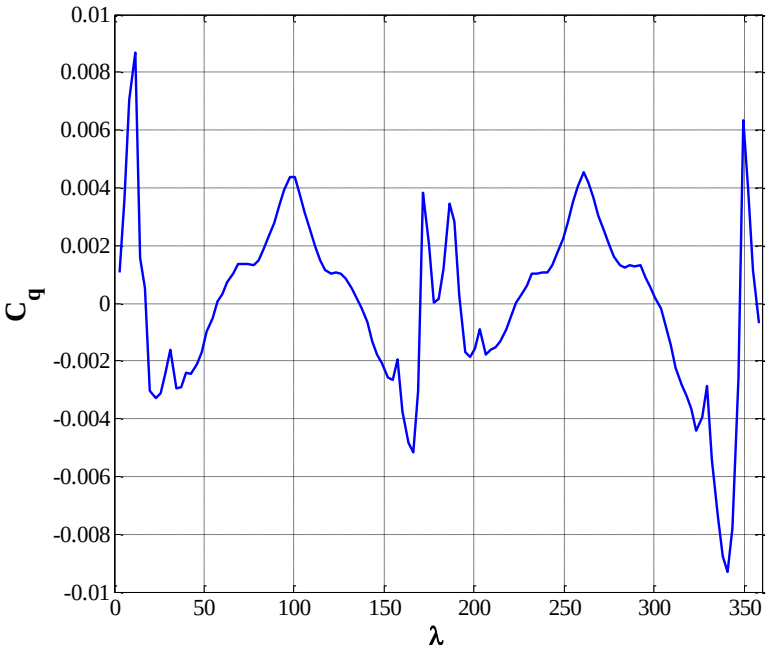

Figure 3. 17: Aerodynamic torque as a function of rotor azimuthal angle.

3.3.4.2 Turbine Control Strategies

Two popular control schemes were considered within this study. These include:

(i) Fixed Speed Control Scheme (FSC): Under this control framework, the angular acceleration is assumed to be zero (i.e. $\dot{\omega}$ = 0). Thus, Equation 3.37 can be rewritten as:

$$T_g = T_m \qquad \text{Equation 3. 38}$$

A perfect FSC turbine model is realised by setting the generator (or applied) torque to exactly the torque generated by the rotor (i.e. aerodynamic torque) hence preventing a change in the rotational speed within the FSC model. The advantages of the FSC model is that the inertial effects of the turbine are not considered and also the effects of time scale on turbine response are not considered (i.e. turbine performance not affected by gust frequency, F_g). Its major disadvantages include inability to modify the system's torque characteristics in order to operate at maximum aerodynamic condition, inability to actively control the turbine system in order to alleviate mechanical loads and improve the power quality of the turbine design while operating within a rapidly fluctuating, complex wind resource, etc. thus making it less suitable to urban wind applications.

(ii) Variable Speed Control Scheme (VSC): This is a popular control design technique widely found in commercial turbine systems. The control considered consists of running the generator such that the turbine system will operate at its peak power producing point (i.e. C_{pmax} as illustrated in Figure 3.8) for any given wind speed. Under this control approach, a standard Region 2 torque control algorithm as described in Refs [83, 264], was employed. Due to its simplicity, this control method was adopted in this study. Unlike the fixed speed control technique, a variable speed control scheme can adjust the rotational speed of the turbine system in order to track the optimum speed as wind speed fluctuates, so as to operate at the peak of the $C_p - \lambda$ curve. The aim is to maximize the power generated for a particular wind speed [265]. Thus, the angular acceleration can be calculated by rewriting Equation 3.37 as :

$$\dot{\omega} = \frac{T_m - T_g}{J} \qquad \text{Equation 3. 39}$$

The generator torque (T_g) is derived from Equation 3.40,

$$T_g = k\omega^2 \quad \text{Equation 3. 40}$$

and the gain k is given as:

$$k = \frac{1}{2}\rho A R^3 \frac{C_{pmax}}{\lambda_{opt}^3} \quad \text{Equation 3. 41}$$

where ρ is the air density, A is the rotor swept area, C_{pmax} is the maximum power coefficient and R is the rotor radius. λ_{opt} is the optimal tip speed ratio at which $C_p = C_{pmax}$. The gain k, as defined in Equation 3.41, is intended to keep the turbine operating at the peak of its $C_p - \lambda$ curve. The turbine rotor torque (T_m) can be calculated using Equation 3.22 or can be rewritten as:

$$T_m = \frac{1}{2}\rho A R^3 \omega^2 \frac{C_{p(\lambda)}}{\lambda} \quad \text{Equation 3. 42}$$

An increase in ambient turbulence intensity results in a corresponding decrease in the optimal operating point of the standard control scheme gain k [264]. Basically, by definition, the local power coefficient is lower or approximately equal to the optimal power coefficient (i.e. $C_p \leq C_{pmax}$). For the purpose of a simple demonstration on how this control strategy works, we will assume the wind speed is constant. When the tip speed ratio is greater than the optimal tip speed (i.e. $\lambda > \lambda_{opt}$), $\dot{\omega}$ will become negative, causing the rotor to decelerate towards $\lambda = \lambda_{opt}$. On the other hand, if the operating tip speed ratio is less than the optimal tip speed ratio (i.e. $\lambda < \lambda_{opt}$), $\dot{\omega}$ will be positive hence accelerating the rotor towards its optimal operating condition (i.e. $\lambda = \lambda_{opt}$) given that

$$C_p \geq \frac{C_{pmax}}{\lambda_{opt}^3}\lambda^3 \quad \text{Equation 3. 43}$$

This principle of changing the rotational speed in a bid to track the optimal operating point (C_{pmax}) is applied within the turbine operation simulated in this study. It is a general consensus that most modelling tools used to determine $C_p - \lambda$ curves for most wind turbines are not perfectly accurate. Hence, control systems designed based on these modelling tools are generally sub-optimal [264]. Even if it is assumed that the gain k was optimal, in reality, wind turbine blades will change over time due to factors such as blade erosion and degradation, bug build-up, etc., thus causing the turbine to perform sub-optimally.

3.3.4.3 Performance analysis of the Vertical Axis Wind Turbine

A list of various certified small wind turbine systems with their technical specifications can be found on the micro-generation certification scheme (MCS) website [190]. For the purpose of this study, a 600 W VAWT system was considered, thus representing a micro-wind turbine system for domestic electricity generation [180]. As stated earlier, the turbine system considered is assumed to be a three straight-bladed NACA0015 VAWT with inertia of 9 kgm^2, rotor diameter and blade height of 1.5 m each and a blade chord length of 0.08815 m. This is simulated in an urban wind resource by using high resolution wind dataset from eight potential turbine sites (as described in Chapters 4 and 5) as inputs. The measured electrical power from the turbine model is related to the measured wind speed with the turbine response equal to the averaging time, averaged over a given burst period (T = 10mins) [45, 266, 267]. Figures 3.18 - 3.19 demonstrate the power outputs of the numerical model employing a very simple fixed-speed and variable-speed control algorithms.

In the FSC operation, the rotor speed is kept constant at different wind conditions thus leading to poor performance under high fluctuating wind speeds. In reality, the rotor speed for the FSC varies very slightly due to the slip in the generator system and when the power generated by the turbine system exceeds its design limits, the generator is shutdown to avoid extra strains on the system. However, various studies have suggested methods of improving the performance of a fixed-speed turbine operation within a built environment [75, 234] which will not be considered within this study. With the VSC system designed to adjust its rotor speed at varying wind speeds in a bid to maintain optimum power generation, it is widely regarded as a better design for urban wind applications [84]. Figures 3.18 and 3.19 demonstrate the performance of the FSC and VSC VAWT systems within a typical suburban/urban site with this specific control observed to show potentials of generating higher power at lower wind speeds than the FSC turbine system if advanced control algorithms were employed. The response time of the turbine output results is 10 s and also demonstrates its ability to respond to turbulent wind resource. However, for the purpose of simplicity, the cut-in wind speed of the VSC system within this study is assumed to be 3 ms^{-1}, which is assumed the minimum cut-in wind speed for most small-scale VSC VAWT systems (See Ref [190]). Unlike the FSC system, the VSC VAWT system leaves room for design improvements in order to achieve system optimization thus resulting to better power outputs while operating in rapidly fluctuating wind environment. This makes it better suited for urban wind applications. Hence, for the purpose of turbine performance analysis presented in Chapter 6, the VSC design presented herein is adopted.

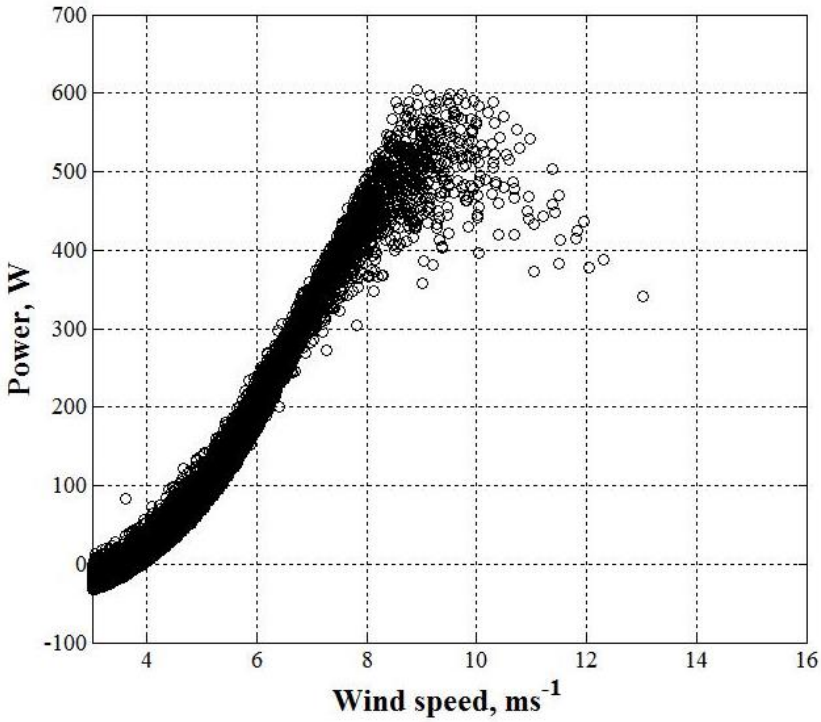

Figure 3. 18: Performance of the VAWT FSC numerical model at different wind speeds for all 8 sites. Dots represent 10 min burst periods.

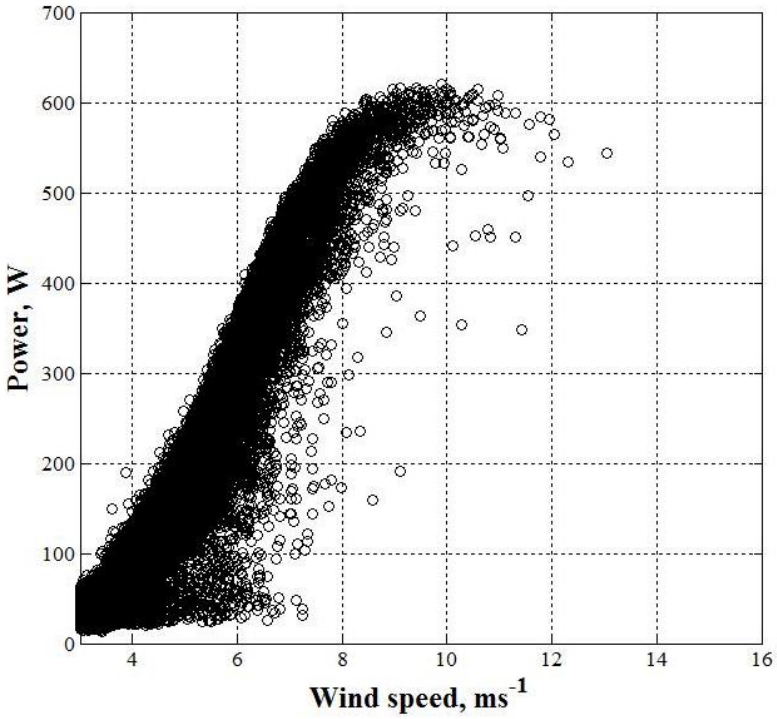

Figure 3. 19: Performance of the VAWT VSC numerical model at different wind speeds for all 8 sites. Dots represent 10 min burst periods.

CHAPTER 4

4 Urban Wind: Characterization of Useful Gust and Energy Capture

4.1 Introduction and Objectives

Small-scale wind turbine operations within a built environment are exposed to high levels of gusts and turbulence compared to flows over less rough surfaces. There is therefore a need for such systems to not only cope with, but to thrive under such fluctuating flow conditions. This chapter focuses on the characterization of typical urban wind resource based on data collected at two urban roof-top locations considered as potential turbine mounting sites within a built environment using high resolution anemometers. The additional energy resource available within high frequency gusts is quantified and is linked to standard measures of turbulence such as turbulence intensity. The effect of averaging time on the available wind power is also highlighted thus demonstrating that the frequency of raw data must be well matched to potential turbine response times in order to make accurate assessments of the excess energy available to a particular turbine within gusts. The sensitivity of this "additional" wind energy to averaging time interval is also explored, providing useful information for the design of gust tracking or dynamic control algorithms for small-scale turbines. An analytical model for predicting the excess energy and/or the total kinetic energy available at a potential turbine site is also proposed in this chapter by assessing the relationship between turbulence intensities and the excess energy available within a built environment.

The structure of the chapter is as follows: Section 4.2 introduces the concepts of gust tracking and gust efficiency and their importance to turbine operation. Section 4.3 presents methods for the characterization of additional energy available within urban wind such as the gust energy coefficient (GEC), and excess energy content (EEC) using high resolution wind measurements from different sites, along with a brief description of the selected urban sites for analysis and data processing methods. Section 4.4.1 presents results obtained from the two approaches in evaluating the additional energy available at these urban sites. The effects of averaging/turbine response time on potential turbine power output are discussed in Section 4.4.2. Here, relationships are drawn between turbulence intensity and excess energy content, and an analytical model for predicting EEC values within built-up areas is proposed. Finally the main conclusions are presented in Section 4.5.

4.2 Background

As discussed in Chapter 2, the wind resource over built environments is characterized by fluctuating, turbulent winds. This could be attributed to various factors like high surface roughness, the interaction between incoming flows and complex local building structures, and atmospheric instabilities caused by local heat sources [48]. The resulting complex, gusty urban wind rapidly changes in both magnitude and direction over a range of length and time-scales which may vary according to the incoming wind direction and therefore upwind roughness characteristics. An example of the gusty nature of real world urban wind speeds is illustrated in Figure 4.1 with the wind speed varying greatly between 0.4 ms^{-1} and 14.5 ms^{-1} within a very short time. These abrupt changes are experienced between points 1 and 2 (a jump in speed from 2.7 ms^{-1} to 13.2 ms^{-1} in $\leq$ 20 s) and points 3 and 4 (a jump from 2.8 ms^{-1} to 14.5 ms^{-1} in $\leq$ 40 s), and are in contrast with observations from coastal/open sea terrain [33] or rural terrain [268]. In this case, they result from increased turbulent drag caused by the high terrain roughness present within built environments [47], rapid changes in flow direction around buildings/structures, and the formation of vortices [144] leading to regions of both flow acceleration and stagnation. These vortices can be influenced by a number of factors ranging from the effect of building area density to the substantial influence of roof heights and shapes on the flow structure within the built environment.

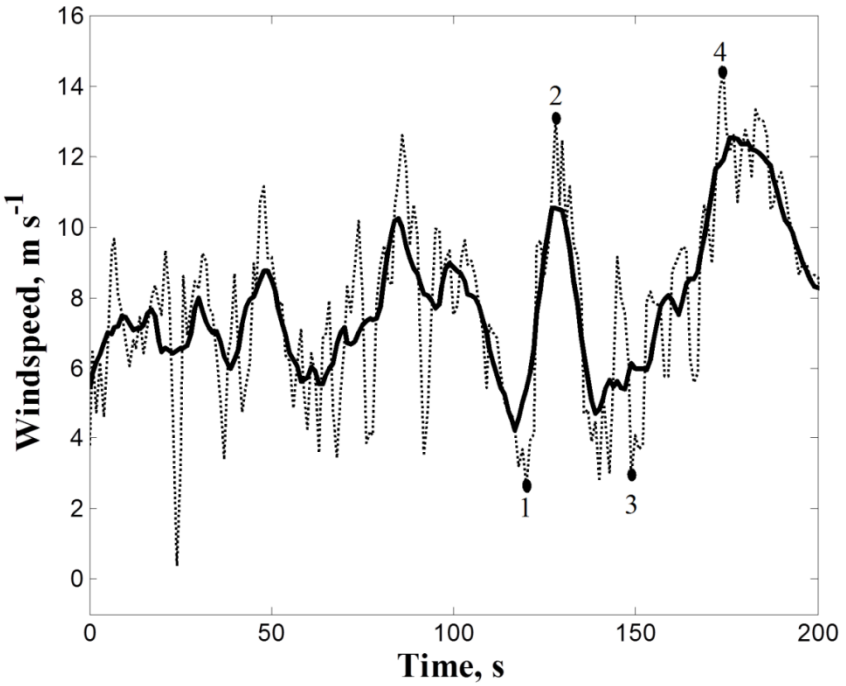

Figure 4. 1: Real world measured urban wind resource at a Manchester roof-top site illustrating a period with high fluctuations of the urban wind resource; the 1 Hz data (dotted lines) and 0.1 Hz data (solid lines).

These complex attributes of the urban wind resource have strong consequences on energy generation. All else being equal, Bertenyi *et al* [12] suggest that a turbine system could experience a 60% loss or gain in power generation if relocated from a coastal/open sea site to an urban environment whereas McIntosh *et al* [234] highlighted the inability of rural-specific turbine rotor designs in tracking the high fluctuations present in the gusty urban wind resource. However, there exists a significant amount of energy stored within the higher frequency components of these gusts (as illustrated in the micrometeorological region in Figure 2.1).

Hence the possible extraction of this energy through the advanced turbine controls discussed in Chapter 3 may partially offset the penalty of wind turbine systems operating in the reduced mean wind speeds experienced close to urban surfaces. However, designing effective controls relies on a detailed understanding of the nature of the available wind resource in order to cope with rapid changes in wind speed (as shown in Figure 4.1) and the generation of rapid torque changes [259]. The assessment of wind turbine system performance within built environments encounters high levels of uncertainty due to unavailability of high temporal resolution monitoring of wind speeds within urban/suburban regions [269]. Computational models of air flow over cities, as discussed in Chapter 2, could potentially provide additional information on wind characteristics and may have the advantage of providing wide spatial coverage

compared to a limited number of measurement sites [48, 270]. Hence it is of interest to determine whether outputs from such models (e.g. mean wind speeds and turbulence levels) could be used to assist in the prior assessment of turbine performance and in turbine system design. For this reason, this chapter focuses on the assessment of turbulence characteristics within urban areas and how measures of turbulence may be used to determine how much energy is available to a well-controlled wind turbine.

It is important that a turbine system to be sited within built environments not only copes with, but thrives in this complex urban wind resource. This may involve the employment of gust tracking technologies in a bid to ensure that the turbine operation is maintained within its region of peak aerodynamic efficiency [12], thus maximizing energy extraction as wind speeds fluctuate. As stated in Chapter 2, the efficiency of a turbine system is commonly characterised by its power coefficient C_p [271-273]. Figure 4.2 presents a power coefficient curve for a vertical axis QR5 wind turbine model as a function of tip speed ratio λ, as measured in a full-scale wind tunnel test by Quiet Revolution [274].

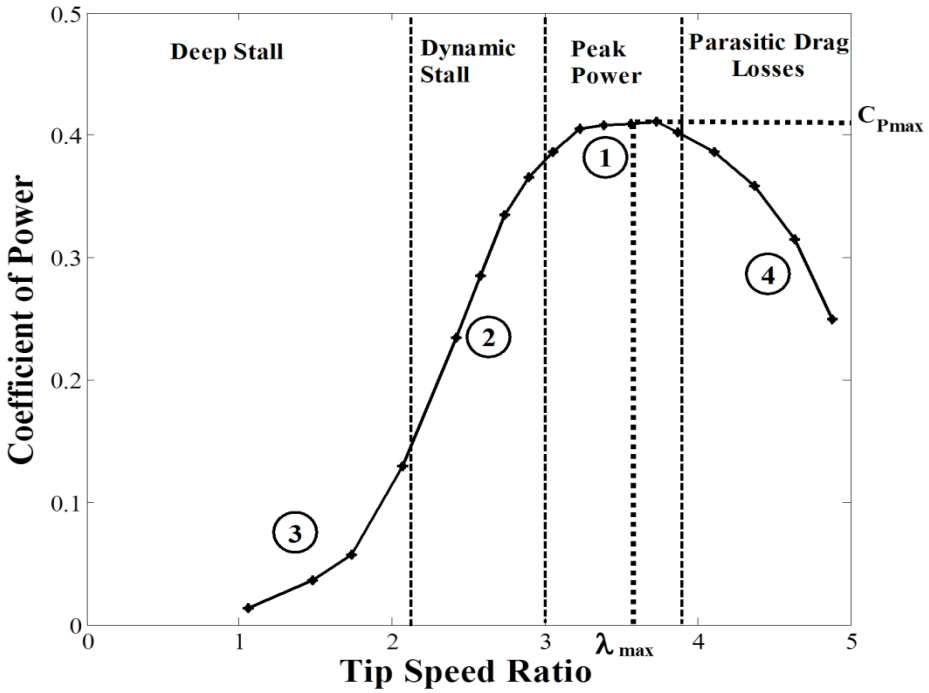

Figure 4. 2: Power coefficient for a QR5 VAWT model as a function of non-dimensional tip speed ratio, measured under a full-scale wind tunnel test by Quiet Revolution highlighting the maximum power coefficient ($\boldsymbol{C_{pmax}}$) and maximum tip speed ratio ($\boldsymbol{\lambda_{max}}$) (Adapted from [12]).

Although the power curve shown in Figure 4.2 is defined for steady flow conditions, the shape of performance curves in unsteady winds have been shown to be similar [234]. Hence the figure serves to illustrate the region of tip speed ratios at which maximum aerodynamic efficiency and therefore peak power can be achieved. Under real world gusts, it is quite possible for the turbine to move from operating at point 1 (peak power) to points 2, 3 or 4 over short time-scales (seconds) if the rotational speed of the turbine is not adjusted.

For better performance in a gusty wind resource, the turbine rotational speed needs to be constantly and precisely adjusted in order to enable the turbine system to operate at its peak aerodynamic efficiency (as shown by C_{pmax} in Figure 4.2). Failure to do so could result in a significant loss in aerodynamic power, especially in situations where the turbine experiences a large gust and its tip speed ratio falls into the region of deep stall [234]. Here, the energy losses and low aerodynamic torque experienced may not be sufficient to allow acceleration back to the turbine's correct speed. Tracking such gusts and avoiding deep stall involves specific design conditions. These include low turbine inertia, real-time operating conditions (as in the case of feedback controls), and a power electronic architecture which allows for active control [275].

While studying flow across buildings/structures within built environments, Cook [276] observed structure-generated turbulence which resulted in the power spectral density containing an additional peak at a higher frequency (i.e. ≥ 0.1 Hz) than typical boundary layer turbulence. The scale of this peak was influenced by the size and shape of inherent structures within a built environment and the frequency range of its fluctuations varied across different sites. Ideally, gust tracking designs would be able to capture all the power contained within this additional peak up to very high frequencies. However, cost limitations may prevent the design of turbines and control architectures which are able to capture this full range of frequencies. In addition, where wind data is used as input to feedback control models, it is usually filtered to remove fast transients which could de-stabilise the selected control model (e.g. simple proportional control [234]). It is therefore of interest to consider different cut-off frequencies which may represent different levels of turbine responsiveness and to evaluate the extent of excess energy which may be captured for the different cut-offs. The upper limit of the frequency range (cut-off frequency F_C) selected is represented in here as the gust frequency (F_G).

The simplest and most popular method of cut-off frequency selection is made by using a low pass filter to extract the lowest frequency components of the wind input. This represents the gust frequency at which the maximum amount of filtering retains a targeted percentage of power content in the turbulent wind within a given period. The targeted power content

percentage tends to vary with different small-scale wind turbine manufacturers as a result of their different design objectives (e.g. 99% below $F_C \approx 0.1$ Hz [234], 98% below $F_C \approx 0.5$ Hz [277]). The selection of different cut-off frequencies tends to affect the performance of the controller as well as the turbine output variables. However, the choice of employing a wind turbine system with little or no gust tracking control within the built environment would entail the system operating at a much lower F_C. This results from the system's time lag which depends on the turbine inertia, controller and aerodynamic response.

The cut-off frequency has been used in this chapter to define the characteristic gust frequency, with F_C employed in averageing the wind input data. A snap shot of the effects of filtering data was shown in Figure 4.1 with an F_C of 0.1 Hz. The averaging time duration ($T_C = 1/F_C$) is an important factor in gust tracking, with the influence of short fluctuations on the turbine operation of a given turbine dependent on the magnitude of the T_C used in averaging the incoming wind speed, turbine RPM and power. T_C therefore varies with different turbine sizes and control models. The analysis of turbulence data at the potential mounting site therefore needs to reflect these characteristics if the excess energy available is to be properly assessed. Various turbine control techniques have been addressed in the literature with the optimum power/torque tracking technique a popular control strategy in achieving optimum power generation [278]. For most control techniques, to run the turbine optimally requires obtaining the $C_p - \lambda$ dependency of the specific turbine and/or the wind speed in calculating the desired rotor speed needed to vary the generator speed [279]. The difficulty and high cost of accurate measurements of urban wind (as discussed in Chapters 2 and 3) and the uncertainty surrounding the application of the turbine manufacturer's $C_p - \lambda$ curve at different turbine sites give rise to errors which will strongly influence the turbine controls. Maximum power point tracking (MPPT) algorithms have been employed in various ways to circumvent these errors but will add to the overall cost of the system [280-282]. In order to evaluate the performance of VAWTs in unsteady winds and the cost effectiveness of control methods, the total energy available to the turbine needs to be estimated and it is here that this Chapter is focused.

Assumptions

The effect of wind direction on the turbine (VAWT) performance within an urban environment was assumed to be negligible [275]. It is also assumed that in an idealised steady wind environment, the GEC and EEC would be 1.0 and 0% respectively [12]. This indicates that the

total integral energy within the sample time period is reflected by the energy derived by employing the mean wind speed within the same sample time period.

4.3 Results and Discussion

4.3.1 Effect of $T.I.$ on power and EEC

Since $T.I.$ is a more commonly presented statistic describing the level of turbulence in built-up areas, it is first interesting to evaluate whether a relationship exists between $T.I.$ and available excess energy. The monthly average wind speed values for the sites analysed are shown in the bottom pane of Figure 4.3. The minimum monthly average wind speed value of 2.1 ms^{-1} was observed in December, while the maximum monthly average wind speed value of 5 ms^{-1} was observed in May, both at the Manchester site. The yearly average wind speeds were found to be 3.3 ms^{-1}, 2.8 ms^{-1} and 3.5 ms^{-1} at the Unileeds (H1 and H2) and Manchester sites respectively, with the longer term (5 years) average values being somewhat higher at 3.74 ms^{-1}, 3.15 ms^{-1} and 3.66 ms^{-1} at each site respectively. Therefore, the sites used in this paper can be considered to possess a low to medium quality wind potential. In the top pane of Figure 4.3, two methods of calculating the power density are shown. The dashed lines correspond to the use of 10 minute averages of wind speeds for the power calculations and the solid lines correspond to the average power calculations at 1 s intervals. The solid line therefore represents the maximum power available if all the energy in the high frequency gusts was to be captured by the wind turbine. There is clearly a marked difference between these two approaches, particularly for the Manchester site which exhibits the highest turbulence intensities for most of the year. Of the two Leeds sites, H2 was shown to exhibit higher turbulence intensities, which is perhaps expected since this mast height is closer to the roof than H1. In addition to generally higher turbulence intensities, higher average wind power is also observed all year round at the Manchester site (excluding the months of November and December) mostly likely due to the fact that it is a tall building (49 m) compared to the local mean building height (14.2 m). If the additional energy in the high frequency gusts was able to be captured at this type of site, it may become viable for turbine siting. In Section 4.4.2, we evaluate how much of this energy may be captured for different turbine response times as represented by T_C.

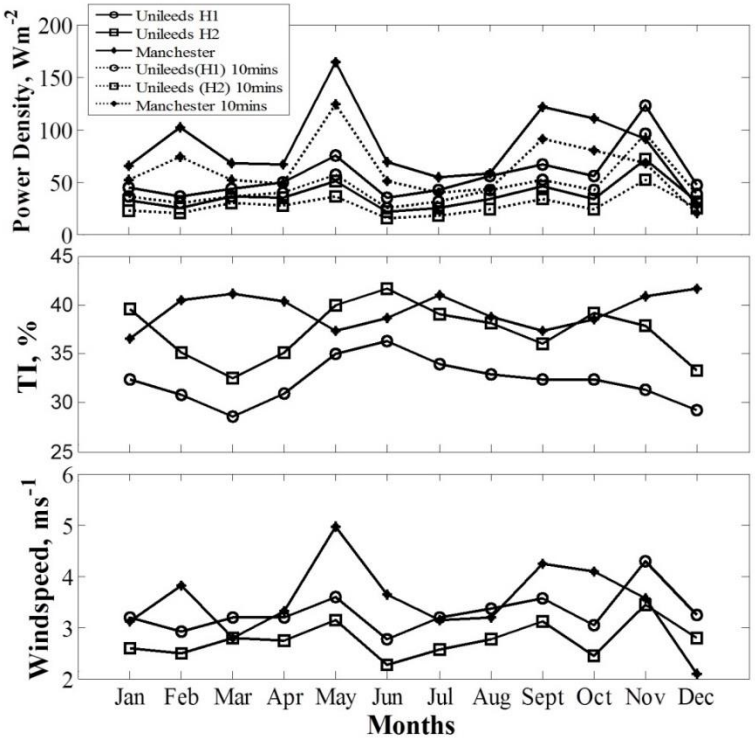

Figure 4. 3: Average monthly power (top), *T.I.* (middle) and mean wind speed (bottom) values at the two sites for a one year data at a sampling frequency of 1 s (solid lines) and an averaging time of 10 mins (dotted lines).

Based on the assertion that the output variables of a VAWT are not affected by rapid changes in wind direction typical of an urban environment [275], it is important to investigate the degree to which the power output is influenced by $T.I.$ at the sites analysed. Methods for estimating the potential energy capture at a specific site by incorporating a measure of turbulence (e.g. $T.I.$) are used by some experts within the wind industry [180]. In addition, $T.I.$ is likely to be a model output when using, for example, computational fluid dynamics, CFD [283, 284] to investigate potential turbine sites. It is therefore useful to investigate how excess energy varies with $T.I.$ thus facilitating the use of such CFD models in the design of gust tracking solutions.

A measure of the influence of $T.I.$ can be highlighted by binning the wind power curve according to different turbulence intensity bands, as shown in Figure 4. 4. This is a common approach employed by most practitioners within the wind industry and provides relevant information as to the turbulence level at which maximum power is observed and beyond which a decline is noticed in the power curve. It is important to note that power curves produced by identical turbines at different sites may lead to different results due to their strong dependence

on the local $T.I.$ distribution, thereby making measured power curves limited in terms of being comparable and transferrable [285].

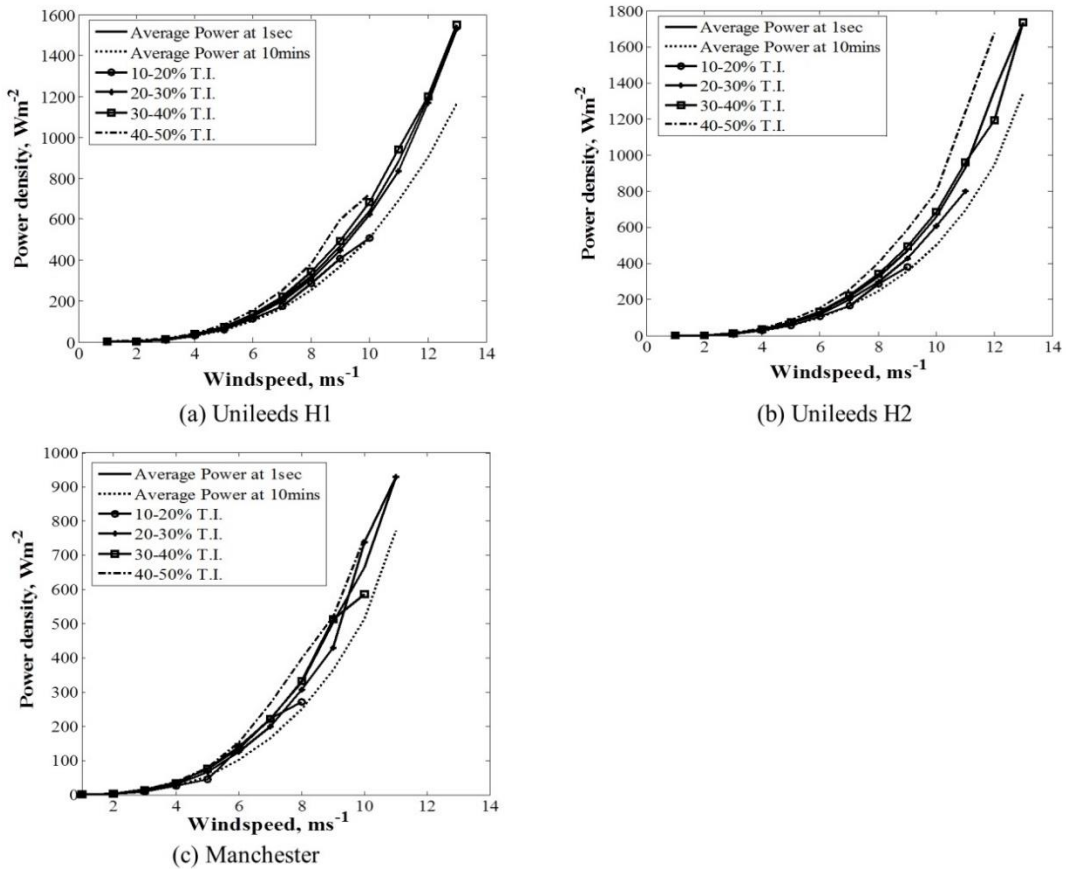

Figure 4. 4: A comparison of the average power curve to power curves sorted by bands of $T.I.$ for one year dataset parsed at 10 min bursts at (a) Unileeds (H1), (b) Unileeds (H2) and (c) Manchester sites.

Figure 4.4 highlights this point, by first showing how different the calculated power curves can be depending on whether 1 s or 10 minute averages in wind speed are assumed. Also shown is the increase in power (at 1 s) with increasing $T.I.$ at both sites with a net reduction in power experienced below $T.I.$ values of 50% at Unileeds (H1 and H2) and Manchester respectively compared to the average power available over all frequencies. The monotonic increase in power with increasing $T.I.$ bands suggests the potential of the turbine for extracting at least a portion of the additional energy observed within these gusty wind resource sites. Implementing fast response controls however, will entail additional capital costs, and hence the level of turbulence experienced at proposed installation sites may give useful information for appropriate turbine design by answering the question: how much excess energy is there worth capturing?

Figure 4.5 shows frequency plots for each site for different bins relating to $T.I.$. It therefore provides relevant information as to the level to which enhanced energy extraction is required within both sites. At the selected sites, the $T.I.$ is almost never less than 10% and is most frequently between 30-40%. A turbine which was able to effectively capture the high frequency energy under such conditions would be able to access an average of over 30% more power than would be estimated using the mean wind speed alone under these conditions as suggested in Table 4.1. For coastal, open country and rural sites where $T.I.$ is more frequently below 20% [22, 45], the average additional excess energy would be much lower (of the order of 10%).

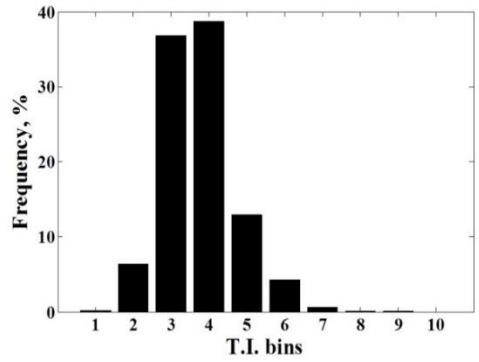

(a) Unileeds H1

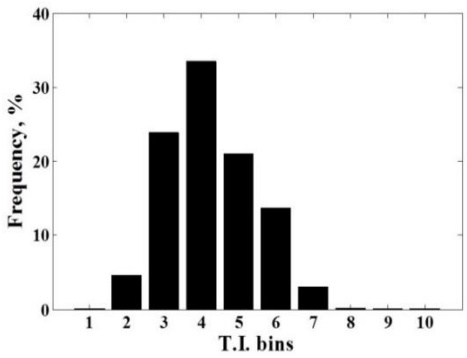

(b) Unileeds H2

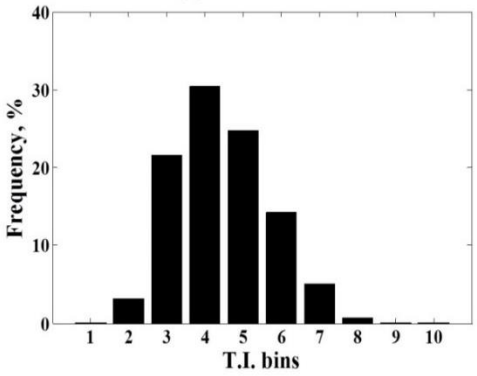

(c) Manchester

T.I. bins	T.I. Range (%)
1	0 – 10
2	10 - 20
3	20 – 30
4	30 – 40
5	40 – 50
6	50 – 60
7	60 – 70
8	70 – 80
9	80 – 90
10	90 – 100

Figure 4. 5: The $T.I.$ distribution for a one year at both sites analysed, for which the power curves are plotted in Figure 4. 4 at = 1 s.

Table 4. 1: Percentage increase across the turbulence intensity bins from the Average Power ($\boldsymbol{P_{10mins}}$) calculated from mean wind speed at 10 mins (as shown in the power plots in Figure 4.4)

Sites	$\boldsymbol{T.I.}$ **Bins**				$\boldsymbol{P_{1s} - P_{10mins}}$
	10 - 20%	**20 - 30%**	**30 - 40%**	**40 - 50%**	
Unileeds(H1)	6.97%	25.77%	34.13%	51.73%	29.79%
Unileeds(H2)	8.04%	18.64%	32.36%	60.01%	33.63%
Manchester	16.57%	25.63%	28.54%	49.55%	28.83%

In a different approach, the EEC, as defined in Section 3.1, quantifies the "excess" energy present in the gusty wind resource. Results from both sites show a yearly average additional energy of 35.3%, 50% and 53.4% at the Unileeds (H1 and H2) and Manchester sites respectively, for a response time of 1 s. An illustration of the EEC at the two sites for a year's wind input is shown in Figure 4.6 and Figure 4.7, with Unileeds (H2) and the Manchester sites showing significantly higher values of EEC. These sites are 6 and 5 m above the roof respectively compared to 10 m for H1, and both sites showed higher $T.I.$ values throughout the year than H1 (see Figure 4.3). Figure 4.7 shows a strong dependence of excess energy on wind speeds as seen in previous studies [12], with strong dependency of turbulence intensity on wind speed also observed (see Figure 4.8), hence suggesting a relationship between the EEC and the turbulence intensities within a given suburban or urban site. Consequently, this suggests the possibility of estimating the additional energy available within a potential turbine site from the knowledge of the $T.I.$ values within the specific site. This, however, will be discussed further later on.

A summary of the mean value of EEC at various sites from both previous and the present studies, categorised according to different levels of terrain roughness, is shown in Table 4.2. The low turbulence sites (i.e. coastal sites) suggest a minor margin of 3.3% of excess energy while the high turbulence sites (i.e. urban environments) suggest a significant margin of above 23% of excess energy available. What is clear from the current work is that in addition to the local roughness parameters, for roof mounted sites it is also important to consider the height above roof when estimating excess energy available.

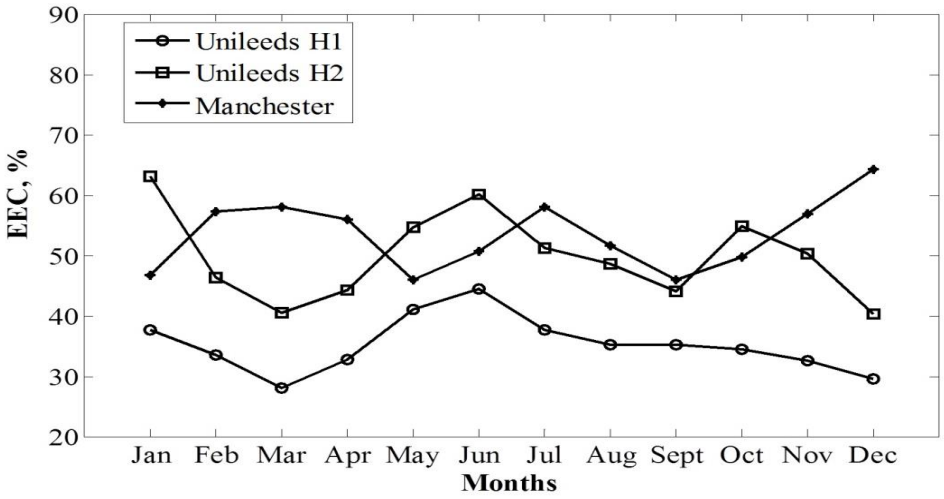

Figure 4. 6: Plot showing the average monthly *EEC* values at the two sites across the year at T_C = 1 s.

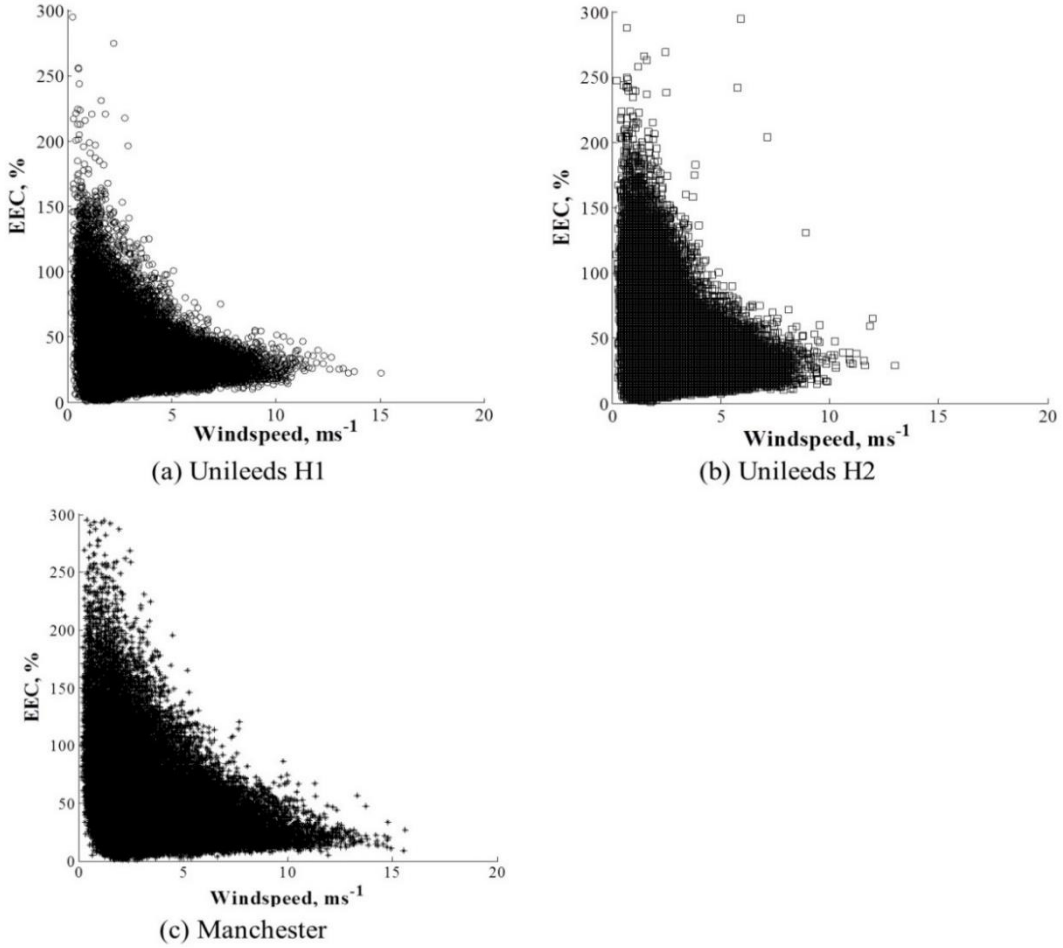

Figure 4. 7: *EEC* at T_C = 1 s for a one year wind input at both sites (Unileeds (H1 and H2) and Manchester). Each point represents 10 min bursts, illustrating the expected potential contribution of gust tracking within both sites.

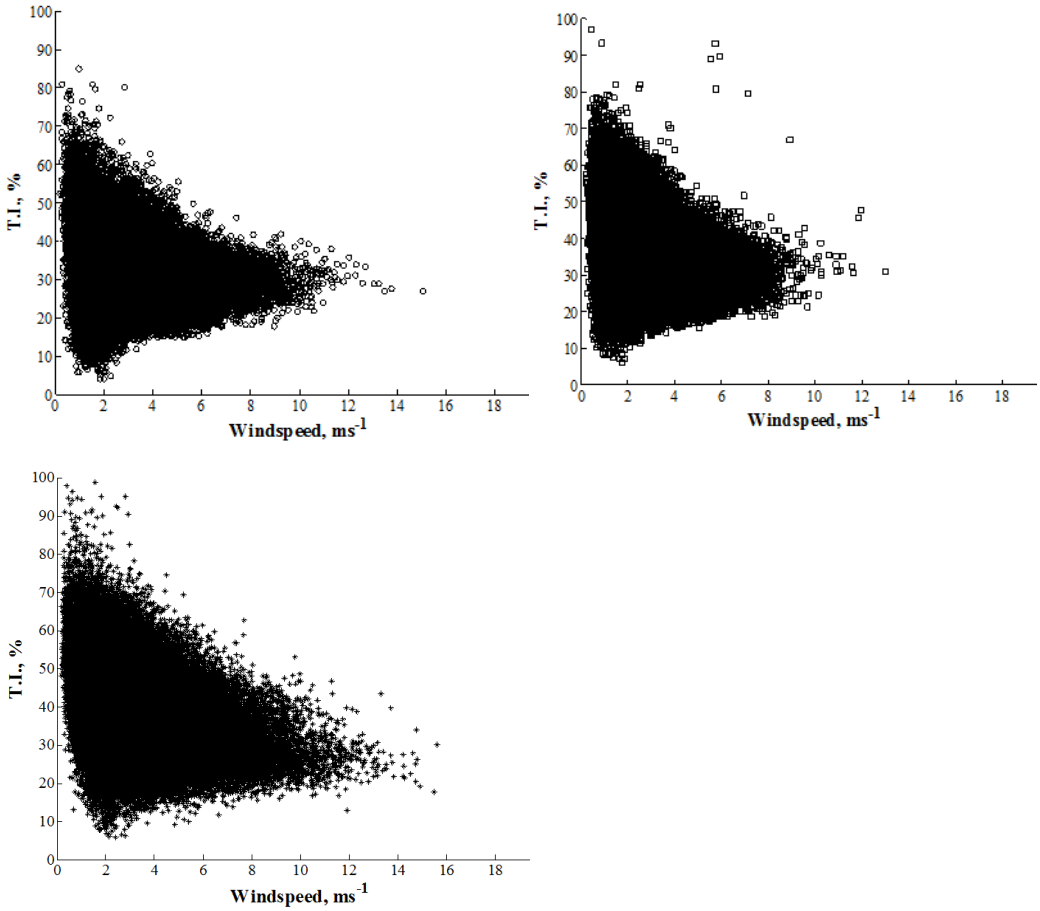

Figure 4. 8: *T.I.* at T_C = 1 s for a one year wind input at both sites (Unileeds (H1 and H2) and Manchester). Each point represents 10 min bursts.

Table 4. 2: A summary of the EEC from some analysed turbine sites with their relative roughness heights (adapted from [12]) and urban sites selected in this paper.

SITE DESCRIPTION	EEC (%)	z_o (m)
Coastal site	3.3	0.005
Open country	16.1	0.05
Semi Urban	22.7	0.2
Urban	> 23	> 0.7
Unileeds (H1)	35.3	1
Unileeds (H2)	50	1
Manchester	53.4	0.9

Thus, from the results presented so far in Section 4.3.1, the two approaches used in evaluating the available "excess" energy at both sites highlight the presence of a sizeable quantity of

additional energy in the gusty urban wind. This could assuage the uncertainties involved in wind assessment within built environments as well as encouraging gust tracking solutions.

4.3.2 Effect of T_c on power and EEC

The average wind speed across the two sites in a year was observed to be greater than 3.1 ms^{-1} and the potential maximum cut off frequency (F_C) likely to be less than 1 Hz (corresponding to the maximum resolvable response frequency of the turbine). Thus, dimensional reasoning, as shown in Equation 4.1, dictates that the minimum length scale (L_u) corresponding to the characteristic maximum gust frequency (F_G) employed in this study is approximately larger in magnitude than the diameter of a small-scale VAWT turbine (e.g. the QR5 with diameter – 3.1 m [275]).

$$L_u = \frac{\bar{V}}{F_c} > D_T \qquad \text{Equation 4. 1}$$

where D_T is the diameter of the turbine.

This means that frequencies, F_C, and/or their corresponding averaging time-scales, T_C, should be less than 1 Hz to be physically resolvable by the turbine. The estimated small-scale wind energy capture for an urban site through a turbine will depend on the turbulence characteristics of the site (measured by $T.I.$) and the response characteristics of the turbine system. T_C characterises the turbine delay in response due to the difference in inertia of the turbine blades and generator (which will depend on turbine size and weight) and the control system architecture [286]. Therefore a range of possible values for T_C could be present for different systems. We present here two case studies and their effects on average available power and EEC.

Case 1 (Tb1): For the first case, the T_C employed (T_C = 10 s) corresponds to the shortest averaging time for anticipated small-scale VAWT response characteristics as suggested in [286].

Case 2 (Tb2): Case 2 represents a VAWT with a much higher system response time (T_C = 60 s), where $F_C << F_G$. This corresponds to the averaging time used in measuring and subsequent data analysis for wind turbines with rotor diameter less than 16 m as described in the relevant standard, IEC 61400 – 12 – 1 (see Annex H of IEC 61400 – 12 – 1 [45])**.**

With the 10 s and 60 s averaging imposed at the two sites we examine the loss in average power and EEC compared to a maximum response frequency of 1 Hz, as shown in Figure 4.9.

Tb1 and Tb2 experience a lower average power loss at Unileeds (H1) as compared to other sites. This may be as a result of reduced blockage and wake effects at the mast height of 10 m above roof at the Unileeds site, and the relatively lower turbulence levels compared to sites nearer the roof (see Figure 4.3). At Unileeds (H1), Figure 4.9 suggests that Tb1 would experience a maximum loss of approximately 6.93% of the available average wind power while Tb2 would experience a maximum power loss of 17.85%. Therefore, the probable increase in cost of a faster responding control system may be easily offset by its potential to capture more energy available in the gusts. A summary of the percentage gain in power available to Tb1 and Tb2 is shown in Table 4.3. Regarding the EEC available at both sites, Figure 4.9 shows that increasing T_C tends to reduce the possible additional energy available, with gust tracking solutions expected to have relatively greater impact at lower mast heights, where $T.I.$ levels are likely to be higher.

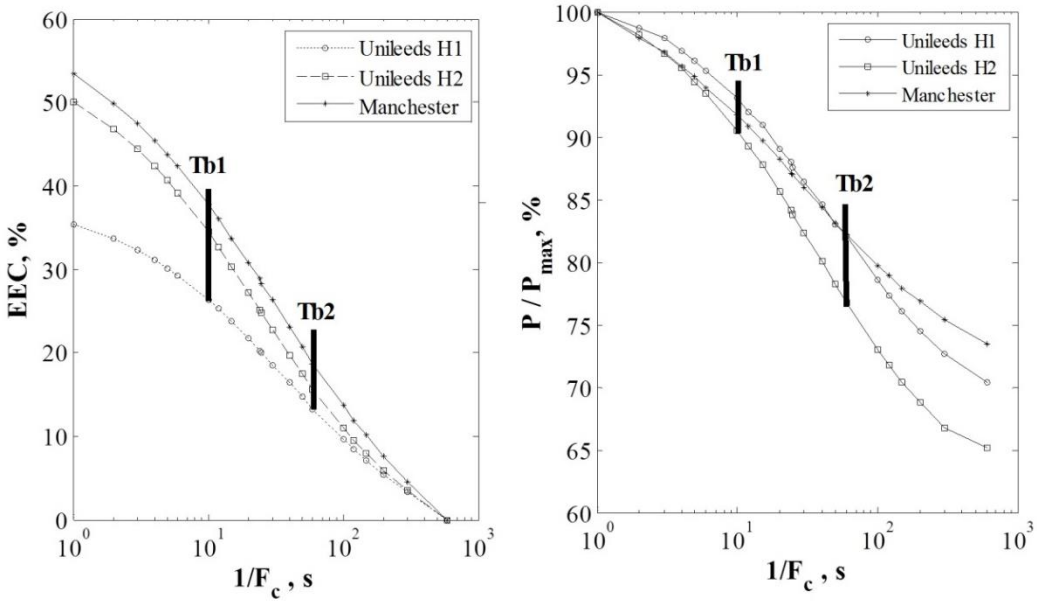

Figure 4. 9: Effect of change in T_C on average *EEC* (left) and wind power (right) at Unileeds and Manchester highlighting power and energy gain with decreasing averaging time.

Table 4. 3: Summary of percentage loss in power deduced from Tb1 and Tb2 operation from assumed maximum operating frequency of 1Hz at both sites for a year.

SITES	TURBINE CONFIGURATIONS	
	Tb1	**Tb2**
Unileeds (H1)	6.93 %	17.85%
Unileeds (H2)	10.68%	23.21 %
Manchester	8.21 %	17.78%

The turbulence spectrum and the location of the turbulent energy peaks will be site dependent and hence large differences may be observed with the use of different time-resolution of the data (T_C) when calculating $T.I.$ at a given site. In addition, when trying to relate the excess energy that may be available to a specific turbine, the use of an appropriate value of T_C is required in order to reflect the potential response time of the turbine. Figure 4.10 demonstrates the impact of increasing T_C on average power, EEC and $T.I.$ at the Manchester site (in this case, $T_C \approx 1/F_C$). Increasing T_C results in decreasing $T.I.$ and decreasing average power and EEC, and vice versa. It is therefore interesting to explore whether, if appropriate averaging times are chosen whether a strong relationship exists between $T.I.$ and EEC.

Such a relationship is demonstrated in Figure 4.11 where EEC values for Leeds (H1 and H2) and Manchester sites are plotted against the equivalent binned values of $T.I.$ for several values of T_C. The figure shows that all the data lie close to a best fit curve which was determined to be a cubic function using a least squares error approach within MATLAB's best fit tool. Thus, EEC values were approximated by an empirical relationship given by the following equation:

$$EEC = 2.2663B^3 + 21.53B^2 + 59.411B - 50.177 \qquad \text{Equation 4. 2}$$

where

$B = (T.I. - 39.913)/21.655$.

with a correlation coefficient value (R^2) of 0.9986. The coefficient was calculated based on the EEC values from site observations (as shown in Figure 4.11), using MATLAB's fitting tool. The high correlation coefficient value (R^2) indicates a good agreement between EEC values from site observations and predicted values.

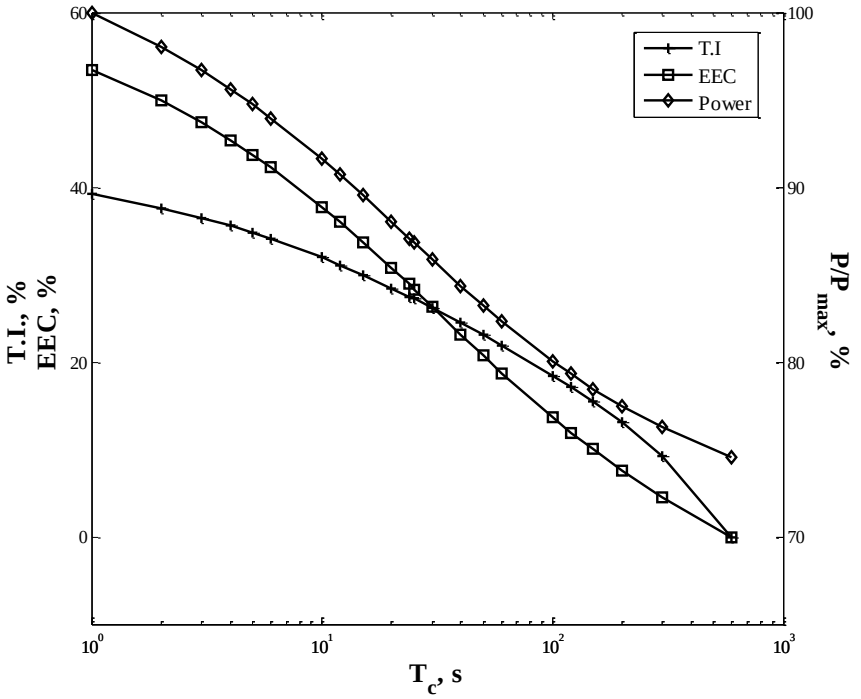

Figure 4. 10: The relationship between average power, *EEC* and *T.I.* with averaging time for a year at the Manchester site demonstrated.

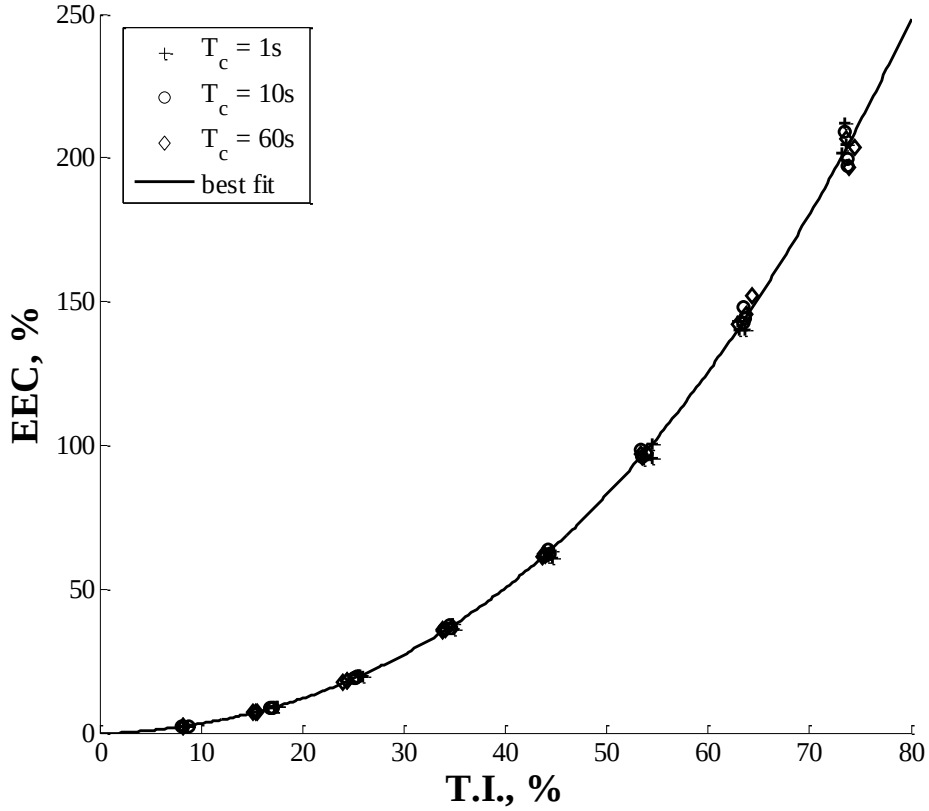

Figure 4. 11: The relationship between *EEC* and *T.I.* with averaging time at both sites.

In assessing the performance of the EEC prediction model given in Equation 4.3, the mean percentage error (MPE, as defined in Equation 4.9) was also used:

$$\text{MPE} = 100 \times \frac{1}{n} \sum \frac{\left| EEC_{obs} - EEC_{pred} \right|}{|EEC_{obs}|} \qquad \text{Equation 4. 3}$$

where n is the number of data points, EEC_{obs} represent the EEC values obtained from observations and EEC_{pred} represent EEC values obtained from Equation 4.2.

Table 4. 4: Mean percentage errors (%) compared over 3 test sites at different T_C using the EEC analytical model.

T_C	**Sites**		**MPE for the different $T.I.$ Bins (%)**							
		T.I.	**0-10**	**10-20**	**20-30**	**30-40**	**40-50**	**50-60**	**60-70**	**70-80**
1s	Unileeds(H1)		8.740	1.035	2.634	0.866	1.447	1.196	0.261	1.611
	Unileeds(H2)		9.780	1.580	2.976	1.499	0.089	0.402	2.641	5.456
	Manchester		11.50	1.485	1.643	3.871	4.831	4.132	1.944	1.506
10s	Unileeds(H1)		8.719	1.429	2.803	1.386	0.349	0.354	1.006	2.507
	Unileeds(H2)		8.796	1.742	3.170	2.373	2.491	3.295	4.129	1.025
	Manchester		9.444	0.251	0.374	0.785	1.177	0.057	0.528	4.419
60s	Unileeds(H1)		8.141	1.626	2.863	2.141	0.835	0.083	3.854	1.777
	Unileeds(H2)		8.366	1.757	3.271	3.151	2.320	2.038	2.245	3.547
	Manchester		8.354	1.195	1.841	0.921	0.336	0.396	1.337	2.734

Table 4.4 compares the MPEs for the EEC model over the 3 test sites at different T_Cs. Model results showed very low error values over the 3 test sites with the largest errors observed within the lowest $T.I.$ bin (i.e. $T.I. = 0 - 10\%$). This suggests that for the sites studied, the EEC available to a particular turbine could be estimated from knowledge of the turbulence intensities so long as the appropriate response time of the turbine was represented by the use of an appropriate value for T_C when calculating $T.I.$

4.4 Summary

High temporal resolution wind measurements from 3 potential urban roof-top sites have demonstrated the gusty and turbulent nature of the urban wind resource and the potential advantages of utilising turbine control systems which are designed to capture the energy available in these gusts. Results demonstrated elevated available additional energy (high EEC) under conditions of higher $T.I.$ values, suggesting that accurate modelling of turbulence intensities could inform calculations of the additional energy available if optimal gust tracking solutions were found. The levels of excess energy were determined not only by local roughness characteristics but also by the above roof elevation of the sites. For short mast roof-top applications, gust tracking could be particularly advantageous. Available power and EEC are shown to decrease with increasing averaging time (T_C) related to the response time of the VAWT, suggesting that faster system response times may be essential to capture the energy within the gusts. Twice the excess energy was available with a 10 s response compared to 60 s. Wind resource and energy systems assessment based on turbulence intensities was shown to vary with different values of T_C illustrating the importance of specifying the data resolution when quoting $T.I.$ values and properly matching T_C to the expected response time of the proposed turbine. Finally, an analytical model for estimating the excess energy available at a potential urban site was proposed by assessing the relationship between $T.I.$ and EEC.

CHAPTER 5

5 A Method for Mapping the Turbulence Intensity and Excess Energy Available to Building Mounted Wind Turbines over a Built-up area

5.1 Introduction and Objectives

Assessing the potential of proposed urban wind installations is hindered by insufficient assessments of both urban wind resource, and the effectiveness of commercial gust control solutions within built up areas. Evaluating the potential performance of a wind turbine within a built environment requires an estimation of the total energy that would be available to it were effective control systems to be used. In this Chapter, a methodology to estimate the level of atmospheric turbulence at a given hub height above a complex urban surface based on parameterisations of the surface aerodynamics is presented. This suggests that such a method can efficiently quantify the total (kinetic) energy resource available to a proposed turbine system across a built-up area. It also allows the investigation of the influence of turbine response time on the energy available to a well-controlled turbine system within a built-up area. This will provide potential customers and manufacturers with relevant information to aid (i) decision making for turbine siting within a built environment, (ii) in the performance evaluation of the proposed turbine system, and (iii) in assessing the cost effectiveness of prospective turbine control systems at potential turbine sites within a built-up area. The methodology may also be relevant to other 'real world' applications such as pollution dispersion modelling and the estimation of wind loading on urban structures.

The methodology proposed within this Chapter consists of three main stages; mean wind speed prediction, turbulence intensity (*T.I.*) prediction and excess energy estimation. The methodology for calculating the mean wind speed as a function of height within an urban environment (known as the MH model) which was introduced in Chapter 3, is employed herein. In Section 5.2, several models for predicting turbulence intensities available from the literature were reviewed and evaluated using meteorological data from the sites described in Section 3.1. Using data from four different cities, an assessment of the accuracy of four $T.I.$ prediction methodologies was carried out. The analytical methodology for predicting EEC proposed in Chapter 4 is further tested for validity in Section 5.3 by assessing its relationship to $T.I.$ across different suburban/urban sites. In Section 5.4.1, these analytical tools were applied at the first test site (i.e. city of Leeds, UK) by mapping the mean wind speed, $T.I.$ and EEC over the city. Further application of this methodology over 3 other major UK cities namely London, Manchester and Edinburgh, is presented in Section 5.4.2. Mapped results of

wind speed, $T.I.$ and EEC at maximum building heights across the four cities are presented in Section 5.4.3. Finally, the main conclusions are presented in Section 5.5.

5.2 Turbulence Intensity ($T.I.$) Prediction Methodology

Comprehensive field studies of atmospheric turbulence over urban environments, in general, are difficult to achieve and as a result limited in scope. Several studies have used different approaches in characterizing atmospheric turbulence with the two dominant environmental controls on turbulence within a built environment being the urban heat island [37, 287] and the high roughness of the suburban/urban surface (buildings, trees and other large structures) [288, 289]. As a result of the absence of a unifying method for characterizing turbulent transfer within a built-up area, much of the recent work has focused on testing the applicability of different concepts within simplified models in different terrains (several of which are presented in Table 5.1) and identifying their ranges of applicability. Table 5.1 lists several approaches proposed by various authors in calculating turbulence intensity for built-up areas.

As can be seen from Table 5.1, three models (2, 3, 4) are based on the local roughness length, two (5, 6) are based on simple corrections related to the mean wind speed, and one (1) is based on the mean building height h_m. Since models 5 and 6 do not contain any representation of the local surface features we do not pursue them further here. From the models presented in Table 5.1, four were selected and tested at the chosen study sites for their ability to predict $T.I.$ Model 1 proposed by Roth [37] estimates $T.I.$ as a function of h_m and Model 2, proposed by Engineering Science Data Unit (ESDU) in 1985 [2, 67] calculates $T.I.$ as a function of the normalised friction velocity u_* taking into account the surface roughness. Within this study, the frictional velocity is calculated as a function of h_m [37]:

$$u_* = 0.094 + 0.353 \exp(-0.946(z/h_m)) \qquad \text{Equation 5. 1}$$

where h_m is the mean building height in the local neighbourhood.

Model 3 proposed by the Danish Standards [290] estimates $T.I.$ as a function of the roughness length z_o. Mertens [291] however, suggested that ignoring the displacement height (as shown in Model 3) would lead to higher errors in estimating $T.I.$ within a built environment and hence suggested the correction in Model 4. Due to the unavailability of LiDAR data used in the calculation of aerodynamic parameters at some sites, the accuracy of each selected model

was tested at four urban sites (Leeds (H1 and H2), Manchester and London) using the measured wind speed data described earlier.

Table 5. 1: Summary of available methodologies used in characterising atmospheric turbulence from previous studies.

No.	Authors	Turbulence Intensity Models
1	Roth [37]	$T.I. = 0.259 + 0.582\exp(-0.943(z/h_m))$ where $0.8 < z/h_m < 6.3$
2	ESDU [2, 67]	$T.I. = \frac{7.5\eta u_*\left(0.538+0.09\ln\left(\frac{z}{z_o}\right)\right)^p}{\left(1+0.156\ \ln\left(\frac{u_*}{fz_o}\right)\right)U}$ where $\eta = 1 - 6fz/u_*$, $p = \eta^{16}$, f = Coriolis parameter, u_* = friction velocity
3	DS 472 [290]	$T.I. = 1/\ln(z/z_o)$
4	Mertens [291]	$T.I. = \frac{1}{\ln\left\|\frac{z-d}{z_o}\right\|}$
5	IEC 61400-1 NTM [292]	$T.I. = T.I._{ref}\ (a + 1.28\alpha + (b + 1.28\beta)/U)$ where a = 0.75; b = 3.8; α =0; $\beta = 1.4$; $T.I._{ref}$ = 18%
6	Ishihara *et al.* [293]	$T.I. = T.I._{ref}\ (a + 1.28\alpha + (b + 1.28\beta)/U)$ where a = 0.75; b = 3.8; $\alpha = 0.27$; $\beta = 2.7$; $T.I._{ref}$ =18%

However, as is true for all rough surfaces, accurate knowledge of the aerodynamic parameters of a built environment is necessary to describe and model the turbulence [37]. Hence, the MH model [47, 63] was employed in calculating the aerodynamic parameters over the study area. The turbulence intensity models were tested using two representations of the mean building height parameters; $h_{hm-local}$ and h_{hmeff}. The former is simply the arithmetic average of the building heights in the neighbourhood region, while the latter accounts for the disproportionate effect of taller buildings on the surface drag, as fully described in [63, 179].

Due to the availability of maps of aerodynamic parameters, 4 sites were considered in assessing the validity of the $T.I.$ models.

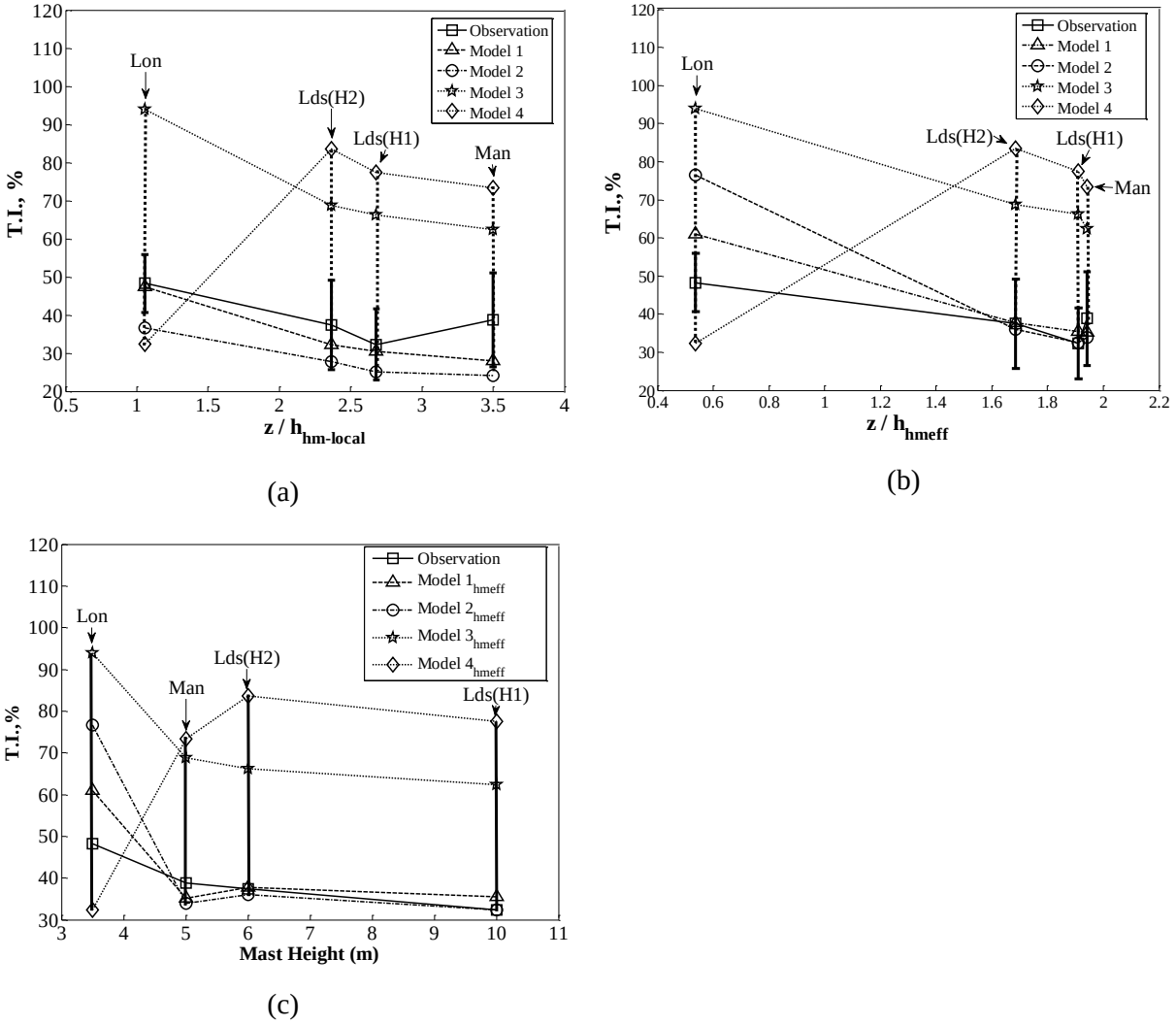

Figure 5. 1: Comparison between observations using high resolution data and four $T.I.$ Models from 4 test sites using (a) local mean building height ($h_{hm-local}$) (b) effective mean building height (h_{hmeff}) (c) Comparing mast heights with $T.I.$ across all test sites. The standard deviation (σ) describing the spread of the measured wind data at the test sites is represented as error bars.

Figure 5.1 demonstrates the relationship between $T.I.$ and normalised height while comparing results from each model with average $T.I.$ observations obtained from measured wind speed data collected at each test site and a spread of the measured wind data represented by error bars shown in Figure 5.1. Turbulence intensity observations from measured data show a decrease in $T.I.$ as normalised height increases (i.e. as the observation site moves further away

from the ground) with a slight discrepancy in the trend observed at the Manchester site which may be a result of the reduced mast height. A plot of variation of $T.I.$ observations with mast height at each test site (as shown in Figure 5.1c) shows a reduction in $T.I.$ as the mast height increases thereby highlighting diminishing turbulence levels as the observations move further away from the roof-top. Unsurprisingly, this supports the idea that higher hub heights for roof mounted turbines would allow them to operate in less turbulent flow regimes.

When using $h_{hm-local}$ as a representation of mean building height, Models 3 and 4 over-predict the turbulence intensities at all test sites except for London where Model 4 under-predicts by 15.9%. Models 1 and 2 substantially under-predict the turbulence intensities at all sites excluding the London and Leeds (H1) sites for Model 1. Substituting $h_{hm-local}$ with h_{hmeff} within each model (i.e. taking into account the disproportionate influence of the taller buildings on surface drag), the results of Models 3 and 4 remain unchanged, whereas Models 1 and 2 reveal significant improvements compared to observations, with both models showing better $T.I.$ predictions at all sites except for the London site which shows an over-prediction of 28.3 % for Model 2 and 12.7% for Model 1. The poor performance of Models 3 and 4 is clearly highlighted in Figure 5.1 with model results lying outside the fluctuations about the average *T.I.* (represented by the error bars) observed at all test sites. However, when h_{hmeff} was employed, Models 1 and 2 showed improvements at all sites except for London. These aberrant model results at the London site may be a result of z being located near to the roof-top within the urban canopy and also below the displacement height (i.e. z < d) where a strong influence of local surrounding structures on the flow properties is observed [198], whereas Model 1 is only expected to be valid at $z/h_{hmeff} > 0.8$ [37].

Studies conducted by Mertens [291] concluded that predicting turbulence intensity within a built environment using the log-law (as employed in Models 3 and 4) will only be valid above a given minimum height (z_{min}). Based on numerous measurements, he proposed z_{min} to be site specific and calculated as:

$$z_{min} = 1.5d \qquad \text{Equation 5. 2}$$

where d is the displacement height. Hence, the accuracy of Model 4 at the London site may be greatly affected as a result of the observation site being located below the z_{min} (as shown in Figure 5.1). A clearer comparison between results from the four models and $T.I.$ observations at all test sites was achieved by using the mean percentage error (*MPE*) as defined in Equation 5.3 with results presented in Figure 5.2.

$$MPE(\%) = 100 \times \frac{1}{n}\sum \frac{\left|T.I._{obs} - T.I._{pred}\right|}{T.I._{obs}} \qquad \text{Equation 5. 3}$$

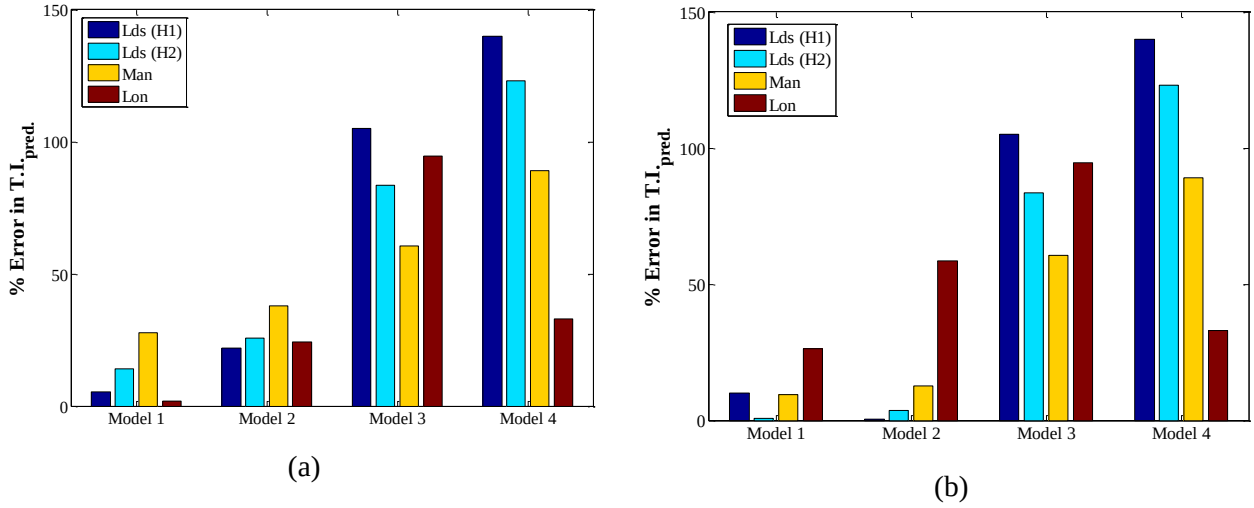

Figure 5. 2: Mean percentage errors for $T.I.$ predictions using Model 1, Model 2, Model 3 and Model 4 across the 4 test sites when using (a) $h_{hm-local}$ (b) h_{hmeff}.

Using the effective mean building height (h_{hmeff}) in Model 1 as demonstrated in Figure 5.2b resulted in a significant reduction in error in predicting $T.I.$ across all sites except London when compared to using $h_{hm-local}$. A maximum average error of 26% was observed at the London site and a minimum of 0.82% at Leeds (H2). Model 2 (h_{hmeff}) likewise showed lower errors in $T.I.$ prediction when compared to Model 2 ($h_{hm-local}$) at all sites except for London with minimum average error of 0.42% observed at Leeds (H1) and a maximum observed at the London site (58.6%). Models 3 and 4 performed poorly across all sites tested, with average errors above 60% observed at all test sites except for London where Model 4 showed a lower average error of 32.9%. Assessing the overall performance of both building height parameters within each model across all test sites as shown in Figure 5.3, the use of h_{hmeff} showed better $T.I.$ prediction accuracy and hence was adopted in subsequent analysis. The results also confirm earlier conclusions of Millward-Hopkins *et al* [63, 179], that it is important to take account of building height variability when predicting above roof flow characteristics over built-up areas. Overall Model 1 using h_{hmeff} gave better $T.I.$ predictions compared to Model 2 using h_{hmeff}. Based on these results and the model's simplicity when compared to the complexity involved in modelling frictional velocity below the blending layer height within a built environment, Model 1 using h_{hmeff} was selected within the rest of the

study. Testing the validity of such a $T.I.$ model over wider regions will require employing further sets of field measurements from suburban/urban sites as well as aerodynamic parameters for each site as they become available.

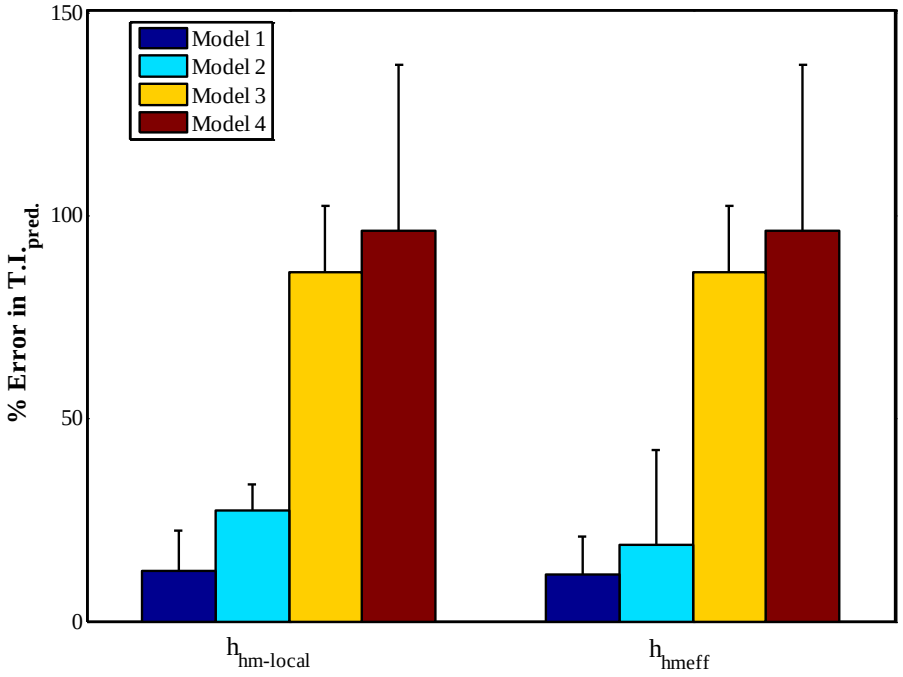

Figure 5. 3: Comparing the mean percentage errors for different models across all test sites when using h_{hmeff} and $h_{hm\text{-}local}$. The standard deviation (σ) of the MPE at all test sites is represented by the error bars.

5.3 Excess energy Prediction Methodology

In order to consider the additional energy available at a given hub height within a built-up area, the EEC prediction model proposed in Section 4.4.2 was adopted. However, the validity of this model was tested over a wider region by employing EEC and $T.I.$ values calculated using high-resolution field measurements from 5 additional urban/suburban potential turbine sites namely Dublin (St Pius and Marrowbone), Helsinki (Suburban and Urban) and London sites which were later made available. Here, filtering of the raw data was necessary at different averaging times (T_C) of 1 s, 10 s and 60 s resolution in order to mimic different turbine response times (as explained in Section 4.3.2) within a burst period of 10 min. These EEC values were plotted against the equivalent binned values of $T.I.$ at the five urban/suburban potential turbine sites. Thus, Figure 5.4 demonstrates a strong relationship between $T.I.$ and EEC, with increases in $T.I.$ resulting in increased additional energy available at the 8

urban/suburban potential turbine sites. This showed strong agreement with results presented in Chapter 4, thereby highlighting the potential impact of employing gust tracking solutions within a built-up area.

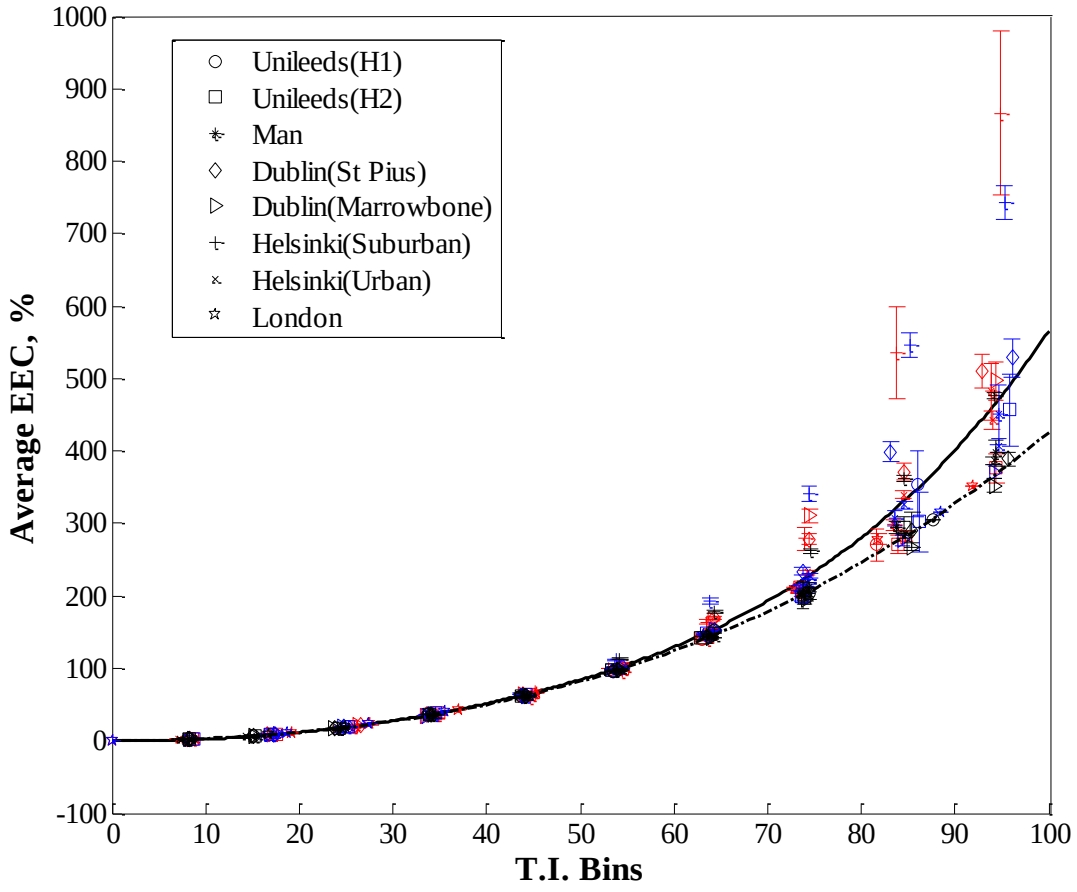

Figure 5. 4: Variation of *EEC* with *T.I.* at 10 min burst periods for 8 test sites (a) markers represent observations from test sites at different T_Cs ; T_C = 1 s (red), T_C = 10 s (blue) and T_C = 60 s (black) (b) the broken line represents *EEC* Model 1 (empirical fit for Equation 4.2), solid line represents *EEC* Model 2 (empirical fit for Equation 5.5) and the error bars the standard error within each *T.I.* bin.

As shown in Figure 5.4, the $EECs$ from individual sites lie close to the empirical fit at $T.I.$ values below 60%. The standard error (defined in Equation 5.4) describing the precision of the $T.I.$ averages within each $T.I.$ bin is represented by error bars in Figure 5.4.

$$s_u = \frac{\sigma_i^{EEC}}{\sqrt{N_i}} \qquad \text{Equation 5. 4}$$

where σ_i^{EEC} is the standard deviation and N_i the number of data points in the i –th bin.

An increase in scatter is observed in *EEC* values as the $T.I.$ increases above 70% across all sites. Whilst the scatter is larger at the higher $T.I.$ values, this may be a result of the smaller sample sizes within these high turbulence bins as suggested by the error bars and a plot of the frequency distributions (see Figure 5.5). The reliability of the empirical fit is likely to be worse for the high turbulence intensity bins but the occurrence of such conditions will be less frequent (See Figure 5.5). For example, even when using 1 s raw data, less than 1% of the data for all sites falls into bins with $T.I.$ greater than 70% whilst less than 7% of mean winds across all sites are less than 1 ms^{-1}. An empirical equation for the prediction of EEC values as a function of $T.I.$ values was determined using the least square errors approach within MATLAB's best fit tool. A polynomial form was assumed and terms up to 10^{th} order were tested. The lowest errors were determined using a 4^{th} order polynomial (and hence *EEC* values are approximated using the following empirical relationship:

$$EEC = 4.2B^4 + 14B^3 + 45B^2 + 99B + 74 \qquad \text{Equation 5. 5}$$

where

$B = (T.I. - 47)/28$.

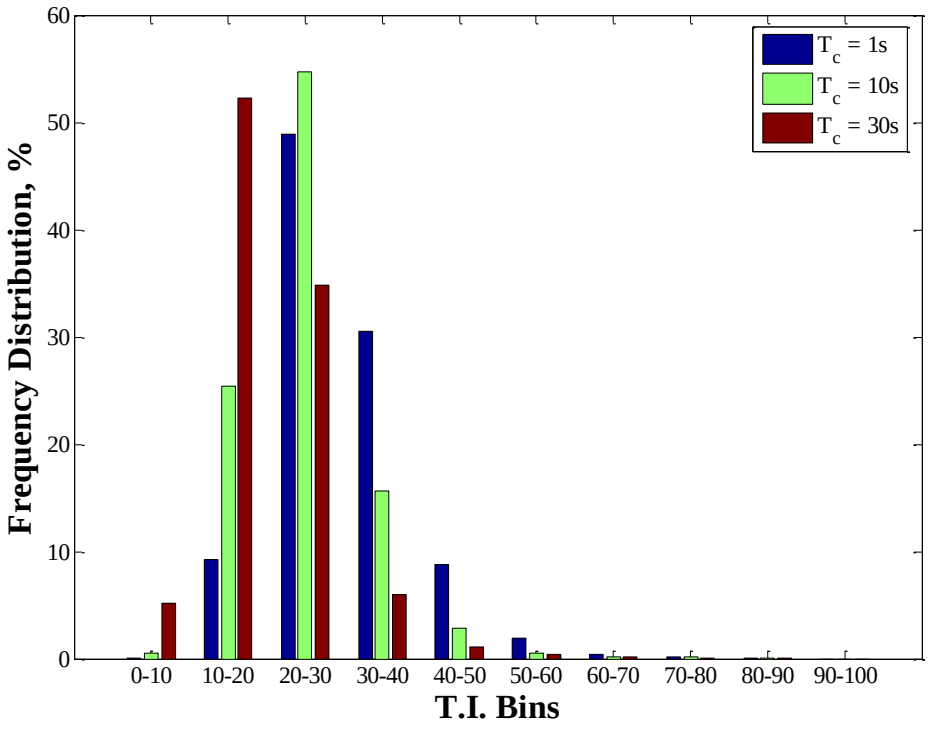

Figure 5. 5: Frequency distribution across different turbulence intensity bins at different $T_c s$ for eight sites.

Figure 5.4 shows a clear comparison between the two empirical fits namely EEC Model 1 (developed using high resolution dataset from three sites and represented by Equation 4.2) and EEC Model 2 (developed using high resolution dataset from eight sites and represented by Equation 5.5). Further analysis showed that an error of less than 9% was observed should either model (i.e. EEC Model 1 or EEC Model 2) be employed at lower turbulence intensities (i.e. < 50%), thus highlighting its reliability within this turbulence intensity range. However, Figure 5.4 showed a clear deviation between both empirical models at higher $T.I.$ bins, with EEC Model 1 under-predicting the excess energy available at higher turbulence intensities when compared to EEC Model 2, thus highlighting the importance of high resolution measurement data from more sites in the development of analytical models. It is important to note that there is very low frequency of occurrence of data in these higher turbulence bins. Also, the data is very scattered in this region and hence any simplified statistical-based model will struggle in these conditions (i.e. likely to be characterised by low mean wind speed or strongly convective flows). Overall, results presented in Figure 5.4 show consistency between the two EEC models (EEC Model 1 and EEC Model 2) at lower turbulence intensities. Although both EEC models are considered less reliable at higher turbulence intensities, EEC

Model 2 demonstrates better accuracy in predicting EEC values at $T.I.$ values greater than 60%, thus suggesting improved EEC prediction model accuracy at higher turbulence intensities should high resolution field measurements from more suburban/urban sites be made available. Hence, for this study, the EEC Model 2 is adopted herein as the excess energy content model. Hence, this suggests that from knowledge of turbulence intensities, the EEC available to a particular turbine could be estimated. However, in the above analysis the 1 s raw data resolution assumes that a turbine could respond to changes in wind speed on this short time-scale.

In reality, the turbulence spectrum is both site dependent and averaging time (T_C) dependant and hence the raw data resolution is important when calculating $T.I.$ at a given site. This has critical implications for assessing the EEC available to a given turbine since the filtering time-scale for the raw data should be based on the estimated response time of a particular turbine. Therefore when estimating EEC, appropriate data filtering should be carried out prior to the calculation of the $T.I.$ Figure 5.6 demonstrates the impact of increasing T_C on average *EEC* with increases in T_C resulting in decreasing EEC and vice versa. For a given site it is clear that the faster the response time, the greater EEC is available to the turbine when compared to the 10 minute mean values with average EEC values greater than 18% observed over the 8 sites at a response time of 30 s (i.e. T_C = 30 s). Up to 80% excess energy is available at a 1 s response time for the most turbulent conditions found close to the roof-top in London. In reality the ability of a turbine and control system to respond on such short time-scales will depend on practical features such as gust tracking control algorithms and power electronics solutions [259, 269, 275]. Thus, it will be interesting to analyse different control methodologies to test whether the predicted excess energy can be realised in practical systems. This will be considered in detail in Chapter 6.

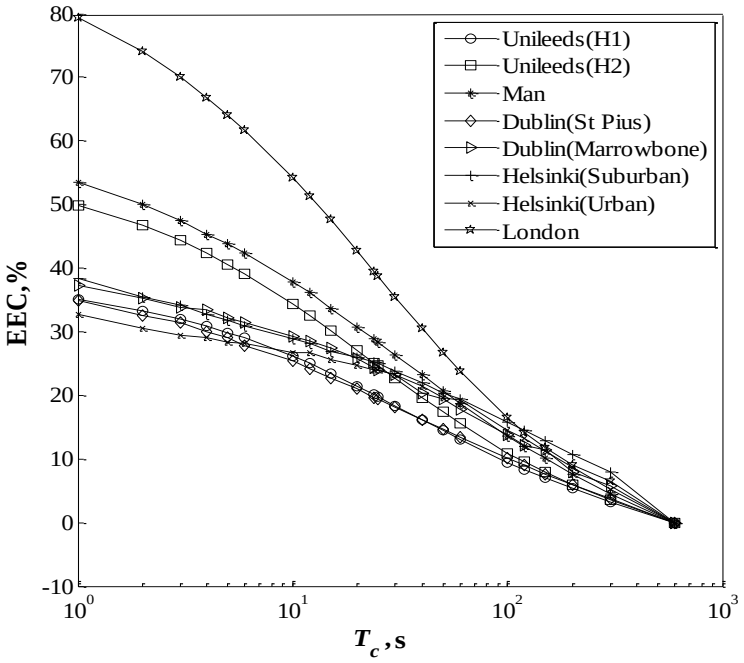

Figure 5. 6: Effect of changes in T_c on average *EEC* at 8 sites highlighting effect of decreasing response time on energy gain.

5.4 City-scale variations in Wind speed, $T.I.$ and *EEC*

5.4.1 First Case Study: The City of Leeds

In this section the city-scale variations of the mean wind speed, $T.I.$ and the *EEC* values predicted by the MH model, $T.I.$ prediction model and the *EEC* prediction model are considered using the city of Leeds as the first test site. Figure 5.7 shows the mean wind speed over Leeds as predicted by the MH model [63, 69] at 10 m above the local mean building height for each neighbourhood region (as illustrated in Figure 5.8). Results show an increase in wind speed at this height as the distance increases from the city centre. This suggests that the urban boundary layer is thicker around the city centre as a result of higher surface roughness (see Figure 5.9). The wind speed map over Leeds, as shown in Figure 5.7, suggests potential turbine sites across the city with the exception of neighbourhoods within the city centre where the minimum predicted wind speed was observed to be approximately 1.1 ms^{-1}. Further analysis showed that wind speeds at this height were expected to be low within the city centre due to the presence of tall buildings/structures (as suggested by increased roughness lengths in Figure 5.9) as well as increased interaction between the local wind and the inherent buildings/structures. However, this may be averted by siting turbine systems above the local maximum building height within the city centre.

Figure 5.10 shows the mean wind speed over Leeds predicted at 10 m above the effective mean building height (h_{hmeff}) for each neighbourhood region. Results show a general increase in wind speeds at this height as the distance increases from the city centre. Generally, wind speeds at this height (i.e. h_{hmeff}, See Figure 5.11) were observed to be higher than that predicted at the local mean building height with an average wind speed of 4.23 ms^{-1} estimated over Leeds. In contrast to the wind map at the local mean building height, the wind speed at h_{hmeff} (as shown in Figure 5.10) suggests potential turbine sites across the city with the exception of a few neighbourhoods with minimum predicted wind speed lower than 2.6 ms^{-1}. Thus, the issue of low wind speeds may be averted by siting turbine systems above the local maximum building height.

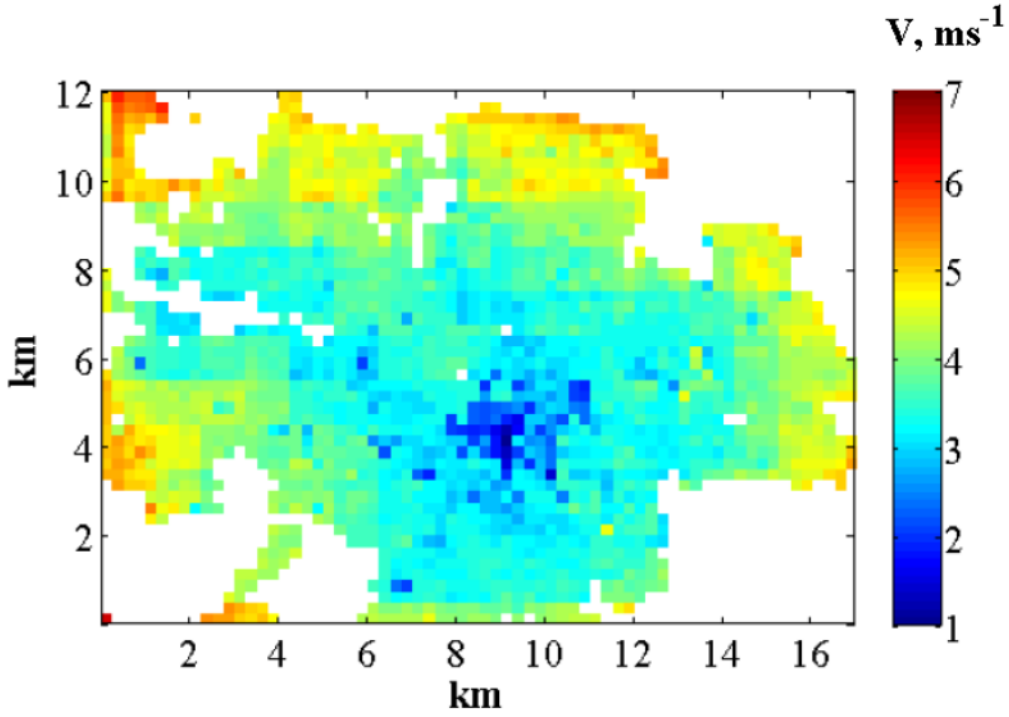

Figure 5. 7: Predicted mean wind speed (ms^{-1}) at 10 m mast height above the local mean building heights over Leeds.

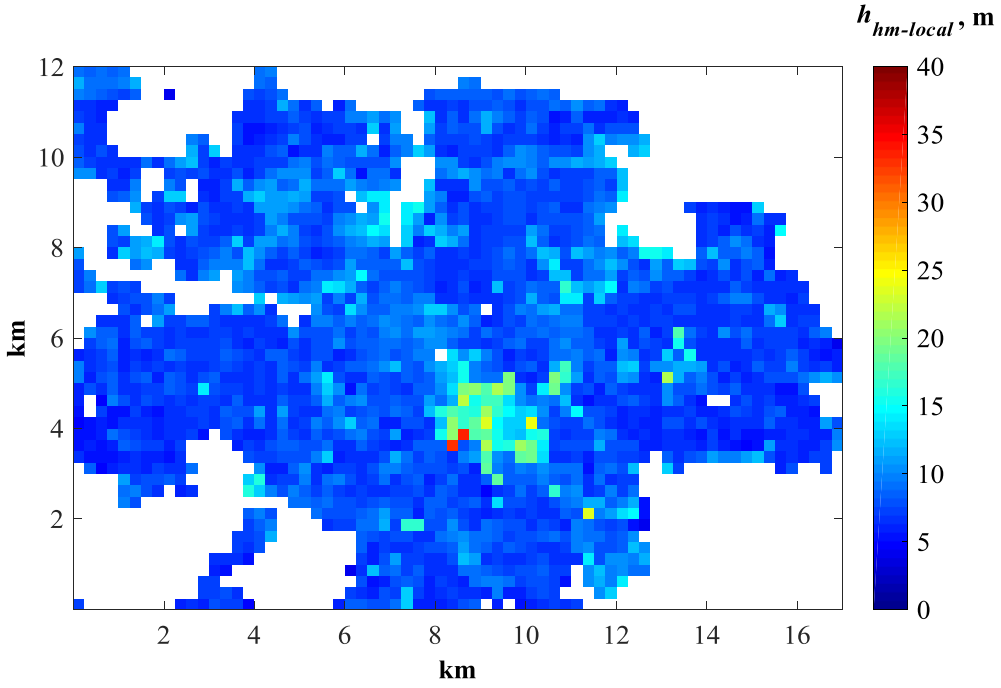

Figure 5. 8: Predicted local mean building height (m) for the neighbourhoods of Leeds.

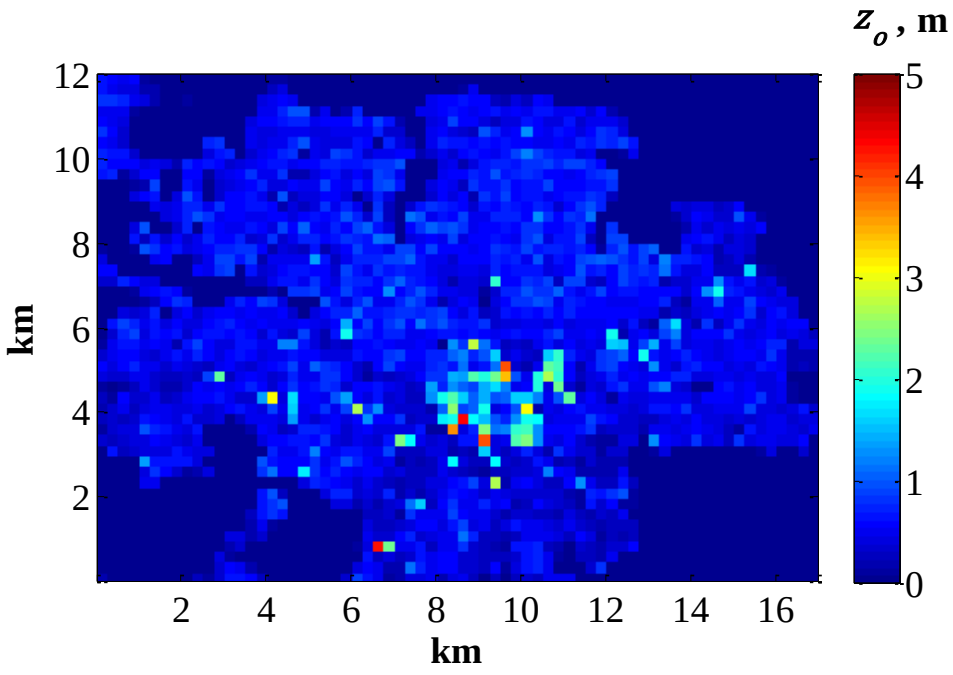

Figure 5. 9: Predicted surface roughness lengths z_o (m) for the neighbourhoods of Leeds.

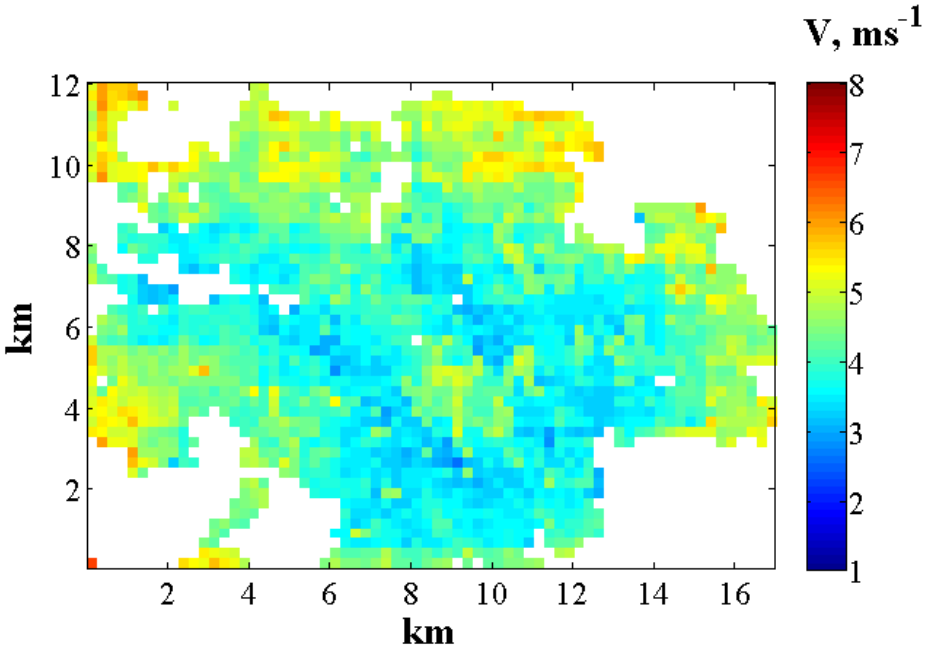

Figure 5. 10: Predicted mean wind speed (ms^{-1}) at 10 m mast height above the mean effective building heights (h_{hmeff}) over Leeds.

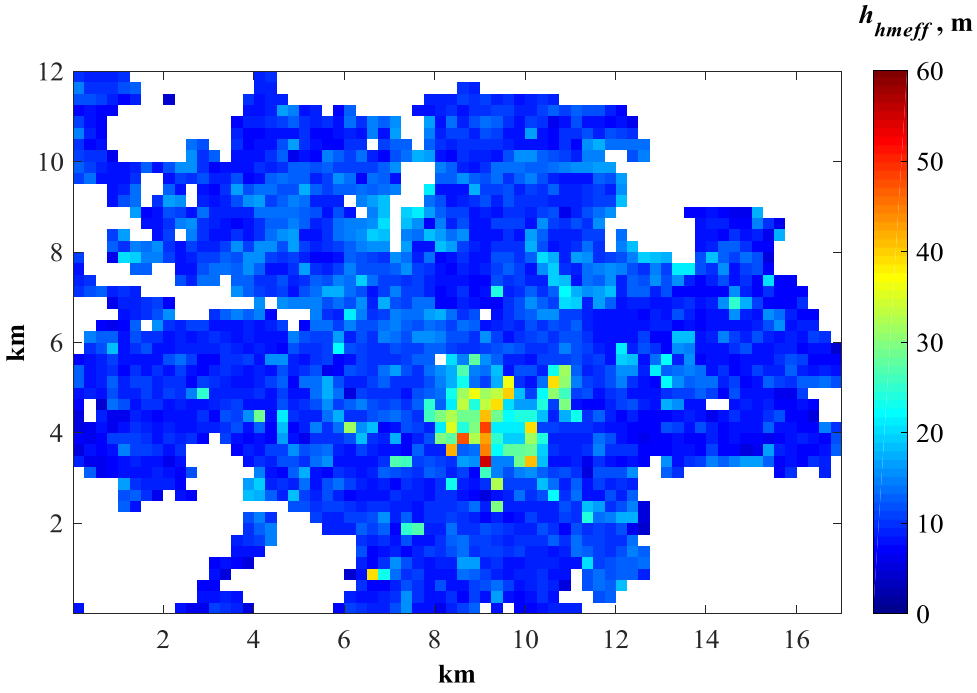

Figure 5. 11: Predicted effective mean building height (m) for the neighbourhoods of Leeds.

Figure 5.12 shows modelled $T.I.$ at a mast height of 10 m above h_{hmeff} over Leeds using the methodology proposed in Section 5.2. The map demonstrates high $T.I.$ values at an average of 40% within the built-up city centre region, with a decrease in predicted $T.I.$ with increasing distance from the city centre. This suggests increased interaction between incoming flows and complex local buildings and other structures around the city centre. Although mapped wind speed results at this height across Leeds city showed higher values (as demonstrated in Figure 5.10), higher turbulence levels within the city centre (as shown in Figure 5.12) makes it less viable for wind turbine siting. Hence, considering the influence of turbulence intensity on turbine performance [12, 193], an efficient wind resource assessment for potential urban wind applications will require an assessment of both wind speeds and local turbulence available within the potential turbine site.

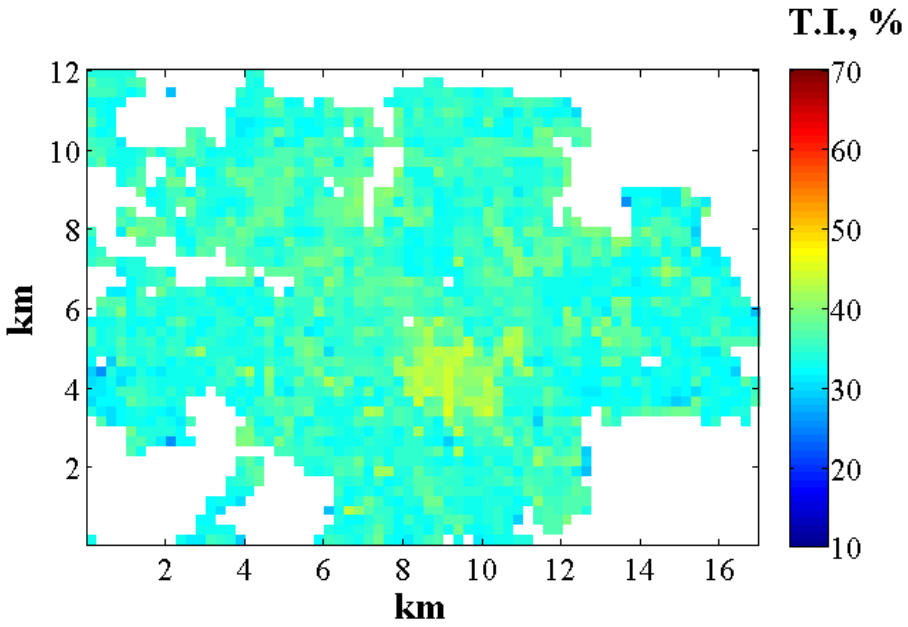

Figure 5. 12: Predicted *T.I.* (%) at 10 m mast height above the mean effective building heights (h_{hmeff}) over Leeds.

Next we mimic the effect of turbine response time by modifying the data filtering time-scale T_c and modelling its effect on the EEC available over Leeds. The aim of this practice is to simply demonstrate the effect of response time on the energy gains available within a built environment. An empirical relationship derived using Matlab software can be established using measured meteorological wind data (as shown in Equation 5.6).

$$EEC_{T_c} = EEC_{1s} \times \left(1 - \left(\frac{E_{loss}}{100}\right)\right) \qquad \text{Equation 5. 6}$$

EEC_{1s} represents the additional energy available calculated at a turbine response time of 1 s and is obtained using Equation 5.5, while E_{loss} is the percentage loss in EEC_{1s} with increasing T_c. An empirical equation for the prediction of E_{loss} values as a function of T_c values was determined using the least square errors approach within MATLAB's best fit tool. A polynomial form was assumed and terms up to 10th order were tested, with Table 5.2 showing the corresponding correlation coefficient (R^2) values for various polynomial fits tested. Based on a "best fit" of the effect of changes in T_c on average EEC at all 8 observation sites as shown in Figure 5.6, E_{loss} was determined to be a 7th order polynomial using the least squares errors approach within MATLAB's best fit tool (as illustrated in Figure 5.13) and is approximated by the empirical relationship:

$$E_{loss} = c_1M^7 - c_2M^6 + c_3M^5 - c_4M^4 - c_5M^3 - c_6M^2 + c_7M + c_8 \qquad \text{Equation 5. 7}$$

where

$M = (T_c - 80.773)/135.92,$

c_1 = 37.681 c_2 = 233.7 c_3 = 379.74 c_4 = 121.66 c_5 = 75.06 c_6 = 2.0584

c_7 = 41.493 c_8 = 65.304.

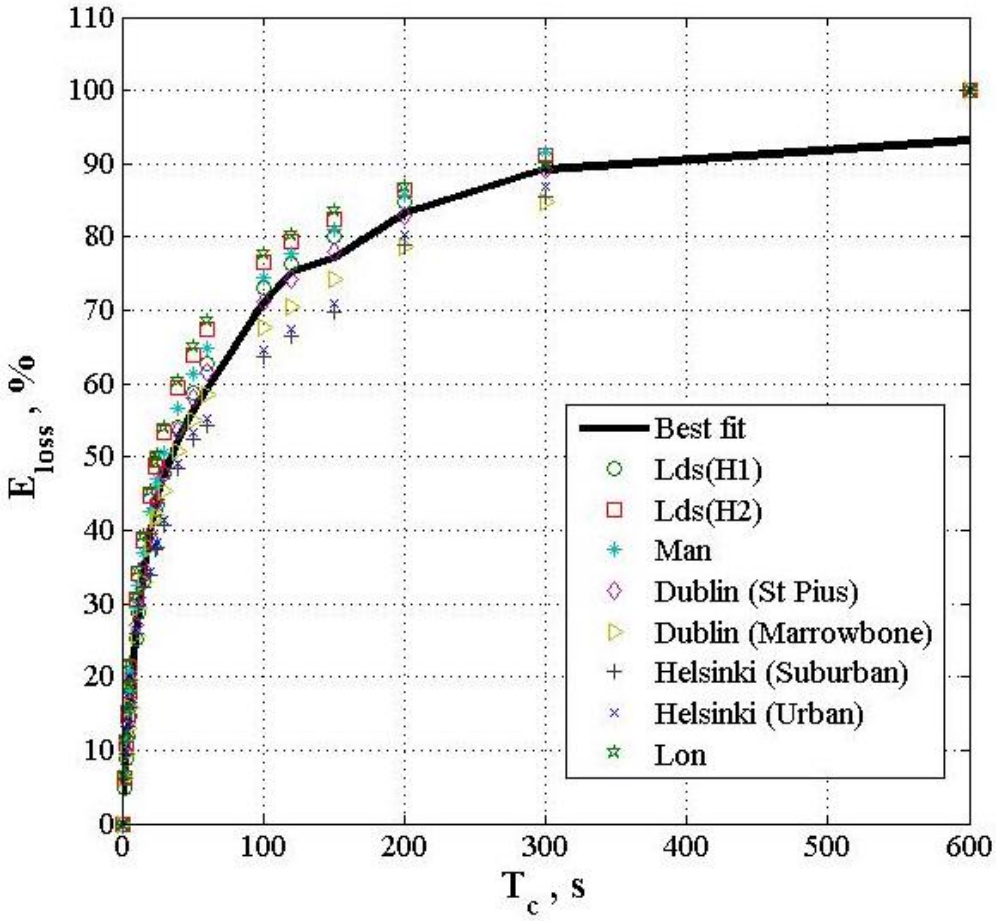

Figure 5. 13: Variation of E_{loss} with T_C at 10 min burst periods for 8 test sites (markers represent observations from test sites).

Table 5. 2: Tests for best fit polynomial with their corresponding correlation coefficient (R^2) values.

No	**Polynomial Order**	**Correlation Coefficient (R^2)**
1	4th Order	0.9594
2	5th Order	0.9753
3	6th Order	0.9792
4	7th Order	0.9831

Incorporating Equation 5.5 into Equation 5.6, an EEC model which accounts for the effect of increasing T_C at 10 m above the h_{hmeff} over Leeds city is developed and results presented in Figure 5.14. A map of energy gains at a turbine response time of 1 s (i.e. T_C = 1 s [294]) over Leeds is shown in Figure 5.14a. An EEC map at response time of 10 s (i.e. T_C = 10 s) which corresponds to the shortest averaging time for anticipated small wind turbine response characteristics suggested by Kooiman [286] is shown in Figure 5.14b. Also, an EEC map at 60 s (i.e. T_C = 60 s; averaging time and subsequent data analysis for wind turbines with rotor diameter less than 16m as described in the relevant standard, IEC 61400-12-1 (see Annex H) [45]), is shown in Figure 5.14c. Considering the EEC model mapped results over Leeds city (as shown in Figure 5.14), energy gains at this height were observed to generally decrease with increasing distance from the city centre. This suggests a strong relationship between surface roughness and EEC with increasing surface roughness resulting in increasing EEC and vice versa.

Results showed that increase in T_C from 1 s to 10 s led to a loss in the average EEC available from 53.2% to 39.2% around the city centre and 45% to 28.6% over the city. A further 50% loss in average EEC (i.e. EEC_{10s}) was observed over the city when T_C is increased from 10 s to 60 s. Figure 5.14d highlights the difference in EEC over Leeds city when T_C is increased from 1 s to 60 s. This suggests that employing a well-controlled turbine system with a faster response time might capture the high additional energy available around the city centre. Finally, it is important to point out that although wind speed model results at 10 m above the mean building height show low values around the city centre, *EEC* model results show high energy gains suggesting an effective tracking of the gust by the turbine system could at least partially counter the problems of reduced power generation experienced within built-up areas. Additional energy content of a maximum of about 67% is predicted to be available to turbine systems with a fast response time within the city of Leeds at 10 m above the urban canopy. This could potentially be achieved by mounting a well-controlled turbine on top of a tall building (i.e. one which is significantly taller than the local average mean building height).

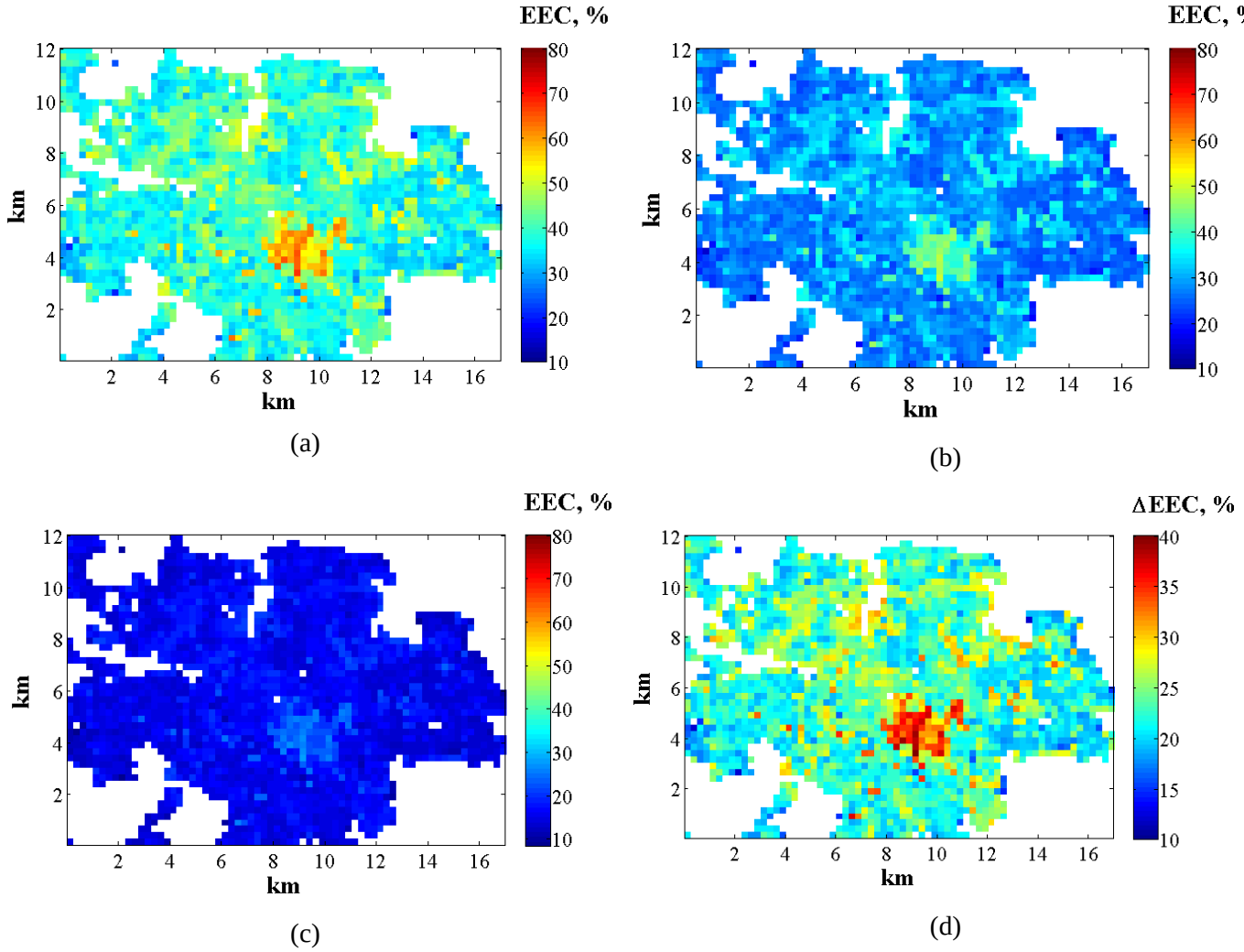

Figure 5. 14: Predicted *EEC* (%) at 10 m mast height above h_{hmeff} over Leeds city (a) at T_C = 1 s (b) at T_C = 10 s (c) at T_C = 60 s (d) difference in the predicted *EEC* at T_C = 1 s and at T_C = 60 s.

5.4.2 City-scale Model Results for London, Manchester and Edinburgh

Having considered city-scale variations for mean wind speed, turbulence intensity and the additional energy available over Leeds, these methodologies were further applied to three major cities in the UK namely London, Manchester and Edinburgh. Figures 5.15 – 5.17 show the mean wind speed at 10 m above h_{hmeff} over the three cities as predicted by the MH model. Mapped wind speed results for London and Manchester show an overall increase in wind speed at this height as the distance from the city centre increases. These low wind speeds observed within neighbourhoods around the city centres in both cities may be as a result of high surface roughness and increased interaction between the local wind and inherent

buildings and complex structures. However, in agreement with mapped wind speed results over Leeds, higher wind speeds were observed within some neighbourhood regions around the city centres in Manchester and London with inherent higher h_{hmeff}.

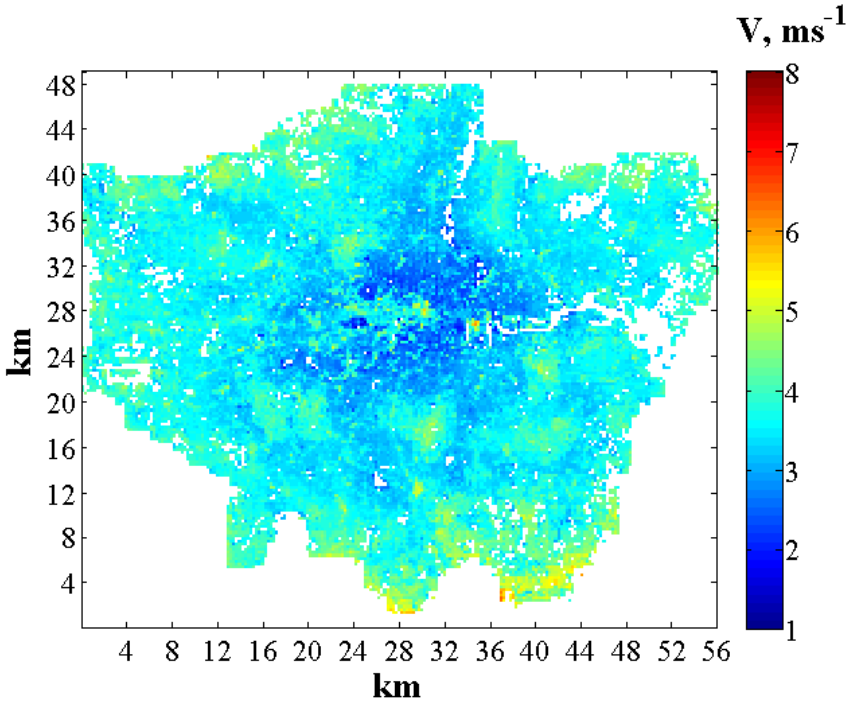

Figure 5. 15: Predicted mean wind speed (ms^{-1}) at 10 m mast height above h_{hmeff} over London.

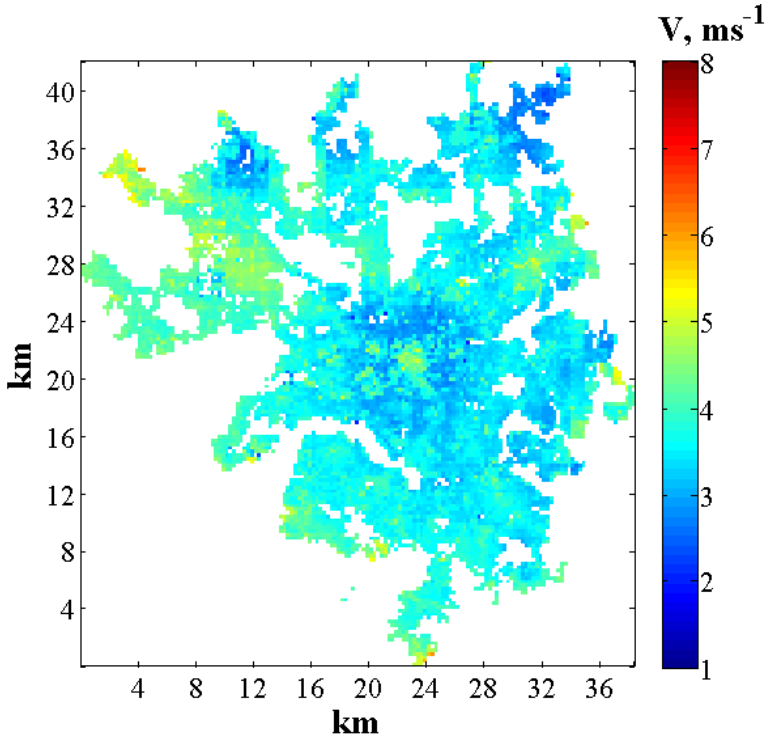

Figure 5. 16: Predicted mean wind speed (ms^{-1}) at 10 m mast height above h_{hmeff} over Manchester.

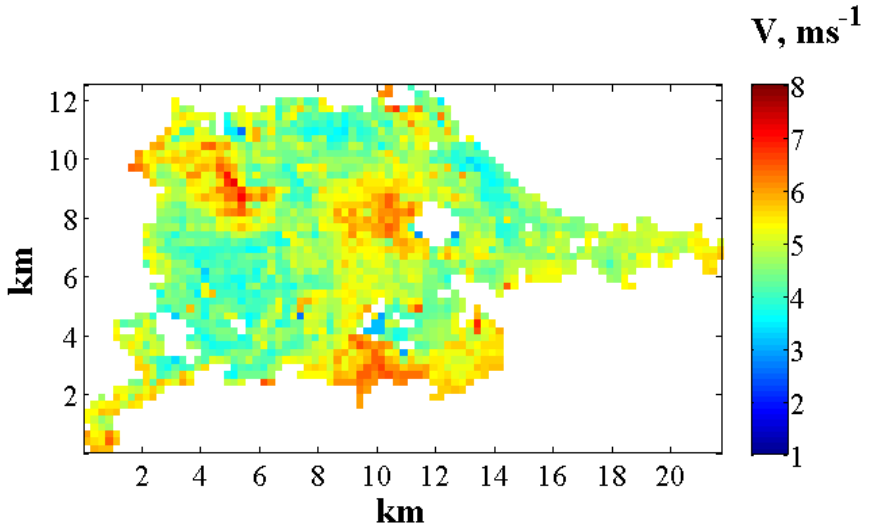

Figure 5. 17: Predicted mean wind speed (ms^{-1}) at 10 m mast height above h_{hmeff} over Edinburgh.

The average wind speeds over both cities were estimated to be 3.6 ms^{-1} and 3.8 ms^{-1} for London and Manchester respectively. However, the maximum wind speeds over London and Manchester were estimated to be 5.98 ms^{-1} and 6.29 ms^{-1} respectively thus showing promise for potential urban turbine sites. In contrast to mapped results over London and Manchester, a different pattern emerges when predicting the wind speeds over Edinburgh. The wind speed map over Edinburgh showed higher wind speeds around the city centre with some neighbourhoods showing average wind speeds above 6 ms^{-1} (See Figure 5.17). This may be due to the presence of open land areas (e.g. parks, golf courses, etc.), elevated grounds (e.g. around the Edinburgh castle), neighbourhoods with lower local building heights and nearness to the North Sea. The average wind speed over Edinburgh was estimated to be 4.9 ms^{-1} with a maximum wind speed of 7.1 ms^{-1} observed over the city, thus suggesting huge potential for urban wind applications across the city.

Figure 5.18 compares the mapped annual mean wind speed over London presented by Drew *et al* [194] using the Macdonald's model to the MH model. From Figure 5.18, the maximum wind speed estimated by Drew et al [194] over London was approximately 5 ms^{-1}, thus under-predicting by 14% when compared to the MH model results. Also, the minimum wind speed estimated over London was shown to significantly over-predict by 63% when compared to the MH model results. These significant discrepancies between both model outputs may be as a result of various factors such as choice of model resolution, with the MH model applying a 250 m by 250 m neighbourhood grid resolution, thus accounting for the variability in the wind speed within the 1 km by 1 km grid resolution employed by Drew *et al* [194]. Other factors include differences in model's description of boundary layer growth,

configuration of obstacles within each gridbox, little or no adjustment of the Macdonald model to account for the disproportionate effect of tall buildings upon the wind flow, thus leading to inaccuracies in estimating surface parameters such as z_0, d and other aerodynamic parameters, as well as the wind profile over London city. Hence, in addition to limitations presented in Section 3.2, this further highlights the problems that may be encountered should the Macdonald's model be used in estimating the wind resource over a built environment. Further information on the MH and Macdonald's wind speed prediction models can be found in Refs [63, 69, 194, 206].

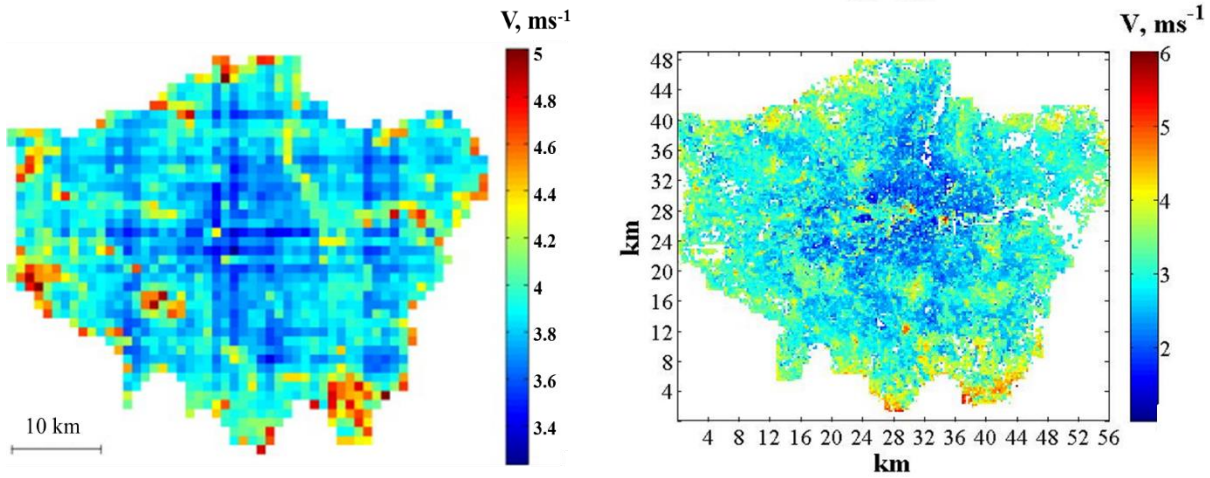

(a) (b)

Figure 5. 18: Comparison between predicted annual mean wind speed over London (a) by Drew *et al* [194] at 5 m mast height above $h_{hm\text{-}local}$, and (b) MH model at 5 m above the h_{hmeff}.

Figures 5.19 - 5.21 show predicted $T.I.$ at a mast height of 10 m above h_{hmeff} over London, Manchester and Edinburgh using the methodology proposed in Section 5.4. The mapped results demonstrate higher $T.I.$ within the city centre, with a decrease in predicted $T.I.$ as the distance from the city centre increases. This, as observed over Leeds (See Section 5.4.1), suggests increased interaction between local wind and complex local buildings and other structures around the city centre. The average $T.I.$ was estimated to be 33.76%, 33.58% and 35.17% over London, Manchester and Edinburgh respectively.

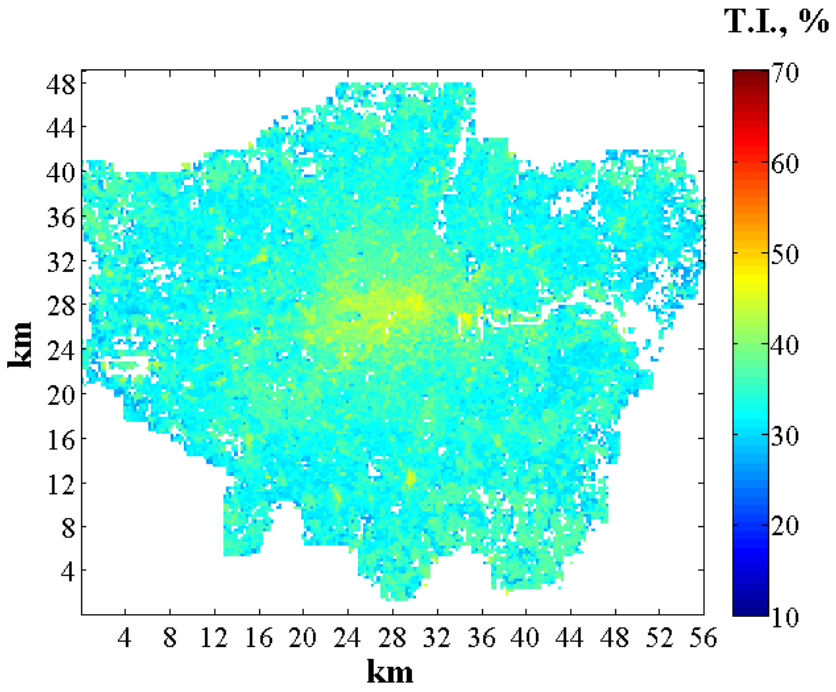

Figure 5. 19: Predicted *T.I.* (%) at 10 m mast height above h_{hmeff} over London.

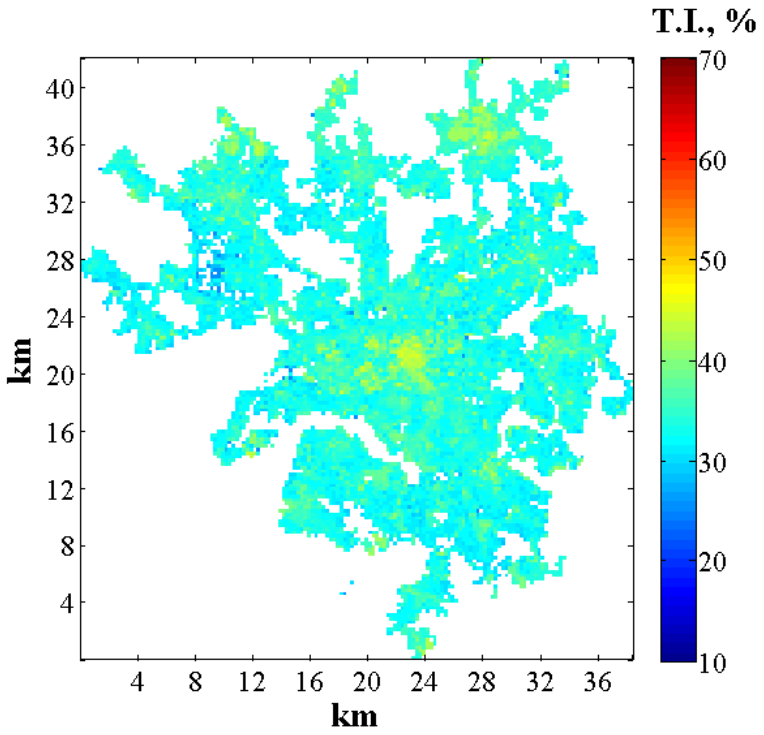

Figure 5. 20: Predicted $T.I.$ (%) at 10 m mast height above h_{hmeff} over Manchester.

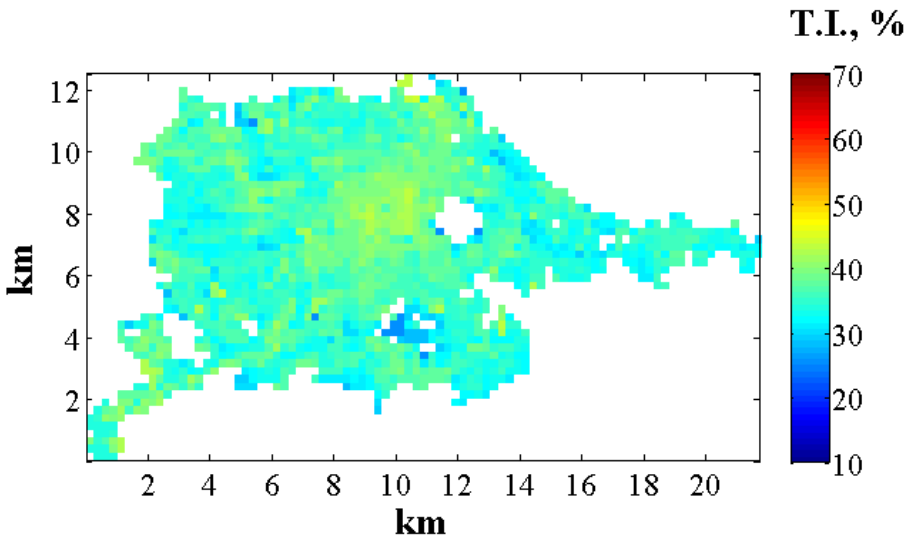

Figure 5. 21: Predicted *T.I.* (%) at 10 m mast height above h_{hmeff} over Edinburgh.

Maps of energy gains over London, Manchester and Edinburgh at 10 m mast height above h_{hmeff} using the methodology proposed in Section 5. 5 are presented in Figures 5.22 – 5.24. Considering the EEC mapped results, energy gains were observed to generally decrease with increasing distance from the city centre. This, as observed over Leeds, suggests a strong relationship between surface roughness and EEC with increasing surface roughness resulting in increasing EEC and vice versa. Further analysis were carried out by calculating the mean percentage error for the predicted EEC values across the wind measurement sites (i.e. Leeds (H1 and H2), Manchester and London). This was achieved by substituting EEC_{obs} (i.e. EEC values calculated using high resolution wind data) and EEC_{pred} (i.e. mapped EEC values predicted at the neighbourhood regions representing the measurement sites using the *EEC* model) for $T.I._{obs}$ and $T.I._{pred}$ in Equation 5.3 respectively. Thus, results presented in Figure 5.25 showed a significant reduction in error in predicting the EEC values using the EEC prediction model across the Leeds and Manchester sites. However, high mean percentage error of approximately 67% was observed at the London site. This may be as a result of the measurement mast height being located near the roof-top and also below the displacement height where a strong influence of the local surrounding structures on flow is observed, as suggested in Section 5.2. Hence, model results showed estimated average energy gains of 36.38%, 35.83% and 39.61% for London, Manchester and Edinburgh respectively thus making these cities potential viable turbine sites. Additional energy contents of a maximum of about 76%, 70% and 64% were estimated to be available to turbine systems with a fast response time within the cities of London, Manchester and Edinburgh respectively at 10 m above the urban canopy.

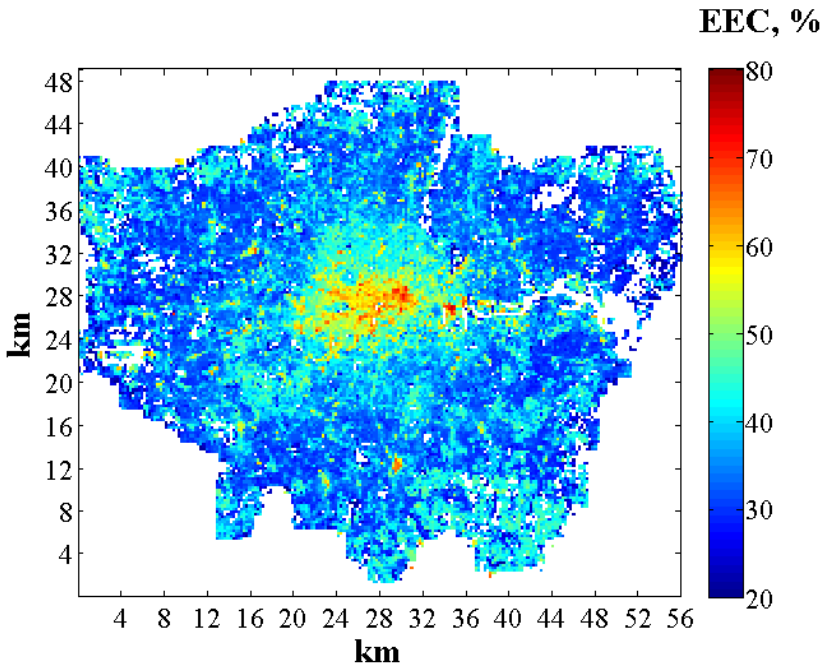

Figure 5. 22: Predicted *EEC* (%) at 10 m mast height above h_{hmeff} over London.

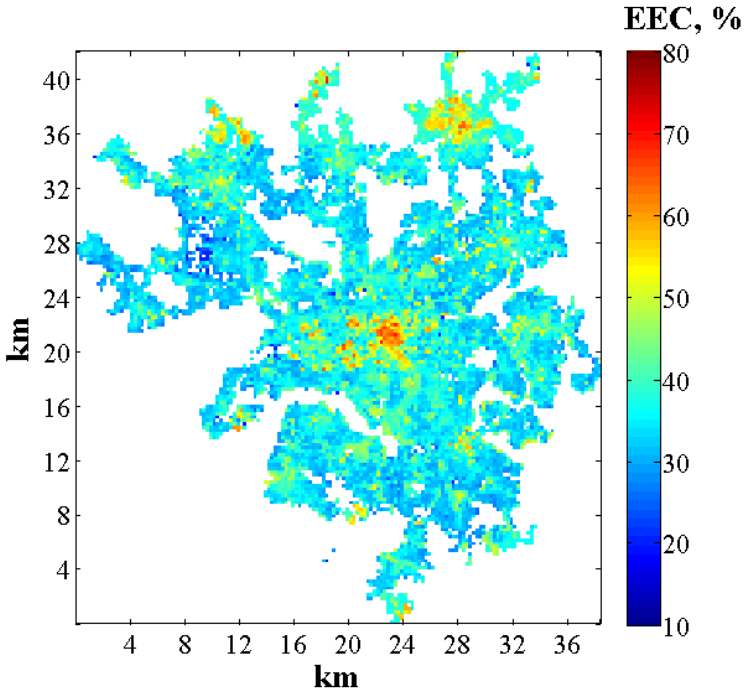

Figure 5. 23: Predicted *EEC* (%) at 10m mast height above h_{hmeff} over Manchester.

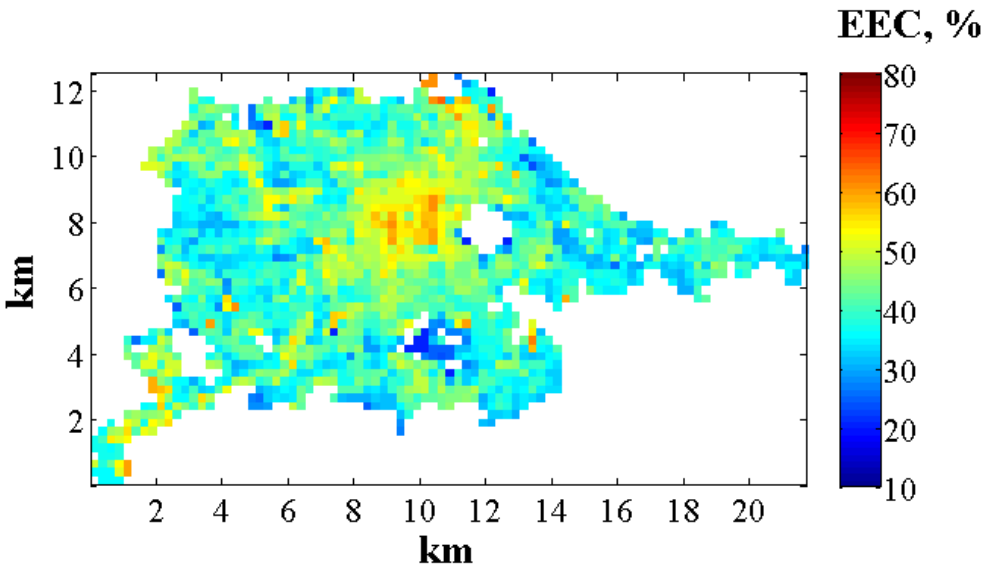

Figure 5. 24: Predicted *EEC* (%) at 10m mast height above h_{hmeff} over Edinburgh.

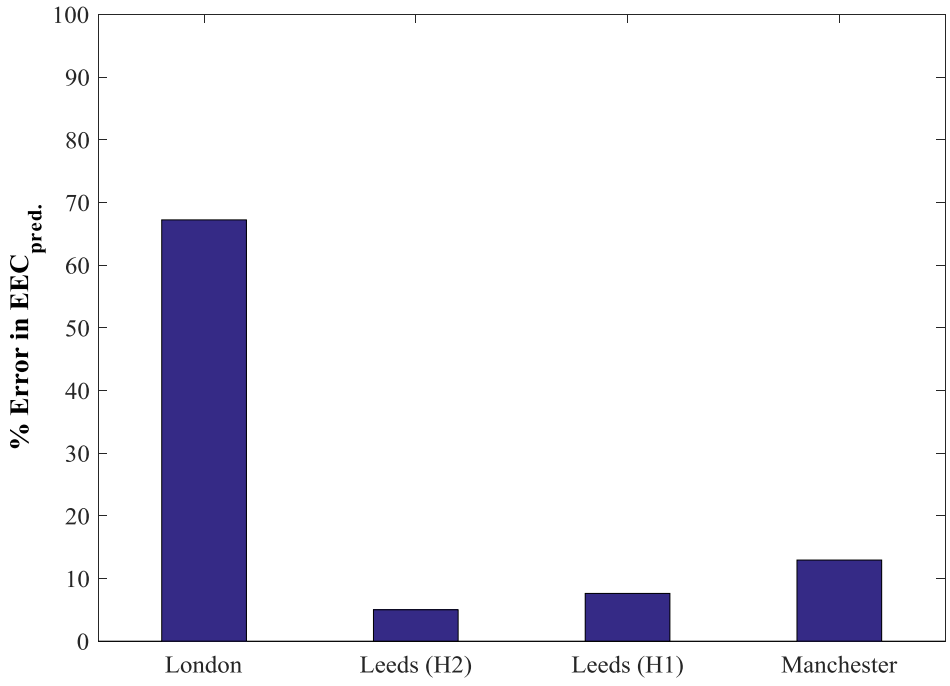

Figure 5. 25 : Mean percentage errors for EEC model predictions across the Leeds (H1 and H2), Manchester and London sites.

5.4.3 City-scale Variation of Wind speed, T.I. and EEC at Maximum Building Height

The city scale variations of the mean wind speed, $T.I.$ and the EEC at a mast height of 10 m above the maximum building heights (i.e. the maximum building height within each

neighbourhood grid) across Leeds, London, Manchester and Edinburgh were considered and results presented in this section. In order to ensure consistency and simplicity in result presentation, a mast height of 10 m was adopted. Compared to wind speed maps presented in Section 5.4.1 and 5.4.2, Figures 5.26 – 5.29 demonstrate huge wind resource potential at maximum building heights across each city. It is important to point out the increased wind speed resource observed at this height within the city centres in each city thus demonstrating significant reduction of the influence of local surface roughness (i.e. tall buildings/structures) on urban wind resource. Hence, higher wind speeds were estimated within Edinburgh with wind speeds above 7 ms^{-1} observed around the city centre. Results show an average wind speed of 4.7ms^{-1}, 4 ms^{-1}, 4.2 ms^{-1} and 5.4 ms^{-1} over Leeds, London, Manchester and Edinburgh respectively. This suggests that siting a turbine at this height tends to address the issues affecting the installation location of small wind turbines within built-up areas, with maximum wind speeds of 7.4 ms^{-1}, 6.7 ms^{-1}, 6.5 ms^{-1} and 7.8 ms^{-1} estimated across Leeds, London, Manchester and Edinburgh respectively.

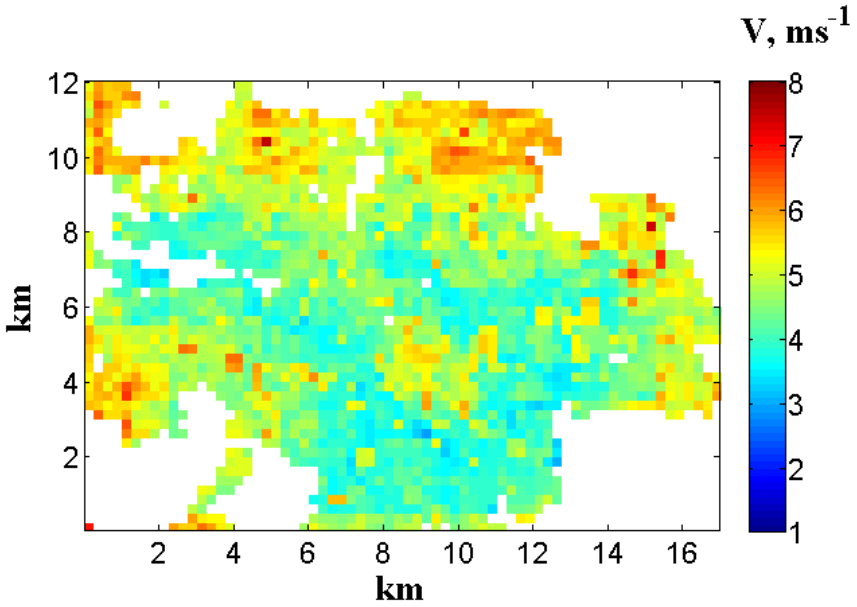

Figure 5. 26: Predicted mean wind speed (ms^{-1}) at 10 m mast height above the maximum building height within neighbourhoods over Leeds.

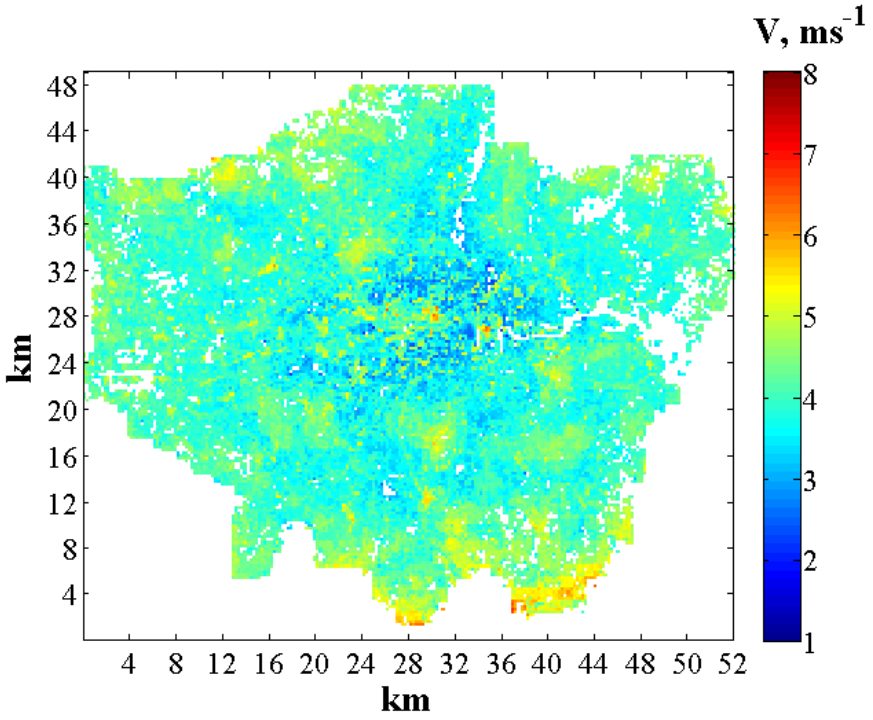

Figure 5. 27: Predicted mean wind speed (ms^{-1}) at 10 m mast height above the maximum building height within neighbourhoods within London.

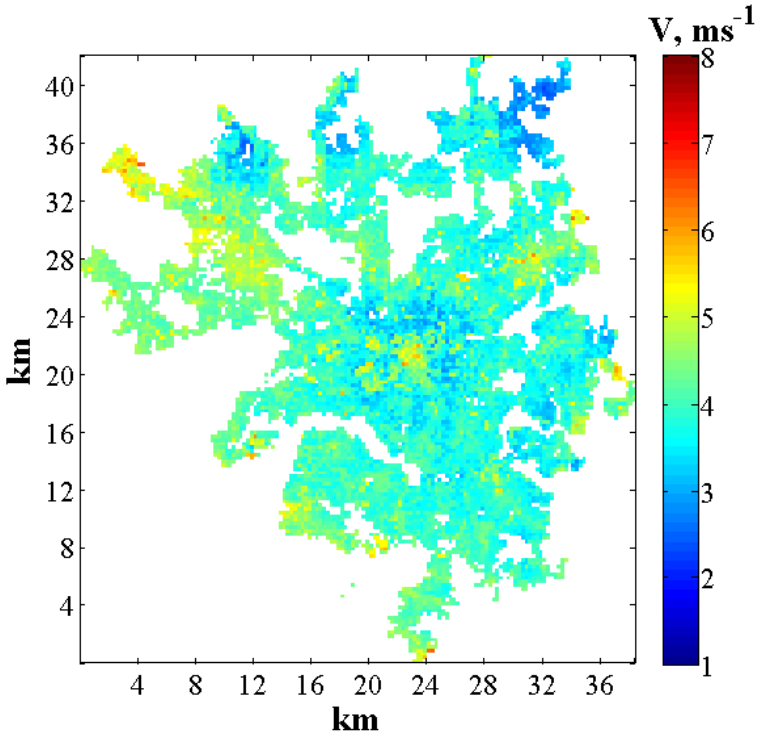

Figure 5. 28: Predicted mean wind speed (ms^{-1}) at 10 m mast height above the maximum building height within neighbourhoods within Manchester.

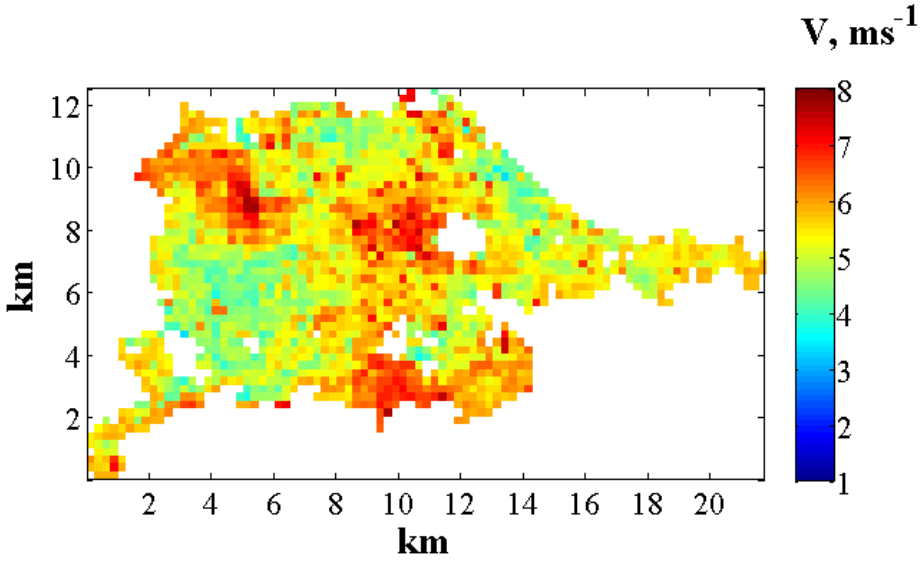

Figure 5. 29: Predicted mean wind speed (ms^{-1}) at 10 m mast height above the maximum building height within neighbourhoods within Edinburgh.

Figures 5.30– 5.33 show modelled $T.I.$ above the maximum building heights across the four cities using the methodology proposed in Section 5.2. These maps demonstrate the reduced effect of local surface roughness on urban wind resource as the vertical distance from the ground increases (as suggested in the wind speed maps). Thus, an estimated 10% decrease in the average $T.I.$ was predicted across each city if a turbine is relocated from the h_{hmeff} to the local maximum building height. This highlights the need for wind turbine systems to be mounted high enough to avoid complex turbulent local winds developed due to enhanced local roughness. This can be achieved by either mounting the turbine system on sufficiently tall masts or locating them on tall buildings/structures or ideally both.

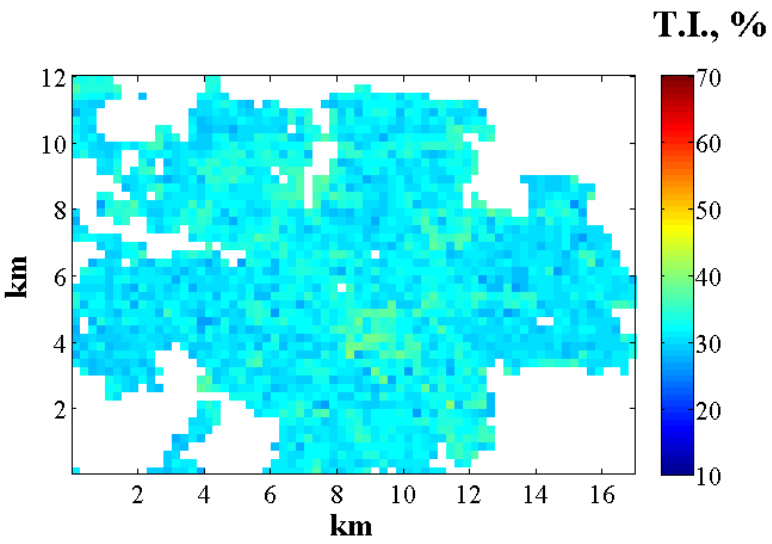

Figure 5. 30: Estimated *T.I.* at 10 m mast height above the maximum building height within neighbourhoods across Leeds.

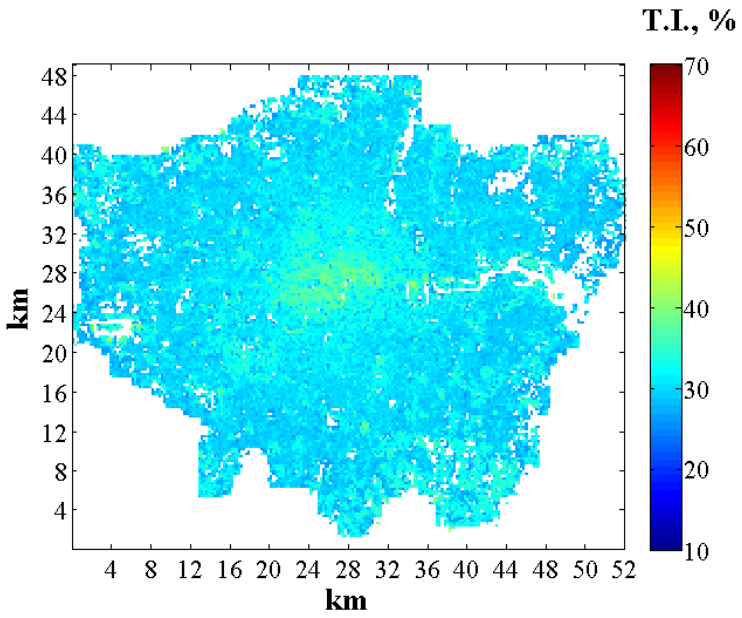

Figure 5. 31: Estimated *T.I.* at 10 m mast height above the maximum building height within neighbourhoods across Manchester.

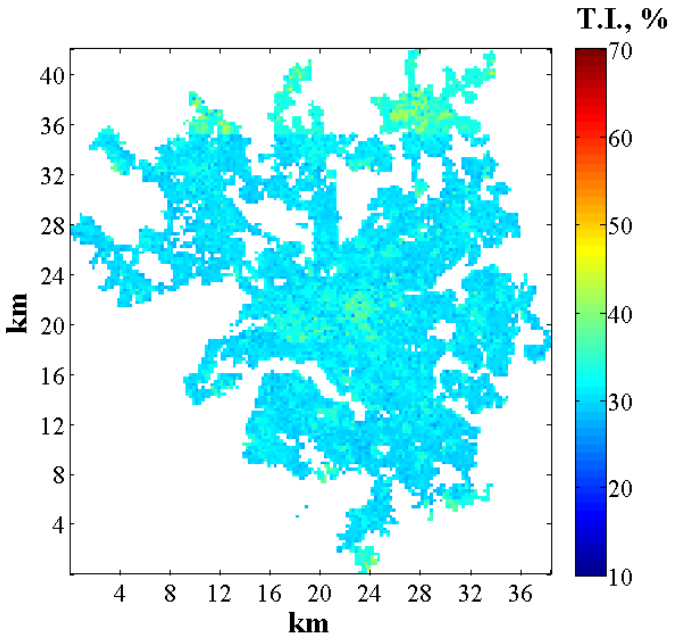

Figure 5. 32: Estimated *T.I.* at 10 m mast height above the maximum building height within neighbourhoods across Manchester.

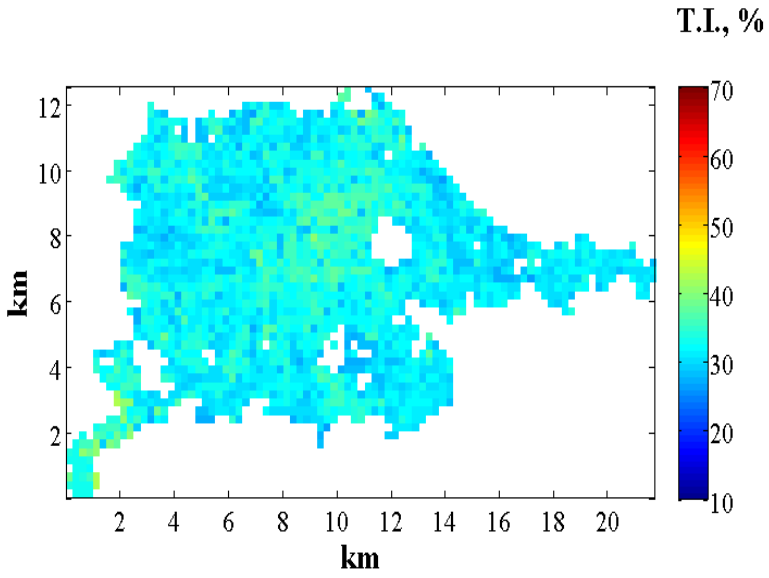

Figure 5. 33: Estimated $T.I.$ at 10 m mast height above the maximum building height within neighbourhoods across Edinburgh.

Lastly, the EEC available at the maximum building heights over Leeds, London, Manchester and Edinburgh cities are presented in Figures 5.34 – 5.37. Results show a loss of 20%, 20%, 17% and 19% in the average excess energy over Leeds, London, Manchester and Edinburgh respectively if the turbine is relocated from the h_{hmeff} to the local maximum height within a

given site. This suggests that the higher a turbine system is, the less cost effective advanced controls may be, hence providing relevant information for urban wind resource assessment for potential wind energy projects. Considering the EEC model mapped results at maximum building heights over the four cities, energy gains were observed to be generally higher around the city centres with a maximum additional energy content of about 52%, 66%, 61% and 59% predicted to be available to a fast response turbine system located on top of tall buildings over Leeds, London, Manchester and Edinburgh respectively. Thus, as shown in Figure 5.38, an increase of approximately 30%, 29%, 23% and 28% in the total integral wind energy was estimated over Leeds, London, Manchester and Edinburgh respectively if the turbine mast height was relocated from the h_{hmeff} to the local maximum building heights. Figure 5.38 demonstrates the overall change (i.e. percentage loss or gain) in the average wind speed, $T.I.$, EEC, average wind energy and the total integral energy in the wind (i.e. taking into account the excess energy available) over Leeds, London, Manchester and Edinburgh by changing the turbine location from h_{hmeff} to the top of a tall building (assumed to be the tallest building/structure within the neighbourhood grid) while considering a response time of 1 s.

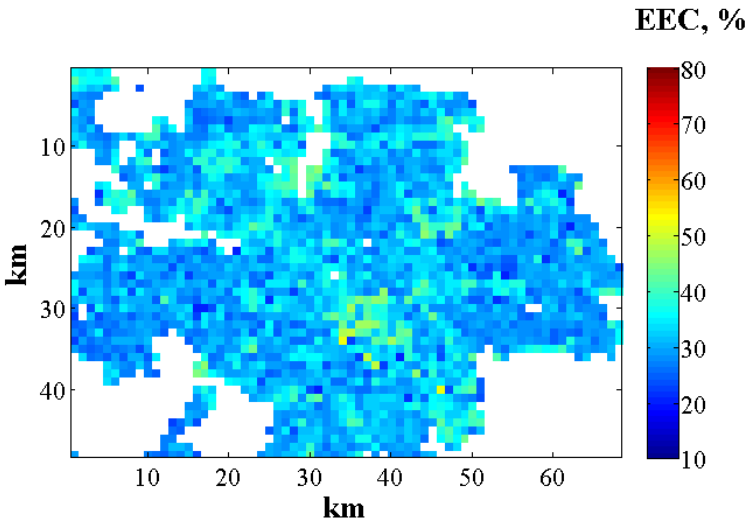

Figure 5. 34: Estimated *EEC* at 10 m mast height above the maximum building height within neighbourhoods across Leeds city.

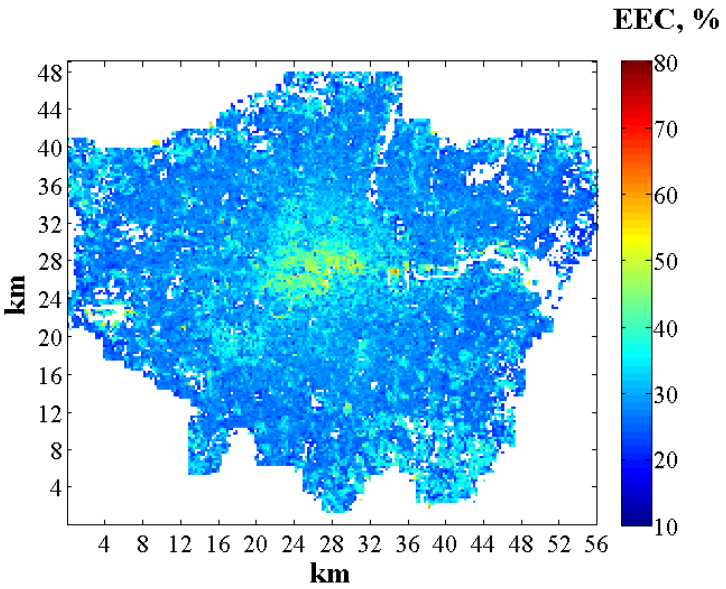

Figure 5. 35: Estimated *EEC* at 10 m mast height above the maximum building height within neighbourhoods across London.

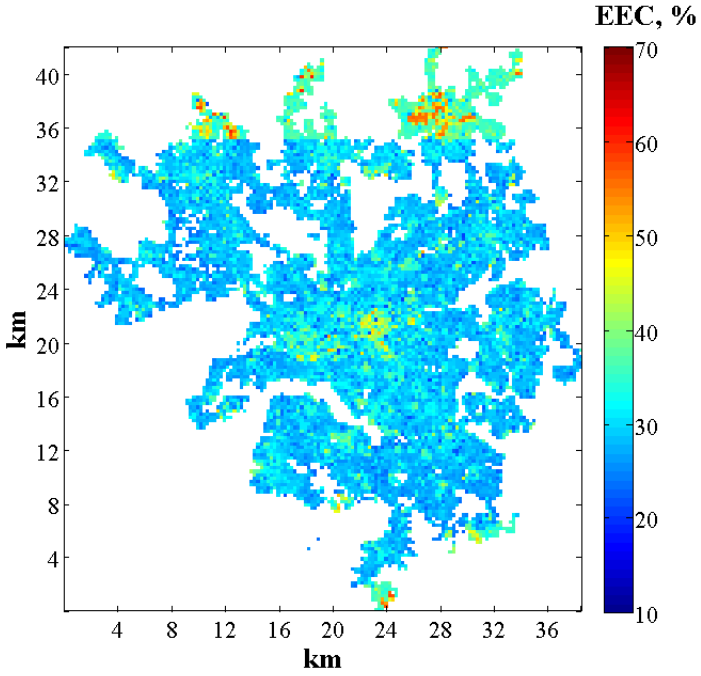

Figure 5. 36: Estimated *EEC* at 10 m mast height above the maximum building height within neighbourhoods within Manchester.

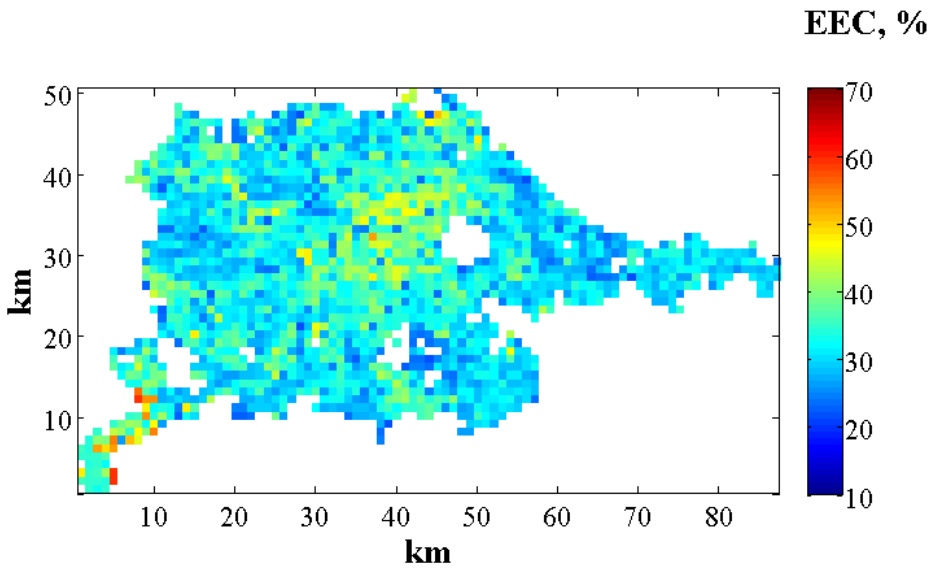

Figure 5. 37: Estimated EEC at 10 m mast height above the maximum building height within neighbourhoods within Edinburgh.

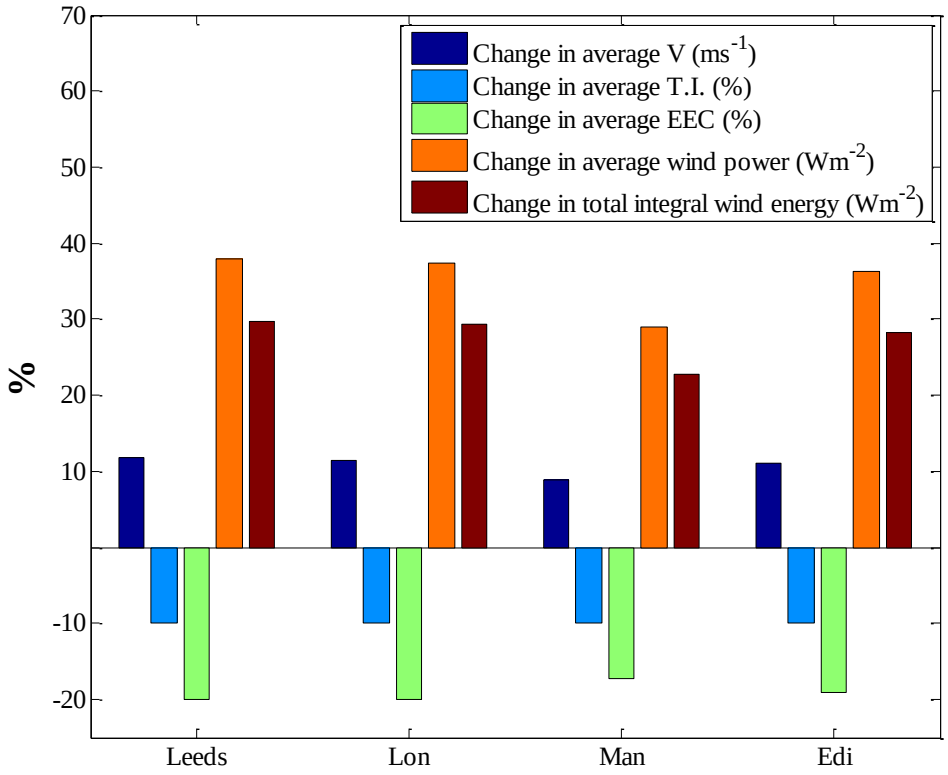

Figure 5. 38: Estimated percentage gain or loss in average wind speed, $T.I.$, EEC, wind power and the total integral wind power with change in mast height from h_{hmeff} to the maximum building height.

5.5 Summary

The possibility of predicting mean wind speeds, turbulence intensities and excess energy potentially available to turbines employing gust tracking at different heights within an urban environment was demonstrated using analytical down-scaling and *T.I.* estimation methods which employed detailed building data to estimate aerodynamic characteristics over the city. High temporal resolution wind measurements from eight potential urban rooftop sites were used in developing a model which was able to estimate excess energy content based on the predicted turbulence intensities. Several simplified models for predicting *T.I.* as functions of roughness length, friction velocity and effective mean building height were tested at 4 potential turbine sites. The accuracy of each model was assessed by comparing model predictions with *T.I.* observations from the test sites. Models 4 and 6, based on a simple log function using roughness length, performed poorly at all test sites. Model 1 and Model 3 showed better accuracies for $^{z}/_{h_{hmeff}}$ > 0.8 with substantial improvements in performance when the effective mean building height (h_{hmeff}) parameter was used instead of the local mean building height, confirming the importance of building height variability in determining the effect of a complex urban surface on the flow above it. Further tests to validate the EEC prediction model proposed in Chapter 4 were carried out. Analysis of measured wind speed data showed increased EEC at higher *T.I.* values signifying the potential to estimate the additional energy available to a turbine if accurate modelling of turbulence intensities is achieved. Hence, an empirical relationship was derived to predict the EEC within a built environment using *T.I.* values obtained at a given turbine response time represented by the appropriate averaging time of the raw data (T_C).

The viability of urban wind energy resource at a city scale was then considered by producing maps of mean wind speed, *T.I.* and EEC across the city using Leeds as a first test site. Mapped results at a mast height of 10 m above the effective mean building height (h_{hmeff}) over Leeds showed mean wind speeds of an average of 4.2 ms^{-1}, an average turbulence intensity of 40% and an average EEC of 38.75% within the city centre area when considering a response time of 1 s. As the distance from the city centre increased, results showed a general increase in the mean wind speed while *T.I.* and EEC decreased, thus highlighting the potential of gust tracking solutions in countering problems of reduced turbine power within the built-up city centre environment. The effect of increasing turbine response time on EEC was also considered. Results showed a decrease in average EEC from 53.2% to 39.2% around the city centre and 38.8% to 28.6% over the city when T_C increased from 1 s to 10 s with a further increase in T_C from 10 s to 60 s leading to a 50% loss in average EEC compared to a response time of 10 s over the city.

Having tested these methodologies over Leeds city, they were further applied to three major UK cities namely London, Manchester and Edinburgh. Mapped results at the mast height of 10 m above h_{hmeff} showed average wind speeds of 3.6 ms^{-1}, 3.8 ms^{-1} and 4.9 ms^{-1}, average turbulence intensities of 33.76%, 33.58% and 35.17%, and average EEC values of 36.38%, 35.83% and 39.61% for London, Manchester and Edinburgh respectively. A comparison between the performance of the MH model and the Macdonald model over London city was also provided, with results suggesting improved accuracy within the MH model in predicting the annual mean wind speed within a built environment. A comparison of the wind resource at different heights within the urban canopy was also carried out by mapping the wind speed, $T.I.$ and EEC at the maximum building heights (assumed to be the height of the tallest building within each neighbourhood grid) across all four cities. Results showed higher wind speed values at this height, with averages of 4.7 ms^{-1}, 4 ms^{-1}, 4.2 ms^{-1} and 5.4 ms^{-1} predicted over Leeds, London, Manchester and Edinburgh respectively. The average $T.I.$ was estimated to decrease by 10% across the four cities if the turbine hub height was changed from h_{hmeff} to the maximum building height. Also, losses of 20%, 20%, 17% and 19% in the average excess energy were predicted over Leeds, London, Manchester and Edinburgh respectively at the maximum building height. The results highlight the potential of a fast response turbine system in extracting the additional energy available within the urban environment. This study also suggests that siting turbine systems above the local maximum building heights may help address the issue of reduced turbine performance due to local turbulence within a built-up area. In future work, it is proposed to map the *T.I.* and *EEC* over more cities when LiDAR building height data are made available. Although considered in Chapter 6, this study proposes more analysis of different control methodologies and field data in a bid to test whether the predicted excess energy can be realised within practical systems.

CHAPTER 6

6 A Method for Estimating the Power extracted by a Micro-wind Turbine system over a Built Environment

6.1 Introduction and Objectives

Although wind energy applications within a built environment have displayed some distinct benefits, they are faced with many challenges. The complicated nature of the urban wind resource and the inability to predict the actual energy generation within a built environment leads to reduced markets as well as yields from micro wind technologies installed within suburban/urban areas. Various wind energy assessments have employed turbine power curves in estimating the power output of a specific turbine system within potential turbine sites [269, 295, 296]. As a result of many investigations, it is broadly acknowledged today that the power curve of a given wind turbine system is influenced by several meteorological and topographical parameters like wind shear, turbulence and inclined airflow, etc.[266]. A major shortcoming in most turbine power assessment studies is that wind speed measurements used in the development of the power curves may not fully represent rapidly fluctuating, turbulent urban wind resource thus making most power curves site dependent. Hence, uncertainties that may arise from assumptions based on local atmospheric conditions while developing turbine power curves or undertaking power performance assessment of turbine systems may lead to under-prediction or over-prediction of the actual power output should generic power curves be applied within built environments. This may have significant implications on the viability of small wind turbine projects within a potential suburban/urban site. The ability of a turbine system to respond to high fluctuations present in an urban wind resource will depend on the response characteristic of the specific system. Although few studies focused on the dependency of energy efficiency of small wind turbines on response time within a suburban/urban area can be found, McIntosh *et al* [234], Kooiman and Tullis [286] and Nguyen and Metzger [262] highlighted the importance of turbine response time and its influence on energy capture within a built environment.

This chapter assesses the potential of micro wind turbine systems as well as proposing a methodology for estimating the power capabilities of the turbine system within a built-up area while considering the influence of local turbulence. Section 6.2 briefly introduces the wind data employed whereas the new model known as the turbine power estimation model (TPE), which comprises of the excess energy coefficient (EEC) model and the turbine performance

coefficient model, is presented in Section 6.3. This model takes into account local turbulence and the excess energy available within a given suburban/urban environment. Section 6.4 considers the effect of response time on the turbine performance coefficient and turbine power estimation model. Section 6.5 analyses the city-scale variation of average power outputs when the turbine power estimation model is applied across four cities namely Leeds, Edinburgh, Manchester and London. Results are presented while considering turbine operation at two different heights within each city; (i) the effective mean building height (ii) local maximum building height. Section 6.6 discusses the influence of turbine response on average power output across the four cities while Section 6.7 presents a brief comparison between the TPE model and the use of a generic power curve. Finally, the main conclusions are presented in Sections 6.8.

6.2 Methodology and Data Processing

For this study, eight high-resolution wind datasets obtained from five different cities namely Leeds, Manchester, London and Dublin and Helsinki were employed. Site descriptions for data employed were presented in Section 3.1.1. For the purpose of this study, the raw wind data was filtered at an averaging time (T_c) of 1 s. Methodologies for processing the wind data, obtaining the $T.I.$ and calculating the excess energy content (EEC) available within a built-up environment were provided in Chapter 3 and are adopted herein. The variable-speed vertical axis wind turbine (VAWT) model, as described in Section 3.3, was employed in this study with input from processed wind data from the 8 potential turbine sites. The turbine power calculated at different response times were parsed into 10-min bursts (i.e. T = 10 min) in order to maintain consistency with $T.I.$ and EEC values used.

6.3 Turbine Power Estimation Model

Generally, power generated by a turbine can be given as [269]:

$$P_T = \frac{1}{2} C_p \rho A \bar{V}^3 \qquad \text{Equation 6. 1}$$

where C_p represents the power coefficient of the turbine system, ρ represents the air density, A represents the rotor swept area and $\bar{V}$ is the mean wind speed over a burst period. Various studies have demonstrated the effect of turbulence on turbine power by adopting measures of factoring turbulence intensity into turbine power estimation. This has been achieved either by directly using $T.I.$ as a form of heuristic safety factor (i.e. reducing the turbine power

estimation by its percentage value [180]) or by adjusting or correcting the manufacturer's power curve for different turbulence intensity values [193]. These require complex methodologies which may not be user-friendly or readily accessible to micro-turbine purchasers or investors. It should be noted that turbine manufacturers are currently not required (by an industry standard or practice) to rate their turbine systems for an arbitrary or more realistic turbulence intensity. Built environments are characterised by fluctuating, turbulent winds as a result of enhanced local roughness. Hence, as turbulence levels within an urban wind resource increase or decrease, the C_p (as represented in Equation 6.1) has to be adjusted to account for inherent local turbulence. In order to estimate the power generated by the VAWT within a characteristic urban wind resource, a methodology is proposed herein. This methodology, which estimates the turbine power from averaged wind over a built environment within a given burst period, is referred to as the turbine power estimation (TPE) model and is mathematically given as:

$$P_T = \frac{1}{2} C_{tc} \rho A \bar{V}^3 \qquad \text{Equation 6. 2}$$

Similar to Equation 6.1, C_p is replaced by a new parameter C_{tc}, which is termed the turbulence induced performance coefficient of the turbine system. C_{tc} is mathematically given as:

$$C_{tc} = C_e(EEC + 1) \qquad \text{Equation 6. 3}$$

where EEC is the excess energy content at a given burst period within the potential turbine site (defined by Equation 3.3) and C_e is the unsteady turbine performance coefficient.

The performance coefficient C_{tc} takes into account the effect of turbulence and response time on the turbine performance while also considering the excess energy content available to the turbine. In order to predict the C_e for a given VAWT system within a built environment, the C_e for a given burst period of 10 min (i.e. T = 10 min) across the year was obtained using Equation 6.4 and plotted against the equivalent binned values of $T.I.$ for the 8 test sites.

$$C_e = \frac{\int_0^T P_{vsc}\, dt}{\int_0^T P_w\, dt} \qquad \text{Equation 6. 4}$$

where P_{vsc} represents the instantenous VAWT power outputs from model simulations using the VSC control model at response time of 1 s using the wind datasets from the eight sites as inputs and P_w represents the instantaneous wind power calculated using Equation 6. 5.

$$P_w = \frac{1}{2}\rho A V_i^3$$ Equation 6. 5

where V_i represents the wind speed measurements at a given averaging time (in this case, T_c = 1 s).

For an ideal (i.e. perfect) turbine operation within an idealised steady wind environment, the C_{tc} would be 0.59 (i.e. C_e and EEC would be 0.59 (Betz limit) and 0 respectively). This indicates that the excess energy and turbine performance calculated reflects the time-series integral. However, due to real world gustiness and losses encountered by the turbine system while operating at potential sites (for example, transmission losses, electrical losses, etc.), this may not be realised. When analysing the unsteady turbine performance, the turbine response was first assumed to be 1 s and the raw wind data was also filtered at an averaging time (T_c) of 1 s, as stated earlier. Losses encountered in turbine operations (i.e. electrical losses, strut losses, mechanical losses, etc.) were not considered herein hence the estimations are likely to be the upper limit compared to what might be realised in practice. Plots of binned C_e values against $T.I$ bins as shown in Figure 6.1 demonstrate a strong relationship between C_e and $T.I.$ with increases in $T.I.$ resulting in decreased turbine performance at all test sites. An empirical equation for the prediction of C_e values as a function of $T.I.$ was determined using the least square errors approach within MATLAB's best fit tool. After various tests to determine the lowest errors, a single-term exponential form was assumed, hence C_e values were approximated using the following empirical relationship:

$$C_e = ae^{cx}$$ Equation 6. 6

where

$x = (T.I. - q)/s$

Table 6.1 presents the coefficients derived from best fit of a $C_e - T.I.$ curve at a response time of 1 s (i.e. T_c = 1) shown in Figure 6.1. This suggests that from the knowledge of turbulence intensities, the performance of a given turbine design could be estimated. However, further analysis showed that increasing the turbine inertia may lead to a decrease in the power generated by the turbine system. This is demonstrated in Figure 6.2, by comparing the performance of the turbine system having a standard baseline inertia (J) with the turbine performance when the standard baseline inertia is increased by 20% (represented by 'J + 20% J' in Figure 6.2). Results show a significant decrease of approximately 24.4% in turbine performance observed at the Leeds (H1) site should the turbine system experience a 20% increase in its inertia. Hence, from Equations 6.2 and 6.3, one can deduce a decrease of

24.4% in the power predicted using the TPE model should the turbine inertia be increased by 20%. This, however, suggests that the turbine inertia has a big impact on the power generated by turbine system, as well as the overall economic benefits for potential urban wind projects. Thus, further sensitivity analysis should be carried out in testing the effects of inertia on the turbine power estimation (TPE) model. This may include testing the performance of the TPE model over various turbine designs and inertia values. This, however, is not covered within this study.

Table 6. 1: Coefficients used in predicting the unsteady power coefficient required for the power estimation model (as given in Equation 6.6).

Constants	
a	23.85
c	-0.7476
q	43.32
s	21.32

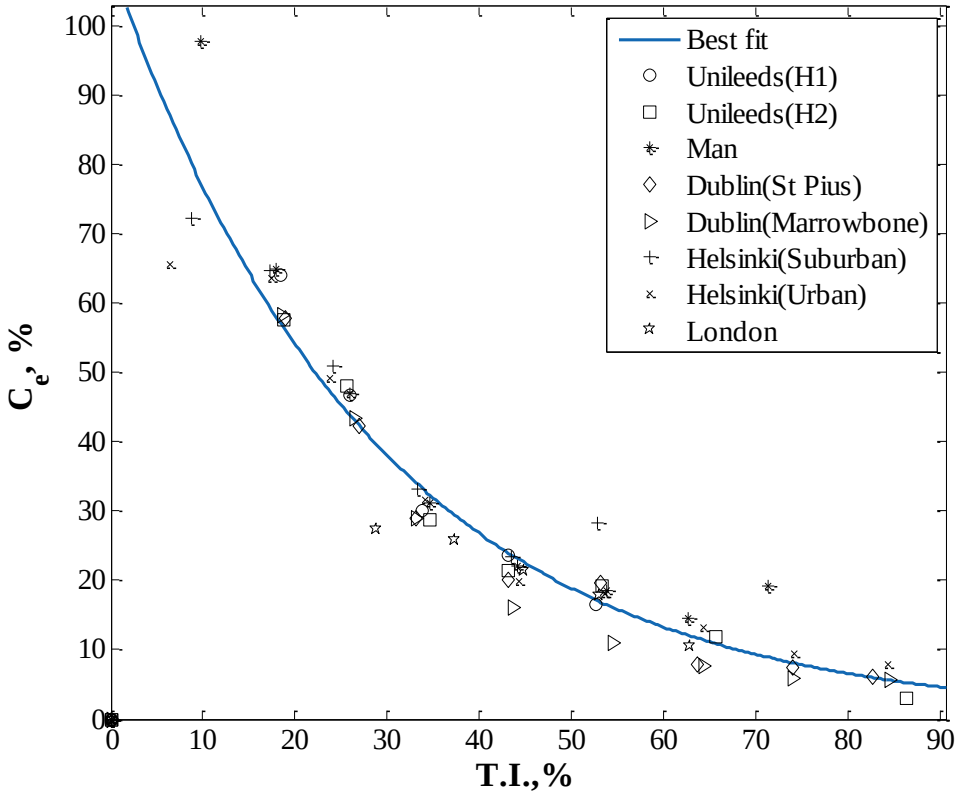

Figure 6. 1: Plots representing best fit for binned C_e at different $T.I.$ bins for all 8 sites at T_c = 1 s (as shown in Equation 6.6 and Table 6.1).

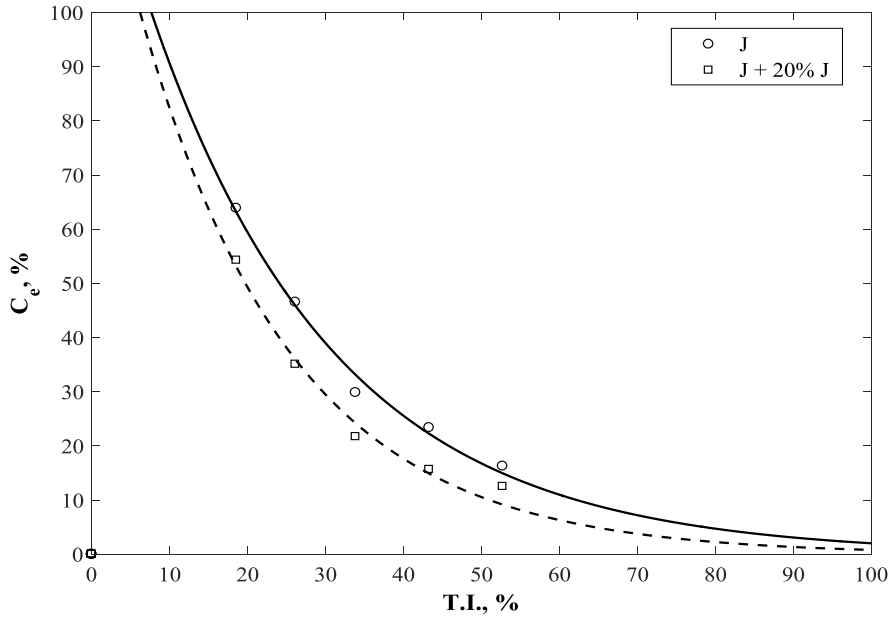

Figure 6. 2: Effect of increase in Inertia on turbine performance at the Leeds (H1) site; solid line represents the best fit for turbine operation with standard baseline Inertia (J), and broken line represents the best fit for turbine operation when the baseline inertia is increased by 20% (represented by 'J + 20%').

EEC values were calculated using the EEC model as proposed in Chapter 5. Thus, incorporating Equation 5.5 and Equation 6.6 into Equations 6.3, the turbine power output at a potential site which takes into account the effect of local turbulence can be estimated using Equation 6.2. A comparison between the turbine power estimation model values (P_{T_pred}) and power output obtained from VSC VAWT model simulations (P_{VSC}) at a burst period of 10 mins using wind data from all 8 sites as input was achieved by using the mean percentage error (MPE) as defined in Equation 6.7. Figure 6.2 presents the MPE at different $T.I.$ bins for all 8 sites.

$$\text{MPE}(\%) = 100 \times \frac{1}{n} \sum \frac{\left| P_{VSC} - P_{T\_pred} \right|}{P_{VSC}} \qquad \text{Equation 6. 7}$$

As demonstrated in Figure 6.3, TPE model errors for $T.I.$ between 40 – 60% were shown to be as low as 15.7%. Further analysis showed higher TPE model errors within Dublin Marrowbone and Helsinki Suburban sites. This may have resulted from lower occurrence within this $T.I.$ bin (See Appendix A), thus suggesting reduced level of model accuracy of the TPE model within 40-60% $T.I.$ bins. Also, TPE model errors within the 20 – 30% $T.I.$ bin were observed to be low across all sites but the London site where the occurrence of such conditions were less frequent (See Appendix A). Hence, the TPE model showed fairly good performance at all sites for turbulence intensities between 20 – 60%, which represented the dominant $T.I.$ demonstrated by the $T.I.$ frequency distribution (as shown in Figure 6.2). Turbine power predictions at $T.I.$ less than 20% and also within the 60 – 70% bin resulted in errors as high as 25.6%. A poor performance was also observed at $T.I.$ higher than 70% across all sites. This was expected at these turbulence intensities as the occurrence of such turbulent conditions will be less frequent within built environments (as demonstrated in Figure 6.3 and Appendix A). As shown in Figure 6. 4, the average power output estimation using TPE model is found to have a positive correlation with VAWT power outputs thus implying better turbine power estimation. It will be interesting to compare average power outputs from turbines using advanced controls and the TPE model. Hence, these results suggest the possibility of predicting fairly well turbine power by a simple model within a built environment as long as the local mean wind speed and $T.I.$ are known.

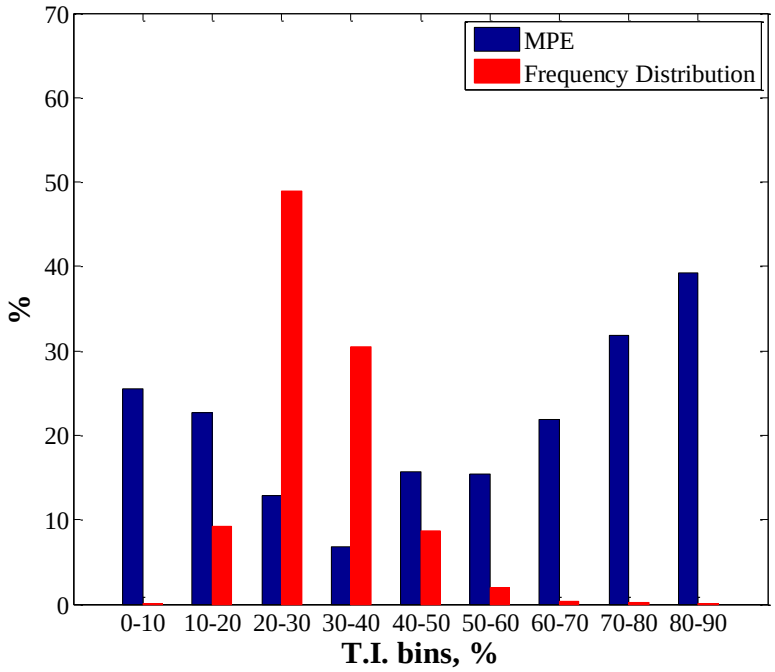

Figure 6. 3: Power estimation errors and frequency distribution compared over eight sites at a response time of 1 s.

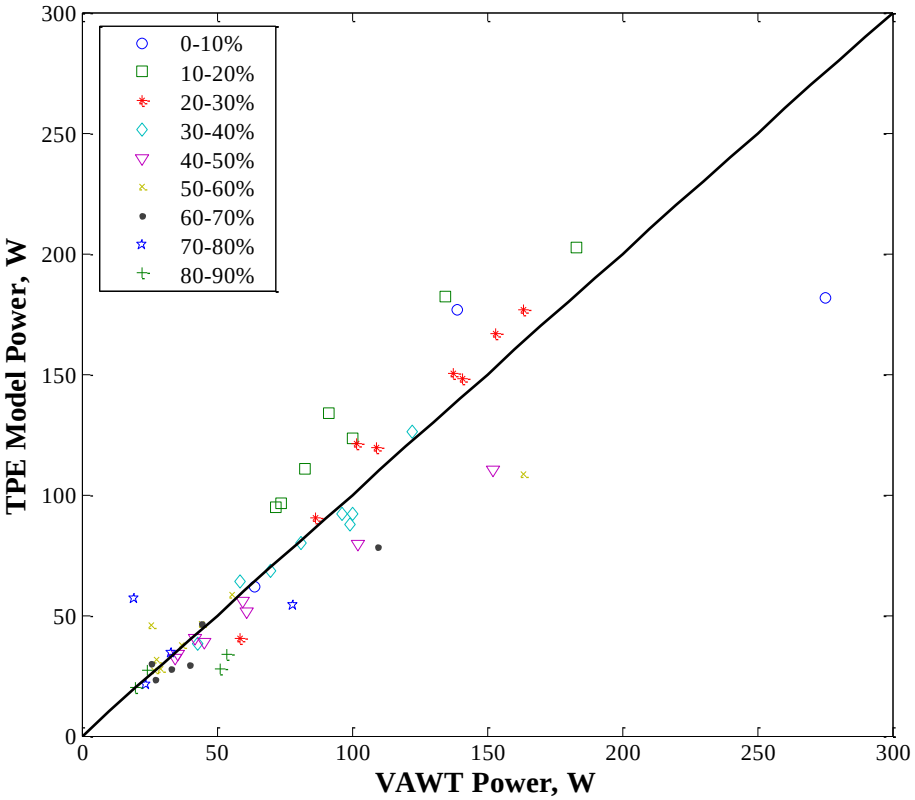

Figure 6. 4: Predicted power output from TPE model versus power outputs from VAWT model for all sites at different turbulence intensities (coloured symbols) and a response time of 1 s. The solid line represents a one-to-one relationship.

6.4 Effect of T_c on C_e and Turbine Power Estimation

Turbine response time has been shown to significantly influence the energy capture within an urban wind resource [262]. Considering the influence of various factors such as turbine inertia, higher local gust frequencies, time lag of experienced by controllers, etc., on turbine operations, turbine systems with a response time of 1 s may not be feasible in real world applications within built environments. Hence, different response times were considered to assess the effect on turbine power output within an urban wind resource for potentially different VAWT designs. This is demonstrated by calculating the unsteady turbine performance coefficient (C_e) at different response times of 10s, 20s and 30s within a burst period of 10 min using Equation 6.4. These C_e values plotted against the equivalent binned values of $T.I.$ at the eight potential turbine sites are presented in Figure 6.5. The best fit for C_e - $T.I.$ plots at different response times were determined using the least square errors approach within MATLAB's best fit tool. After various tests to determine the lowest errors, a two-term exponential form was assumed for response times of 10 s, 20 s and 30 s. Hence, C_e values were approximated using the following empirical relationship:

$$C_e = ae^{cx} + be^{dx} \qquad \text{Equation 6. 8}$$

where

$x = (T.I. - q)/s$

A summary of the coefficients of the two-term exponential for the different response times are provided in Table 6. 2. The maximum response time considered within this study was 30 s above which the turbine system may be considered uneconomical for operations within a built environment.

Table 6. 2: Summary of the coefficients for the best fit for $C_e - T.I.$ plots at different response times across the 8 sites.

Constants	**Turbine Response time (s)**		
	10	**20**	**30**
a	19.02	23.51	0.6099
b	3.789	1.045	19.84
c	-0.4299	-0.5336	-3.342
d	-1.806	-2.881	-0.2464
q	41.19	35.99	35.79
s	21.2	21.03	20.95

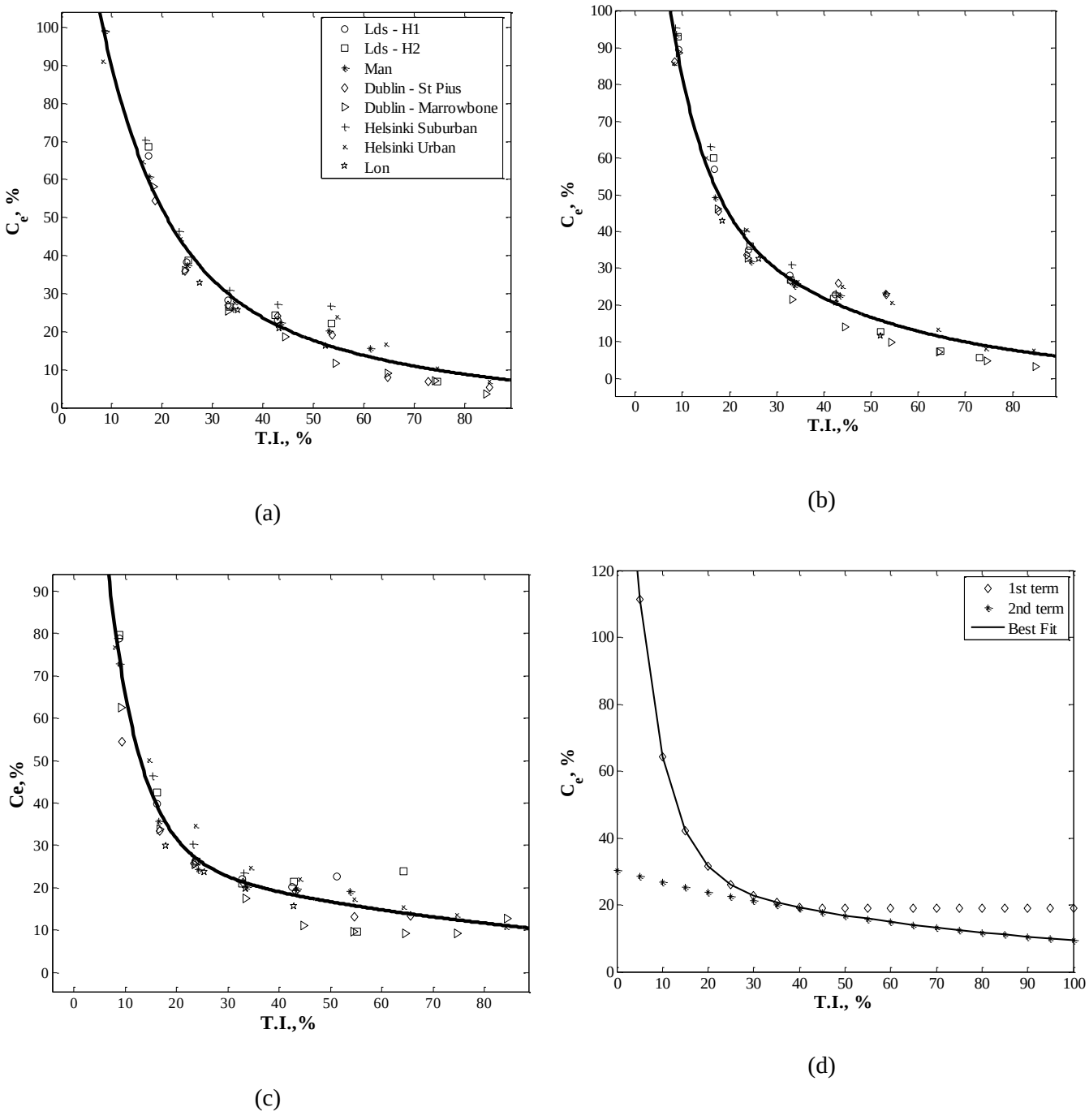

Figure 6. 5: Plots representing best fit for binned C_e at different $T.I.$ bins for all 8 sites at different $T_c s$ (a) 10 s (b) 20 s (c) 30 s (d) Description for the best fit at T_c = 30 s.

As shown in Figure 6.5, it was observed that as the response time of the turbine increased, the C_e - $T.I.$ curve was observed to be steeper at lower turbulence intensities (represented by the first term of the exponential in Equation 6.8) and flatter at higher turbulence intensities (represented by the second term of the exponential). A simple plot distinguishing the first and second terms of the exponential in Equation 6.8 is demonstrated in Figure 6.5d. Thus,

Figure 6.5 suggests that as the response time approaches 30 s, less significant changes in the turbine's power output may be observed at higher turbulence intensities, whereas a steep increase in power may be observed at lower turbulence intensities as the turbine becomes less sensitive to wind fluctuations. Consequently, in order to adequately reflect the variation in the steepness of the C_e - $T.I.$ curve at lower turbulence and the degree of sensitivity of the turbine system at higher turbulence as a result of changes in response times (as shown in Figure 6.5), four empirical models were employed (See Table 6.1 and 6.2). Hence, the development and validation of a single systematic C_e - $T.I.$ empirical model that reflects the effect of varying turbine response times will require further sets of field measurements and turbine tests as they become available. These relationships obtained at different response times (as represented by the coefficients in Table 6. 2) were employed in calculating the turbulence induced power coefficient (C_{tc}) using Equation 6. 3. Thus, they served as inputs in estimating the turbine power across the 8 potential sites using Equation 6.2.

The VAWT model power outputs across the 8 potential sites were obtained by using wind data filtered at averaging times of 10 s, 20 s and 30 s as input to the turbine model with VSC controls. These outputs were compared with turbine power prediction model outputs using the mean percentage error (MPE) parameter defined by Equation 6.7. Figure 6.6 presents MPE plots across different $T.I.$ bins at different response times for all eight sites. Results show good TPE performance at a response time of 10 s, with power prediction errors less than 16% at turbulence intensities below 40%. Further analysis showed over 90% of the wind resource across the 8 test sites to have occurred at $T.I.$ below 40%. High TPE model errors were observed at higher turbulence intensities (i.e. $T.I.$ > 50 %) which represent a very small percentage of the wind resource at the test sites. The TPE model demonstrated good power predictions at the response times of 20 s and 30 s (as shown in Figure 6.6). However, higher errors were observed in less frequent turbulence intensity bins (i.e. 10 – 20% $T.I.$ bin and at $T.I.$ > 50%). This is in agreement with results obtained at a response time of 10 s (as shown in Figure 6.6 a). Further analysis showed these high errors were as a result of poor model accuracy at Helsinki (suburban and urban) and Dublin Marrowbone sites due to these turbulence intensity bins being less frequent. Figure 6.7 presents the overall average MPE for different response times at all eight sites with average model errors of 14.11%, 14.51%, 15.64% and 13.33% suggested at response times of 1 s, 10 s, 20 s and 30 s respectively. It is important to clearly state that this study demonstrates the effect of response time on the turbine performance within a built environment. However, development of a more systematic C_{tc} function which reflects the variation in response time as well as testing and validity of such a turbine power estimation model over a wider region will require further sets of field measurements from suburban/urban sites as they become available, further study on VAWT

modelling and performance assessments (i.e. vortex modelling and design optimization), advanced controls system modelling and analysis, wind tunnel tests, etc.

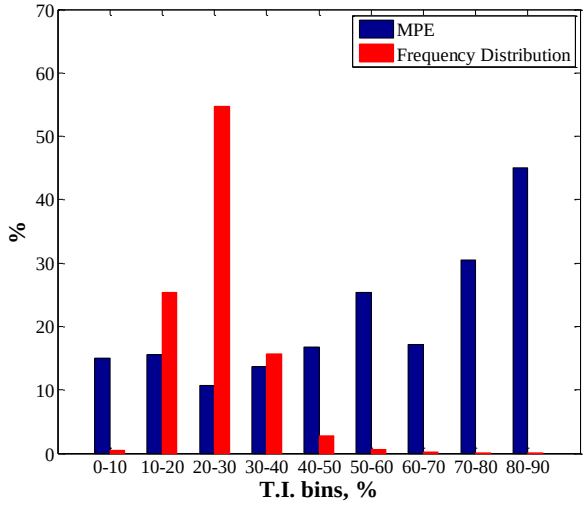

(a)

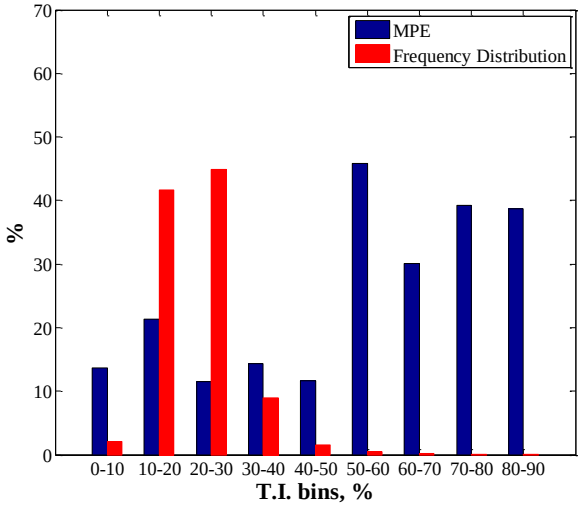

(b)

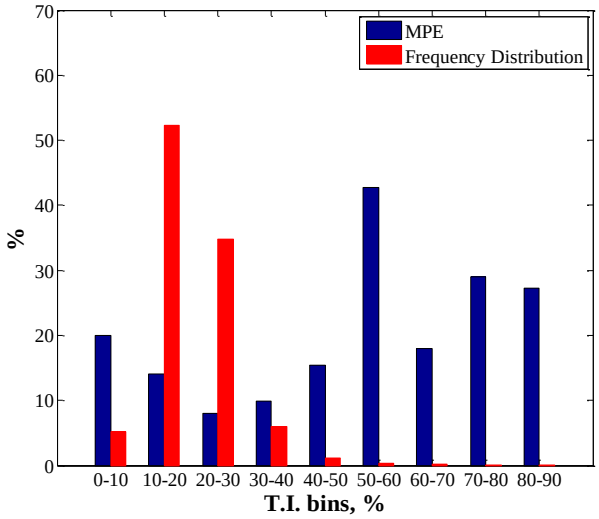

(c)

Figure 6. 6: Power estimation errors and $T.I.$ frequency distribution compared over eight sites at different response times (a) 10 s (b) 20 s (c) 30 s.

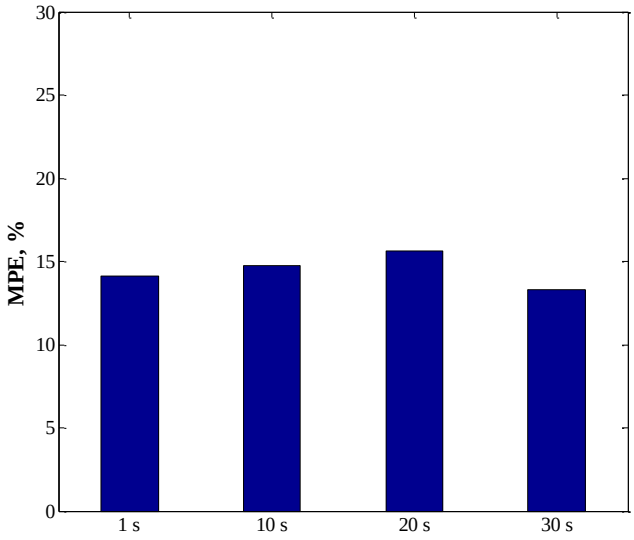

Figure 6. 7: Overall Average TPE model errors at different response times for all eight potential turbine sites.

6.5 City-Scale Variation of the Power Estimation Model

6.5.1 Performance at Effective Mean Building Height

Before considering the city scale variation of turbine power by using the TPE model at a given hub height across a built environment, the turbulence induced performance coefficient (C_{tc}) for the turbine system at a response time of 1 s was estimated. This was achieved by incorporating the turbulence intensity estimation model (as presented in Chapter 5) into Equation 6.6 in estimating the unsteady performance coefficient (C_e) of the turbine system. This, together with the EEC estimation model presented in Chapter 5, served as inputs in predicting the C_{tc} values using Equation 6.3. This was tested over four major UK cities. For the purpose of simplicity in result presentation and analysis, the C_{tc} values were multiplied by 100 and thus presented in percentages (%). Figure 6.8 demonstrates the city-scale variation of C_{tc} at 10 m above the effective mean building height (h_{hmeff}) for each neighbourhood region over four cities namely; Leeds, London, Manchester and Edinburgh.

Not taking into account turbine system losses (for example, strut losses, electrical losses, etc.), mapped C_{tc} estimation over all four cities generally showed higher values as the distance from the city centre increases. Low C_{tc} values were generally observed in neighbourhoods around the city centre which may be due to higher turbulence observed as a result of increased interaction between the local wind and the inherent buildings/structures (as demonstrated in

Figure 5.9) thus leading to reduced turbine performance. Results showed average C_{tc} values of 44.56%, 44.31%, 45.59% and 45.49% for Leeds, Edinburgh, Manchester and London respectively. Further analysis across all four cities showed minimum C_{tc} value of 36.21% observed over London whereas a maximum C_{tc} value of 52.86% was observed in all four cities. This higher C_{tc} value was observed in neighbourhood regions with lower turbulence intensities.

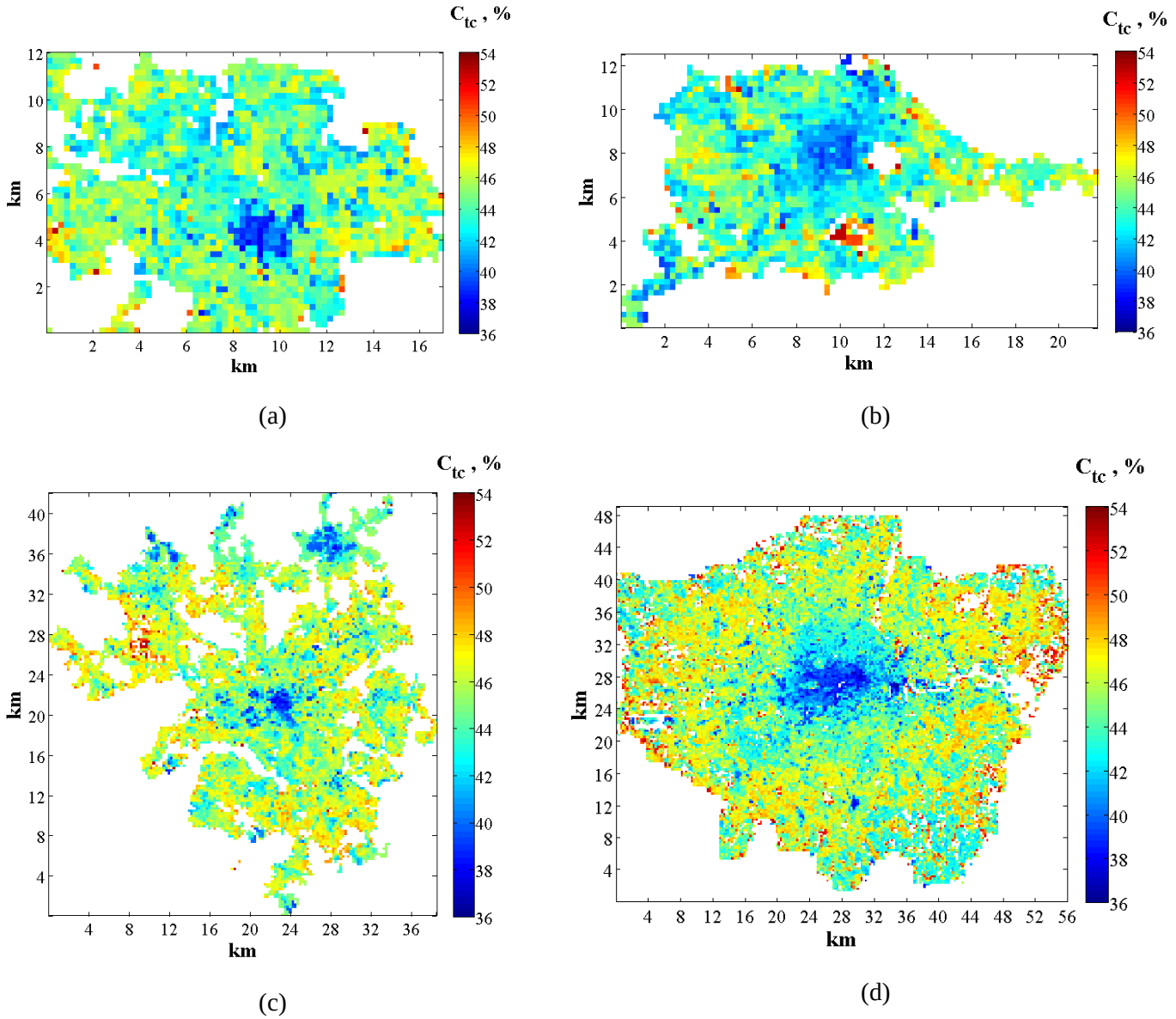

Figure 6. 8: Map of the C_{tc} for the VAWT model at 10 m above the effective mean building height over all four cities (a) Leeds (b) Edinburgh (c) Manchester (d) London.

In order to estimate the turbine power from average wind at a given hub height over a built-up area, the TPE model (as defined by Equation 6.2) was developed by combining the $T.I.$

and EEC estimation models presented in Chapter 5, the C_e estimation model as proposed earlier in Section 6.3 and the wind speed prediction model (MH model) which is based on long term wind speed averages (details of the MH model were provided in Chapter 3). Figure 6.9 represents mapped city-scale variation of the turbine power at 10 m above the effective mean building height (h_{hmeff}) over the four cities. Results showed low power outputs over each city excluding Edinburgh where higher power outputs of above 120 W were observed within neighbourhood regions around the city centre. Estimated average power outputs of 47.95 W, 71.38 W, 35.43 W and 30.09 W were observed over Leeds, Edinburgh, Manchester and London respectively. However, model results for all four sites showed a minimum power output of 5.62 W within Manchester and maximum power outputs of 176.72 W, 195.77 W, 131 W and 145.97 W over Leeds, Edinburgh, Manchester and London respectively. A summary of observations at all four sites is presented in Table 6.3.

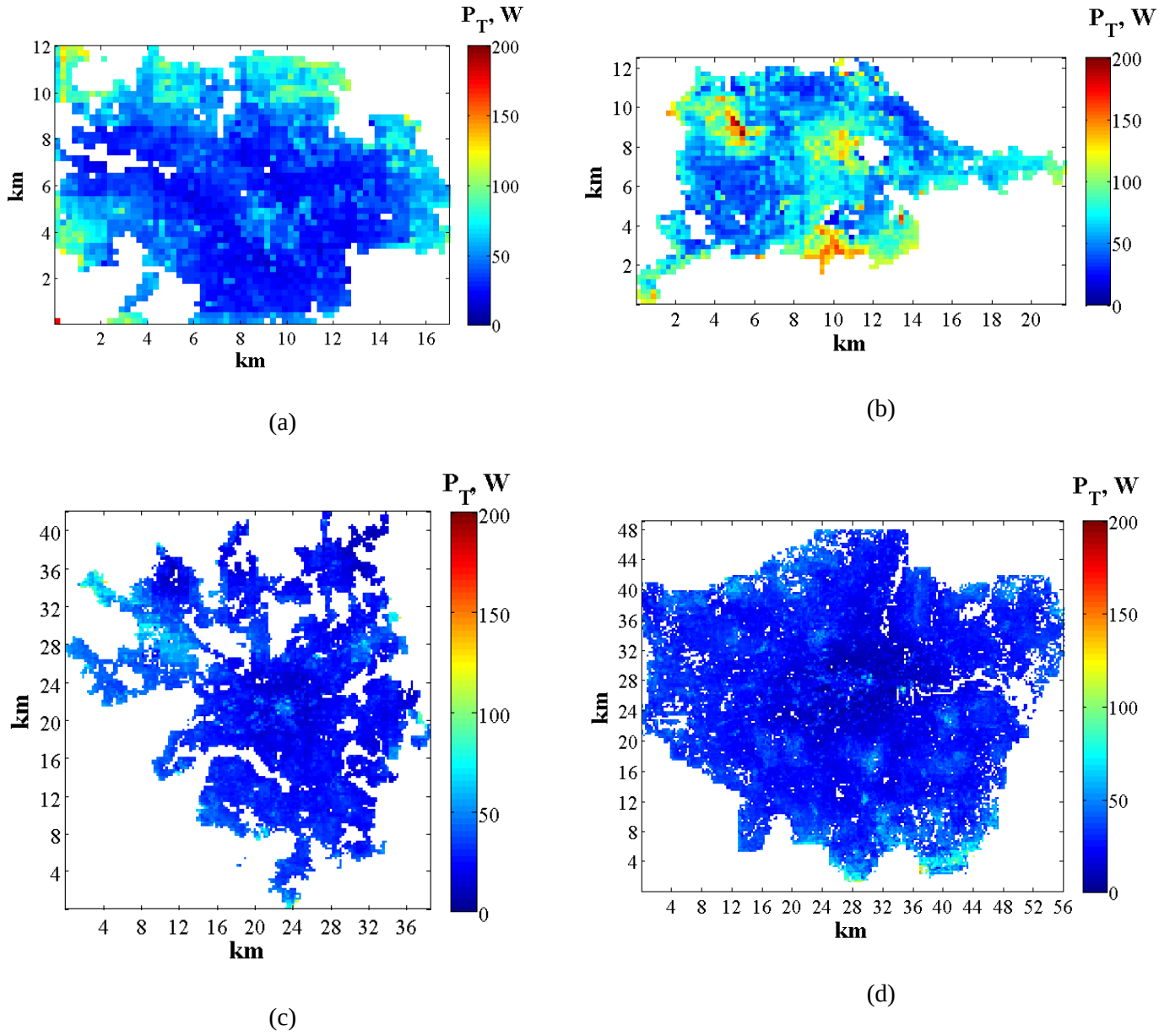

Figure 6. 9: Map of the power output for the VAWT model at effective mean building height over all four cities (a) Leeds (b) Edinburgh (c) Manchester (d) London.

Table 6. 3: Summary of results from the TPE and the C_{tc} estimation models at 10 m above h_{hmeff} over four cities at a response time of 1 s.

Leeds			
	Min	**Average**	**Max**
Power	11.57	47.95	176.72
C_{tc}	37.5873	44.56	52.86
Edinburgh			
	Min	**Average**	**Max**
Power	11.46	71.38	195.77
C_{tc}	38.16	44.31	52.86
Manchester			
	Min	**Average**	**Max**
Power	5.62	35.44	131.01
C_{tc}	37.10	45.59	52.86
London			
	Min	**Average**	**Max**
Power	2.24	30.09	145.97
C_{tc}	36.21	45.49	52.85

6.5.2 Performance at Local Maximum Building Height

City scale variations of C_{tc} and power output obtained using the TPE model at a mast height of 10 m above the local maximum building heights (h_{max}) within each neighbourhood region over the four cities at a response time of 1 s were considered and the results are presented in Figures 6.10 and 6.11. Mapped results at this height showed higher C_{tc} values when compared with that estimated at effective mean building heights with average C_{tc} values of 47.43%, 47.01%, 48.01% and 48.33% observed over Leeds, Edinburgh, Manchester and London respectively. As shown in Figure 6.10, high average C_{tc} values of about 52.85% were observed within neighbourhoods in London with higher building height. It is important to note that these values do not account for other losses (e.g. strut losses, electrical losses, etc.) encountered by the turbine system leading to high C_{tc} values. Further analysis showed

improved turbine performance and lower EEC at this height within these specific neighbourhoods. Considering the power output over all four cities, results showed lower values of approximately 16.62 W, 25.44 W, 7.27 W and 2.78 W were observed within Leeds, Edinburgh, Manchester and London, with the maximum power output of 300.78 W observed within Edinburgh. However, as demonstrated in Figure 6.11, the average power values of 70.8 W, 103.89 W, 48.3 W and 44.11 W were estimated over Leeds, Edinburgh, Manchester and London respectively. This suggests that relocating the turbine from h_{hmeff} to the tallest building within a given neighbourhood region within a city may result in an increase of about 32% in power output. A summary of the predicted turbine performance at a 10 m mast height above the h_{max} over the four cities considered is presented in Table 6.4.

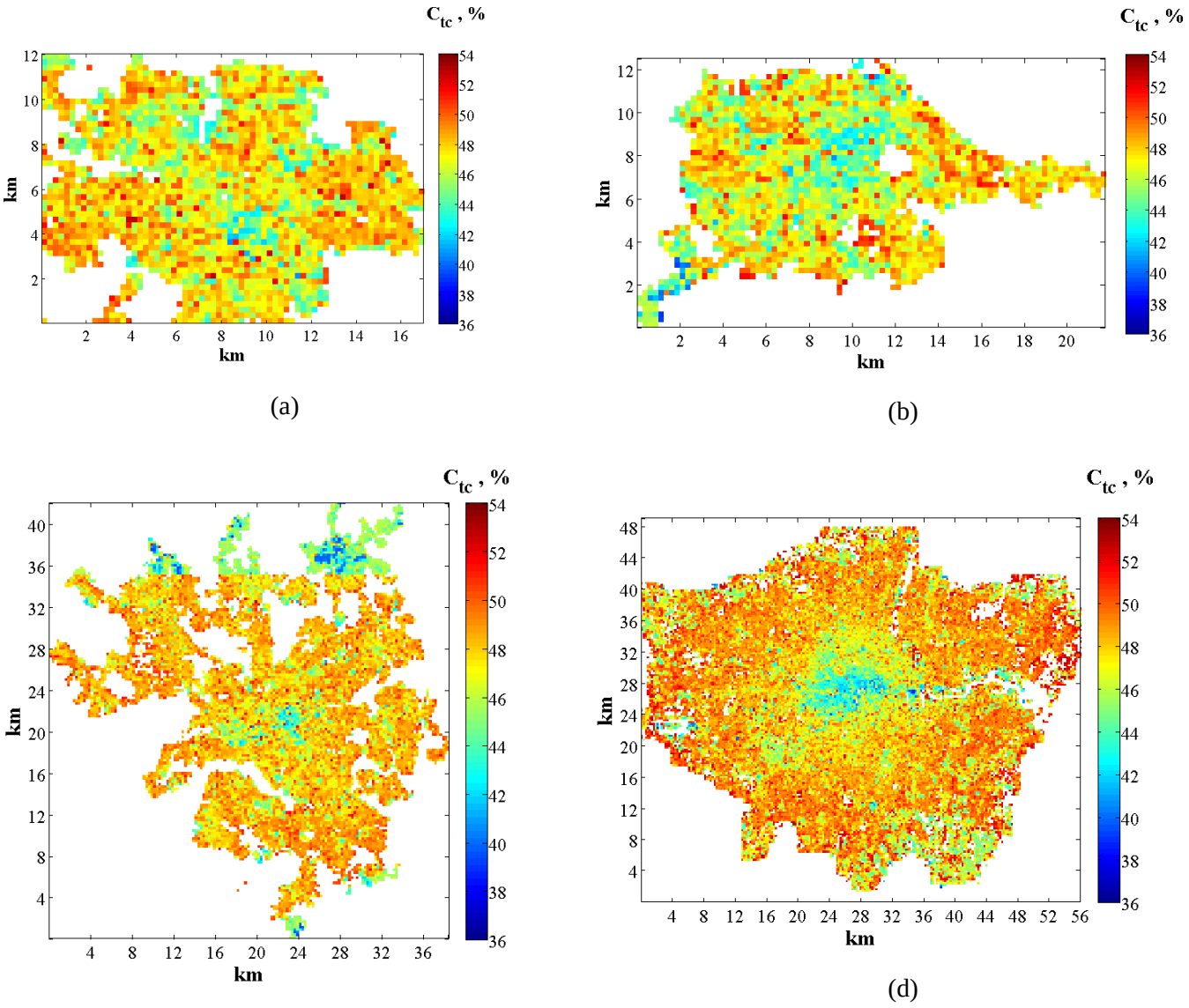

Figure 6. 10: Map of the C_{tc} for the VAWT model at 10 m above the h_{max} over all four cities at 1 s (a) Leeds (b) Edinburgh (c) Manchester (d) London.

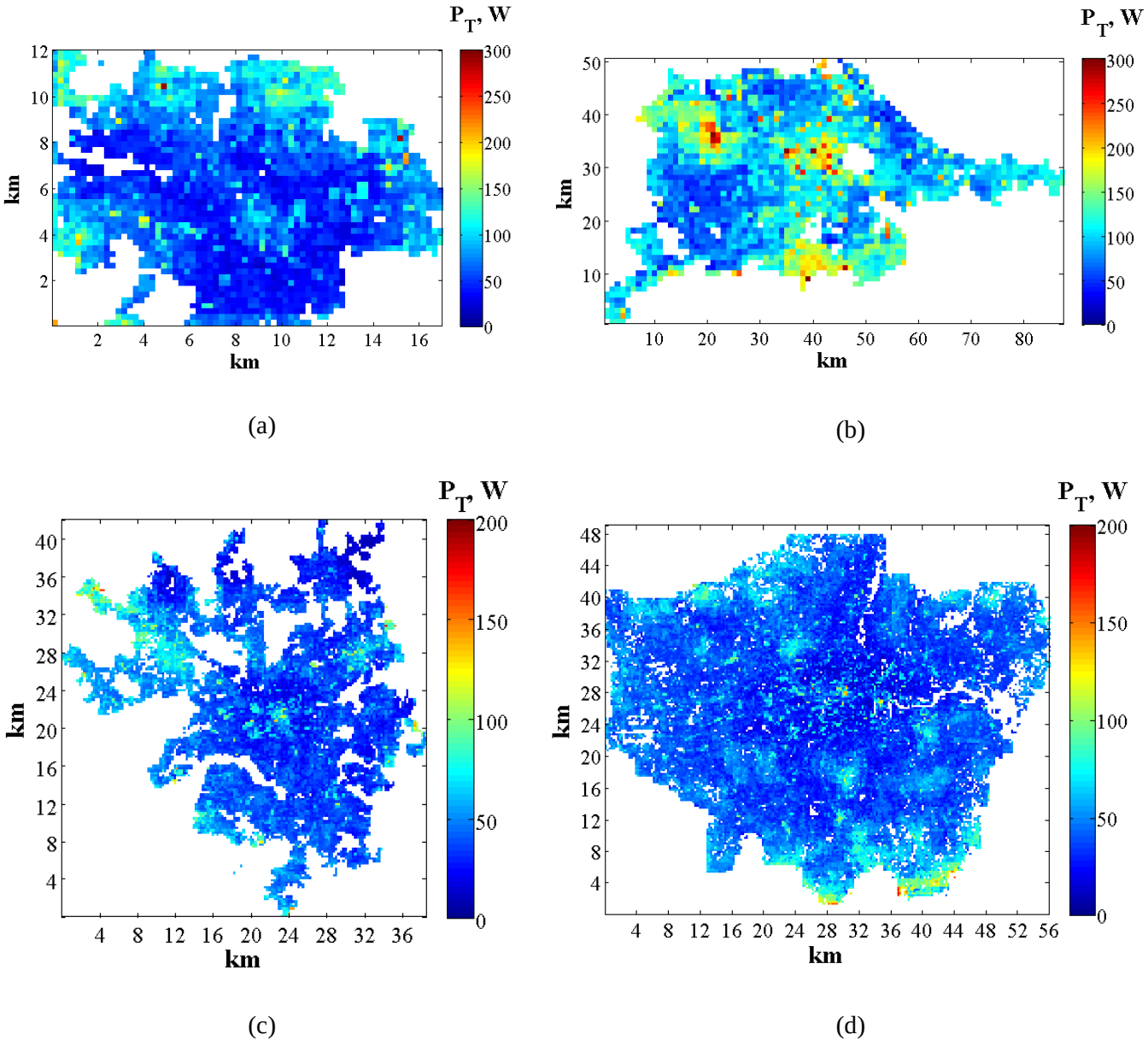

Figure 6. 11: Map of the power output for the VAWT model at 10 m above the h_{max} over all four cities (a) Leeds (b) Edinburgh (c) Manchester (d) London.

Table 6. 4: Summary of results from the TPE and the C_{tc} estimation models at 10 m above h_{max} across four cities.

Leeds			
	Min	**Average**	**Max**
Power	16.62	70.80	286.81
C_{tc}	40.55	47.43	52.84
Edinburgh			
	Min	**Average**	**Max**
Power	25.44	103.89	300.78
C_{tc}	39.08	47.01	52.15
Manchester			
	Min	**Average**	**Max**
Power	7.27	48.30	173.72
C_{tc}	38.71	48.01	52.70
London			
	Min	**Average**	**Max**
Power	2.78	44.11	175.61
C_{tc}	37.81	48.33	52.85

6.6 Effect of T_c on City Scale Variation of the Power Estimation Model

6.6.1 Performance at Mean Building Height

The high variability of wind speed and direction within an urban wind resource affects the operations of urban wind applications. These fluctuations usually at time-scales on order of 10 s or lower [286], will independently impact the turbine blade and will not necessarily equally compensate losses or gains from other blades thus significantly influencing turbine output. Although it is anticipated that turbine systems will be sensitive to these fluctuations, improvements on the response of commercial turbine systems to this very fast fluctuating complex urban wind resource are still in progress. Hence, in order to mimic response times realizable within commercial turbine systems, various response times were tested and analysis presented within this section. First, we consider the city-scale variation of turbine performance

and output with response time (T_c) on order of 10 s. Figures 6.12 and 6.13 demonstrate the turbine performance at 10 m above the effective mean building height for each neighbourhood region over four cities.

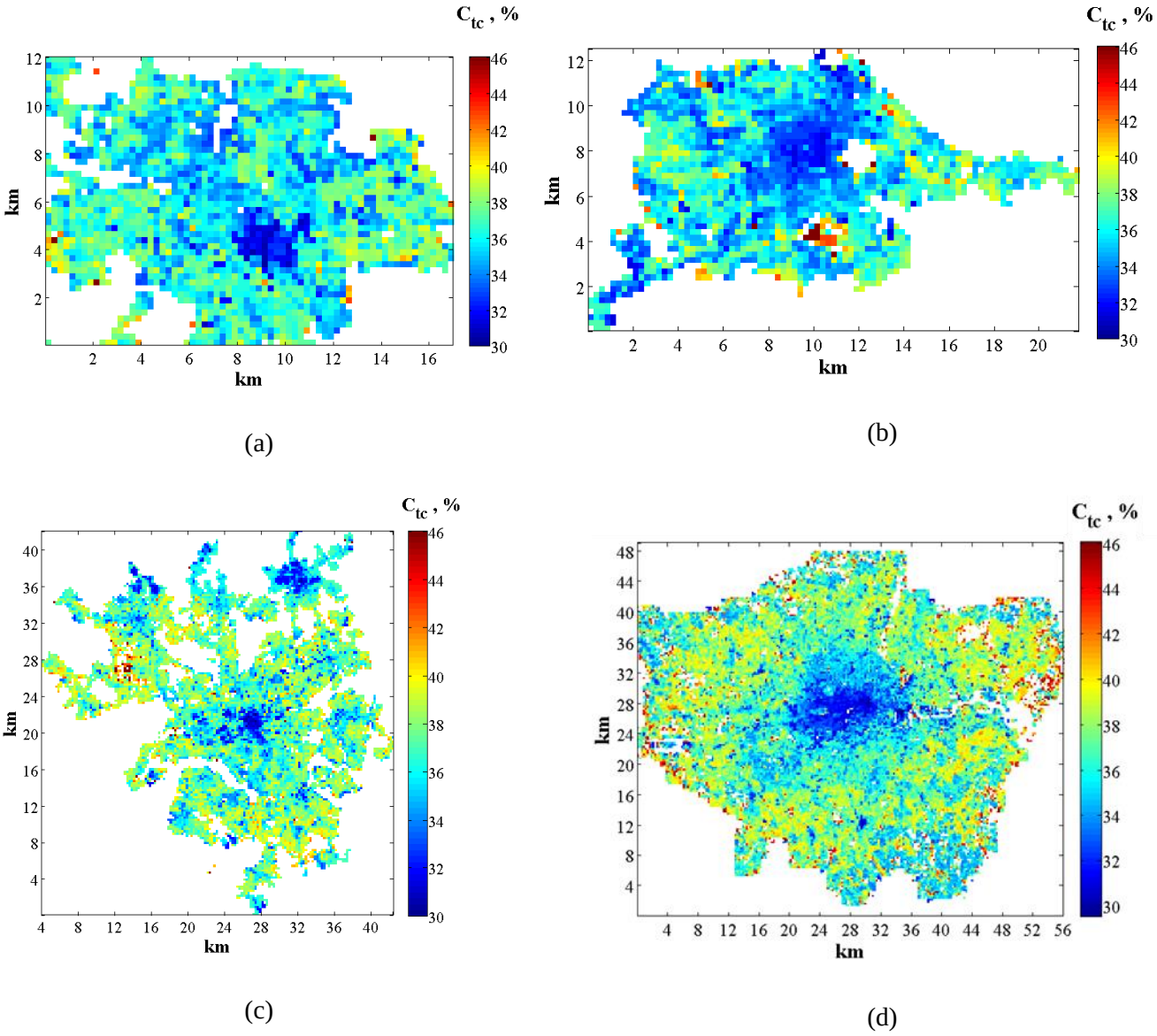

Figure 6. 12: Map of the C_{tc} for the VAWT model at T_c = 10 s and 10 m above h_{hmeff} across all four cities (a) Leeds (b) Edinburgh (c) Manchester (d) London.

Figure 6.12 showed low C_{tc} values within the city centres with values increasing as the distance from the city centre increases across all four cities. Thus, as the response time was adjusted from 1 s to 10 s, average C_{tc} values were shown to decrease by approximately 18% across all four cities with lower C_{tc} values of approximately 29.5% observed within neighbourhoods around London city centre (as demonstrated in Figure 6.12d). Further

analysis carried out suggests this low C_{tc} value may be due to higher turbulence intensities (i.e. up to 47.7%) observed at this height within those neighbourhoods around London city centre thus leading to lower C_e values. Due to enhanced local roughness, lower C_{tc}values were also observed in some neighbourhood regions outside the city centres in Leeds, Manchester and Edinburgh. Turbine power output estimated from average wind speed over each city was observed to decrease by approximately 18% when the response time was changed from 1 s to 10 s thus highlighting the influence of response time on turbine operations within an urban wind resource. Mapped power output results over the four cities (as shown in Figure 6.13) showed a minimum power output of approximately 1.87 W within London and a maximum of approximately 157.44 W over Edinburgh city. Compared with turbine performance at T_c = 1 s, further tests at 20 s and 30 s response times resulted in an average 29% and 44% decrease respectively in average C_{tc} values and power output over all four cities. A summary of average C_{tc} values and power outputs at a response time of 10 s is presented in Table 6.5 while results at response times (T_cs) of 20 s and 30 s are presented in Appendices B and C.

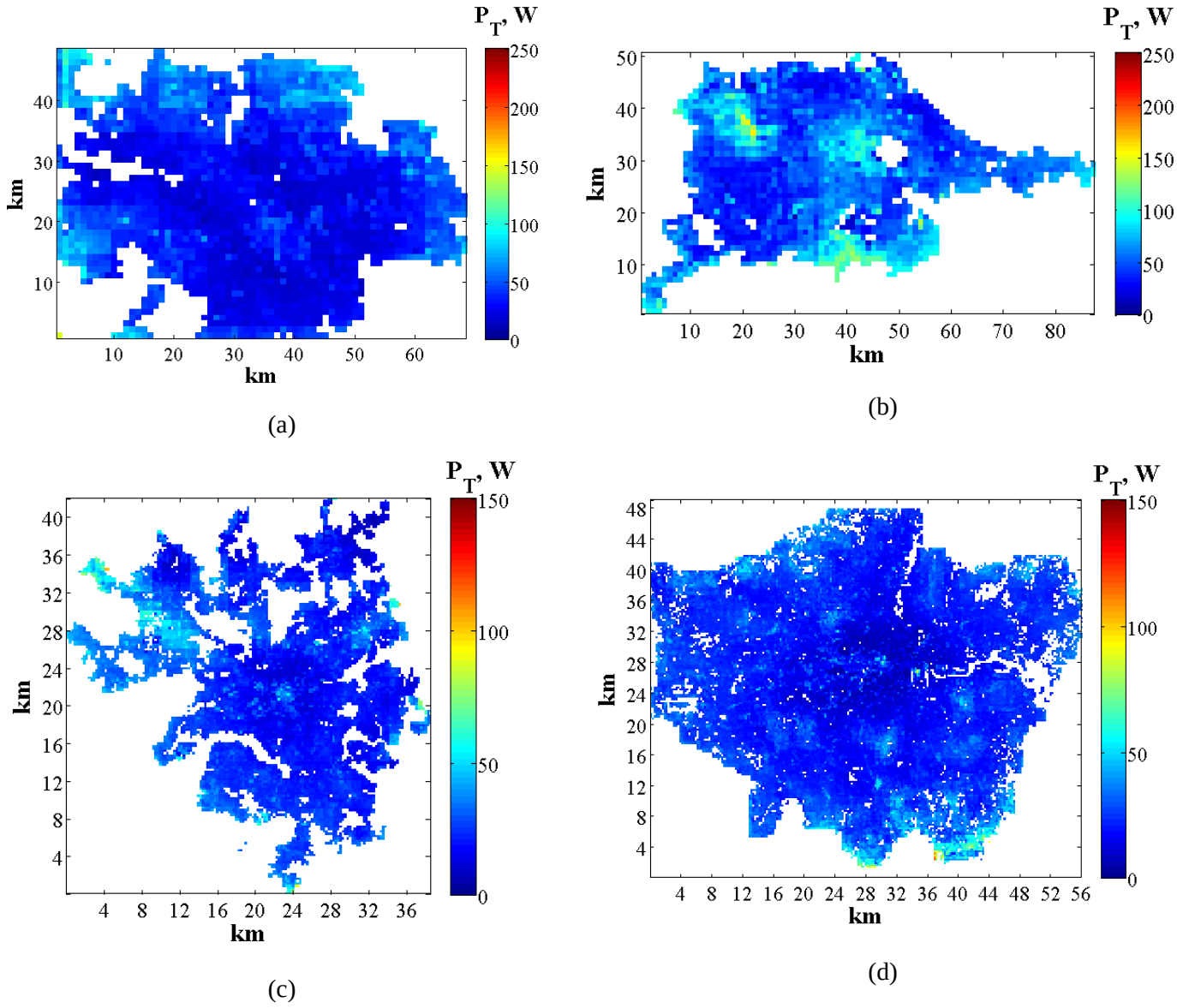

Figure 6. 13: Map of the power output for the VAWT model at T_c = 10 s and 10m above effective mean building height across all four cities (a) Leeds (b) Edinburgh (c) Manchester (d) London.

Table 6. 5: Summary of results from the TPE and the C_{tc} estimation models at 10 m above h_{hmeff} across four cities at T_c = 10 s.

Leeds			
	Min	**Average**	**Max**
Power	11.57	47.95	176.72
C_{tc}	30.41	36.30	45.84
Edinburgh			
	Min	**Average**	**Max**
Power	11.46	71.38	195.77
C_{tc}	30.81	36.08	45.84
Manchester			
	Min	**Average**	**Max**
Power	5.62	35.44	131.01
C_{tc}	30.09	37.35	45.84
London			
	Min	**Average**	**Max**
Power	2.24	30.09	145.97
C_{tc}	29.53	37.30	45.84

6.6.2 Performance at Maximum Building Height

The effect of varying turbine response times on turbine operations at local maximum building heights (h_{max}) across the four cities was also considered. Figure 6.14 demonstrates the city-scale variation of the turbine performance at a response time (T_c) of 10 s. Results showed an estimated 17% decrease in average C_{tc} and average power output values across all four cities when the response time was adjusted from 1 s to 10 s at this height. Comparing turbine performance across the four cities, minimum and maximum C_{tc} values of 30.56% and 45.84% were observed in London. These higher C_{tc} values were as a result of lower turbulence which may be due to higher building heights observed within the city of London. However, lower C_{tc} values resulting from enhanced local turbulence were observed within some neighbourhoods across London with inherent higher surface roughness. Compared with turbine performances with the same response time, results across the four cities showed an

increase of 7.7% approximately in the C_{tc} values when the turbine height was changed from h_{hmeff} to h_{max}. Considering the power outputs from average wind across each city, average power values of 58.64 W, 85.77 W, 40.18 W and 36.76 W were estimated for Leeds, Edinburgh, Manchester and London respectively with minimum and maximum turbine power outputs observed within London and Edinburgh respectively (see Figure 6.15).

It is interesting to point out that average power outputs from turbine systems with a response time (T_c) of 10 s and located at h_{max} were observed to be higher than outputs from a more sensitive turbine (i.e. T_c = 1 s) located at h_{hmeff}. Thus, in agreement with results presented in Chapter 5, this highlights the importance of siting turbine systems further away from local turbulence (i.e. above the local maximum building height) within a potential suburban/urban location. A summary of turbine performances at this height over all four sites is presented in Table 6.6. Compared with turbine performance at a response time of 1 s, further tests at h_{max} showed a decrease in the average C_{tc} values and average power output of approximately 29% at response time of 20 s and between 43 and 45% at 30 s over all four cities. It is assumed that turbines with faster response are capable of instantaneously tracking fluctuations in the wind and thus successfully capturing excess energy contents within a gusty urban wind. However, average turbine power outputs at h_{max} at response time (T_c) of 20 s (as presented in Appendix D) were shown to be approximately 4.95%, 3.29% and 4.6% higher than that generated by a fast response turbine (i.e. T_c = 1 s) operating at h_{hmeff} over Leeds, Edinburgh and London cities respectively. Thus, with excess energy higher at h_{hmeff} (in agreement with results presented in Chapter 5), this study highlights the significance of gust tracking solutions in urban wind applications at heights below the local maximum building height within a built environment (i.e. $h_{hmeff} \leq h \leq h_{max}$). Summaries of the turbine performances at response times (T_cs) of 20 s and 30 s are presented in Appendices D and E respectively.

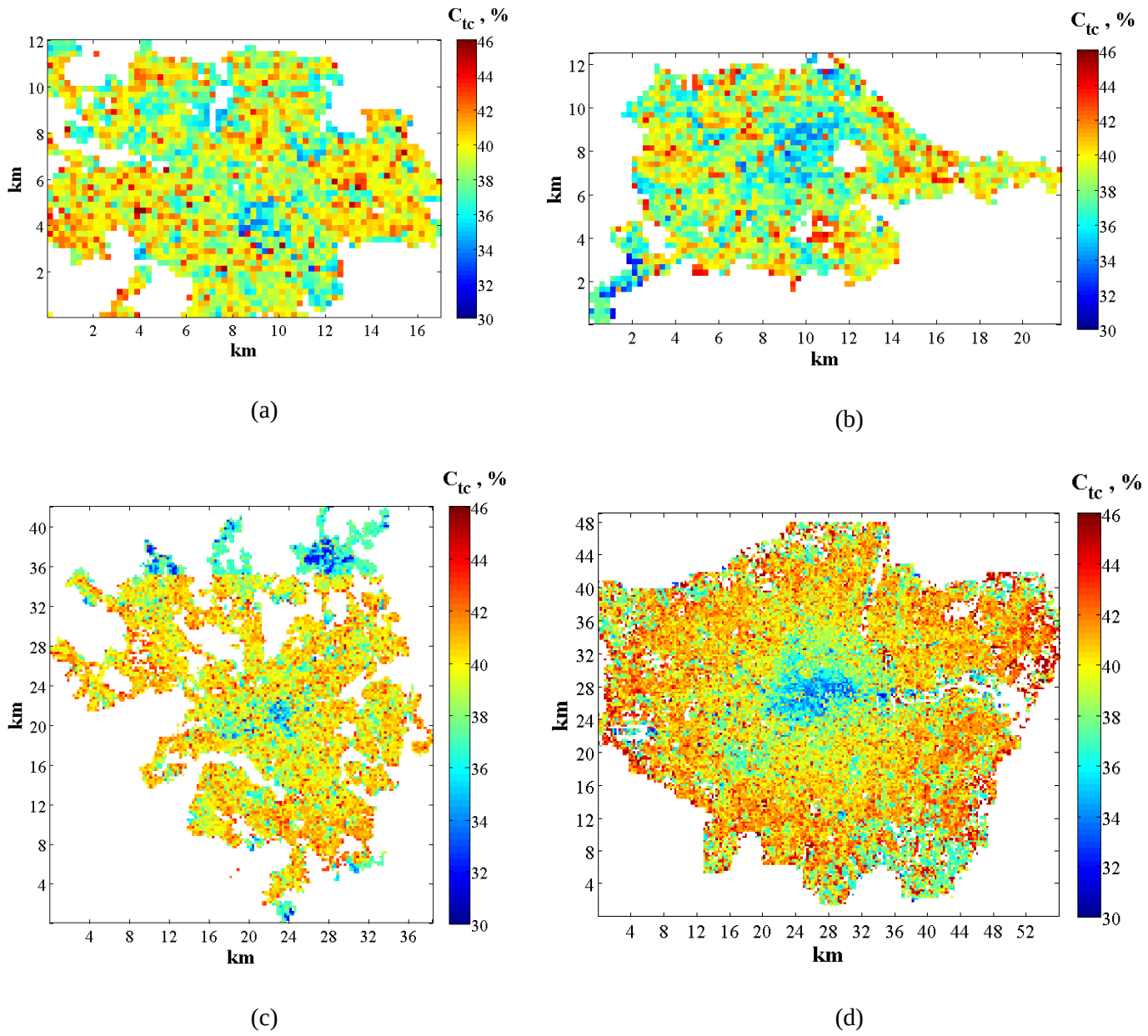

Figure 6. 14: Map of the C_{tc} for the VAWT model at T_c = 10 s and 10 m above the h_{max} across all four cities (a) Leeds (b) Edinburgh (c) Manchester (d) London.

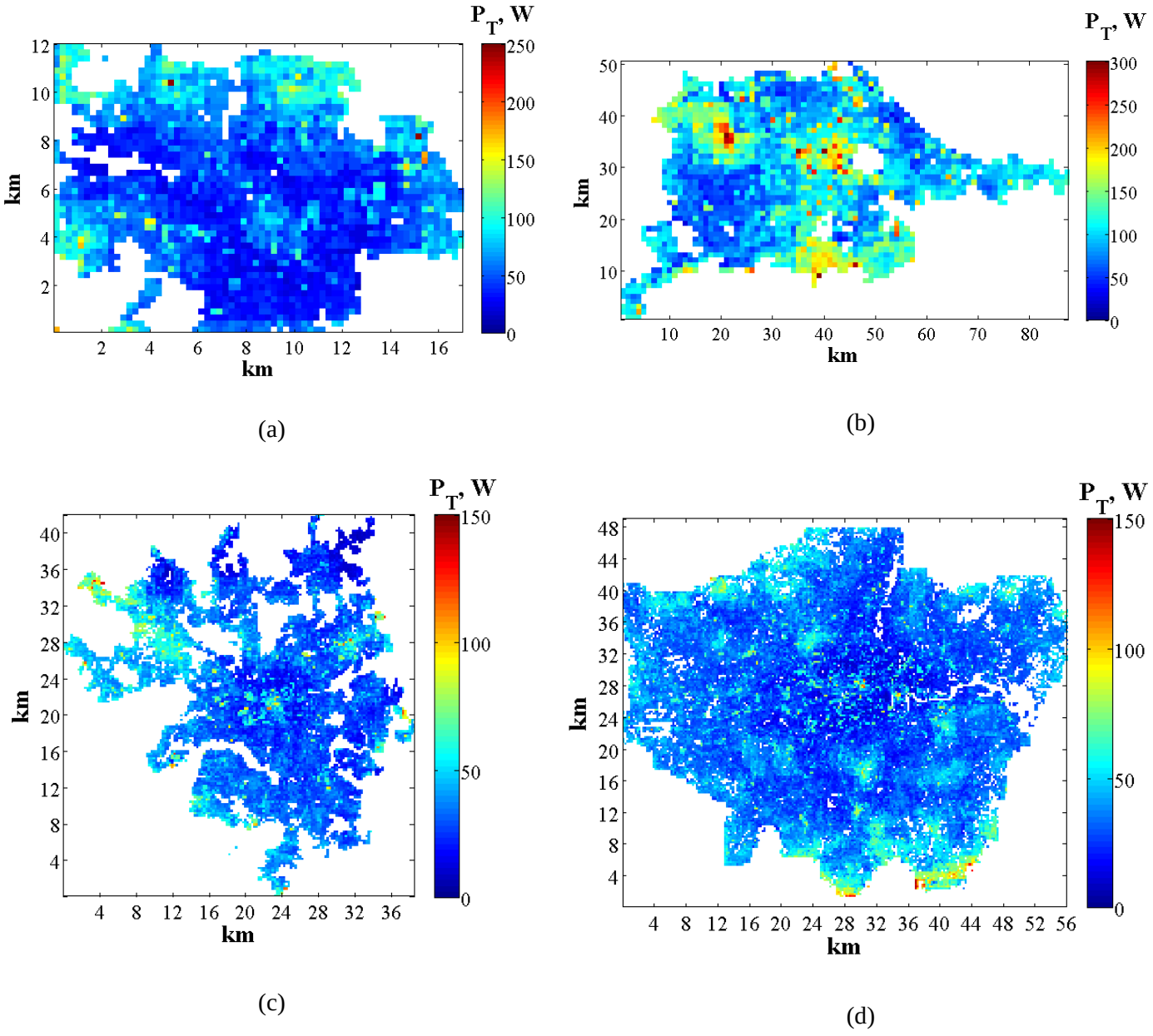

Figure 6. 15: Map of the power output for the VAWT model at T_c = 10 s and 10 m above h_{max} over four cities (a) Leeds (b) Edinburgh (c) Manchester (d) London.

Table 6. 6: Summary of results from the TPE and the C_{tc} estimation models at 10 m above h_{max} over four cities at T_c = 10 s.

Leeds			
	Min	**Average**	**Max**
Power	11.57	47.95	176.72
C_{tc}	32.61	39.29	45.82
Edinburgh			
	Min	**Average**	**Max**
Power	11.46	71.38	195.77
C_{tc}	31.47	38.85	44.91
Manchester			
	Min	**Average**	**Max**
Power	5.62	35.44	131.01
C_{tc}	31.20	39.93	45.64
London			
	Min	**Average**	**Max**
Power	2.24	30.09	145.97
C_{tc}	30.56	40.33	45.84

6.7 Comparison between Power Estimation from Turbine Power Curve and the Turbine Power Estimation (TPE) Model

As a standard part of the manufacturer's technical specification [269], power curves demonstrate the dependency of turbine system's power output on wind speed. Hence, one can estimate the power output of a given turbine system for different average wind speeds by merely using the turbine's power curve. Generic power curves of different wind turbine systems are supplied by manufacturers assuming ideal meteorological and topographical conditions [267]. In reality, wind turbine systems are never employed in ideal conditions. Thus, these generic power curves provided could be significantly different from the power

curves obtained from different sites due to various factors like turbine location and topography, air density, wind speed distribution and direction, uncertainties in measurements, type of controls employed, mechanical issues, etc. Considering real world gustiness, these power curves may either under-report or over-report the real value of turbine outputs at varying wind speeds within a built environment [193]. Although various studies have suggested different methods for adjusting turbine power curves to account for the influence of local terrain on turbine power outputs [193, 297-301], this study considered a simple application of a turbine power curve in estimating the turbine system's power output. This is a popular approach used by various studies in the wind energy industry for turbine performance assessments and analysis [180, 265, 269, 296, 302, 303]. In order to illustrate the errors encountered by employing turbine power curves within urban wind resources, power outputs obtained by applying a simple turbine curve from the eight potential sites were compared to the TPE model power outputs. From the VSC power outputs presented in Figure 3.19, a generic power curve represented by an 8th degree polynomial (as shown in Equation 6.9) is presented in Figure 6.16. Employing this generic power curve, the power output (P_{pc}) at the eight test sites were estimated at a response time of 10 s (i.e. using the wind datasets from the eight sites as inputs and filtered at T_c = 10 s) over a burst period of 10 min.

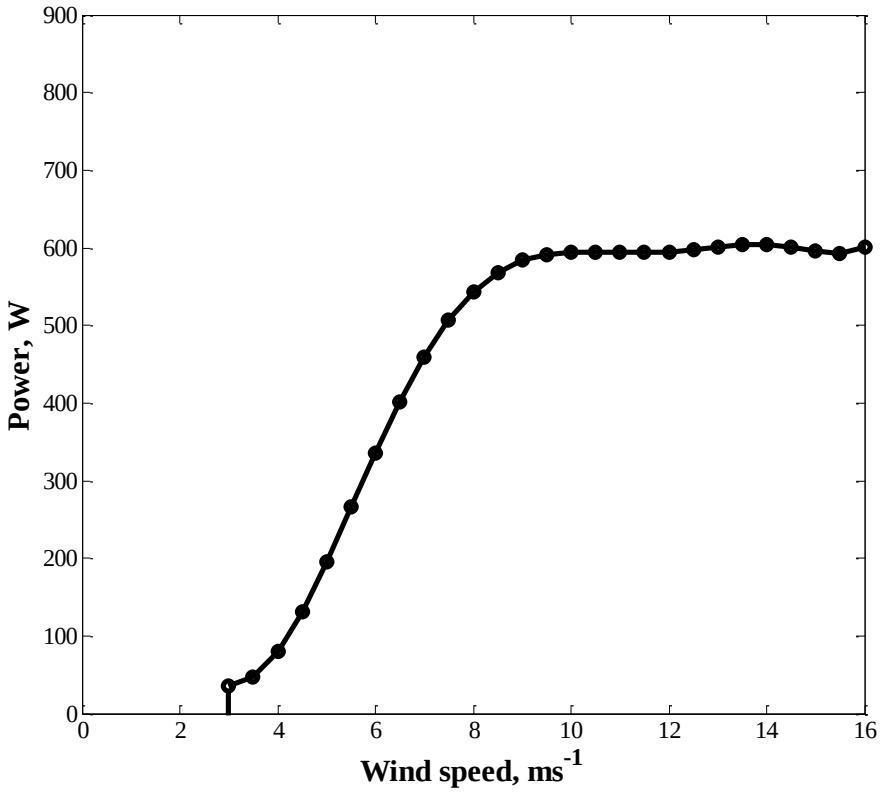

Figure 6. 16: Vertical axis wind turbine power curve adapted from turbine power outputs presented in Figure 3.19.

$$P_{pc} = 17.388Y^7 + 11.796Y^6 - 117.77Y^5 - 0.444Y^4 + 241.32Y^3 - 181.08Y^2 + 41.139Y + 591.56 \quad \text{Equation 6. 9}$$

where

$Y = (V - 9.5)/4.183$

A comparison between the power outputs estimated using the power curve (P_{pc}) and power output values estimated from average wind using the TPE model (as shown in section 6.3 and 6.4) was achieved by using the mean percentage error (MPE) as provided in Equation 6.10 and results presented in Figure 6.17.

$$\text{MPE}(\%) = 100 \times \frac{1}{n} \sum \frac{|P_{T\_VSC} - P_{pc}|}{P_{T\_VSC}} \quad \text{Equation 6. 10}$$

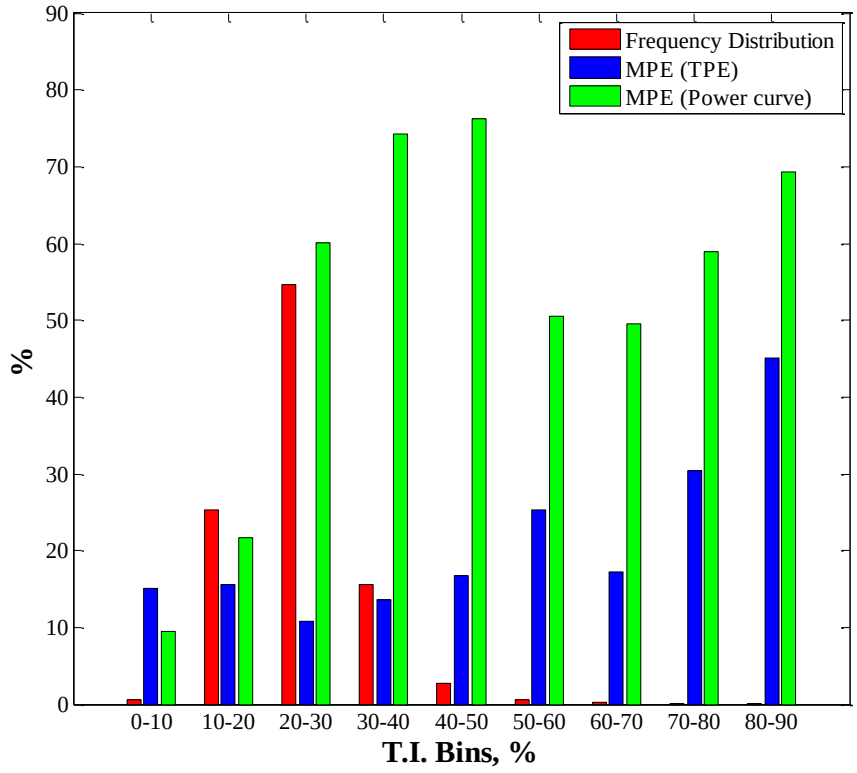

Figure 6. 17: Power estimation errors using a power curve and the TPE model compared over eight sites at response time of 10 s.

Comparing both approaches in Figure 6.17, the generic power curve tends to perform better at turbulence intensities lower than 10 %. However, the TPE model shows better overall prediction accuracy at $T.I.$ lower than 50%. Although both approaches perform poorly at higher turbulence intensities (i.e. $T.I.$ > 50%), the TPE model tends to perform better when compared with the generic power curve. The annual energy production over a built environment can simply be estimated by combining the TPE model outputs with the Weibull probability density function for all of the velocities within the operating range of a specific turbine design [194]. This, however, has not been included within this study. Various studies have carried out energy analysis and power assessment of small wind turbines within a suburban/urban environment while neglecting the effect of turbulence [194, 269, 296, 304, 305]. Thus, the TPE model demonstrates a simple and cost effective method of incorporating turbulence effect while effectively estimating turbine power from averaged wind measurements over a given burst period, thus suggesting improved accuracy of annual energy production estimates. These results can be compared to estimated installed power (i.e. maximum possible power output as provided by the manufacturer) in order to assess the viability of a potential urban wind project. These results and cost implications, however, are not presented within this study, thus suggesting relevant areas for future research.

Also, it will be interesting to test accuracy of the TPE model at higher turbulence by using a different modelling approach (e.g. vortex model), advanced control algorithms (e.g. PID feedback controls) and high resolution wind measurements from more suburban/urban sites. Hence, results presented in Figure 6.17 tends to support the assumption that generic power curves are site dependent and significantly under-predict or over-predict when applied within a different fluctuating, turbulent wind environment (i.e. urban wind resource). Thus, instead of producing different power curves for different turbulence intensities, this study suggests that manufacturers could produce a single C_e - $T.I.$ curve which could be used in combination with the EEC - $T.I.$ curve in estimating the power capabilities of a specific turbine system within a built environment as has been demonstrated in the TPE model. Various studies have suggested different methods for adjusting turbine power curves to account for turbulence when estimating the turbine power outputs within a turbulent wind resource [193, 297-301]. Hence, it will be interesting to assess the performance these different methods with that of the TPE model within a built environment, however, this was not considered in this study.

As described in Section 2.3.4, the viability of a turbine system configuration within a potential site can be assessed by its capacity factor. Figure 6.18 demonstrates the city-scale variation of the capacity factor at the local maximum building height over four cities namely Leeds, Edinburgh, Manchester and London. The capacity factor (CF) was derived from the TPE

model estimates while considering long term wind speed averages (as defined by the MH model) and is defined by Equation 6.11.

$$CF\ (\%) = \frac{average\ power\ output\ from\ TPE\ model}{Maximum\ rated\ power} \times 100\% \qquad \text{Equation 6. 11}$$

where the maximum rated power for the micro VSC vertical axis wind turbine considered herein is 600 W.

From results, significant potentials for a micro wind turbine was suggested over Edinburgh with maximum capacity factor of 43.17% predicted at neighbourhoods within the city (not accounting for other losses). As shown in Figure 6.18, low capacity factors were observed generally within each city (excluding Edinburgh) with these values increasing as the distance from the city centre increases. The lowest capacity factor within a neighbourhood region was predicted for London with average capacity factors of 9.77%, 14.30%, 6.1270 % and 6.70% predicted over Leeds, Edinburgh, London and Manchester respectively. A summary of the capacity factor over the four cities is presented in Table 6.7. The implication of these results is that the capacity factor of a specific turbine design within a potential suburban/urban site can be fairly estimated by a simple model thus providing relevant information for decision making for potential urban turbine projects as well as turbine manufacturers. Given the variability of predicted capacity factor over short distances within the city, it is clear that the type of model developed here provides a very useful scoping tool for initial site viability assessment.

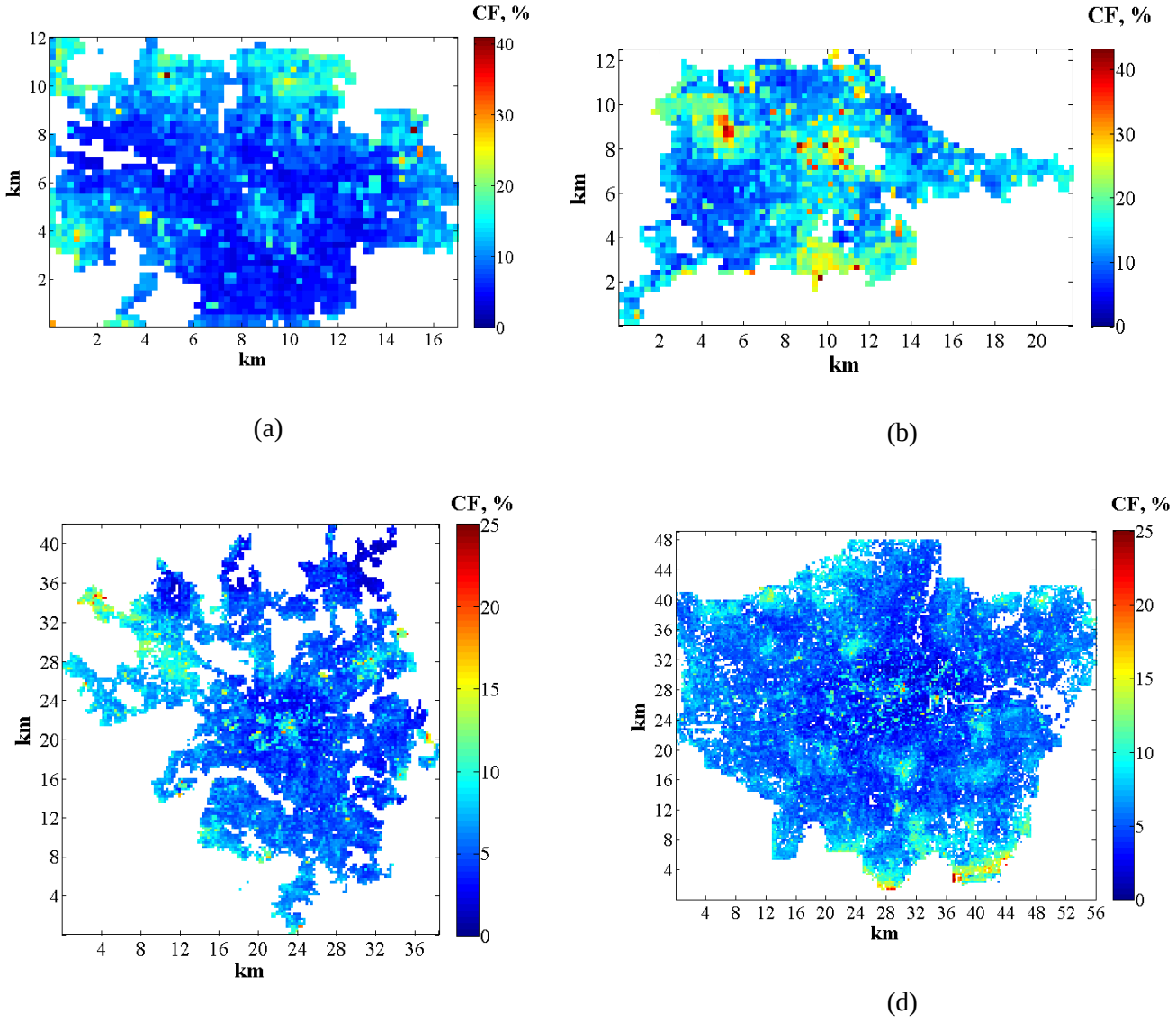

Figure 6. 18: Map of the CF for the VAWT model at T_c = 10 s and 10 m above h_{max} across all four cities (a) Leeds (b) Edinburgh (c) Manchester (d) London.

Table 6. 7: Summary of results from the capacity factor estimated using the TPE model at 10 m above h_{max} over four cities at T_c = 10 s.

Capacity Factors			
	Min	**Average**	**Max**
Leeds	2.35	9.77	40.87
Edinburgh	3.60	14.30	43.17
Manchester	0.99	6.70	24.70
London	0.40	6.13	24.81

It is quite interesting to point out the relationship existing between the excess energy available within a built environment and the performance of the VAWT model represented by the unsteady performance coefficient (C_e) employed in this study. Figure 6.19 demonstrates a good $EEC - C_e$ relationship thus suggesting that less than 25% excess energy is available when the turbine is performing at 40% of its maximum capacity. However, the turbine performance is shown to be below 40 % at higher excess energy contents. This may be due to various factors such as choice of control systems or the effect of turbine inertia, increased wake effects, strut losses and losses from multiple blade elements, etc. which were not considered in this study. Advanced control systems designs and gust tracking solutions may lead to improvements in the turbine power output thus moving the curve towards the right (as shown in Figure 6.19). This may serve as a measure for assessing the performance of a given control systems design and/or gust tracking solutions employed within a turbine system for urban wind applications. Thus, improvements in current controls could be assessed as well as its cost effectiveness when compared to how much excess energy it is willing to harness within a potential turbine site.

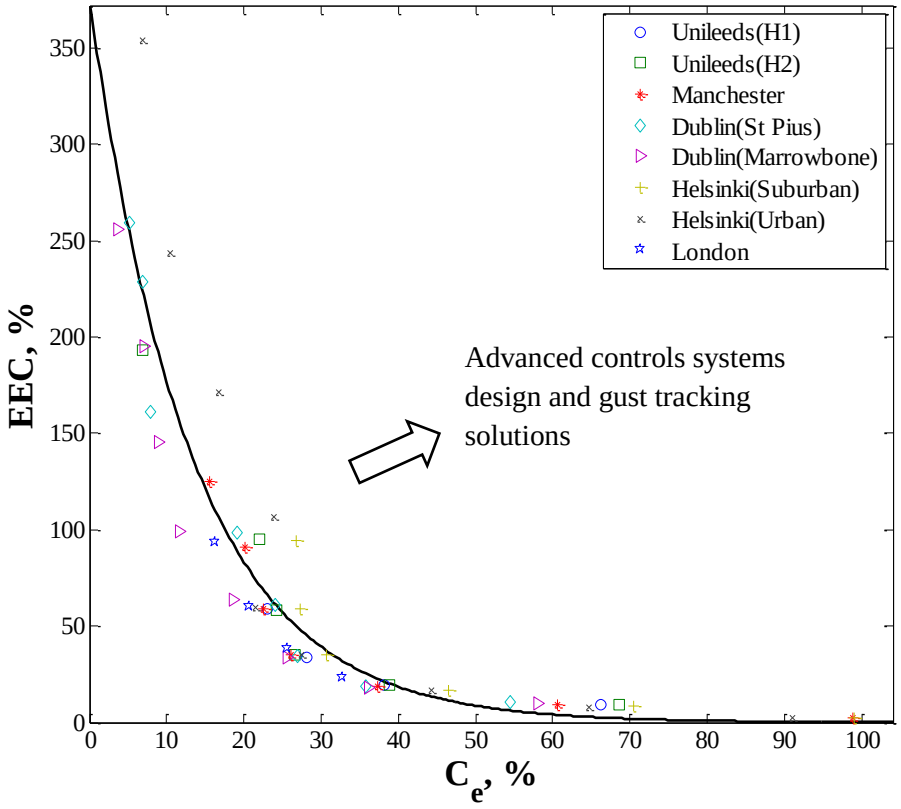

Figure 6. 19: Relationship between excess energy content and turbine performance within a built environment at response time of 1s (best fit represented by solid line).

6.8 Summary

A new turbine performance parameter known as the turbulence induced performance coefficient (C_{tc}) was introduced in this Chapter. This parameter aims to assess the performance of a turbine system while taking into account the effect of turbulence (as represented by the unsteady performance coefficient, C_e) and excess energy available within a potential turbine site. An analytical model for predicting C_e at different turbulence intensities was developed using data collected from eight suburban/urban sites. Hence, a method of estimating the turbine power output within a gusty wind resource was proposed by multiplying the C_{tc} value with the wind energy available to the turbine system at a given burst period. The effect on turbine response time on turbine performance was also presented and discussed. City-scale variations of the C_{tc} and turbine power for four (4) cities was demonstrated at different response times at a mast height of h_{hmeff} over each city. Results at this height showed average C_{tc} values of 44.56%, 44.31%, 45.59% and 45.49%, and an average power of 47.95 W, 71.38 W, 35.43 W and 30.09 W at a response time of 1 s over Leeds, Edinburgh,

Manchester and London respectively. A change in response time from 1 s to 10 s led to approximately 18% loss in the average C_{tc} and power values across all four cities. Further changes in response time to 20 s and 30 s led to further decreases in average C_{tc} and power outputs thus highlighting the importance of response time on turbine performance within a built environment. The turbine performance at the local maximum building height (h_{max}) over all four cities was also considered. Results show an overall improvement in turbine performance at this height when compared with the turbine performance at h_{hmeff} over each city. Hence, at a response time of 1 s, an increase of 47.6%, 45.5%, 36.3% and 46.6% in the average power output was estimated over Leeds, Edinburgh, Manchester and London cities when the mast height was altered from h_{hmeff} to h_{max}. These improvements in turbine performance as a result of a change in mast height were also observed at varying response times (i.e. 10 s, 20 s and 30 s). This highlights the importance of mounting turbines at the tallest building in a neighbourhood region. A comparison between the TPE model and the use of a generic power curve was also drawn. Results showed better accuracy in estimating the turbine power output within a turbulent, fluctuating wind resource using the TPE model. Hence, instead of providing many power curves for different turbulence intensities, this study suggests manufacturers provide a single C_e - $T.I.$ curve which would be incorporated into the TPE model in predicting the power capabilities of a given VAWT model within a specific built environment. Mapped results demonstrating the city-scale variation of the turbine's capacity factor was predicted over Leeds, Edinburgh, Manchester and London. Results showed better capacity factors within Edinburgh and the minimum average capacity factor within London. This suggests that the viability of a small turbine project within a suburban/urban area can be assessed using a simple less-expensive model if the turbulence intensity and wind speeds at the potential sites are provided. Finally, the performance of control systems employed within urban wind applications can be assessed by comparing the unsteady performance of the turbine with the excess energy available to the system. This was demonstrated by a C_e - EEC curve obtained from observations from eight different potential sites.

CHAPTER 7

7 Final Discussion and Conclusions

7.1 Research summary

There is great potential for harnessing power via small-scale wind turbines if carefully sited within suburban/urban areas thus encouraging electricity supply through renewable energy technologies. However, in order to sustain the growth of these renewable urban wind applications (especially small-scale wind turbines) within the UK, efficient and cost effective methods of assessing of the wind resource within a potential suburban/urban site and predicting the power performance of a potential turbine design configuration should be made available. While the large-scale wind industry has benefited from decades of research which has led to the development of detailed site assessment procedures, the small-scale industry is still in its embryonic stage. The research described in this Thesis however, has addressed the challenge of developing a cost effective methodology for estimating the atmospheric turbulence (represented by the turbulence intensity parameter) as well as total kinetic (wind) energy available to building mounted wind turbines in suburban/urban areas. It also addresses the challenge of estimating the power capabilities of a small wind turbine operating within an urban wind resource while considering its impact on the total investment cost. In order to investigate how accurate the total kinetic (wind) energy, turbulence intensity as well as turbine power estimations are, a number of high resolution wind measurements from sonic anemometers mounted on roof tops within suburban/urban areas have been analysed. Thus, novel models have been developed utilising techniques and principles based upon boundary layer meteorology.

Chapter 2 introduced the concepts of turbulence with respect to boundary layer and urban meteorology and presented the relevant contributions of various studies towards modelling atmospheric turbulence thus highlighting the importance of this study. In order to assess the performance of a small turbine system, Chapter 2 also presented an overview of various types of turbine systems and their applications. It also presented the basic fundamentals, aerodynamics principles within a standard turbine operation and various methods of control employed thus laying the foundation for the development of a simple low-cost small vertical axis wind turbine model which was later employed within this study. Chapter 3 introduced the high resolution wind measurements employed within this study, as well as brief descriptions of the sites at which these measurements were collected. A brief description of the wind prediction methodology proposed by Millward-Hopkins *et al* [63](referred to as the MH model) was also presented in Chapter 3. A framework for the development of a simple

low-cost vertical-axis wind turbine model was introduced in Chapter 3. This model was later employed for the purpose of assessing the power capabilities of a vertical axis wind turbine within a typical suburban/urban area, as presented in Chapter 6. Due to major challenges always encountered in assessing the wind resource within a built environment as highlighted in Chapter 2, characterisation of this urban wind resource was presented in Chapter 4 by employing high resolution wind datasets collected from different typical urban sites. Further analysis led to the development of a new analytical model that estimates the excess energy available within a potential turbine site while taking into account the effect of local turbulence. This model, which was termed the EEC model, together with the turbulence intensity estimation ($T.I.$) model and the wind speed prediction model (referred to as the MH model) presented in Chapter 5 were tested in four major UK cities. The city-wide variation of wind speed, turbulence intensity and excess energy available at a potential turbine site at different hub heights was demonstrated over Leeds, Manchester, Edinburgh and London. However, a novel model for estimating turbine power outputs from average wind while accounting for turbulence and the excess energy at different averaging/response times was developed and presented in Chapter 6. This methodology also suggested further room for improvement in the predictive accuracy of turbine power capabilities if gust tracking solutions were to be employed.

7.2 Results and Implications

Chapter 2 highlighted the limitations of different modelling approaches based on either wind tunnel experiments or CFD models in fully modelling atmospheric turbulence for city-wide wind energy assessment. This led to adopting a time/spatially averaged approach while employing high resolution wind measurements from various sites with turbulence expressed in terms of simple quantities such as turbulence intensity ($T.I.$). However, the exact magnitude of turbulence received by building mounted wind turbines are likely to be difficult to predict accurately without site specific assessment. Thus, Chapter 4 provides a detailed characterisation of a typical urban wind resource available to a building mounted wind turbine. It was observed that there was a significant amount of excess energy available in the complex, rapidly fluctuating wind resource present within a built environment. This excess energy (represented in this study as the excess energy content (EEC)) was shown to possess a strong relationship with turbulence intensity and averaging time. Hence, Chapter 4 proposed a new analytical model which aims to predict the excess energy available by quoting the $T.I.$ values within a given time interval.

The implications of these results are that the additional energy available is usually under-represented by the use of mean wind speeds in quantifying the total wind energy available to a turbine system operating within a built environment. Previous wind systems assessment studies have shown that turbulence affects the performance of wind turbines, thus higher turbulence level leading to lower power outputs and vice versa [2, 193, 286, 299]. Results from this research study indicate that effectively harnessing a portion of this excess energy available within gusty wind conditions could compensate for the lower mean power outputs were a gust tracking solution to be employed. Thus, the accuracy of wind energy assessments (especially within suburban/urban areas) could improve significantly if the excess energy, usually neglected, was accounted for. Also, in estimating the excess energy available within a potential turbine site, it is important to note that EEC is sensitive to averaging time interval considered, thus underlining the potential of faster response turbines in capturing more power.

In Chapter 5, various turbulence intensity estimation models based on parameterisation of the surface aerodynamics were tested. The accuracy of each model was assessed by comparing model predictions to $T.I.$ values obtained from site observations. Evaluation of model results showed Model 1, which estimates the $T.I.$ as a function of local mean building height, to have better accuracy compared to other models, hence it was selected as the primary $T.I.$ estimation model in this study. Improvements in predictive accuracy of the $T.I.$ model were achieved by substituting the local mean building height ($h_{hm-local}$) with the effective mean building height (h_{hmeff}) thus accounting for the disproportionate effect of taller buildings (as fully described in Section 5.2). The implications of these results are that it may be acceptable to overlook the wake turbulence and other complexities inherent in turbulence exchange within suburban/urban areas and obtain reasonably accurately estimates of atmospheric turbulence at different heights within a built environment. By accounting for height variability, the EEC model earlier proposed was combined with the $T.I.$ model to estimate the EEC values at different heights within a typical suburban/urban area. Mapped results over four cities (i.e. Leeds, Edinburgh, London and Manchester) suggested $T.I.$ and EEC values to be higher at lower hub heights and vice versa.

The implications of these results are that the high costs of obtaining data from potential turbine sites for analysis could be circumvented by employing simple analytical models. Also, the higher costs that may be incurred in employing advanced turbine controls could also be avoided due to recommendations based on results from these models (as demonstrated in Chapters 5 and 6). Thus, decisions on turbine siting, performance evaluation of a proposed turbine system as well as assessing the cost effectiveness of prospective turbine control system

at potential turbine sites within a built environment could be made at lower cost and computer power. This is in contrast to the case of CFD models, wind tunnel experiments or extensive field measurements.

Chapter 2 presented the basic fundamentals, aerodynamic characteristics and various controls employed in wind turbine operations. This provided a foundation upon which a simple-low cost was developed in Chapter 3 and tests carried out at different operating conditions. This simplified turbine low-cost model was developed within the MATLAB software to represent a lightly-loaded small wind turbine which was employed for the purpose of turbine performance analysis within a suburban/urban environment. Comparison between the unsteady performance coefficient (C_e) of the turbine and $T.I.$ was made, and analysis suggested turbine systems perform better at lower atmospheric turbulence. Hence, in agreement with results presented in Chapter 5, turbine systems operations are suggested to be cost effective at higher hub heights (i.e. away from the effect of local roughness). Instead of employing the widely popular power coefficient (C_p) parameter in estimating turbine power outputs, a novel coefficient known as the turbulence induced performance coefficient (C_{tc}) was proposed in Chapter 6. From results of power outputs predicted from average wind, this coefficient was shown to provide better accuracy in power estimation thus correcting for the effect of atmospheric turbulence on turbine power while accounting for the excess energy available at potential sites. This, therefore, suggests improvements in methods employed for wind energy systems evaluation while assessing their performance and operation within a built environment. One implication of this methodology is that it does not consider the different losses (electrical losses, strut losses, etc.) experienced by the turbine system while estimating power outputs within these potential suburban/urban sites.

The effect of response time on unsteady turbine performance (C_e) was also tested across eight potential suburban/urban sites thus confirming the importance of response time on turbine power output. Thus, an analytical model that estimates C_e by quoting the $T.I.$ for different time intervals was developed from the strong relationship between C_e and $T.I.$ (as described in Chapter 6). A combination of the Millward-Hopkins (MH) mean wind prediction model, $T.I.$ and EEC estimation models (presented in Chapter 5) and the C_e prediction model led to the development of the turbine power estimation model (TPE). The implication of results from the TPE model is that the power output from a given turbine design at a potential site could be estimated if the $T.I.$ and EEC at that specific site were to be provided. City-scale variation of turbine power outputs from average wind at different response times across four cities (Leeds, Edinburgh, London and Manchester) were demonstrated by employing the TPE model. It can be deduced from the predicted power outputs at different hub heights that turbine

systems with faster response times located at lower hub heights (for example, h_{hmeff}) tend to perform poorly compared to slower response turbines located at the tallest building within the same neighbourhood region. Considering the higher EEC values experienced at lower heights (as demonstrated in Chapter 5), mapped TPE results over each city highlight the importance of advanced controls (such as gust tracking control algorithms) if turbines were to be located at hub heights closer to the effective mean building height (h_{hmeff}) or below. Overall, height variability appeared to be a crucial in the siting of a building mounted wind turbines.

In addition, due to the tests carried out at few sites, these models may be best suited for preliminary potential turbine site evaluation or city-scale assessment as well as a useful tool for scoping the potential of small wind turbines at different heights within a built environment. However, onsite wind measurements may be needed to confirm the availability of wind resource as well as the atmospheric turbulence experienced at potential turbine sites. The measured wind speed and $T.I.$ could be incorporated into the TPE model in evaluating the performance of a potential turbine design within a specific site. Finally, having carried out a preliminary comparison between power estimation using a generic power curve and the TPE model, results showed better power predictions using the power curve at $T.I.$ lower than 10% whereas performing poorly at $T.I.$ higher than 10% (which is frequently more likely to occur within a built environment). The implication of this result is that complexities involved in the production and application of various power curves representing different turbulence intensities for a more effective turbine performance assessment can be avoided by providing a single C_e - $T.I.$ curve. A city-scale variation of the capacity factor of the chosen turbine configuration was produced over four major UK cities. This suggests that the viability of an urban wind project can be assessed by using a simple model provided the $T.I.$ and the wind speeds at the potential site are provided. It can also be recommended that the portion of the excess energy harnessed by a wind energy system can be assessed by comparing the EEC - C_e curve before and after employing a control system thus evaluating its performance in turbine operations within a specific turbine site.

7.3 Limitations and Opportunities for Future work

In Chapters 4 and 5, the major limitations of the analysis undertaken were determined by the availability of high-resolution wind datasets. The datasets available provided the needed support for testing and validation of the $T.I.$ and EEC estimation models. Another limitation was the unavailability of aerodynamic parameters for some sites with available high-resolution wind measurements, resulting in the evaluation of the $T.I.$ model at fewer sites. Hence, it may be beneficial for the $T.I.$ model as well as the EEC model to be tested and

validated at more suburban/urban sites provided the aerodynamic parameters and high-resolution wind datasets are available.

There were important limitations encountered in the vertical-axis wind turbine design in Chapter 3, including employing a simple standard control method, the choice of a less advanced modelling approach, etc. Due to the high cost that could be incurred if other modelling approaches such as vortex modelling (which for example, incorporates the wake effects as well as other secondary effects) were to be employed, this study was limited to the scope of stream tube modelling. Further investigations need to be undertaken by considering various modelling approaches such as vortex models (which are considered the most accurate models). Although this research study was limited to the performance of a simple straight-bladed VAWT, it would be interesting to evaluate the performance of curved-bladed VAWT (a common design found in commercial wind turbines). The use of a simple standard control method may have suggested poor tracking of the C_{pmax} due to poor estimation of the control gain k while operating in rapidly varying wind condition. Hence the use of advanced control algorithms such as PID feedback controllers may go a long way in improving the performance of the turbine system. This may lead to improvements in the C_e prediction model and hence an overall improvement in the accuracy of the TPE model.

One obvious limitation in Chapter 6 which may affect the city-scale variation in turbine power outputs may arise from the simplifications that were made in the development of the wind speed prediction model (also known as the MH model). Although the effects of building-scale flow features and local topography below the neighbourhood scale were not accounted for in the MH model, the $T.I.$ model was assumed to account for these local features in predicting turbine power. However, given the complex nature of the local atmospheric environment of suburban/urban areas and considering the fact that physical and aerodynamic properties do not fully characterise the nature of turbulence exchange (especially wake turbulence) within this environment, a further limitation in the accuracy of the $T.I.$ model in estimating atmospheric turbulence within a potential suburban/urban site ensues. Hence, it is recommended that more research should be carried out on transfer processes within the urban canopy (for example, within the main region of momentum, heat and mass exchange) and the exchange at higher heights above the urban canopy in order to fully understand the urban-turbulence system. An additional limitation in Chapter 6 may exist as the TPE model performance was only compared to a generic power curve. However, it is recommended that a detailed comparison between the TPE model and different methodologies proposed by various studies for adjusting power curves in order to account for local turbulence is carried out. Also, further tests to validate the capacity factors predicted in Chapter 6 are required. This

could require more high resolution wind datasets, physical and aerodynamic properties for various sites and also computer time.

7.4 Impact of this Research

7.4.1 Impact in the field of urban meteorology

It is expected that the findings of this research study will have significant impacts in the field of urban meteorology and the wind energy industry in general (especially urban wind energy). The most significant findings for urban meteorology are those of Chapters 4 and 5. This is because comprehensive field study of atmospheric turbulence over complex (inhomogeneous) environments in general is difficult and costly to accomplish. Also, previous urban-turbulence studies carried out have been mostly for the purpose of understanding and modelling pollution dispersion, wind loading on buildings and other structures, etc. [37]. Few studies on atmospheric turbulence within the suburban/urban environment for the sole purpose of wind energy analysis can be found. Thus, this study aims to provide the relevant background for understanding and analysing turbulent transfer over complex (inhomogeneous) environments.

The models proposed in Chapters 4 and 5 could be used to estimate the turbulence intensity, excess energy and total kinetic (wind) energy available at different heights within the suburban/urban environment. This provides a platform for analysing city-scale variations of urban atmospheric properties. Also, given the large inaccuracies observed when using the Macdonald's model [47], the MH model offers improvements in predicting the z_0, d, wind speed and various aerodynamic parameters by considering the building height variations within a built environment. This has been demonstrated in Chapter 5. This, consequently, leads to improved accuracy in predicting the $T.I.$ and EEC within a potential suburban/urban turbine site. It is useful to note that the $T.I.$ model could also be used to estimate the drag coefficient, friction velocity and other turbulence properties over a built environment for use in other areas of research such as pollution dispersion, wind loading analysis on buildings/structures, etc.

7.4.2 Impact in the field of urban wind energy

The primary goal of this research study was to develop models to assist in the development of wind energy and its applications in suburban/urban areas. This could be achieved by increasing the understanding of the urban wind resource and how inherent atmospheric conditions affect the energy available as well as estimating the power outputs were small wind turbines to be installed. Accordingly, in Chapter 6, the works of Chapters 1 to 5 were brought

together in the development of a new wind energy resource assessment tool known as the turbine power prediction (TPE) model. This TPE model comprises of various sub-models which is represented in Figure 7.1.

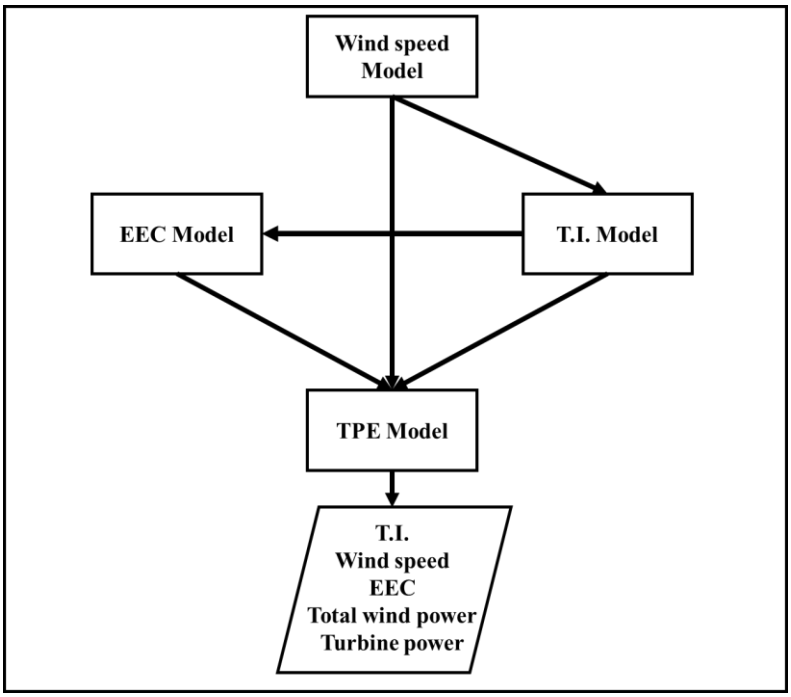

Figure 7. 1: A simple layout of the turbine power estimation (TPE) model and its sub-models.

The promising results reported in Chapters 5 and 6, using the models shown in Figure 7.1, highlight several areas that could benefit from further study. Such a study would allow a more detailed investigation into urban meteorology and small wind applications within built environment, which is rarely found. In order to maximize the impact of this research, it is recommended that a map of the wind speed, turbulence intensity, excess energy, power output and also capacity factor for specific turbine designs at different heights over the various study areas are made available so that they can be easily assessed by the public or interested parties. It would be informative as well as encouraging if this methodology is extended to a much greater number of cities/towns. Hence, this would allow the financial implications of potential wind turbine projects within a wider area to be evaluated.

The big picture

Models proposed in this research could also be transformed into an online tool. Figure 7.2 is a snapshot of a tool developed by the Energy Research Institute, University of Leeds. This tool is quite user-friendly, compatible with google chrome and aims to predict the average wind speed at different heights over six different cities namely Leeds, Edinburgh, Manchester, London, Birmingham and Nottingham.

More features such as turbulence intensity, excess energy and turbine power estimations using models presented in Chapters 4 to 6 could also be incorporated into this tool. Hence, by quoting their postcode and the proposed hub height, a user could find out not just the wind speed, but the estimated turbulence intensity, excess energy and potential turbine power output around their property thus bringing renewable energy technologies closer to the public and also encouraging urban wind energy development. The scope of this tool could be extended to other cities and areas within the UK. However, this may require availability of physical and aerodynamic properties for various cities (preferably LiDAR data that has recently been made freely available for large areas of the UK [306]), extending the urban wind meteorology defined by MH model to those cities, more tests and validation of the $T.I.$ and EEC models, obtaining a $C_e - T.I.$ curve from small wind turbine manufacturers and finally testing and validating the TPE model within different suburban/urban environments.

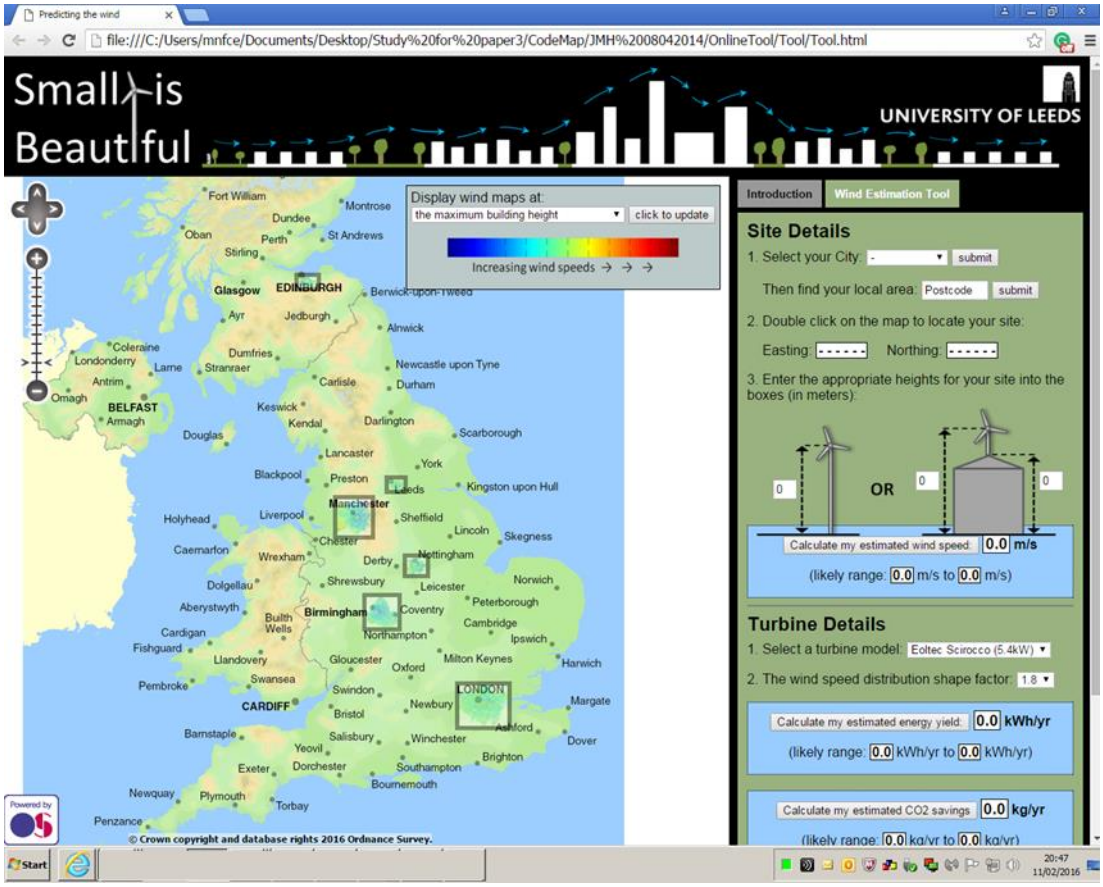

Figure 7. 2: A snapshot of the wind energy prediction tool developed by the Energy Research Institute, University of Leeds.

APPENDIX A

Mean Percentage Error (MPE) for turbine power prediction model across all 8 sites at averaging time (T_c) of 1 s.

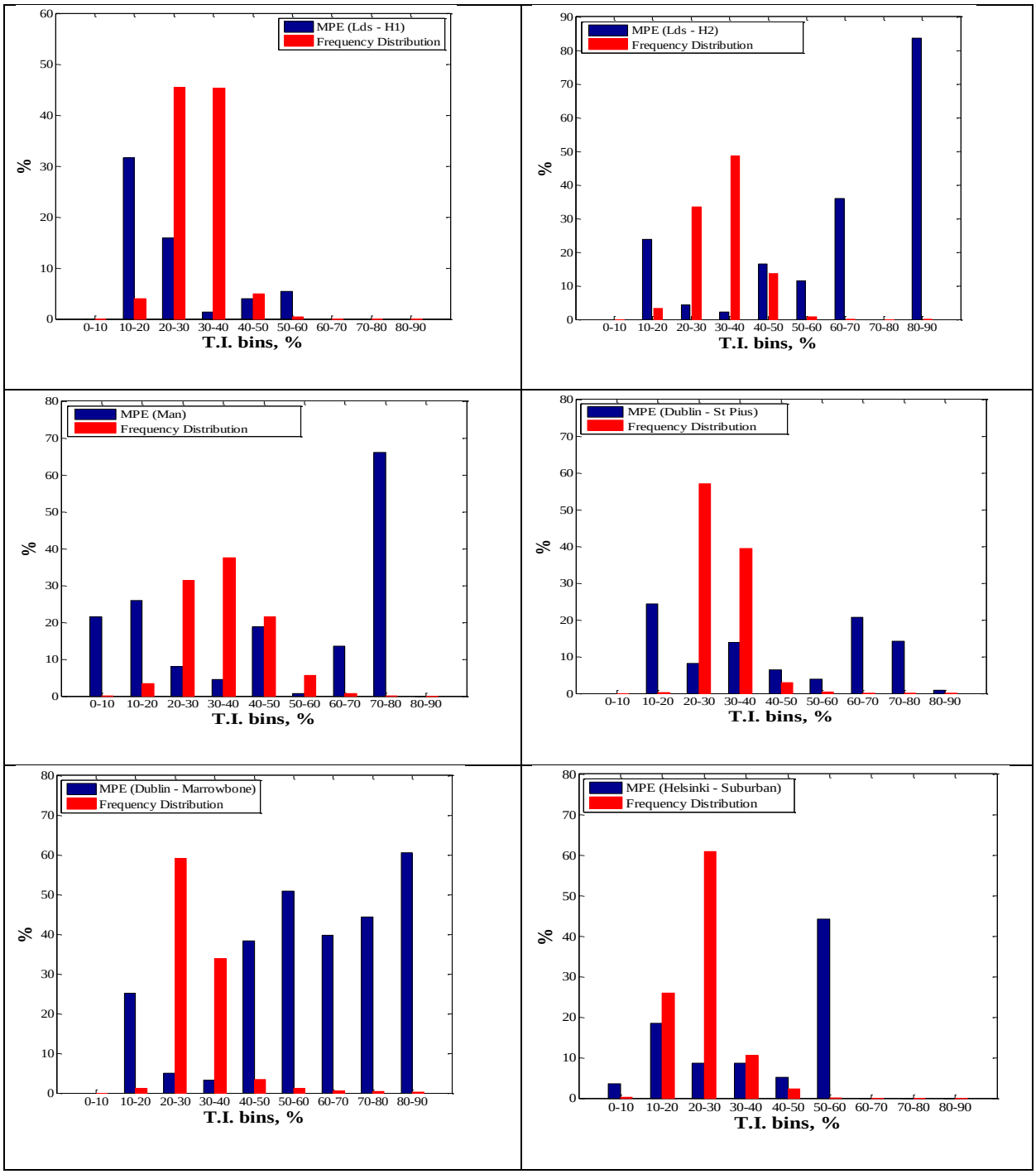

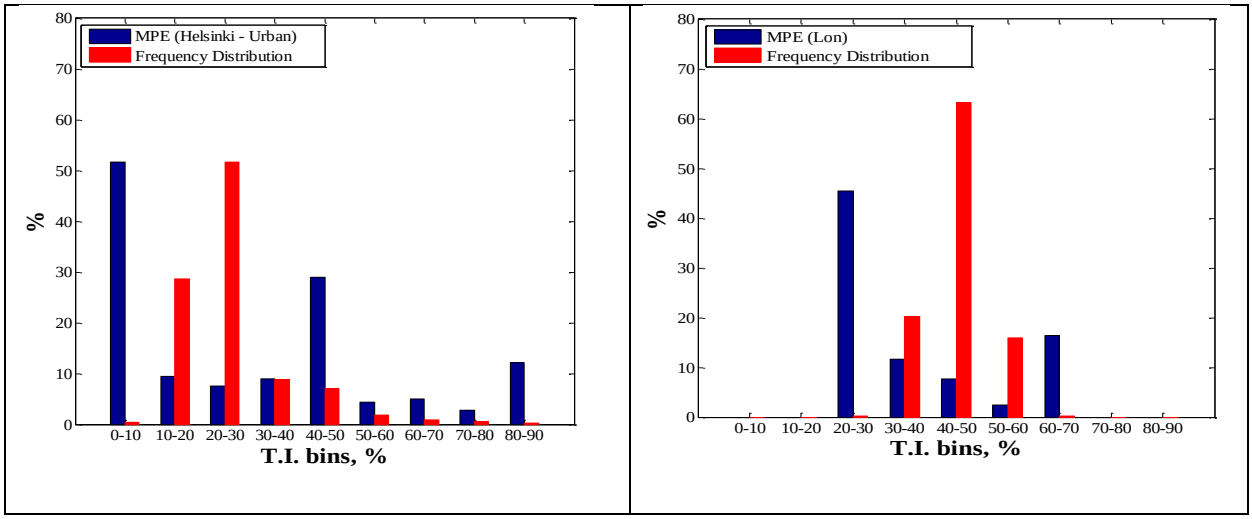
MPE (Helsinki - Urban)
Frequency Distribution
%
0-10
10-20
20-30
30-40
40-50
50-60
60-70
70-80
80-90
T.I. bins, %
MPE (Lon)
Frequency Distribution
%
0-10
10-20
20-30
30-40
40-50
50-60
60-70
70-80
80-90
T.I. bins, %

APPENDIX B

Summary of results from the TPE and the C_{tc} estimation models at 10 m above h_{hmeff} across four cities at T_c= 20 s.

Leeds			
	Min	**Average**	**Max**
Power	8.29	33.81	124.77
C_{tc}	26.67	31.43	38.75
Edinburgh			
	Min	**Average**	**Max**
Power	8.40	50.32	137.85
C_{tc}	27.03	31.26	38.75
Manchester			
	Min	**Average**	**Max**
Power	4.12	25.05	92.09
C_{tc}	26.38	32.23	38.75
London			
	Min	**Average**	**Max**
Power	1.60	21.27	102.66
C_{tc}	25.86	32.19	38.74

APPENDIX C

Summary of results from the TPE and the C_{tc} estimation models at 10 m above h_{hmeff} across four cities at T_c = 30 s.

Leeds			
	Min	**Average**	**Max**
Power	6.16	27.02	97.35
C_{tc}	24.22	25.02	27.91
Edinburgh			
	Min	**Average**	**Max**
Power	6.05	40.51	117.95
C_{tc}	24.23	24.98	27.91
Manchester			
	Min	**Average**	**Max**
Power	2.97	19.67	76.02
C_{tc}	24.22	25.26	27.91
London			
	Min	**Average**	**Max**
Power	1.20	16.81	86.26
C_{tc}	24.22	25.27	27.91

APPENDIX D

Summary of results from the TPE and the C_{tc} estimation models at 10 m above local maximum building heights across four cities at T_c = 20 s.

Leeds			
	Min	**Average**	**Max**
Power	12.00	50.33	208.00
C_{tc}	28.55	33.72	38.73
Edinburgh			
	Min	**Average**	**Max**
Power	18.35	73.73	219.28
C_{tc}	27.60	33.38	38.02
Manchester			
	Min	**Average**	**Max**
Power	5.13	34.45	125.78
C_{tc}	27.37	34.20	38.59
London			
	Min	**Average**	**Max**
Power	2.03	31.47	126.57
C_{tc}	26.81	34.51	38.74

APPENDIX E

Summary of results from the TPE and the C_e estimation models at 10 m above local maximum building heights across four cities at T_c = 30 s.

Leeds			
	Min	**Average**	**Max**
Power	8.81	38.45	151.72
C_{tc}	24.37	25.74	27.91
Edinburgh			
	Min	**Average**	**Max**
Power	13.49	56.77	159.79
C_{tc}	24.26	25.64	27.55
Manchester			
	Min	**Average**	**Max**
Power	4.01	26.09	92.23
C_{tc}	24.25	25.92	27.83
London			
	Min	**Average**	**Max**
Power	1.47	23.83	100.18
C_{tc}	24.22	26.06	27.91

REFERENCES

[1] Elvidge C, Safran J, Nelson I, Tuttle B, Ruth Hobson V, Baugh K, Dietz J, Erwin E, Lunetta R, Lyon J. *Area and positional accuracy of DMSP nighttime lights data.* CRC Press: Boca Raton, FL, USA, 2004.

[2] Burton T, Sharpe D, Jenkins N, Bossanyi E. *Wind Energy Handbook.* John Wiley & Sons Ltd, West Sussex, UK, 2001.

[3] Makkawi A, Celik AN, Muneer T. Evaluation of micro-wind turbine aerodynamics, wind speed sampling interval and its spatial variation. *Services Engineering Research and Technology* 2009, **30**(1), pp.7-14.

[4] Gipe P. Wind energy comes of age. 1995.

[5] Allen SR, Hammond GP, McManus MC. Prospects for and barriers to domestic micro-generation: A United Kingdom perspective. *Applied Energy*, 2008, **85**(6), pp.528-544.

[6] Twidell J, Weir T. *Renewable Energy Resources.* New York: Taylor and Francis, 1986.

[7] McKendry IG, Sturman AP, Owens IF. A Study of Interacting Multi-Scale Wind Systems, Canterbury Plains, New Zealand. *Meteorol. Atmos. Phys.*, 1986, **35**, pp.242-252.

[8] Munteanu I, Bratcu AI, Cutululis N-A, Ceanga E. *Optimal control of wind energy systems: towards a global approach.* Springer Science & Business Media, 2008.

[9] Sathyajith M. *Wind energy: fundamentals, resource analysis and economics.* Springer Science & Business Media, 2006.

[10] Petersen EL, Mortensen NG, Landberg L, Hùjstrup J, Frank HP. Wind Power Meteorology. Part II: Siting and Models. *Wind Energy*, 1998, **1**, pp.55-72.

[11] Van der Hoven I. Power spectrum of horizontal wind speed in the frequency range from 0.0007 to 900 cycles per hour. *Journal of Meteorology*, 1957, **14**(2), pp.160-164.

[12] Berténvi T, Wickins C, McIntosh S. Enhanced energy capture through gust-tracking in the urban wind environment. *In: 48th AIAA Aerospace Sciences Meeting*, Orlando, Florida, USA. American Institute of Aeronautics and Astronautics, 2010.

[13] Petersen EL, Mortensen NG, Landberg L, Hojstrup J, Frank HP. Wind Power Meteorology. *Riso National Laboratory*, 1997.

[14] Blaabjerg F, Ma K. Future on power electronics for wind turbine systems. *Emerging and Selected Topics in Power Electronics, IEEE Journal of*, 2013, **1**(3), pp.139-152.

[15] Panofsky HA, Van der Hoven I. *Structure of small scale and middle scale turbulence at Brookhaven.* Pennsylvania State University, Mineral Industries Experiment Station, Department of Meteorology, 1956.

[16] Lang S, McKeogh E. LIDAR and SODAR measurements of wind speed and direction in upland terrain for wind energy purposes. *Remote Sensing*, 2011, **3**(9), pp.1871-1901.

[17] Bailey BH, McDonald SL, Bernadett DW, Markus MJ, Elsholz KV. Wind Resource Assessment Handbook: Fundamentals for Conducting a Successful Monitoring Program. TAT-5–15283–01. Golden, CO, USA., 1997.

[18] Senjyu T, Sakamoto R, Urasaki N, Funabashi T, Fujita H, Sekine H. Output power leveling of wind turbine generator for all operating regions by pitch angle control. *Energy Conversion, IEEE Transactions on*, 2006, **21**(2), pp.467-475.

[19] Larsen GC, Hansen KS. Database on wind characteristics. *Structure and Philosophy, RISO*, 2004.

[20] Politis ES, Chaviaropoulos PK. Micrositing and Classification of Wind Turbines in Complex Terrain. *In: Proceedings of the 2008 European Wind Energy Conference & Exhibition*, 31 March–3 April, Brussels. 2008, pp.126-130.

[21] Politis ES, Prospathopoulos J, Cabezon D, Hansen KS, Chaviaropoulos P, Barthelmie RJ. Modeling wake effects in large wind farms in complex terrain: the problem, the methods and the issues. *Wind Energy*, 2012, **15**(1), pp.161-182.

[22] Davidson PA. *Turbulence: an introduction for scientists and engineers.* Oxford University Press, 2015.

[23] Chorin AJ. Numerical solution of the Navier-Stokes equations. *Mathematics of computation*, 1968, **22**(104), pp.745-762.

[24] Karniadakis GE, Israeli M, Orszag SA. High-order splitting methods for the incompressible Navier-Stokes equations. *Journal of Computational Physics*, 1991, **97**(2), pp.414-443.

[25] Foias C. What do the Navier-Stokes equations tell us about turbulence? *Contemporary Mathematics*, 1997, **208**, pp.151-180.

[26] Seinfeld JH, Pandis SN. *Atmospheric chemistry and physics: from air pollution to climate change.* John Wiley & Sons, 2016.

[27] Truesdell C. Notes on the History of the General Equations of Hydrodynamics. *The American Mathematical Monthly*, 1953, **60**(7), pp.445-458.

[28] Hoffman J. Weak uniqueness of the Navier-Stokes equations and adaptive turbulence simulation. *In: Proceedings of the 12th Leslie Fox Prize Meeting*, 2005.

[29] Qian J. Variational approach to the closure problem of turbulence theory. *Physics of Fluids (1958-1988)*, 1983, **26**(8), pp.2098-2104.

[30] Mansour N, Kim J, Moin P. Near-wall k-epsilon turbulence modeling. *AIAA journal*, 1989, **27**(8), pp.1068-1073.

[31] Weber RO. Remarks on the Definition and Estimation of Friction Velocity. *Boundary-Layer Meteorology*, **93**(2), pp.197-209.

[32] Petersen EL, Mortensen NG, Landberg L, Højstrup J, Frank HP. Wind power meteorology. Part I: Climate and turbulence. *Wind Energy*, 1998, **1**(s 1), pp.25-45.

[33] Wieringa J. Gust factors over open water and built-up country. *Boundary-Layer Meteorology*, 1973, **3**(4), pp.424-441.

[34] Harstveit K. Full scale measurements of gust factors and turbulence intensity, and their relations in hilly terrain. *Journal of Wind Engineering and Industrial Aerodynamics*, 1996, **61**(2–3), pp.195-205.

[35] Holton JR, Hakim GJ. *An introduction to dynamic meteorology*. Academic press, 2012.

[36] Frederickson PA, Davidson KL, Edson JB. A Study of Wind Stress Determination Methods from a Ship and an Offshore Tower. *Journal of Atmospheric and Oceanic Technology*, 1997, **14**(4), pp.822-834.

[37] Roth M. Review of atmospheric turbulence over cities. *Quarterly Journal of the Royal Meteorological Society*, 2000, **126**, pp.941–990.

[38] Zeman O, Jensen NO. Modification of turbulence characteristics in flow over hills. *Quarterly Journal of the Royal Meteorological Society*, 1987, **113**(475), pp.55-80.

[39] Ly LN. Effect of the Angle between Wind Stress and Wind Velocity Vectors on the Aerodynamic Drag Coefficient at the Air-Sea Interface. *Journal of Physical Oceanography*, 1993, **23**(1), pp.159-163.

[40] Rotach MW. Turbulence Close to a Rough Urban Surface Part I: Reynolds Stress. *Boundary-Layer Meteorol*, 1993, **65**, pp.1–28.

[41] Geernaert GL, Hansen F, Courtney M, Herbers T. Directional attributes of the ocean surface wind stress vector. *Journal of Geophysical Research: Oceans*, 1993, **98**(C9), pp.16571-16582.

[42] Harstveit K. Full scale measurements of gust factors and turbulence intensity, and their relations in hilly terrain. *J. Wind. Eng. Ind. Aerod.*, 1996, **61(2–3)**, pp.195–205.

[43] Solari G, A. , Kareem A. On the formulation of ASCE7-95 gust effect factor. *J. Wind Eng. Ind. Aerodyn.*, 1998, **77-78**, pp.673–684.

[44] Greenway ME. An analytical approach to wind velocity gust factors. *J. Ind. Aerodyn*, 1979, **5**, pp.61–91.

[45] IEC 61400-12-1. Wind Turbines – Part 12-1 : Power performance measurement of Electricity producing wind turbines. Ed, 2005.

[46] Kaimal JC, Finnigan JJ. *Atmospheric boundary layer flows: their structure and measurement.* Oxford University Press, USA, 1994.

[47] Millward-Hopkins JT, Tomlin AS, Ma L, Ingham D, Pourkashanian M. Estimating aerodynamic parameters of urban-like surfaces with heterogeneous building heights. *Boundary-Layer Meteorology*, 2011, **141**(3), pp.443-465.

[48] Britter R, Hanna S. Flow and dispersion in urban areas. *Annual Review of Fluid Mechanics*, 2003, **35**(1), pp.469-496.

[49] Oke TR. *Boundary Layer Climates.* New York: Methuen and Co., 1987.

[50] Shaw RH, Pereira AR. Aerodynamic roughness of a plant canopy: A numerical experiment. *Agricultural Meteorology*, 1982, **26**(1), pp.51-65.

[51] Sakagami Y, Santos PA, Haas R, Passos JC, Taves FF. Logarithmic Wind Profile: A Stability Wind Shear Term. *arXiv preprint arXiv:1405.5158*, 2014.

[52] Millward-Hopkins JT. *Predicting the wind resource available to roof-mounted wind turbines in urban areas*. thesis, University of Leeds, 2013.

[53] Oke TR. Street design and urban canopy layer climate. *Energy and Buildings*, 1988, **11**(1), pp.103-113.

[54] Arnfield AJ. An approach to the estimation of the surface radiative properties and radiation budgets of cities. *Physical Geography*, 1982, **3**(2), pp.97-122.

[55] Millward-Hopkins JT, Tomlin AS, Ma L, Ingham D, Pourkashanian M. The predictability of above roof wind resource in the urban roughness sublayer. *Wind Energy*, 2012, **15**(2), pp.225-243.

[56] CarbonTrust. Small-scale wind energy - technical report. Available from: http://www.carbontrust.co.uk/technology/technologyaccelerator/small-wind.htm. 2008. [Accessed].

[57] Garratt JR. The Internal Boundary-Layer - A Review. *Boundary-Layer Meteorology*, 1990, **50(1-4)**, pp.171-203.

[58] Millward-Hopkins JT, Tomlin AS, Ma L, Ingham D, Pourkashanian M. Aerodynamic Parameters of a UK City Derived from Morphological Data. *Boundary-Layer Meteorology*, 2012, pp.1-22.

[59] Hanna SR, Britter RE. Wind Flow and Vapor Cloud Dispersion at Industrial Sites. [online], 2002.

[60] Bou-Zeid E, Parlange MB, Meneveau C. On the Parameterization of Surface Roughness at Regional Scales. *Journal of the Atmospheric Sciences*, 2007, **64**(1), pp.216-227.

[61] Bou-Zeid E, Meneveau C, Parlange MB. Large-eddy simulation of neutral atmospheric boundary layer flow over heterogeneous surfaces: Blending height and effective surface roughness. *Water Resources Research*, 2004, **40**(2), pp.n/a-n/a.

[62] UK Met Office. Small-scale wind energy Technical Report. Available from: www.carbontrust.com/media/85174/small-scale-wind-energy-technical-report.pdf. 2008. [Accessed 7/7/2014].

[63] Millward-Hopkins J, Tomlin A, Ma L, Ingham D, Pourkashanian M. Mapping the wind resource over UK cities. *Renewable Energy*, 2013, **55**(Complete), pp.202-211.

[64] Cheng H, Castro IP. Near wall flow over urban-like roughness. *Boundary-Layer Meteorology*, 2002, **104(2)**, pp.229-259.

[65] Cheng H, Hayden P, Robins AG, I.P. C. Flow over cube arrays of different packing densities. *Journal of Wind Engineering and Industrial Aerodynamics*, 2007, **95(8)**, pp.715-740.

[66] Mertens S. *Wind energy in the built environment.* Multi Science Publishing Company, 2005.

[67] ESDU. Characteristics of atmospheric turbulence near the ground. Part III: Variations in space and time for strong winds (neutral atmosphere). ESDU 75001, UK. Engineering Sciences Data Unit, 1985.

[68] MacDonald RW. Modelling the mean velocity profile in the urban canopy layer. *Boundary-Layer Meteorology*, 2000, **97**, pp.25–45.

[69] Millward-Hopkins JT, Tomlin AS, Ma L, Ingham D, Pourkashanian M. Assessing the potential of urban wind energy in a major UK city using an analytical model. *Renewable Energy*, 2013, **60**, pp.701-710.

[70] Oke TR. The Distinction between Canopy and Boundary-Layer Urban Heat Island'. *Atmosphere*, 1976, **14**, pp.269-277.

[71] Carlin PW, Laxson AS, Muljadi E. The history and state of the art of variable-speed wind turbine technology. *Wind Energy*, 2003, **6**(2), pp.129-159.

[72] Schubel PJ, Crossley RJ. Wind turbine blade design. *Energies*, 2012, **5**(9), pp.3425-3449.

[73] Hansen AD, Hansen LH. Wind Turbine Concept Market Penetration over 10 Years (1995–2004). *Wind Energy*, 2007, **10 (1)**, pp.81-97.

[74] Vestas. World's most powerful wind turbine now operational. Available from: http://www.vestas.com/en/media/news#!140128_nr_vws. 2014. [Accessed 06/08/2015].

[75] McIntosh SC. *Wind energy for the built environment*. thesis, University of Cambridge, 2009.

[76] Hansen A, Butterfield C. Aerodynamics of horizontal-axis wind turbines. *Annual Review of Fluid Mechanics*, 1993, **25**(1), pp.115-149.

[77] Aeolos Wind Turbine. Horizontal Axis Wind Turbine Instructions. Available from: http://www.windturbinestar.com/horizontal-axis-wind-turbine-2.html. 2013. [Accessed 18/01/2013].

[78] Eldridge FR. *Wind machines.* Van Nostrand Reinhold Co., 1980.

[79] Islam M, Ting D, Fartaj A. Aerodynamic Models for Darrieus-type Straight-bladed Vertical Axis Wind Turbines. *Renewable and Sustainable Energy Reviews*, 2008, **12(4)**, pp.1087-1109.

[80] Blackwell BF. SLA-74-0160. Vertical-axis wind turbine: How It Works. Sandia Laboratories., Albuquerque, N. Mex.(USA), 1974.

[81] Johnston Jr SF. Proceedings of the vertical axis wind turbine (VAWT) design technology seminar for industry. Sandia Labs., Albuquerque, NM (USA), 1980.

[82] Kirke BK. *Evaluation of self-starting vertical axis wind turbines for stand-alone applications*. thesis, GRIFFITH UNIVERSITY GOLD COAST, 1998.

[83] Bianchi FD, De Battista H, Mantz RJ. *Wind turbine control systems: principles, modelling and gain scheduling design.* Springer Science & Business Media, 2006.

[84] Eriksson S, Bernhoff H, Leijon M. Evaluation of different turbine concepts for wind power. *Renewable and Sustainable Energy Reviews*, 2008, **12**(5), pp.1419-1434.

[85] Aslam Bhutta MM, Hayat N, Farooq AU, Ali Z, Jamil SR, Hussain Z. Vertical axis wind turbine–A review of various configurations and design techniques. *Renewable and Sustainable Energy Reviews*, 2012, **16**(4), pp.1926-1939.

[86] Lazauskas L. Three pitch control systems for vertical axis wind turbines compared. *Wind Engineering*, 1992, **16**(5), pp.269-282.

[87] Renewable UK. Generate your Own Power. Available from: http://www.renewableuk.com/en/publications/index.cfm/gyop1. 2013. [Accessed 18/01/2013].

[88] Renewable UK. Small Wind Systems: UK market report. 2011.

[89] US Energy Department. Energy Efficiency and Renewable Energy. Available from: http://www1.eere.energy.gov/wind/wind_how.html. 2012. [Accessed 7/12/2012].

[90] Nahas MN. A Self-Starting Darrieus-Type Windmill. *Energy and Power Engineering Journal*, 1993, **18**(9), pp.899 - 906.

[91] Manwell JF, McGowan JG, Rogers AL. *Wind Energy Explained: Theory, Design and Application.* Second ed. John Wiley & Sons Ltd, West Sussex, UK, 2002.

[92] Miley SJ. A catalog of low Reynolds number airfoil data for wind turbine applications. 1982.

[93] Tangier J, Smith B, Kelley N, Jager D. Measured and Predicted Rotor Performance for the SERI Advanced Wind Turbine Blades. NREL TP-257-4594, National Renewable Energy Laboratory, Golden, CO, 1992.

[94] Habali S, Saleh I. Design and testing of small mixed airfoil wind turbine blades. *Renewable Energy*, 1995, **6**(2), pp.161-169.

[95] Hau E. Wind Turbines-Fundamentals, Technologies, Application, Economics. *IEEE Electrical Insulation Magazine*, 2003, **19**(2), p.48.

[96] Ragheb M, Ragheb AM. Wind Turbines Theory - The Betz Equation and Optimal Rotor Tip Speed Ratio, Fundamental and Advanced Topics in Wind Power. *Rupp Carriveau (Ed.)*, 2011, **InTech**, pp.http://www.intechopen.com/articles/show/title/wind-turbines-theory-the-betz-equation-and-optimal-rotor-tip-speed-ratio.

[97] Baroudi JA, Dinavahi V, Knight AM. A review of power converter topologies for wind generators. *Renewable Energy*, 2007, **32**(14), pp.2369-2385.

[98] Coton FN, Wang T. The prediction of horizontal axis wind turbine performance in yawed ow using an unsteady prescribed wake model. *Proceedings of the Institution of Mechanical Engineers, Part A: Journal of Power and Energy*, 1999, **213 (1)**, pp.33-43.

[99] Johnson KE, Pao LY, Balas MJ, Fingersh LJ. Control of variable-speed wind turbines: standard and adaptive techniques for maximizing energy capture. *Control Systems, IEEE*, 2006, **26**(3), pp.70-81.

[100] Bellarmine GT, Urquhart J. Wind Energy for the 1990s and Beyond. *Energy Conversion and Management Journal*, 1996, **37**(12), pp.1741-1752.

[101] Tong W. *Wind power generation and wind turbine design.* Wit Pr/Computational Mechanics, 2010.

[102] Pao LY, Johnson KE. A Tutorial on the Dynamics and Control of Wind Turbines and Wind Farms. *In: American Control Conference*, June,2009, St. Louis, Missouri USA. 2009.

[103] Hansen AD, Hansen LH. Market penetration of different wind turbine concepts over the years. *In: 2007 European Wind Energy Conference and Exhibition*, 2007.

[104] Muljadi E, Butterfield C. Wind farm power system model development. *In: World Renewable Energy Congress VIII, Colorado*, 2004.

[105] Shukla RD, Tripathi R, Gupta S. Power electronics applications in wind energy conversion system: A review. *In: Power, Control and Embedded Systems (ICPCES), 2010 International Conference on*: IEEE, 2010, pp.1-6.

[106] Thiringer T, Petersson A. Control of a variable-speed pitch-regulated wind turbine. *Dept. of Energy and Environ., Chalmers Univ. of Technol., Göteborg, Sweden*, 2005.

[107] Laks JH, Pao LY, Wright AD. Control of wind turbines: Past, present, and future. *In: American Control Conference, 2009. ACC'09.*: IEEE, 2009, pp.2096-2103.

[108] Stol KA. Disturbance tracking control and blade load mitigation for variable-speed wind turbines. *Journal of solar energy engineering*, 2003, **125**(4), pp.396-401.

[109] Wright A, Fingersh L. Advanced control design for wind turbines. Part I: control design, implementation and initial tests. National Renewable Energy Laboratory. NREL/TP-500-42437, Golden, Colorado, 2008.

[110] Koutroulis E, Kalaitzakis K. Design of a maximum power tracking system for wind-energy-conversion applications. *Industrial Electronics, IEEE Transactions on*, 2006, **53**(2), pp.486-494.

[111] Yaoqin J, Zhongqing Y, Binggang C. A new maximum power point tracking control scheme for wind generation. *In: Power System Technology, 2002. Proceedings. PowerCon 2002. International Conference on*: IEEE, 2002, pp.144-148.

[112] Komatsu M, Miyamoto H, Ohmori H, Sano A. Output Maximization Control of Wind Turbine Based on Extremum Control Strategy. *In: Proc. Amer. Ctrl. Conf.*, June. 2001, pp.1739–1740.

[113] Song Y, Dhinakaran B, Bao X. Variable speed control of wind turbines using nonlinear and adaptive algorithms. *Journal of Wind Engineering and Industrial Aerodynamics*, 2000, **85**(3), pp.293-308.

[114] Boukhezzar B, Siguerdidjane H, Hand MM. Nonlinear control of variable-speed wind turbines for generator torque limiting and power optimization. *Journal of solar energy engineering*, 2006, **128**(4), pp.516-530.

[115] Frost SA, Balas MJ, Wright AD. Direct adaptive control of a utility-scale wind turbine for speed regulation. *International Journal of Robust and Nonlinear Control*, 2009, **19**(1), pp.59-71.

[116] Kumar A, Stol K. Scheduled model predictive control of a wind turbine. *In: Proceedings of AIAA/ASME Wind Energy Symposium*, 2009.

[117] Miller A, Muljadi E, Zinger DS. A variable speed wind turbine power control. *IEEE Transactions on Energy Conversion*, 1997, **12**(2).

[118] Haniotis AE, Soutis KS, Kladas AG, Tegopoulos J. Grid connected variable speed wind turbine modeling, dynamic performance and control. *In: Power Systems Conference and Exposition, 2004. IEEE PES*: IEEE, 2004, pp.759-764.

[119] Ahmed A, Ran L, Bumby JR. New constant electrical power soft-stalling control for small-scale VAWTs. *Energy Conversion, IEEE Transactions on*, 2010, **25**(4), pp.1152-1161.

[120] Hwang IS, Min SY, Jeong IO, Lee YH, Kim SJ. Efficiency improvement of a new vertical axis wind turbine by individual active control of blade motion. *Smart Structures and Materials 2006: Smart Structures and Integrated Systems*, 2006, **6173**, pp.316-323.

[121] Paraschivoiu I, Trifu O, Saeed F. H-Darrieus wind turbine with blade pitch control. *International Journal of Rotating Machinery*, 2009, **2009**.

[122] Samsonov V, Baklushin P. Comparison of different way for VAWT aerodynamic control. *Journal of Wind Engineering and Industrial Aerodynamics*, 1992, **39**, pp.427-433.

[123] Vashkevitch K, Samsonov V. Investigation of HAWT and VAWT aerodynamics for large WEC design. *In: European Community Wind Energy Conference*, Madrid, Spain. 1990, pp.316 - 318.

[124] Pao LY, Johnson KE. Control of wind turbines. *Control Systems, IEEE*, 2011, **31**(2), pp.44-62.

[125] Suryanarayanan S, Dixit A. On the dynamics of the pitch control loop in horizontal-axis large wind turbines. *In: American Control Conference, 2005. Proceedings of the 2005*: IEEE, 2005, pp.686-690.

[126] Kumar V, Paraschivoiu M, Paraschivoiu I. Low Reynolds number vertical axis wind turbine for Mars. *Wind Engineering*, 2010, **34**(4), pp.461-476.

[127] Yamamoto G, Shiotani M. Atmospheric turbulence over the large city—Turbulence in the free atmosphere. *Geophys. Mag. Cent. Meteor. Observ. Japan*, 1950, **21**, pp.134-147.

[128] Finnigan J, Raupach M, Bradley EF, Aldis G. A wind tunnel study of turbulent flow over a two-dimensional ridge. *Boundary-Layer Meteorology*, 1990, **50**(1-4), pp.277-317.

[129] Santamouris M, Papanikolaou N, Koronakis I, Livada I, Asimakopoulos D. Thermal and air flow characteristics in a deep pedestrian canyon under hot weather conditions. *Atmospheric Environment*, 1999, **33**(27), pp.4503-4521.

[130] Lee SH, Park SU. A vegetated urban canopy model for meteorological and environmental modelling. *Boundary-Layer Meteorology*, 2008, **126**(1), pp.73-102.

[131] Leitl B, Schatzmann M. Compilation of Experimental Data for Validation Purposes. *CEDVAL (Meteorology Institute, Hamburg University)*, 1998.

[132] Nielsen M. Turbulent ventilation of a street canyon. *Environmental monitoring and assessment*, 2000, **65**(1), pp.389-396.

[133] Nakamura Y, Oke T. Wind, temperature and stability conditions in an east-west oriented urban canyon. *Atmospheric Environment (1967)*, 1988, **22**(12), pp.2691-2700.

[134] Arnold S, ApSimon H, Barlow J, Belcher S, Bell M, Boddy J, Britter R, Cheng H, Clark R, Colvile R. Introduction to the DAPPLE air pollution project. *Science of the Total Environment*, 2004, **332**(1), pp.139-153.

[135] Christen A, Vogt R, Rotach M. Profile measurements of selected turbulence characteristics over different urban surfaces. *In: Proc. 4th Int. Conf. on Urban Air Quality*, 2003, pp.408-411.

[136] Wood CR, Barlow JF, Belcher SE, Dobre A, Arnold SJ, Balogun AA, Lingard JJ, Smalley RJ, Tate JE, Tomlin AS. Dispersion experiments in central London: the 2007 DAPPLE project. *Bulletin of the American Meteorological Society*, 2009, **90**(7), pp.955-969.

[137] Allwine KJ, Shinn JH, Streit GE, Clawson KL, Brown M. Overview of URBAN 2000: A multiscale field study of dispersion through an urban environment. *Bulletin of the American Meteorological Society*, 2002, **83**(4), pp.521-536.

[138] Nielsen M. Turbulent ventilation of a street canyon. *Environmental monitoring and assessment*, 2000, **65**(1-2), pp.389-396.

[139] Zajic D, Fernando HJ, Brown MJ, Kim J-J, Baik J-J. Flow and turbulence in simulated city canyons; Measurements and computations. *In: Proc. of Fifth International Conference on Urban Climate, Lodz, Poland, September*, 2003, pp.1-5.

[140] Johnson G, Hunter L. Some insights into typical urban canyon airflows. *Atmospheric Environment*, 1999, **33**(24), pp.3991-3999.

[141] Louka P, Belcher S, Harrison R. Coupling between air flow in streets and the well-developed boundary layer aloft. *Atmospheric Environment*, 2000, **34**(16), pp.2613-2621.

[142] Christen A, Vogt R, Rotach MW, Parlow E. P1. 4 FIRST RESULTS FROM BUBBLE II: PARTITIONING OF TURBULENT HEAT FLUXES OVER URBAN SURFACES. *Rn*, 2002.

[143] Brown MJ, Boswell D, Streit G, Nelson M, McPherson T, Hilton T, Pardyjak ER, Pol S, Ramamurthy P, Hansen B. Joint urban 2003 street canyon experiment. *In: 84th AMS Meeting, Paper J*, 2004.

[144] Eliasson I, Offerle B, Grimmond CSB, Lindqvist S. Wind fields and turbulence statistics in an urban street canyon. *Atmospheric Environment*, 2006, **40**, pp.1-16.

[145] Taylor P, Teunissen H. The Askervein Hill project: overview and background data. *Boundary-Layer Meteorology*, 1987, **39**(1-2), pp.15-39.

[146] Mason P, King J. Measurements and predictions of flow and turbulence over an isolated hill of moderate slope. *Quarterly Journal of the Royal Meteorological Society*, 1985, **111**(468), pp.617-640.

[147] Coppin PA, Bradley EF, Katen PC. The Evolution of Atmospheric Turbulence over a Two-Dimensional Ridge. *In: 9th Australasian Fluid Mechanics Conference, Auckland, N.Z*, University of Auckland. 1986, pp.569-572.

[148] Finnigan JJ. Air flow over complex terrain. *In: Flow and Transport in the Natural Environment: Advances and Applications*. Denmead WLSaOT, ed. Berlin: Springer, 1988, pp.183-229.

[149] Xie Z-T, Coceal O, Castro IP. Large-Eddy Simulation of Flows over Random Urban-like Obstacles. *Boundary-Layer Meteorology*, 2008, **129**(1), pp.1-23.

[150] Zaki SA, Hagishima A, Tanimoto J, Ikegaya N. Aerodynamic parameters of urban building arrays with random geometries. *Boundary-Layer Meteorology*, 2011, **138**(1), pp.99-120.

[151] Carpentieri M, Robins AG, Baldi S. Three-Dimensional Mapping of Air Flow at an Urban Canyon Intersection. *Boundary-Layer Meteorology*, 2009, **133**(2), pp.277-296.

[152] Rafailidis S. Influence of building areal density and roof shape on the wind characteristics above a town. *Boundary-Layer Meteorology*, 1997, **85**(2), pp.255-271.

[153] Kastner-Klein P, Fedorovich E, Rotach M. A wind tunnel study of organised and turbulent air motions in urban street canyons. *Journal of Wind Engineering and Industrial Aerodynamics*, 2001, **89**(9), pp.849-861.

[154] Meroney RN, Pavageau M, Rafailidis S, Schatzmann M. Study of line source characteristics for 2-D physical modelling of pollutant dispersion in street canyons. *Journal of Wind Engineering and Industrial Aerodynamics*, 1996, **62**(1), pp.37-56.

[155] Hagishima A, Tanimoto J, Nagayama K, Meno S. Aerodynamic parameters of regular arrays of rectangular blocks with various geometries. *Boundary-Layer Meteorology*, 2009, **132**(2), pp.315-337.

[156] Ghobadian A, Goddard AJH, Gosman AD, Nixon W. Numerical simulation of coastal internal boundary layer development and a comparison with simple models. *In: 14th International Technical Meeting on Air Pollution Modelling and its Application*, Copenhagen. 1983.

[157] El Tahry S, Gosman A. The two-and three-dimensional dispersal of a passive scalar in a turbulent boundary layer. *International journal of heat and mass transfer*, 1981, **24**(1), pp.35-46.

[158] Modi AS. *Direct numerical simulation of turbulent flow*. Unpublished, 1999.

[159] Launder BE, Spalding DP. The numerical computation of turbulent flows. *Computer Methods in Applied Mechanics and Engineering,*, 1974, **3**, pp.269-289.

[160] Launder BE, Sharma BI. Application of the energy-dissipation model of turbulence to the calculation of flow near a spinning disc. *Letters in Heat and Mass Transfer*, 1974, **1**, pp.131-138.

[161] Yakhot V, Smith LM. The renormalization group, the ε-expansion and derivation of turbulence models. *Journal of Scientific Computing*, 1992, **7**(1), pp.35-61.

[162] Wilcox DC. *Turbulence modeling for CFD.* DCW industries La Canada, CA, 1998.

[163] Menter FR. Two-equation eddy-viscosity turbulence models for engineering applications. *AIAA Journal*, 1994, **32**, pp.1598-1605.

[164] Gosman A. Developments in CFD for industrial and environmental applications in wind engineering. *Journal of Wind Engineering and Industrial Aerodynamics*, 1999, **81**(1), pp.21-39.

[165] Breuer M, Lakehal D, Rodi W. Flow around a surface mounted cubical obstacle: comparison of LES and RANS-results. *In: Computation of Three-Dimensional Complex Flows*. Springer, 1996, pp.22-30.

[166] Murakami S. Comparison of various turbulence models applied to a bluff body. *Journal of Wind Engineering and Industrial Aerodynamics*, 1993, **46**, pp.21-36.

[167] Emejeamara FC, Tomlin AS. A method for mapping the turbulence intensity and excess energy available to building mounted wind turbines over a UK City. *Wind Energy*, 2015, pp.n/a-n/a.

[168] Staffelbach G, Senoner JM, Gicquel LYM, Poinsot T. Large eddy simulation of combustion on massively parallel machines. *In: 8th International meeting High performance computing for computational science*. 2008, pp.444-464,.

[169] Schmidt RC, Kerstein AR, Wunsch S, Nilsen V. Near-wall LES closure based on one-dimensional turbulence modeling. *Journal of Computational Physics*, 2003, **186**(1), pp.317-355.

[170] Hoffman J, Johnson C. A new approach to computational turbulence modeling. *Computer Methods in Applied Mechanics and Engineering*, 2006, **195**(23), pp.2865-2880.

[171] Drikakis D. Advances in turbulent flow computations using high-resolution methods. *Progress in Aerospace Sciences*, 2003, **39**(6), pp.405-424.

[172] Orszag SA, Patterson Jr G. Numerical simulation of three-dimensional homogeneous isotropic turbulence. *Physical Review Letters*, 1972, **28**(2), p.76.

[173] Rogallo RS. *Numerical experiments in homogeneous turbulence.* National Aeronautics and Space Administration, 1981.

[174] Kim J, Moin P, Moser R. Turbulence statistics in fully developed channel flow at low Reynolds number. *Journal of fluid mechanics*, 1987, **177**, pp.133-166.

[175] Feiereisen WJ, Reynolds WC, Ferziger JH. Numerical simulation of a compressible homogeneous, turbulent shear flow. 1981.

[176] Le H, Moin P, Kim J. Direct numerical simulation of turbulent flow over a backward-facing step. *Journal of fluid mechanics*, 1997, **330**, pp.349-374.

[177] Na Y, Moin P. Direct numerical simulation of turbulent boundary layers with adverse pressure gradient and separation. Rep. TF-68. *Mechanical Engineering Department, Stanford University*, 1996.

[178] Spalart PR. Direct simulation of a turbulent boundary layer up to R θ= 1410. *Journal of fluid mechanics*, 1988, **187**, pp.61-98.

[179] Millward-Hopkins J, Tomlin A, Ma L, Ingham D, Pourkashanian M. Aerodynamic parameters of a UK city derived from morphological data. *Boundary-Layer Meteorology*, 2013, **146**(3), pp.447-468.

[180] Allen S, Hammond G, McManus M. Energy analysis and environmental life cycle assessment of a micro-wind turbine. *Proceedings of the Institution of Mechanical Engineers, Part A: Journal of Power and Energy*, 2008, **222**(7), pp.669-684.

[181] Bahaj A, Myers L, James P. Urban energy generation: influence of micro-wind turbine output on electricity consumption in buildings. *Energy and Buildings*, 2007, **39**(2), pp.154-165.

[182] Weekes SM. *Small-scale wind energy: methods for wind resource assessment*. thesis, University of Leeds, 2014.

[183] HM Government. Feed-in Tariff: get money for generating your own electricity. Available from: https://www.gov.uk/feed-in-tariffs. 2015. [Accessed 4/9/2015].

[184] Sissons MF, James PAB, Bradford J, Myers LE, Bahaj AS, Anwar A, Green S. Pole-mounted horizontal axis micro-wind turbines: UK field trial findings and market size assessment. *Energy Policy*, 2011, **39**(6), pp.3822-3831.

[185] RenewableUK. Small and Medium Wind UK Market Report. 2015.

[186] World Wind Energy Association. Small Wind World Report. 2015.

[187] Creutzig F, Baiocchi G, Bierkandt R, Pichler P-P, Seto KC. Global typology of urban energy use and potentials for an urbanization mitigation wedge. *Proceedings of the National Academy of Sciences*, 2015, **112**(20), pp.6283-6288.

[188] Walker SL. Building mounted wind turbines and their suitability for the urban scale—A review of methods of estimating urban wind resource. *Energy and Buildings*, 2011, **43**, pp.1852 - 1862.

[189] DCLG. Department for Communities and Local Government. Code for Sustainable Homes: A step change in sustainable home building practice. (Cmnd:06 BD 04224). London, UK, Ed, 2006.

[190] MCS UK. The Microgeneration Certification Scheme. Available from: http://www.microgenerationcertification.org/. 2016. [Accessed 12/01/2016].

[191] Walters R, Fanucci J, Hill P, Migliore P. Vertical axis wind turbine development: Executive summary. *Final Report, 1 Mar. 1976-30 Jun. 1977 West Virginia Univ., Morgantown. Dept. of Aerospace Engineering.*, 1979, **1**.

[192] Adam K, Hoolohan V, Gooding J, Knowland T, Bale CSE, Tomlin AS. Methodologies for city-scale assessment of renewable energy generation potential to inform strategic energy infrastructure investment. *Cities*.

[193] Sunderland K, Woolmington T, Blackledge J, Conlon M. Small wind turbines in turbulent (urban) environments: A consideration of normal and Weibull distributions for power prediction. *Journal of Wind Engineering and Industrial Aerodynamics*, 2013, **121**, pp.70-81.

[194] Drew D, Barlow J, Cockerill T. Estimating the potential yield of small wind turbines in urban areas: A case study for Greater London, UK. *Journal of Wind Engineering and Industrial Aerodynamics*, 2013, **115**, pp.104-111.

[195] Drew DR, Barlow JF, Cockerill TT, Vahdati MM. The importance of accurate wind resource assessment for evaluating the economic viability of small wind turbines. *Renewable Energy*, 2015, **77**, pp.493-500.

[196] UK Met Office. UK Climate Summaries. Available from: http://www.metoffice.gov.uk/climate/uk/. 2013. [Accessed August, 2013].

[197] NOABL database. Available from: http://www.rensmart.com/Weather/BERR. 2014. [Accessed 09/10/2014].

[198] Barlow J, Dobre A, Smalley R, Arnold S, Tomlin A, Belcher S. Referencing of street-level flows measured during the DAPPLE 2004 campaign. *Atmospheric Environment*, 2009, **43**(34), pp.5536-5544.

[199] Balogun AA, Tomlin AS, Wood CR, Barlow JF, Belcher SE, Smalley RJ, Lingard JJ, Arnold SJ, Dobre A, Robins AG. In-street wind direction variability in the vicinity of a busy intersection in central London. *Boundary-Layer Meteorology*, 2010, **136**(3), pp.489-513.

[200] Järvi L, Hannuniemi H, Hussein T, Junninen H, Aalto PP, Hillamo R, Mäkelä T, Keronen P, Siivola E, Vesala T. The urban measurement station SMEAR III: Continuous monitoring of air pollution and surface-atmosphere interactions in Helsinki, Finland. *Boreal environment research*, 2009, **14**, pp.86-109.

[201] Nordbo A, Järvi L, Haapanala S, Moilanen J, Vesala T. Intra-city variation in urban morphology and turbulence structure in Helsinki, Finland. *Boundary-Layer Meteorology*, 2013, **146**(3), pp.469-496.

[202] Wieringa J. Representative roughness parameters for homogeneous terrain. *Boundary-Layer Meteorology*, 1993, **63**(4), pp.323-363.

[203] Grimmond CSB, Oke TR. Aerodynamic Properties of Urban Areas Derived From Analysis of Surface Form. *Journal of Applied Meteorology*, 1999, **38**, pp.1262-1292.

[204] Elliott WP. The growth of the atmospheric internal boundary layer. *Transactions, American Geophysical Union*, 1958, **39**, pp.1048-1054.

[205] Jiang D, Jiang W, Liu H, Sun J. Systematic influence of different building spacing, height and layout on mean wind and turbulent characteristics within and over urban building arrays. *Wind and Structures*, 2008, **11**(4), pp.275-289.

[206] Macdonald RW, Griffiths RF, Hall DJ. An improved method for the estimation of surface roughness of obstacle arrays. *Atmospheric Environment*, 1998, **32**(11), pp.1857-1864.

[207] Kastner-Klein P, Rotach MW. Mean Flow and Turbulence Characteristics in an Urban Roughness Sublayer. *Boundary-Layer Meteorology*, 2004, **111**(1), pp.55-84.

[208] Di Sabatino S. A Simple Model for Spatially-averaged Wind Profiles Within and Above an Urban Canopy. *Boundary-Layer Meteorology*, 2008, **127**, pp.131-151.

[209] Leonardi S, Castro IP. Channel flow over large cube roughness: a direct numerical simulation study. *Journal of Fluid Mechanics*, 2010, **651**, pp.519-539.

[210] Ratti C, Di Sabatino S, Britter R, Brown M, Caton F, Burian S. Analysis of 3-D Urban Databases with Respect to Pollution Dispersion for a Number of European and American Cities. *Water, Air and Soil Pollution: Focus*, 2002, **2**(5), pp.459-469.

[211] Raupach MR. Drag and drag partition on rough surfaces. *Boundary-Layer Meteorology*, 1992, **60**(4), pp.375-395.

[212] Raupach MR. Simplified expressions for vegetation roughness length and zero-plane displacement as functions of canopy height and area index. *Boundary-Layer Meteorology*, 1994, **71**(1), pp.211-216.

[213] Bottema M. Roughness parameters over regular rough surfaces: Experimental requirements and model validation. *Journal of Wind Engineering and Industrial Aerodynamics*, 1996, **64**(2), pp.249-265.

[214] Bottema M. Urban roughness modelling in relation to pollutant dispersion. *Atmospheric Environment*, 1997, **31**(18), pp.3059-3075.

[215] Templin R. Aerodynamic performance theory for the NRC vertical-axis wind turbine. National Aeronautical Establishment, Ottawa, Ontario (Canada), 1974.

[216] Noll RB, Ham N.D. Analytical evaluation of the aerodynamic performance of a high-reliability vertical-axis wind turbine. 1980, **Proceedings of AWEA national conference, USA**.

[217] Wilson R, Lissaman P. Applied aerodynamics of wind power machines. *NASA STI/Recon Technical Report N*, 1974, **75**, p.22669.

[218] Strickland JH. A performance prediction model for the darrieus turbine. *International Symposium on wind energy systems, Cambridge, UK, September 7-9*, 1976, **C3-39-54**.

[219] Muraca RJ, Stephens MV, Dagenhart JR. Theoretical Performance of Cross-Wind Axis Turbines with results for a Catenary Vertical Axis Configuration. *NASA TMX-72662, USA*, 1975.

[220] Sharpe D. *A theoretical and experimental study of the Darrieus vertical axis wind turbine.* Polytechnic School of Mechanical, Aeronautical and Production Engineering, 1977.

[221] Paraschivoiu I. Double-multiple streamtube model for darrieus wind turbines. 1981, **Second DOE/NASA wind turbines dynamics workshop, NASA CP-2186, Cleveland, OH**, pp.19–25.

[222] Lapin EE. Theoretical performance of vertical axis wind turbines. 1975, **ASME paper, 75-WA/Ener-1, The winter annual meeting, Houston, TX, USA**.

[223] Larsen HC. Summary of a vortex theory for the cyclogiro. 1975, **Proceedings of the second US national conferences on wind engineering research, Colorado state university**, pp.V8-1–3.

[224] Fanucci JB, Walter, R.E. Innovative wind machines: the theoretical performance of a vertical-axis windturbine. 1976, **Proceedings of the vertical-axis wind turbine technology workshop, Sandia laboratories, SAND 76-5586**, pp.iii-61-95,.

[225] Wilson RE. Wind-turbine aerodynamics. *J Wind Eng Ind Aerodynam*, 1980, pp.357–72.

[226] Holme OA. Contribution to the aerodynamic theory of the vertical axis wind turbine. 1976, **International symposium. on wind energy systems, September 7th–9th, Cambridge, England**, pp.C4-55–71.

[227] Strickland JB, Webster B, Nguyen T. A Vortex Model of the Darrieus Turbine: An Analytical and Experimental Study. 1980, **Technical report SAND81-7017, Sandia National Laboratory**.

[228] Cardona JL. Flow curvature and dynamic stall simulated with an aerodynamic freevortex model for VAWT. *Wind Eng*, 1984, **8**, pp.135–43.

[229] Migliore PG, Wolfe, W.P., Fanucci, J.B. Flow curvature effects on Darrieus turbine blade aerodynamics. *J Energy*, 1980, **4(2)**, pp.49–55.

[230] Currie IG. Fundamental mechanics of fluid. 1974, **New York: McGraw-Hill**.

[231] Pawsey N, C,K. Development and evaluation of passive variable-pitch vertical axis wind turbines. 2002, **Doctoral thesis, The University of New South Wales**.

[232] Hirsch H, Mandal, A.C. A cascade theory for the aerodynamic performance of darrieus wind turbines. *Wind Eng*, 1987, **11(3)**, pp.164–75.

[233] Mandal AC, Burton JD. The effects of dynamic stall and flow curvature on the aerodynamics of darrieus turbines applying the Cascade model. *Wind Eng*, 1994, **18(6)**, pp.267–82.

[234] McIntosh S, Babinsky H, Bertenyi T. Optimizing the Energy Output of Vertical Axis Wind Turbines for Fluctuating Wind Conditions. *In: 45th AIAA Aerospace Sciences Meeting and Exhibit*. Reno, Nevada, USA: American Institute of Aeronautics and Astronautics, 2007.

[235] Beri H, Yao Y. Double Multiple Stream Tube Model and Numerical Analysis of Vertical Axis Wind Turbine. *Energy and Power Engineering Journal*, 2011, **3**, pp.262-270.

[236] Paraschivoiu I. *Wind turbine design: with emphasis on Darrieus concept.* Presses inter Polytechnique, 2002.

[237] Shires A. Development and evaluation of an aerodynamic model for a novel vertical axis wind turbine concept. *Energies*, 2013, **6**(5), pp.2501-2520.

[238] Paraschivoiu I, Delclaux F, Fraunie P, Beguier C. Aerodynamic analysis of the Darrieus rotor including secondary effects. *Journal of Energy*, 1983, **7**(5), pp.416-422.

[239] Parra-Santos T, Gallegos-Muñoz A, Rodriguez-Beneite MA, Uzarraga-Rodriguez C, Castro-Ruiz F. Numerical Modeling of Vertical Axis Wind Turbines. *In: ASME 2014 4th Joint US-European Fluids Engineering Division Summer Meeting collocated with the ASME 2014 12th International Conference on Nanochannels, Microchannels, and Minichannels*: American Society of Mechanical Engineers, 2014, pp.V01DT39A004-V01DT39A004.

[240] Sheldahl RE, Klimas PC. Aerodynamic characteristics of seven symmetrical airfoil sections through 180-degree angle of attack for use in aerodynamic analysis of vertical axis wind turbines. Sandia National Labs., Albuquerque, NM (USA), 1981.

[241] Jacobs EN, Ward KE, Pinkerton RM. The characteristics of 78 related airfoil sections from tests in the variable-density wind tunnel. 1933.

[242] Moriarty PJ, Hansen, A. C. AeroDyn Theory Manual,. *National Renewable Energy Laboratory*, 2005, **NREL/EL-500-36881 - January 2005**.

[243] Buhl Jr LM. A new empirical relationship between thrust coefficient and induction factor for the turbulent windmill state. *National Renewable Energy Laboratory Technical report* 2005, **NREL/TP-500-36834—August 2005**.

[244] Glauert H. *The analysis of experimental results in the windmill brake and vortex ring states of an airscrew*. HM Stationery Office, 1926.

[245] Sharpe D. Wind turbine aerodynamics. *Wind energy conversion systems*, 1990, pp.54-118.

[246] Homicz GF. Numerical Simulation of VAWT Stochastic Aerodynamic Loads Produced by Atmospheric Turbulence: VAWT-SAL Code. *Sandia Laboratories Energy Report*, 1991, **SAND91 - 1124**.

[247] James G. *Modern engineering mathematics.* Pearson Education, 2007.

[248] Gormont RE. An Analytical Model of Unsteady Aerodynamics and Radial Flow for Application to Helicopter Rotors. *U.S. Army Air Mobility Research and Development Laboratory Technical Report*, 1973, **72-67**.

[249] Masson C, Leclerc C, Paraschivoiu I. Appropriate Dynamic-Stall Models for Performance Predictions of VAWTs with NLF Blades. *International Journal of Rotating Machinery*, 1998, **4 - 2**, pp.129-139.

[250] Paraschivoiu I, Desy P, Masson C. Blade-Tip, Finite-Aspect-Ratio and Dynamic-Stall Effects on the Darrieus Rotor. *AIAA Journal of Propulsion and Power*, 1988, **2**(5), pp.73-80.

[251] Brochier G, Fraunie P, Beguier C, Paraschivoiu I. Water Channel Experiments of Dynamic Stall on Darrieu Wind Turbine Blades. *Journal of Propulsion and Power*, 1986, **2**, pp.445 - 449.

[252] Laneville A, Vittecoq P. Effect of turbulence on Dynamic Stall. *Wind Turbine Aerodynamics Seminar*, 1985, **Sandia National Laboratories, Albuquerque, New Mexico**.

[253] Masse B. Description de deux programmes d'ordinateur pour le calcul des perofrmances et des charges aerodynamiques pour les eoliennes a axes vertical. *IREQ-2379*, 1981.

[254] Berg DE. An Improved Double-Multiple Streamtube Model for the Darrieus-Type Vertical Axis Wind Turbine. *Sixth Biennal Wind Energy Conference and Workshop*, 1983, pp.231-233.

[255] McGowan R, Lozano R, Raghav V, Komerath N. Vertical Axis Micor Wind Turbine Design for Low Tip Speed Ratios. *In: Design and Modeling in Science, Education and Technology: DeMset 2012*, March 25th - 28th, 2012, Orlando, Florida USA. 2012.

[256] Ge M, Tian D, Deng Y. Reynolds Number Effect on the Optimization of a Wind Turbine Blade for Maximum Aerodynamic Efficiency. *Journal of Energy Engineering*, 2014, **142**(1), p.04014056.

[257] Blackwell BF, Sheldahl RE, Feltz LV. Wind Tunnel Performance Data for the Darrieus Wind Turbine with NACA0012 Blades. *Sandia Laboratories Energy Report*, 1976, **SAND76-0130**.

[258] Sheldahl RE, Klimas PC, Feltz LV. *Aerodynamic performance of a 5-metre-diameter Darrieus turbine with extruded aluminum NACA-0015 blades.* National Technical Information Service, 1980.

[259] Scelba G, Consoli A. Gust tracking capability of small direct-drive wind turbines. *In: Sustainable Energy Technologies (ICSET), 2010 IEEE International Conference*, Kandy, Sri Lanka. IEEE, 2010, pp.1-6.

[260] Morren J, Pierik J, de Haan SWH. Inertial response of variable speed wind turbines. *Electric Power Systems Research*, 2006, **76**(11), pp.980-987.

[261] Komass T. VERTICAL AXIS WIND TURBINE WITH PERMANENT MAGNET SYNCHRONOUS GENERATOR SIMULATION IN MATHLAB SIMULINK. *Engineering for Rural Development (Latvia)*, 2013.

[262] Nguyen L, Metzger M. Enhanced energy capture by a vertical axis wind turbine during gusty winds in an urban/suburban environment. *Journal of Renewable and Sustainable Energy*, 2015, **7**(5), p.053118.

[263] Baker J. Features to aid or enable self starting of fixed pitch low solidity vertical axis wind turbines. *In: Wind Engineering 1983 3C: Proceedings of the Sixth international Conference on Wind Engineering, Gold Coast, Australia, March 21-25, And Auckland, New Zealand, April 6-7 1983; held under the auspices of the International Association for Wind Engineering*: Elsevier, 2012, p.369.

[264] Johnson KE, Fingersh LJ, Balas MJ, Pao LY. Methods for Increasing Region 2 Power Capture on a Variable-Speed Wind Turbine. *Journal of solar energy engineering*, 2004, **126**(4), pp.1092-1100.

[265] Zinger DS, Muljadi E. Annualized wind energy improvement using variable speeds. *Industry Applications, IEEE Transactions on*, 1997, **33**(6), pp.1444-1447.

[266] Wagner R, Antoniou I, Pedersen SM, Courtney MS, Jørgensen HE. The influence of the wind speed profile on wind turbine performance measurements. *Wind Energy*, 2009, **12**(4), pp.348-362.

[267] Shokrzadeh S, Jozani MJ, Bibeau E. Wind Turbine Power Curve Modeling Using Advanced Parametric and Nonparametric Methods. *Sustainable Energy, IEEE Transactions on*, 2014, **5**(4), pp.1262-1269.

[268] Jackson PS. The evaluation of windy environments. *Building and Environment*, 1978, **13**(4), pp.251-260.

[269] Acosta JL, Combe K, Djokic SZ, Hernando-Gil I. Performance assessment of micro and small-scale wind turbines in urban areas. *Systems Journal, IEEE*, 2012, **6**(1), pp.152-163.

[270] Hanna SR, Brown MJ, Camelli FE, Chan ST, Coirier WJ, Kim S, Hansen OR, Huber AH, Reynolds RM. Detailed simulations of atmospheric flow and dispersion in downtown Manhattan: An application of five computational fluid dynamics models. *Bulletin of the American Meteorological Society*, 2006, **87**(12), pp.1713-1726.

[271] Baskut O, Ozgener O, Ozgener L. Second law analysis of wind turbine power plants: Cesme, Izmir example. *Energy*, 2011, **36**(5), pp.2535-2542.

[272] Shamshirband S, Petković D, Saboohi H, Anuar NB, Inayat I, Akib S, Ćojbašić Ž, Nikolić V, Mat Kiah ML, Gani A. Wind turbine power coefficient estimation by soft computing methodologies: comparative study. *Energy Conversion and Management*, 2014, **81**, pp.520-526.

[273] Abdullah M, Yatim A, Tan C, Saidur R. A review of maximum power point tracking algorithms for wind energy systems. *Renewable and Sustainable Energy Reviews*, 2012, **16**(5), pp.3220-3227.

[274] Penna P. Wind tunnel tests of the Quiet Revolution Ltd. QR5 vertical axis wind turbine. *Institute for Aerospace Research, National Research Council Canada, Rept. LTR-AL-2008-0004*, 2008.

[275] Bertenyi T, Young T. Power electronics solutions for Vertical Axis urban wind turbines. *In: Electrical Power & Energy Conference (EPEC)*. IEEE, 2009, pp.1-7.

[276] Cook NJ. Designers guide to wind loading of building structures. Part 1. 1986.

[277] Nakamura M, Nanayakkara N, Yoshida H, Hatazaki H. Modelling and Prediction of Effective Wind speed for Wind Turbine Operations *In: Proceedings - International Conference on Automation ICAUTO-95*, December 11-14, Indore, India. Allied Publishers Limited, 1995, pp.225-228.

[278] Haque ME, Negnevitsky M, Muttaqi KM. A novel control strategy for a variable speed wind turbine with a permanent magnet synchronous generator. *In: Industry Applications Society Annual Meeting, 2008. IAS'08. IEEE*: IEEE, 2008, pp.1-8.

[279] Eriksson S, Kjellin J, Bernhoff H. Tip speed ratio control of a 200 kW VAWT with synchronous generator and variable DC voltage. *Energy Science & Engineering*, 2013, **1**(3), pp.135-143.

[280] Thongam J, Bouchard P, Ezzaidi H, Ouhrouche M. Wind speed sensorless maximum power point tracking control of variable speed wind energy conversion systems. *In: Electric Machines and Drives Conference, 2009. IEMDC'09. IEEE International*: IEEE, 2009, pp.1832-1837.

[281] Jeong HG, Seung RH, Lee KB. An improved maximum power point tracking method for wind power systems. *Energies*, 2012, **5**(5), pp.1339-1354.

[282] Zhu Y, Cheng M, Hua W, Wang W. A Novel Maximum Power Point Tracking Control for Permanent Magnet Direct Drive Wind Energy Conversion Systems. *Energies*, 2012, **5**(5), pp.1398-1412.

[283] Abohela IMMM. Effect of roof shape, wind direction, building height and urban configuration on the energy yield and positioning of roof mounted wind turbines. 2012.

[284] Ledo L, Kosasih P, Cooper P. Roof mounting site analysis for micro-wind turbines. *Renewable Energy*, 2011, **36**(5), pp.1379-1391.

[285] Kaiser K, Langreder W, Hohlen H, Hojstrup J. Turbulence Correction of Power Curve. *In: Wind Energy: Proceedings of the Euromech Colloquium*. Peinke J, Schaumann P and Barth S, eds. New York: Springer, 2007, pp.159-162.

[286] Kooiman S, Tullis S. Response of a vertical axis wind turbine to time varying wind conditions found within the urban environment. *Wind Engineering*, 2005, **34**(4), pp.389-401.

[287] Oke T. The heat island of the urban boundary layer: characteristics, causes and effects. *In: Wind Climate in Cities*. Netherlands: Springer, 1995, pp.81-107.

[288] Voogt JA, Oke TR. Complete urban surface temperatures. *Journal of Applied Meteorology*, 1997, **36**(9), pp.1117-1132.

[289] Hamlyn D, Britter R. A numerical study of the flow field and exchange processes within a canopy of urban-type roughness. *Atmospheric Environment*, 2005, **39**(18), pp.3243-3254.

[290] Danish Standard. Code of practice for loads and safety of wind turbine constructions. DS 472, 1992.

[291] Mertens S. *Wind energy in the built environment: concentrator effects of buildings.* Brentwood, UK: Multi Science Publishing Company, 2006.

[292] IEC 61400-1. Wind turbines – Part 1: Design requirements. Ed3, 2005.

[293] Ishihara T, Yamaguchi A, Sarwar MW. A Study of the Normal Turbulence Model in IEC 61400-1. *Wind Engineering*, 2012, **36**(6), pp.759-766.

[294] James P, Sissons M, Bradford J, Myers L, Bahaj A, Anwar A, Green S. Implications of the UK field trial of building mounted horizontal axis micro-wind turbines. *Energy Policy*, 2010, **38**(10), pp.6130-6144.

[295] Kaiser K, Langreder W, Hohlen H, Højstrup J. Turbulence Correction for Power Curves. *In: Wind Energy*. Peinke J, Schaumann P and Barth S, eds. Springer Berlin Heidelberg, 2007, pp.159-162.

[296] Acosta JL. Assessment of renewable wind resources in UK urban areas. *In: MELECON 2010-2010 15th IEEE Mediterranean Electrotechnical Conference*: IEEE, 2010, pp.1439-1444.

[297] Heath MA, Walshe JD, Watson SJ. Estimating the potential yield of small building-mounted wind turbines. *Wind Energy*, 2007, **10**(3), pp.271-287.

[298] El-Shimy M. Optimal site matching of wind turbine generator: Case study of the Gulf of Suez region in Egypt. *Renewable Energy*, 2010, **35**(8), pp.1870-1878.

[299] Albers A, Hinsch C. Influence of different meteorological conditions on the power performance of large WECS. *DEWI Magazin*, 1996, **9**, pp.40-49.

[300] Hu S-y, Cheng J-h. Performance evaluation of pairing between sites and wind turbines. *Renewable Energy*, 2007, **32**(11), pp.1934-1947.

[301] Jangamshetti SH, Rau VG. Normalized power curves as a tool for identification of optimum wind turbine generator parameters. *Energy Conversion, IEEE Transactions on*, 2001, **16**(3), pp.283-288.

[302] Carrillo C, Obando Montaño AF, Cidrás J, Díaz-Dorado E. Review of power curve modelling for wind turbines. *Renewable and Sustainable Energy Reviews*, 2013, **21**, pp.572-581.

[303] Thiringer T, Linders J. Control by variable rotor speed of a fixed-pitch wind turbine operating in a wide speed range. *Energy Conversion, IEEE Transactions on*, 1993, **8**(3), pp.520-526.

[304] Simic Z, Havelka JG, Bozicevic Vrhovcak M. Small wind turbines – A unique segment of the wind power market. *Renewable Energy*, 2013, **50**, pp.1027-1036.

[305] Hayes BP, Djokic SZ. Modelling of wind generation at all scales for transmission system analysis. *IET Generation, Transmission & Distribution*, 2013, **7**(10), pp.1144-1154.

[306] Data.gov.uk. LiDAR Composite DSM - 1m - Datasets. Available from: https://data.gov.uk/dataset/lidar-composite-dsm-1m1. 2016. [Accessed 18/02/2016].